Improved Nanocomposite Performance Using Carboxylated Cellulose Nanocrystals

By

Parisa Bayat

Thesis submitted to the University of Ottawa in partial fulfillment of requirements for degree of Ph.D. in Chemical Engineering

Department of Chemical and Biological Engineering

Faculty of Engineering

University of Ottawa, Ottawa, Canada

Abstract

This thesis aims to develop sustainable polymer nanocomposites by capitalizing on the unique properties of carboxylated cellulose nanocrystals (cCNCs)—a bio-based nanomaterial derived from wood pulp via an environmentally friendly hydrogen peroxide oxidation process. cCNCs are hydrophilic, making dispersion in hydrophobic polymers challenging. This thesis explores strategies to enhance polymer performance while addressing dispersion issues through surface changes and processing techniques. Two important industrial polymer systems were selected: polylactic acid (PLA) and latex-based pressure-sensitive adhesives (PSAs), which both stand to benefit from renewable nanofillers that can boost performance without compromising sustainability.

In the first project, a commercial PSA formulation was introduced into a seeded, semi-batch emulsion polymerization (2-ethyl hexyl acrylate/methyl methacrylate/styrene), which successfully achieved high tack and peel strength. Yet, the shear adhesion remained insufficient for industrial applications. By integrating cCNCs, the PSA films demonstrated simultaneous increases in tack, peel strength, and shear adhesion, avoiding the property trade-off between tack and peel strength, and shear adhesion. Key to these gains was cCNC reassembly: dried-redispersed cCNCs, especially under sonication, were more prone to forming nanofibril-like networks, reinforcing the adhesive film and substantially boosting shear adhesion (by >1,300% in some cases). Systematic experiments revealed that cCNC dispersion and subsequent end-to-end realignment into nanofibrillar networks proved vital to maximizing adhesive performance.

Building on this framework, the second study investigated whether cCNCs' compatibility with the hydrophobic polymer matrix could be further improved by acetylation. Through a systematic variation of degrees of substitution (DS), the hydrophilic cCNC surfaces became increasingly hydrophobic. cCNCs with the highest DS (0.42) demonstrated noticeably better PSA performance than unmodified cCNCs. Improved dispersion and latex particle coalescence were encouraged by lower interfacial tension, which ultimately led to higher tack, peel strength, and shear adhesion. Overall, these findings reinforce how fine-tuning cCNC surface chemistry can enhance nanoparticle networks and mechanical performance in latex-based PSAs.

To investigate the further potential of cCNCs and their surface modification, we explored their influence on the crystallization behaviour of polylactic acid (PLA). While PLA's renewable origin and biodegradability make it attractive, commonly used solvents for dispersing CNCs—such as chloroform and dimethyl formamide—undercut its environmental appeal. Here, ethyl lactate (EtLa) was adopted as a safer, bio-based solvent that also acts as a plasticizer, enhancing chain mobility and lowering PLA's cold crystallization temperature. Incorporating cCNCs in EtLa not only accelerated PLA crystallization but also improved mechanical performance, as evidenced by polarized optical microscopy, X-ray diffraction, and differential scanning calorimetry results. Acetylated cCNCs (AcCNCs) further refined nucleation efficiency, with lower DS AcCNCs achieving superior dispersion and fostering rapid spherulitic growth. Though higher DS AcCNCs increased the storage modulus, they were comparatively less effective in nucleation efficiency due to suboptimal interactions in EtLa. Consequently, balancing DS emerged as the key to delivering enhanced crystallization, better mechanical robustness, and an overall more sustainable PLA nanocomposite—achieved without relying on harmful solvents.

The adaptability of cCNC-based nanocomposites is highlighted overall in this thesis, which demonstrates how specific surface alterations and processing condition adjustments might narrow the performance and sustainability gap. The insights here offer a foundation for future research, from large-scale acetylation protocols to alternative green solvents, ensuring that cCNCs continue to drive innovation across various polymer applications.

Resumé

Cette thèse vise à développer des nanocomposites polymères durables en tirant parti des propriétés uniques des nanocristaux de cellulose carboxylée (cCNCs), un nanomatériau biosourcé dérivé de la pâte de bois par un procédé d'oxydation du peroxyde d'hydrogène respectueux de l'environnement. Les cCNCs sont hydrophiles, ce qui rend la dispersion dans les polymères hydrophobes difficile. Cette thèse explore des stratégies pour améliorer la performance des polymères tout en abordant les problèmes de dispersion par des changements de surface et des techniques de traitement. Deux systèmes de polymères industriels importants ont été sélectionnés : l'acide polylactique (PLA) et les adhésifs sensibles à la pression (PSA) à base de latex, qui bénéficient tous deux de nanocharges renouvelables qui peuvent améliorer les performances sans compromettre la durabilité.

Dans le cadre du premier projet, une formulation commerciale de PSA a été introduite dans une polymérisation en émulsion semi-discontinue (acrylate de 2-éthyle hexyle/méthacrylate de méthyle/styrène), qui a permis d'obtenir une résistance élevée à l'adhérence et au pelage. Pourtant, l'adhérence au cisaillement est restée insuffisante pour les applications industrielles. En intégrant des cCNCs, les films PSA ont démontré des augmentations simultanées de l'adhérence, de la résistance au pelage et de l'adhérence au cisaillement, évitant ainsi le compromis entre la résistance à l'adhérence et au pelage et l'adhérence au cisaillement. La clé de ces gains a été le réassemblage des cCNCs : les cCNCs séchées-redispersées, en particulier sous sonication, étaient plus susceptibles de former des réseaux de type nanofibrille, renforçant le film adhésif et augmentant considérablement l'adhérence au cisaillement (de >1 300% dans certains cas). Des expériences systématiques ont révélé que la dispersion des cCNCs et le réalignement subséquent de bout en bout dans les réseaux nanofibrillaires se sont avérés essentiels pour maximiser la performance de l'adhésif.

En s'appuyant sur ce cadre, la deuxième étude a cherché à déterminer si la compatibilité des cCNCs avec la matrice polymère hydrophobe pouvait être améliorée par l'acétylation. Grâce à une variation systématique des degrés de substitution (DS), les surfaces cCNC hydrophiles sont devenues de plus en plus hydrophobes. Les cCNCs ayant le DS le plus élevé (0,42) ont démontré une performance nettement meilleure du PSA que les cCNCs non modifiées. L'amélioration de la

dispersion et de la coalescence des particules de latex a été encouragée par une tension interfaciale plus faible, ce qui a finalement entraîné une adhérence plus élevée, une résistance au pelage et une adhérence au cisaillement plus élevées. Dans l'ensemble, ces résultats renforcent la façon dont le réglage fin de la chimie de surface cCNC peut améliorer les réseaux de nanoparticules et les performances mécaniques des PSAs à base de latex.

Pour explorer davantage le potentiel des cCNCs et leur modification de surface, nous avons étudié leur influence sur le comportement de cristallisation de l'acide polylactique (PLA). Bien que l'origine renouvelable et la biodégradabilité du PLA le rendent attrayant, les solvants couramment utilisés pour la dispersion des cCNCs, comme le chloroforme et le diméthylformamide, nuisent à son attrait environnemental. Ici, le lactate d'éthyle (EtLa) a été adopté comme solvant biosourcé plus sûr qui agit également comme plastifiant, améliorant la mobilité de la chaîne et abaissant la température de cristallisation à froid du PLA. L'incorporation de cCNC dans EtLa a non seulement accéléré la cristallisation du PLA, mais a également amélioré les performances mécaniques, comme en témoignent les résultats de la microscopie optique polarisée, de la diffraction des rayons X et de la calorimétrie différentielle à balayage. Les CNC acétylées (AcCNCs) ont affiné l'efficacité de la nucléation, les DS plus faibles atteignant une dispersion supérieure et favorisant une croissance sphérulitique rapide. Bien que des AcCNCs au DS plus élevés augmentent le module de stockage, ils sont comparativement moins efficaces dans l'efficacité de la nucléation en raison d'interactions sous-optimales dans EtLa. Par conséquent, l'équilibrage de la DS est apparu comme la clé pour offrir une cristallisation améliorée, une meilleure robustesse mécanique et un nanocomposite PLA globalement plus durable, réalisé sans dépendre de solvants nocifs.

L'adaptabilité des nanocomposites à base de cCNCs est soulignée dans l'ensemble de cette thèse, qui démontre comment des modifications de surface spécifiques et des ajustements des conditions de traitement peuvent réduire l'écart de performance et de durabilité. Les connaissances ici offrent une base pour de futures recherches, des protocoles d'acétylation à grande échelle aux solvants verts alternatifs, garantissant que les cCNCs continuent de stimuler l'innovation dans diverses applications de polymères.

Preface

Dedications

I dedicate this thesis to my dearest parents, who have been my guiding light through every moment of self-doubt. Whenever I felt I wasn't enough, you reminded me of my strengths and taught me to be brave—your unwavering faith in me has truly been my greatest source of motivation (and a cure for procrastination). To my sister, who stood by me during my very first panic attack in the first year of my PhD. At that moment, she told me, "You won't die," and prescribed lemon juice for every moment I was convinced otherwise. Your kindness and reassurance carried me through one of my darkest moments, and you still manage to make me laugh when I'm convinced the sky is falling. To my brother, for always making me feel supported, even when you teased me about possibly blowing up the lab. Your clever "motivational speeches" ("Don't fail, or else…") kept me on my toes, and your belief in me proved stronger than any coffee I consumed along the way.

To my cousin, Ghazaleh, though you are miles away, you never failed to cheer me on. Thank you for being my private therapist, offering top-notch advice in exchange for nothing but a good laugh and a few emojis.

To all my friends, who brought so much joy throughout this journey—thank you, Marc, Emile, and Josh, for introducing me to acroyoga, where I learned how to stay balanced even when life felt upside down (let's be honest, that is still easier than finishing a PhD, LOL). There have been many ups and downs along the way, and I could not have overcome them without each of you. Your heartfelt support and belief in me have made this achievement possible. I am forever grateful.

And finally, to myself. For the days I felt like giving up but didn't. For the countless late nights, early mornings, and moments when exhaustion felt overwhelming. For standing back up after every setback, pushing forward through every challenge, and proving to myself that I am stronger than my doubts. Through every hard day, I kept going—and I did it.

Acknowledgements

This journey would not have been possible without the unwavering support, guidance, and encouragement of many incredible individuals, to whom I am deeply grateful.

First and foremost, I extend my heartfelt gratitude to my supervisor, **Prof. Marc A. Dubé**, for his exceptional mentorship, patience, and unwavering support throughout my PhD. Your insightful guidance, constructive feedback, and ability to push me toward critical thinking have been invaluable in shaping my research and personal growth. Beyond academia, your leadership course was nothing short of life-changing—I signed up expecting professional development but ended up reevaluating my entire perspective on leadership, communication, and even life itself (fun fact: I still don't know whether I took a leadership or a philosophy course!). Thank you for always believing in me, challenging me to think bigger, and supporting me through both my academic and personal growth.

I am also immensely grateful to my co-supervisor, **Prof. Kelly M. Meek**, whose expertise, thoughtful advice, and continuous support have been instrumental in refining my research. Your attention to detail and insightful perspectives have strengthened the quality of this work, and I deeply appreciate the time and effort you dedicated to guiding me through this journey.

Throughout this PhD, I faced many challenging moments, and you—**Marc and Kelly**—were always the first people I turned to. I could not have been luckier to have not just incredible supervisors, but also two of my closest friends and mentors. I will always cherish the deep conversations we had—especially those moments when I shared my fears about turning 30, questioning the unknowns that lay ahead. **Kelly**, I will never forget your words: "Your journey may be even more beautiful after 30, just as mine was." That reassurance, that simple but profound perspective, gave me the courage to embrace whatever comes next.

A special acknowledgment to **Dr. Andrew Anstey**, for his invaluable contributions and guidance throughout the third part of my project. Your expertise, patience, and willingness to discuss ideas and provide constructive feedback played a crucial role in shaping my understanding and strengthening this research.

I would also like to express my deepest gratitude to **Dr. Vida Gabriel**—you were one of the first people to welcome me and guide me through this journey. From teaching me how to

start working with the reactor to introducing me to CBEGSA, you not only supported me academically but also showed me the true richness of friendship beyond nationalities. Thank you for motivating me, inviting me to your engagement surprise party, and making me feel at home through potlucks, gatherings, and endless support. Your kindness and generosity made an immeasurable impact on my experience, and I am forever grateful.

To **Dr. Maryam Movafagh** and **Dr. Fatemeh Abedi**, the best friends I could have ever made along this journey—you were more than just colleagues; you became my support system, my cheerleaders, and my safe space. I was so incredibly lucky to have both of you not only helping me in the workplace but also in my life. Your kindness, endless encouragement, and moments of laughter made even the most difficult days manageable, and I will cherish our friendship forever.

A huge thank you to **CBEGSA** (Chemical and Biological Engineering Graduate Student Association)—being part of this organization as a departmental representative was one of the most enriching experiences of my PhD. Through this role, I had the opportunity to engage with an incredible community, advocate for students, and discover new strengths within myself that I never knew I had.

Finally, I extend my gratitude to the **Department of Chemical and Biological Engineering** for their continuous support and for always providing me with the opportunity to explore and realize my full potential. The encouragement and resources provided throughout my PhD journey have been invaluable.

This journey has been filled with challenges and triumphs, and I am beyond grateful to have had such an incredible support system. Thank you all for your encouragement, guidance, and belief in me—it has truly made all the difference.

Statement of Contributions

This research was made possible through the support and contributions of numerous individuals and collaborators.

Prof. Michael Cunningham (Queen's University) contributed editorial feedback on the manuscripts entitled "The Effect of Cellulose Nanocrystal Reassembly on Latex-Based Pressure-Sensitive Adhesive Performance" and "Enhancing Pressure-Sensitive Adhesive Performance Using Acetylated Carboxylated Cellulose Nanocrystals." Additionally, **Prof. Pascale Champagne** (Queen's University) participated in discussions related to this work.

Prof. Emily D. Cranston (University of British Columbia) provided valuable research guidance and assisted with Atomic Force Microscopy (AFM) experiments related to the characterization of carboxylated cellulose nanocrystals (cCNCs).

Rahil Ghalamboland (University of Ottawa) performed AFM experiments, while **Dr. Reza Frouzanmehr** (University of Ottawa) provided access to his laboratory for Differential Scanning Calorimetry (DSC) and Dynamic Mechanical Analysis (DMA). Further instrumental support was provided by **Nichole Cheung** and **Dr. Patrick Lee** (University of Toronto) for Polarized Optical Microscopy (POM) experiments.

Prof. Benoît Lessard (University of Ottawa) secured funding for the AFM measurements, and **Prof. Christopher Lan** (University of Ottawa) facilitated access to a centrifuge. Additionally, **Patrick Pageau** and **Franco Ziroldo** (University of Ottawa) provided technical support throughout the research. **Xiaotan Zhu** (University of Ottawa) assisted in operating the freeze-dryer for sample preparation. A special acknowledgment goes to **Mike Mascioli** for his invaluable assistance in reactor repair, which was instrumental in maintaining laboratory operations.

Dr. Andrew Anstey provided invaluable **contributions and guidance** in the preparation of the manuscript entitled "*Effect of Carboxylated Cellulose Nanocrystal Acetylation on PLA Nanocomposite Properties.*" His insights were instrumental in refining the discussion and analysis of this study.

Finally, my supervisors, **Prof. Marc A. Dubé** and **Prof. Kelly M. Meek**, provided scientific guidance, continuous support, and contributions to the revision and editing of the manuscripts

presented in this thesis. Their collective expertise and support were instrumental in the successful completion of this research, and I extend my sincere gratitude to each of them.

Statement of Originality

I certify that the research presented in this thesis is my own work, and all referenced work performed by others is explicitly stated using standard methods.

Table of Contents

List of Figures

List of Tables

Nomenclature

2-EHA	2-Ethyl Hexyl Acrylate
AcCNC	Acetylated Carboxylated Cellulose Nanocrystals
AFM	Atomic Force Microscopy
cCNC	Carboxylated Cellulose Nanocrystals
CNC	Cellulose Nanocrystals
DMA	Dynamic Mechanical Analysis
DMSO	Dimethyl Sulfoxide
DMF	Dimethylformamide
DS	Degree of Substitution
DSC	Differential Scanning Calorimetry
ΔH_{cc}	Enthalpy change associated with cold crystallization
EtLa	Ethyl Lactate
FTIR	Fourier Transform Infrared Spectroscopy
MMA	Methyl Methacrylate
NaPS	Sodium Persulfate
NMR	Nuclear Magnetic Resonance
POM	Polarized Optical Microscopy
PLA	Polylactic Acid
PSA	Pressure-Sensitive Adhesive
SDS	Sodium Dodecyl Sulfate
sCNC	Sulfated Cellulose Nanocrystals
STY	Styrene
$t_{1/2}$	Crystallization Half-Time
T_{cc}	Cold Crystallization Temperature
TGA	Thermogravimetric Analysis
THF	Tetrahydrofuran
T_g	Glass Transition Temperature
VOC	Volatile Organic Compound
XRD	X-ray Diffraction
σ (Sigma)	Surface charge density
θ (Theta)	Contact angle, indicating surface hydrophilicity or hydrophobicity

Chapter 1

Introduction

1.1 Sustainable polymer nanocomposites

In recent years, polymeric materials have been combined with a diverse spectrum of organic,[1] organically modified,[2] and inorganic nanomaterials in the form of nano-spheres[3] to dramatically improve their properties. Compared to conventional synthetic polymers and composites, polymer nanocomposites have many advantages, such as superior barrier qualities, heat resistance, decreased flammability, and higher strength and modulus.[4,5] However, because the accumulation of millions of tons of plastic garbage continues to pose serious ecological dangers, concerns over their influence on the environment remain substantial.[6] Sustainability is a key consideration when addressing environmental concerns and is defined as maintaining necessary benefits while minimizing future harm. Over the past few decades, polymer reaction engineers have increasingly concentrated on identifying methods to reduce or eliminate the impact of polymers by implementing sustainable production guidelines. For instance, applying the 12 principles of green chemistry to polymer manufacturing and focusing on renewable feedstock.[7]

In the context of polymers, sustainability involves relative comparisons to traditional practices and encompasses aspects such as using renewable feedstocks, producing materials through eco-friendly processes with minimal waste, energy, and water use, and ensuring the polymer can reintegrate into the environment after its useful life without causing harm to humans, animals, or ecosystems. A truly sustainable polymer minimizes environmental impact throughout its entire lifecycle, from material extraction and manufacturing to usage and end-of-life disposal.

To promote the use of renewable resources, significant research has focused on developing various bio-based composites using wood-derived nanomaterials. These abundant nanomaterials pose minimal safety risks[8] and include cellulose nanocrystals (CNCs)[9], starch nanospheres[10] and lignin nanoparticles[11]. CNCs are a promising alternative to synthetic

nanoparticles thanks to their non-toxic nature (as classified by Environment Canada), cost-effectiveness, biocompatibility, high aspect ratio, and exceptional mechanical properties.[12] Sourced primarily from wood pulp, CNCs are the crystalline regions of cellulose microfibrils, obtained by selectively removing the amorphous regions through controlled acid hydrolysis. The surface functional groups of the CNC surface are strongly influenced by the acid used during CNC extraction from wood pulp.[13,14] By replacing some surface hydroxy groups, sulfated CNCs—which are typically created by hydrolyzing with sulfuric acid—acquire anionic sulfate half-ester groups. As a result, the colloidal stability of CNC dispersions in water is greatly improved.[15] On the other hand, Anomera Inc. has developed a more ecologically friendly method of extracting CNCs by oxidation with hydrogen peroxide.[12] Carboxylated CNCs (cCNCs) are produced by this technique, which substitutes carboxylate groups for certain surface hydroxy groups. Compared to sulfated CNCs, these cCNCs have a reduced surface charge density.[13]

According to theoretical and experimental investigations, the fundamental cellulose crystal has a very high longitudinal modulus of about 150 GPa, which is the basis for the promise of cellulose-derived composites.[9] Because of these qualities, CNCs are ideal for altering the properties of polymers and promoting the sustainability of polymer nanocomposites. However, direct dispersion into nonpolar, hydrophobic polymer matrices is difficult due to CNCs' hydrophilic nature.[16,17] Because CNC surfaces are rich in hydroxy (OH) groups, these environmentally friendly nanoparticles are perfect candidates for functionalization, which could enhance their compatibility with hydrophobic polymers and improve their dispersion in polar polymer matrices. [18,19]

Previous studies conducted by the Dubé group demonstrated using both hydrophilic and partially hydrophobic CNCs in producing nanocomposite pressure-sensitive adhesives (PSAs) through conventional emulsion polymerization.[20,21] It was observed that partially hydrophobic CNCs enhanced PSA performance compared to unmodified, hydrophilic CNCs. However, the specifics of the hydrophobic modification on the CNCs remained undisclosed due to corporate confidentiality, as the CNCs were supplied by Celluforce Inc.

Our research team has devised a simple and ecologically safe method for altering the hydrophilicity of CNC surfaces.[22] The esterification of OH groups, which substitutes acetyl groups

for hydroxymethyl groups, is the basis of the technique. As a result, the CNCs are more soluble in nonpolar organic fluids and less hydrophilic. By altering the degree of substitution (DS) of the acetyl groups in a controlled manner, the CNCs' hydrophilicity and dispersibility in organic or aqueous solutions can be manipulated.[23]

In this work, we modified cCNCs through acetylation to yield a controllable range of hydrophobicity/hydrophilicity. These modified cCNCs were then used to investigate their effect on the properties of two commercially important polymers: an acrylic PSA and polylactic acid (PLA), a biodegradable and biocompatible polymer.[24,25]

PSAs are indispensable across various industries due to their ability to adhere to surfaces with minimal pressure.[26] Acrylic PSAs are particularly dominant, valued for their excellent transparency, adhesion properties, and resistance to ultraviolet (UV) light. Meanwhile, emulsion-based and low-VOC PSAs have been increasingly adopted, driven by environmental regulations and the growing preference for sustainable products.[27] Despite their environmental benefits, the compartmentalized nature of polymer particles suspended in water (i.e., in emulsion polymerization) makes achieving a continuous network in the dried adhesive film more challenging, leading to decreased performance when compared to solution polymerization, specifically in the matter of shear adhesion. The range of desired shear adhesion is broad and depends on the specific application.[26] Thus, the emulsion polymers often require additional modification to achieve similar adhesive performance; this is where using a nanocomposite can provide benefits.[28,29] Combining emulsion polymerization and a bio-based nanomaterial, such as CNCs, leads to a more sustainable PSA manufacturing process and has also been shown to improve latex-based adhesive properties.[30] This approach, however, is not without its challenges. Introducing charged materials such as cCNCs can destabilize the latex, necessitating precise control of variables such as pH, particle size, solids content, and molecular weight. Finally, using a more hydrophobic acetylated cCNC could enhance polymer-nanomaterial compatibility and improve adhesive properties.

PLA's inherently slow crystallization kinetics and limited thermal and mechanical properties present challenges for their broader industrial adoption.[31] CNCs have been shown to enhance polymer crystallization and mechanical properties by acting as nucleating agents while

maintaining biodegradability.[24,32–34] Incorporating CNCs into polymer matrices such as PLA also presents challenges due to their hydrophilic nature. The abundance of hydroxy groups on the CNCs leads to strong interactions resulting in their aggregation and poor compatibility with hydrophobic matrices such as PLA. This limits their ability to reinforce the material effectively, undermining the mechanical and thermal properties of the composite. Modifying the CNC surfaces, such as through acetylation, can reduce their hydrophilicity and offer improved dispersion.

Alanalp et al. investigated the effect of solvents on crystallization behaviour and kinetics, discovering that dimethyl sulfoxide (DMSO) had a lower onset temperature for cold crystallization and a broader exothermic peak than dimethylformamide (DMF)-based samples.[35] However, polar solvents used in similar research, such as DMF,[35,36] chloroform,[37] and dichloromethane,[38] are more hazardous. In this work, we propose the potential of cCNCs and acetylated cCNCs dispersed in a less hazardous solvent, ethyl lactate, to improve PLA's crystallization behaviour and thermal and mechanical properties. This could lead to the expected environmental benefits and significantly broaden the range of applications where PLA can be used. Furthermore, this approach could be extrapolated to other polymer nanocomposite applications.

1.2 Objectives, hypothesis, and thesis structure

In this thesis, we hypothesize that the controlled acetylation of cCNCs improves their compatibility with hydrophobic polymers, which will lead to improved performance of these nanocomposite materials. As two examples of proof-of-concept, the well-dispersed modified cCNCs will be shown to enhance PSA performance and PLA mechanical properties.

Our objectives were:

1- To investigate the use of cCNCs in a commercially important PSA formulation.
2- To modify cCNCs using an acetylation process to yield cCNCs with a controlled range of hydrophobicity
3- To incorporate the acetylated cCNCs into PSAs and PLA and measure the impact on their properties.

This thesis includes a total of 6 chapters, described below:

Chapter 2 provides a background on adhesives and PLA, discusses the emulsion polymerization process, and introduces the renewable nanomaterials, CNCs, used to improve the properties of our hydrophobic polymer nanocomposites.

Chapter 3 was published in Biomacromolecules and explores the influence of CNC reassembly and the formation of nanofibril-like structures in latex-based pressure-sensitive adhesives (PSAs).

Chapter 4, published in Industrial & Engineering Chemistry Research, explores the influence of acetylation of cCNC on the properties of latex-based PSAs (i.e., tack, peel strength, shear adhesion).

Chapter 5 is to be submitted to a refereed journal and discusses the effects of cCNCs and acetylated cCNCs on PLA crystallinity, and thermal and mechanical properties.

Chapter 6 provides a general discussion and summarizes the most important findings in this thesis. The discussion concludes by proposing new, more effective approaches for sustainably improving the properties of sustainable polymers for broader applications.

Finally, Appendices I-III contain supporting information related to chapters 3 to 5, respectively; Appendix IV provides a report on health and safety considerations for this project, and Appendix V contains a list of publications and conference attendance.

1.3 References

(1) Cummings, S.; Zhang, Y.; Smeets, N.; Cunningham, M.; Dubé, M. On the Use of Starch in Emulsion Polymerizations. *Processes* **2019**, *7* (3), 140. https://doi.org/10.3390/pr7030140.

(2) Kango, S.; Kalia, S.; Celli, A.; Njuguna, J.; Habibi, Y.; Kumar, R. Surface Modification of Inorganic Nanoparticles for Development of Organic–Inorganic Nanocomposites—A Review. *Prog Polym Sci* **2013**, *38* (8), 1232–1261. https://doi.org/10.1016/j.progpolymsci.2013.02.003.

(3) Sinha Ray, S.; Okamoto, M. Polymer/Layered Silicate Nanocomposites: A Review from Preparation to Processing. *Prog Polym Sci* **2003**, *28* (11), 1539–1641. https://doi.org/10.1016/j.progpolymsci.2003.08.002.

(4) Rahmat, M.; Hubert, P. Carbon Nanotube–Polymer Interactions in Nanocomposites: A Review. *Compos Sci Technol* **2011**, *72* (1), 72–84. https://doi.org/10.1016/j.compscitech.2011.10.002.

(5) Mittal, G.; Dhand, V.; Rhee, K. Y.; Park, S.-J.; Lee, W. R. A Review on Carbon Nanotubes and Graphene as Fillers in Reinforced Polymer Nanocomposites. *J of I&ECR* **2015**, *21*, 11–25. https://doi.org/10.1016/j.jiec.2014.03.022.

(6) Lau, W. W. Y.; Shiran, Y.; Bailey, R. M.; Cook, E.; Stuchtey, M. R.; Koskella, J.; Velis, C. A.; Godfrey, L.; Boucher, J.; Murphy, M. B.; Thompson, R. C.; Jankowska, E.; Castillo Castillo, A.; Pilditch, T. D.; Dixon, B.; Koerselman, L.; Kosior, E.; Favoino, E.; Gutberlet, J.; Baulch, S.; Atreya, M. E.; Fischer, D.; He, K. K.; Petit, M. M.; Sumaila, U. R.; Neil, E.; Bernhofen, M. V.; Lawrence, K.; Palardy, J. E. Evaluating Scenarios toward Zero Plastic Pollution. *Science (1979)* **2020**, *369* (6510), 1455–1461. https://doi.org/10.1126/science.aba9475.

(7) Dubé, M. A.; Gabriel, V. A.; Pakdel, A. S.; Zhang, Y. Sustainable Polymer Reaction Engineering: Are We There Yet? *Can J Chem Eng* **2021**, *99* (1), 31–60. https://doi.org/10.1002/cjce.23865.

(8) Lin, N.; Huang, J.; Dufresne, A. Preparation, Properties and Applications of Polysaccharide Nanocrystals in Advanced Functional Nanomaterials: A Review. *Nanoscale* **2012**, *4* (11), 3274. https://doi.org/10.1039/c2nr30260h.

(9) Dufresne, A. *Nanocellulose*; Huang, J., Dufresne, A., Lin, N., Eds.; Wiley, 2019. https://doi.org/10.1002/9783527807437.

(10) Le Corre, D.; Bras, J.; Dufresne, A. Starch Nanoparticles: A Review. *Biomacromolecules* **2010**, *11* (5), 1139–1153. https://doi.org/10.1021/bm901428y.

(11) Duval, A.; Lawoko, M. A Review on Lignin-Based Polymeric, Micro- and Nano-Structured Materials. *React Funct Polym* **2014**, *85*, 78–96. https://doi.org/10.1016/j.reactfunctpolym.2014.09.017.

(12) Habibi, Y.; Lucia, L. A.; Rojas, O. J. Cellulose Nanocrystals: Chemistry, Self-Assembly, and Applications. *Chem Rev* **2010**, *110* (6), 3479–3500. https://doi.org/10.1021/cr900339w.

(13) Delepierre, G.; Vanderfleet, O. M.; Niinivaara, E.; Zakani, B.; Cranston, E. D. Benchmarking Cellulose Nanocrystals Part II: New Industrially Produced Materials. *Langmuir* **2021**, *37* (28), 8393–8409. https://doi.org/10.1021/acs.langmuir.1c00550.

(14) Masese, F. K.; Njenga, P. K.; Ndaya, D. M.; Kasi, R. M. Recent Advances and Opportunities for Cellulose Nanocrystal-Based Liquid Crystalline Polymer Hybrids and Composite Materials. *Macromolecules* **2023**, *56* (17), 6567–6588. https://doi.org/10.1021/acs.macromol.3c00369.

(15) Kedzior, S. A.; Marway, H. S.; Cranston, E. D. Tailoring Cellulose Nanocrystal and Surfactant Behavior in Miniemulsion Polymerization. *Macromolecules* **2017**, *50* (7), 2645–2655. https://doi.org/10.1021/acs.macromol.7b00516.

(16) Klemm, D.; Kramer, F.; Moritz, S.; Lindström, T.; Ankerfors, M.; Gray, D.; Dorris, A. Nanocelluloses: A New Family of Nature-Based Materials. *Angew. Chem., Int. Ed.* **2011**, *50* (24), 5438–5466. https://doi.org/10.1002/anie.201001273.

(17) Miao, C.; Hamad, W. Y. Critical Insights into the Reinforcement Potential of Cellulose Nanocrystals in Polymer Nanocomposites. *Curr. Opin. Solid State Mater. Sci.* **2019**, *23* (4), 100761. https://doi.org/10.1016/j.cossms.2019.06.005.

(18) Ferreira, F. V.; Pinheiro, I. F.; Gouveia, R. F.; Thim, G. P.; Lona, L. M. F. Functionalized Cellulose Nanocrystals as Reinforcement in Biodegradable Polymer Nanocomposites. *Polym. Compos.* **2018**, *39* (S1), E9–E29. https://doi.org/10.1002/pc.24583.

(19) Hokkanen, S.; Bhatnagar, A.; Sillanpää, M. A Review on Modification Methods to Cellulose-Based Adsorbents to Improve Adsorption Capacity. *Water Res* **2016**, *91*, 156–173. https://doi.org/10.1016/j.watres.2016.01.008.

(20) Pakdel, A. S.; Cranston, E. D.; Dubé, M. A. Incorporating Hydrophobic Cellulose Nanocrystals inside Latex Particles via Mini-Emulsion Polymerization. *Macromol. React. Eng.* **2021**, *15* (5), 2100023. https://doi.org/10.1002/mren.202100023.

(21) Pakdel, A. S.; Niinivaara, E.; Cranston, E. D.; Berry, R. M.; Dubé, M. A. Cellulose Nanocrystal (CNC)–Latex Nanocomposites: Effect of CNC Hydrophilicity and Charge on Rheological, Mechanical, and Adhesive Properties. *Macromol. Rapid. Commun.* **2021**, *42* (3), 2000448. https://doi.org/10.1002/marc.202000448.

(22) Abedi, F.; Emadzadeh, D.; Dubé, M. A.; Kruczek, B. Modifying Cellulose Nanocrystal Dispersibility to Address the Permeability/Selectivity Trade-off of Thin-Film Nanocomposite Reverse Osmosis Membranes. *Desalination* **2022**, *538*, 115900. https://doi.org/10.1016/j.desal.2022.115900.

(23) Biswas, A.; Berfield, J. L.; Saha, B. C.; Cheng, H. N. Conversion of Agricultural By-Products to Methyl Cellulose. *Ind Crops Prod* **2013**, *46*, 297–300. https://doi.org/10.1016/j.indcrop.2013.01.039.

(24) Mokhena, T. C.; Sefadi, J. S.; Sadiku, E. R.; John, M. J.; Mochane, M. J.; Mtibe, A. Thermoplastic Processing of PLA/Cellulose Nanomaterials Composites. *Polymers (Basel)* **2018**, *10* (12), 1363. https://doi.org/10.3390/polym10121363.

(25) Arrieta, M. P.; Peltzer, M. A.; López, J.; Peponi, L. PLA-Based Nanocomposites Reinforced with CNC for Food Packaging Applications: From Synthesis to Biodegradation. In *Industrial Applications of Renewable Biomass Products*; Springer International Publishing: Cham, 2017; pp 265–300. https://doi.org/10.1007/978-3-319-61288-1_11.

(26) Jovanović, R.; Dubé, M. A. Emulsion-Based Pressure-Sensitive Adhesives: A Review. *Journal of Macromolecular Science, Part C: Polymer Reviews* **2004**, *44* (1), 1–51. https://doi.org/10.1081/MC-120027933.

(27) Gabriel, V. A.; Dubé, M. A. Toward a Fully Biobased Pressure-Sensitive Adhesive. *Ind. Eng. Chem. Res.* **2023**, *62* (1), 478–488. https://doi.org/10.1021/acs.iecr.2c03756.

(28) Tobing, S. D.; Klein, A. Molecular Parameters and Their Relation to the Adhesive Performance of Emulsion Acrylic Pressure-Sensitive Adhesives. II. Effect of Crosslinking. *J. Appl. Polym. Sci.* **2001**, *79* (14), 2558–2564. https://doi.org/10.1002/1097-4628(20010401)79:14<2558::AID-APP1065>3.0.CO;2-Y.

(29) Fu, S.; Sun, Z.; Huang, P.; Li, Y.; Hu, N. Some Basic Aspects of Polymer Nanocomposites: A Critical Review. *Nano Mater. Sci.* **2019**, *1* (1), 2–30. https://doi.org/10.1016/j.nanoms.2019.02.006.

(30) Gabriel, V. A.; Cranston, E. D.; Dubé, M. A. Pushing the Limits with Cellulose Nanocrystal Loadings in Latex-Based Pressure-Sensitive Adhesive Nanocomposites. *Macromol. React. Eng.* **2020**, *14* (6), 2000027. https://doi.org/10.1002/mren.202000027.

(31) Kubowicz, S.; Booth, A. M. Biodegradability of Plastics: Challenges and Misconceptions. *Environ Sci Technol* **2017**, *51* (21), 12058–12060. https://doi.org/10.1021/acs.est.7b04051.

(32) Sarul, D. S.; Arslan, D.; Vatansever, E.; Kahraman, Y.; Durmus, A.; Salehiyan, R.; Nofar, M. Preparation and Characterization of PLA/PBAT/CNC Blend Nanocomposites. *Colloid Polym Sci* **2021**, *299* (6), 987–998. https://doi.org/10.1007/s00396-021-04822-9.

(33) Eichers, M.; Bajwa, D.; Shojaeiarani, J.; Bajwa, S. Biobased Plasticizer and Cellulose Nanocrystals Improve Mechanical Properties of Polylactic Acid Composites. *Ind Crops Prod* **2022**, *183*, 114981. https://doi.org/10.1016/j.indcrop.2022.114981.

(34) Gois, G. da S.; Santos, A. S. F.; Hernandéz, E. P.; Medeiros, E. S.; Almeida, Y. M. B. Biodegradation of PLA/CNC Composite Modified with Non-Ionic Surfactants. *Polymer Bulletin* **2023**, *80* (10), 11363–11377. https://doi.org/10.1007/s00289-022-04618-z.

(35) Alanalp, M. B.; Ozdemir, B.; Nofar, M.; Durmus, A. Isothermal and Non-Isothermal Cold Crystallization Kinetics of Polylactide/Cellulose Nanocrystal (PLA/CNC) Nanocomposites. *J Therm Anal Calorim* **2022**, *147* (24), 14211–14227. https://doi.org/10.1007/s10973-022-11598-9.

(36) Bagheriasl, D.; Carreau, P. J.; Riedl, B.; Dubois, C.; Hamad, W. Y. Shear Rheology of Polylactide (PLA)–Cellulose Nanocrystal (CNC) Nanocomposites. *Cellulose* **2016**, *23* (3), 1885–1897. https://doi.org/10.1007/s10570-016-0914-1.

(37) Vatansever, E.; Arslan, D.; Nofar, M. Polylactide Cellulose-Based Nanocomposites. *Int. J. Biol. Macromol.* **2019**, *137*, 912–938. https://doi.org/10.1016/j.ijbiomac.2019.06.205.

(38) Mukherjee, T.; Tobin, M. J.; Puskar, L.; Sani, M.-A.; Kao, N.; Gupta, R. K.; Pannirselvam, M.; Quazi, N.; Bhattacharya, S. Chemically Imaging the Interaction of Acetylated Nanocrystalline Cellulose (NCC) with a Polylactic Acid (PLA) Polymer Matrix. *Cellulose* **2017**, *24* (4), 1717–1729. https://doi.org/10.1007/s10570-017-1217-x.

Chapter 2

Background

A background on adhesive theory and characterization, emulsion polymerization and nanocomposites is presented below. Note that a general background on CNCs in polymer nanocomposites is discussed here and that details pertaining to cCNCs and acetylated cCNCs in PSAs are discussed in Chapters 3 and 4. More discussion regarding cCNCs and acetylated cCNCs in PLA is presented in Chapter 5.

2.1 Cellulose nanocrystals (CNCs)

Cellulose, the primary structural component of biomass, is a polysaccharide made up of linear chains of D-glucose units ($C_6H_{11}O_5$) connected through β(1 → 4) glycosidic bonds (Fig. 2.1). CNCs can be extracted by hydrolyzing the amorphous regions in cellulose microfibrils, typically found in biomass sources such as wood pulp, using strong acid catalysts.[1–7] The dimensions of CNCs vary depending on their source, ranging from 5 to 30 nm in diameter and 100 nm to 3 μm in length.[8]

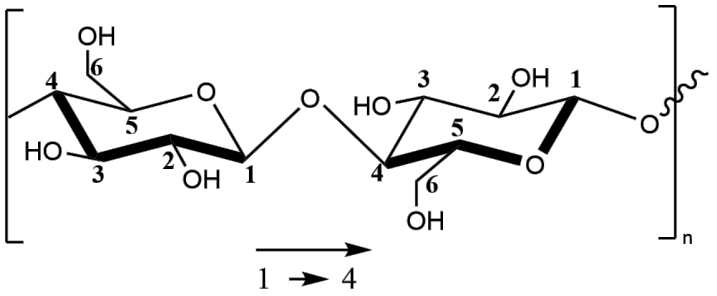

Figure 2.1. Chemical structure of cellulose rings and β 1–4 glucosidic bonds.

The acid used during extraction determines the chemical properties of the CNC surface, thus, using different acids for hydrolysis can yield CNCs with unique surface functional groups.[9] Sulfuric acid introduces anionic sulfate half-ester groups, resulting in sulfated CNCs (sCNCs) that form stable colloidal dispersions in water. In contrast, hydrochloric acid produces CNCs without surface charges, leading to strong aggregation due to hydrogen bonding, which hinders their

dispersion.[10] Anomera Inc. (Montreal, QC), however, employs a more sustainable method of hydrogen peroxide oxidation to isolate CNCs, introducing carboxylate groups to the surface to yield carboxylated CNCs (cCNCs), marketed as DextraCel™.[11]

Anomera Inc. obtains cCNCs through two distinct reactions (Fig 2.2).[11] The carboxyl functional group is present on the CNC surfaces in all of them. However, their locations vary slightly: 1. carboxyl group on the C_6 position of the cellulose chain, which is often produced by oxidizing the primary hydroxy groups; and 2. Carboxylic acid groups are found exclusively at the reducing ends of the CNCs, which can be obtained due to the chemistry of the highly reactive aldehyde functional group. Additional information regarding the reactions is proprietary.[11]

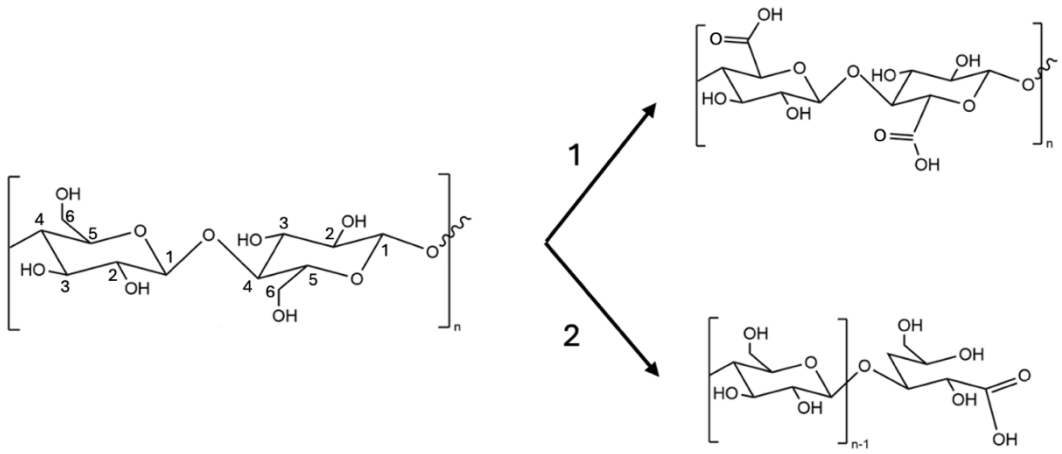

Figure 2.2. Chemical structure of carboxylated CNC.

DextraCel™ or cCNCs are 100–200 nm long and have an average diameter of 5 nm. In comparison, sCNCs are smaller and have a lower surface charge.[9] A study conducted by the Cranston group found significant performance changes due to the different surface groups on cCNCs.[9] In contrast to sCNCs, which break down at 150°C, cCNCs have better colloidal stability in water and higher thermal stability in both their acid and sodium forms, with a thermal degradation onset at 250°C.[2,9] The addition of latex monomers containing carboxyl groups has been shown to impact film formation.[12] This raises the question of whether adding carboxyl

groups as cCNCs will improve an adhesive film's quality and performance, which would be comparable to adding carboxylate moieties to the monomers.

CNCs have garnered considerable interest due to their minimal health hazards (i.e., CNCs are classified as "non-toxic" by Environment Canada),[13] composability,[14,15] biocompatibility,[16–19] exceptional mechanical,[20] optical [21], and rheological qualities[22], affordability, and a low thermal expansion coefficient[23]. With its high aspect ratio and rod-like or whisker-like shape, CNCs are very distinctive; instead of the compact monolayers that are frequently observed with spherical nanoparticles, this property allows them to form networks within a matrix or at interfaces.[2] CNCs, therefore, have a wide range of potential for cutting-edge, environmentally friendly uses in green chemistry.[24] Numerous studies and real-world implementations have shown that these qualities make them a desirable option for various creative applications.[25,26]

2.1 CNC modification methodologies

The difficulty of integrating CNCs, which are hydrophilic, into hydrophobic polymers has prompted the development of a number of CNC modification techniques.[27] The CNC surfaces' hydroxy groups serve as ideal reactive sites, opening the door for chemical alterations that can strengthen the mechanical and adhesive qualities of the resultant polymer composites and improve dispersion in hydrophobic latexes.[28,29] These changes are essential for resolving the fundamental incompatibilities between hydrophobic matrices and CNCs. Various chemical modification techniques are employed to address these issues, emphasizing how these tactics can maximize the performance of CNC-polymer nanocomposites in various applications.[8]

One well-known method for making CNC surfaces hydrophobic so they can be used with more hydrophobic fluids is the esterification of OH groups.[30–32] Acetylation is a traditional CNC esterification method that involves condensing carboxylic acid and hydroxy groups to produce acetyl functional groups ($COCH_3$) on CNC surfaces (Fig. 2.3).[33–35] When CNCs undergo acetylation, the intermolecular hydrogen bonds are disrupted, reducing their hydrophilicity and enhancing their ability to disperse in hydrophobic polymers.[36] This improvement is indicated by a noticeable increase in the water contact angle of CNC nanocomposite films, demonstrating enhanced hydrophobicity.[37,38] Our research team recently developed a straightforward, eco-friendly

method to introduce acetyl groups to CNCs.[35] This process allows for controlled acetylation, enabling adjustment of CNC hydrophilicity and dispersibility in both organic and aqueous solvents.[39] The degree of acetylation can be fine-tuned using acetic anhydride and iodine as a catalyst, which regulates the extent of substitution.[40] The findings demonstrate that, in comparison to unmodified CNCs, acetylated CNCs have noticeably better hydrophobicity and thermal stability.[41] To date, no acetylation or any other modifications have been performed on cCNCs. A major focus of our work is the preparation of acetylated cCNCs for inclusion into nanocomposites using this technique.

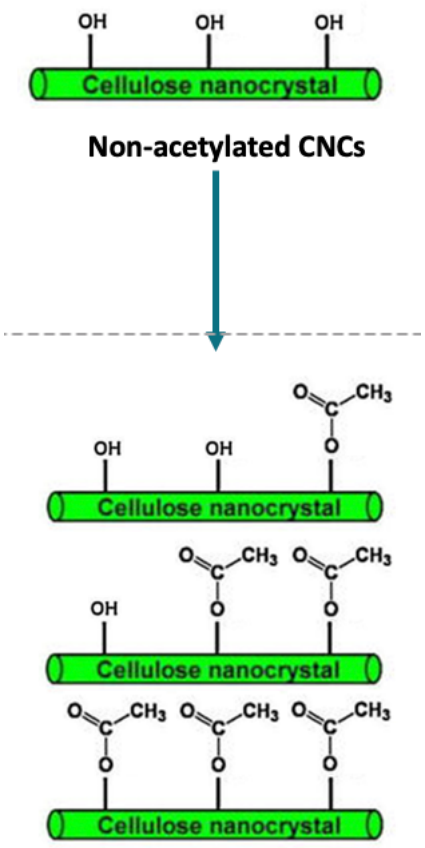

Figure 2.3. Acetylation of CNCs

The performance of polymer nanocomposites is largely determined by the shape, dispersion quality, and functionality of the nanomaterial added. Many nanomaterials that have been studied are spherical. When extracted, CNCs have an anisotropic rod-like shape, and their

high length-to-width ratio (i.e., aspect ratio) is responsible for their remarkable strength effects in polymer nanocomposites.[42,43]

As noted earlier, CNCs are compatible with water-based systems and can be suspended in aqueous media.[44] This makes the dispersion of the CNCs in emulsion polymerization, for example, relatively straightforward. Stable CNC-latex dispersions were first reported using miniemulsion polymerization, where CNCs improved the storage modulus of nanocomposite films in the rubbery state.[45,46] A recent study showed significant improvement in polymeric films cast from styrene-butyl acrylate latex formulations with CNCs.[47] Our research group has pioneered the use of sulfated CNCs in latex-based adhesive formulations, along with experimental methods describing incorporating CNCs for producing latexes for adhesive applications.[48–50]

2.3 Pressure-sensitive adhesives

PSAs are unique polymeric materials that adhere to surfaces with light contact pressure while maintaining a fluid-like state after adhesion.[51] While cohesion refers to the interactions between molecules of the same substance, adhesion is characterized by the bonding of one material to another and specifies the forces acting across an interface.[52] The distinctive balance between adhesive and cohesive forces is possible due to a polymer's viscoelastic profile; it facilitates PSA flowability and energy dissipation during the bonding process via interfacial and interstitial crosslinking and polymer chain entanglement.[53,54] Key performance metrics for PSAs include tack, peel strength (adhesion), and shear adhesion (cohesion) (Figure 2.4). This combination of properties makes them highly versatile, catering to the needs of industries such as automotive, packaging, construction, electronics, healthcare, and consumer products. [55,56]

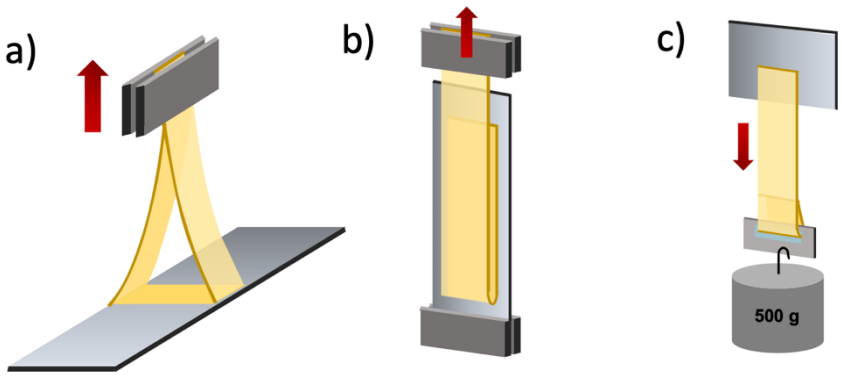

Figure 2.4. PSA property tests: (a) tack, (b) peel strength, and (c) shear adhesion.

Tack represents the separation energy after brief contact under light pressure, indicating the force required to detach the PSA immediately after it adheres to a surface (Figure 2.4a). Peel adhesion measures the PSA's ability to resist removal by peeling, determined by the force needed to peel it from a substrate after applying standard pressure during the bonding step (Figure 2.4b). Shear adhesion demonstrates the material's ability to withstand constant shear forces, reflecting its cohesive resistance to flow or creep under an applied load during bonding (Figure 2.4c).[53,54,57–59] Tack and peel tests involve both bonding and debonding steps, where the loading rate is critical, while shear adhesion is evaluated under static conditions.[60]

Following World War II, acrylic-based PSAs emerged as the second most widely used type, surpassed only by rubber-based PSAs, due to their balance of processability, properties and compatibility with additives.[52,61] Polymers with a low glass-transition temperature (T_g), preferably ranging from -70 to -20°C, are widely utilized in PSA formulations because they can maintain their fluidity and tackiness at room temperature.[56] In general, the required T_g for PSAs is achieved by combining “soft” monomers (i.e., low polymer T_g) with “hard” monomers (i.e., high polymer T_g). Several factors significantly influence the properties of latex-based adhesives. Particle size plays a crucial role, with smaller particles providing larger surface areas and tighter packing during film formation, resulting in smoother surfaces that enhance substrate wetting, tack, and peel strength.[51,62] Molecular weight also impacts performance, as higher molecular weights promote fibril formation during debonding, improving tack and peel strength until a

critical maximum is reached.[63] Beyond this point, increased entanglement density enhances shear adhesion but reduces tack.[64] Finally, gel content, determined by molecular weight and crosslinking density, affects the balance between cohesive and adhesive strength; higher gel content typically increases shear adhesion while lowering tack and peel strength.[25,51,65]

The push to reduce volatile organic compounds (VOCs) shifted the focus of acrylic PSA production methods toward water-based alternatives.[66] Unlike solvent-based PSAs, which benefit from a continuous gel network, water-based PSAs rely on polymer diffusion and chain entanglements during film formation.[56] Emulsion polymerization is a sustainable and environmentally friendly method for producing water-based PSAs. Originally developed during World War II to address natural rubber shortages, this heterogeneous polymerization process involves water, monomers, surfactants, initiators, and optional modifiers.[52,61] Latex, the resulting stable polymer particle dispersion, relies on surfactants (e.g., sodium dodecyl sulfate, Dowfax 2A1™) for particle stability and nucleation.[67] Water, which typically constitutes 50–60% of the reaction volume, reduces viscosity, facilitates heat dissipation, and aids monomer and emulsifier transfer. Emulsion polymerization commonly uses anionic surfactants for cost-effective particle stabilization and water-soluble initiators (e.g., sodium persulfate or NaPS). Additional ingredients, such as chain transfer and crosslinking agents, are used to control molecular weight and tailor polymer properties.

Emulsion polymerization can be conducted in batch, semi-batch, or continuous modes, with the semi-batch process being used in this work.[68] This method involves an initial particle seed stage followed by controlled monomer feeding, enabling better control of reaction rates, latex composition, and particle count. The process occurs in three intervals (Figure 2.5). Interval I begins with the formation of monomer droplets stabilized by surfactant, monomers dissolved in water, and micelles formed above the critical micelle concentration.[69] Polymer particles nucleate when hydrophobic oligomeric radicals enter micelles, driven by micellar nucleation. This interval ends when all micelles are consumed, and particle numbers stabilize. Interval II involves polymerization within the particles, with monomer droplets acting as reservoirs. Monomer diffuses to the particles to maintain equilibrium, resulting in a constant polymerization rate until the droplets are depleted. Interval III completes the reaction by polymerizing the remaining

monomer in the particles and water phase. This simplified mechanism highlights key stages and omits less relevant variations.

Recent innovations have improved emulsion-based PSA performance, offering benefits like process flexibility, lower costs, and sustainability.[12,49,50,70] However, challenges remain, particularly in balancing tack, peel strength, shear adhesion, water resistance, and surface wettability.[56] Nanoparticles are frequently used to boost shear adhesion but often compromise tack and peel strength in PSA nanocomposites.[71–73] The uOttawa Polymer Reaction Engineering group has extensive experience with renewably sourced nanoparticles, and in particular, CNCs,[74–76] for PSA property improvement. As noted, CNCs have garnered significant attention thanks to their biodegradability, biocompatibility, and nontoxicity.[8] In 2017, the groundbreaking work of Dastjerdi et al. revealed *simultaneous* significant improvement of all three PSA characteristics by adding CNCs.[77]

In a comparative study of in-situ and blending techniques for synthesizing latex-based PSAs, Dastjerdi et al. observed that higher CNC loadings increased gel content and elasticity in PSAs due to restricted chain mobility, enhancing shear adhesion in both methods.[49] However, PSAs produced using the in-situ method demonstrated superior performance across all adhesive properties, attributed to better nanomaterial dispersion and enhanced interactions with the polymer matrix during synthesis. Additionally, incorporating pre-dispersed nanomaterials during polymerization eliminated the need for post-synthesis blending, reducing production time and costs.[50,78]

Many attempts have been made so far to resolve the long-standing puzzle of CNC aggregation in dispersions.[79–81] For example, Ouzas et al. pointed out that hydrophobic monomers such as ethyl hexyl acrylate (EHA) resist the CNCs, causing the CNCs to aggregate and lose their efficacy in latex dispersions.[50] Additionally, the solids content threshold needed for film formation can be lowered by CNCs.[50] Gabriel et al. achieved stable latex with 40% solids using 4 phm CNC by optimizing water utilization during seed and feed stages.[82] However, achieving high solids content in emulsion polymerizations introduces challenges in CNC dispersion. To mitigate these issues with cCNCs, Gabriel et al. developed a modified semi-batch polymerization method using dual surfactants and initiators, maintaining low ionic strength to stabilize the latex.[83]

Regarding adhesive performance (tack, peel strength, and shear adhesion), nanocomposite films with CNCs perform better than their base case formulations.[74] Larger viscosity is correlated with larger CNC loadings, suggesting that the CNCs are present outside of the latex particles, as demonstrated by AFM.[84] Ultrasonication, a common method for breaking CNC aggregates, has been shown by the Dubé group to have minimal impact on adhesive improvements compared to non-sonicated CNCs. Non-ultrasonicated CNCs maintain cCNC-cCNC interactions, acting like nanofibers and enhancing mechanical properties.[84] Eliminating the ultrasonication step could reduce costs, energy consumption, and industrial resistance to this technique. Regardless of the CNC type, addition method, or ultrasonication, incorporating CNCs consistently improves PSA properties, including tack, peel strength, and shear adhesion, highlighting their versatility in acrylic polymer formulations.[84]

Although using CNCs' hydrophilic nature for emulsion polymerization and simultaneously improving three PSA characteristics offer intriguing benefits, their hydrophilicity makes it challenging to disperse them into nonpolar hydrophobic polymeric matrices.[7,85,86] To increase the compatibility of hydrophobic latexes with hydrophilic CNCs, Pakdel et al.[75] incorporated hydrophobic (with a water contact angle of 70.4°) and partially hydrophobic sCNCs (with a water contact angle of 50.8°). They demonstrated that incorporating partially hydrophilic CNCs in conventional emulsion polymerizations improved PSA performance compared to unmodified, hydrophilic CNCs.[76] Nevertheless, all three of the PSA's primary performance characteristics deteriorated when very hydrophobic CNCs were used inside polymer particles during a mini-emulsion polymerization.[75] However, for proprietary reasons, the exact nature and properties of the hydrophobic and partially hydrophobic CNCs in that study were not provided.[75,76]

2.4 PLA

One of the most promising bio-sourced polymers with applications in packaging, textiles, drug delivery, and biomedical equipment, polylactic acid (PLA), has attracted significant attention due to its biodegradability, biocompatibility, and UV stability.[87,88] Depending on the stereoisomer concentration of L- and D-type stereoisomers as well as other process parameters, PLA can be manufactured in either amorphous or semi-crystalline forms.[89] Despite its advantages, the slow

crystallization rate of PLA leads to extended processing times, reduced mechanical properties, and poor thermal stability during processing, limiting its potential for broader applications.[90,91] Many attempts have been made to address these challenges, such as copolymerization[92], blending with other polymers[93], and incorporating nanofillers [89]. Nanofillers, such as carbon nanotubes, layered silicates, hydroxyapatite, layered titanate, and aluminum hydroxide, can enhance polymer properties even at low concentrations due to their unique "nano-effect."[94] However, a key drawback of these nanofillers is that most of them are not biodegradable or biocompatible.[89] CNCs with exceptional mechanical properties, low thermal expansion, high aspect ratio, and unique rheological behaviour have drawn more attention as ideal nanoparticles for improving PLA crystallization rates as an environmentally friendly nucleating agent.[95,96] All the studies so far were on adding sCNCs to PLA, enhancing its cold crystallization by promoting faster and more uniform crystal formation, as the sCNCs act as nucleating agents.[9,93,95,97–99] This results in a reduction in cold crystallization temperature due to the sCNCs weakening the intermolecular interactions between PLA chains in the rubbery state.[100] The incorporation of sCNCs resulted in reduced thermal stability, with higher sCNC content causing lower degradation onset temperatures.[101] In contrast, cCNCs demonstrate significantly higher thermal stability, with degradation onset temperatures around 250°C, compared to the lower 150°C onset for sCNCs.[102] This difference highlights the potential of cCNCs to enhance the thermal stability of PLA nanocomposites.

A key challenge with nanocomposite materials is achieving a uniform dispersion within the matrix.[97] Numerous studies have shown that dispersing CNCs in PLA through solution casting is more effective than direct melt mixing, as it facilitates the wetting of the hydrophilic CNCs and prevents irreversible agglomeration after drying.[93,103–105] The impact of solvents on crystallization behaviour and kinetics has been explored, finding that dimethyl sulfoxide (DMSO) resulted in a lower onset temperature for cold crystallization and a broader exothermic peak compared to dimethylformamide (DMF)-based samples.[100] However, many polar solvents used in similar research, such as DMF[100,104], chloroform[89], and dichloromethane[106], are hazardous. To address this, PLA processed with ethyl lactate, a bio-based, benign, and economically viable solvent, is

proposed in this work as a suitable alternative. CNC dispersion in ethyl lactate is achieved through a solvent exchange process, maintaining high environmental and safety standards.

CNCs' hydrophilicity, which leaves them vulnerable to quick aggregation in hydrophobic matrices such as PLA, reduces the efficiency of solution casting in achieving uniform CNC dispersions in PLA. The hydroxy groups on the CNC surfaces interact to produce this hydrophilicity, which makes it more difficult for them to disperse within the hydrophobic PLA matrix, diminishing the potential of CNCs as reinforcing agents. [107] Several surface modification approaches have been investigated to improve their usefulness as PLA nanofillers and lessen their hydrophilicity.[38,108] Acetylated sCNCs have demonstrated encouraging outcomes, boosting capacity and crystallization rates without sacrificing thermal stability. [108]

2.5 Knowledge gaps to fill

This work aims to apply the principles of Green Chemistry to design more sustainable polymers, focusing specifically on PSAs and PLA. While replacing petroleum-based components with bio-based alternatives presents technical challenges, we will leverage various engineering techniques to address colloidal instabilities and performance changes that may arise from these substitutions. Despite the focus of most studies on sCNCs, cCNCs have gained attention due to the sustainable processes used to produce them and their superior colloidal stability.

This study addresses that while adding cCNCs can improve the mechanical properties of polymeric materials, the hydrophilic nature of cCNCs complicates their dispersion in hydrophobic matrices. The environmentally benign acetylation process used in this study[35] allows us to generate a spectrum of cCNCs with adjustable hydrophilic/hydrophobic properties through acetylation, aiming to better understand how these surface characteristics influence their incorporation into polymers and improve their performance. Acetylating cCNCs further enhances their thermal stability by substituting hydroxy groups with acetyl groups, which is crucial for blending CNCs with PLA in high-temperature processes such as extrusion.[38] This research could open new avenues for understanding the effects of CNC surface properties on their role in the final properties of two commercially important hydrophobic systems, with potential applications extending to a broader range of polymer systems.

2.6 References

(1) Hamad, W. Y.; Hu, T. Q. Structure-Process-Yield Interrelations in Nanocrystalline Cellulose Extraction. *Can J Chem Eng* **2010**, n/a-n/a. https://doi.org/10.1002/cjce.20298.

(2) Moon, R. J.; Martini, A.; Nairn, J.; Simonsen, J.; Youngblood, J. Cellulose Nanomaterials Review: Structure, Properties and Nanocomposites. *Chem Soc Rev* **2011**, *40* (7), 3941. https://doi.org/10.1039/c0cs00108b.

(3) Trache, D.; Hussin, M. H.; Haafiz, M. K. M.; Thakur, V. K. Recent Progress in Cellulose Nanocrystals: Sources and Production. *Nanoscale* **2017**, *9* (5), 1763–1786. https://doi.org/10.1039/C6NR09494E.

(4) Revol, J.-F.; Godbout, L.; Dong, X.-M.; Gray, D. G.; Chanzy, H.; Maret, G. Chiral Nematic Suspensions of Cellulose Crystallites; Phase Separation and Magnetic Field Orientation. *Liq Cryst* **1994**, *16* (1), 127–134. https://doi.org/10.1080/02678299408036525.

(5) Pereira, A. L. S.; Nascimento, D. M. do; Souza Filho, M. de sá M.; Morais, J. P. S.; Vasconcelos, N. F.; Feitosa, J. P. A.; Brígida, A. I. S.; Rosa, M. de F. Improvement of Polyvinyl Alcohol Properties by Adding Nanocrystalline Cellulose Isolated from Banana Pseudostems. *Carbohydr Polym* **2014**, *112*, 165–172. https://doi.org/10.1016/j.carbpol.2014.05.090.

(6) Favier, V.; Canova, G. R.; Cavaillé, J. Y.; Chanzy, H.; Dufresne, A.; Gauthier, C. Nanocomposite Materials from Latex and Cellulose Whiskers. *Polym Adv Technol* **1995**, *6* (5), 351–355. https://doi.org/10.1002/pat.1995.220060514.

(7) Miao, C.; Hamad, W. Y. Critical Insights into the Reinforcement Potential of Cellulose Nanocrystals in Polymer Nanocomposites. *Curr. Opin. Solid State Mater. Sci.* **2019**, *23* (4), 100761. https://doi.org/10.1016/j.cossms.2019.06.005.

(8) Dufresne, A. *Nanocellulose*; Huang, J., Dufresne, A., Lin, N., Eds.; Wiley, 2019. https://doi.org/10.1002/9783527807437.

(9) Delepierre, G.; Vanderfleet, O. M.; Niinivaara, E.; Zakani, B.; Cranston, E. D. Benchmarking Cellulose Nanocrystals Part II: New Industrially Produced Materials. *Langmuir* **2021**, *37* (28), 8393–8409. https://doi.org/10.1021/acs.langmuir.1c00550.

(10) Van den Berg, O.; Capadona, J. R.; Weder, C. Preparation of Homogeneous Dispersions of Tunicate Cellulose Whiskers in Organic Solvents. *Biomacromolecules* **2007**, *8* (4), 1353–1357. https://doi.org/10.1021/bm061104q.

(11) Lam, E.; Hemraz, U. D. Preparation and Surface Functionalization of Carboxylated Cellulose Nanocrystals. *Nanomaterials* **2021**, *11* (7), 1641. https://doi.org/10.3390/nano11071641.

(12) Khanjani, J.; Zohuri, G. H.; Gholami, M.; Shojaei, B.; Dalir, R. Emulsion Semi-Batch Terpolymerization Process Using Hybrid Emulsifiers for Synthesizing New Emulsion Pressure Sensitive Adhesives (EPSAs). *J Adhes* **2014**, *90* (2), 174–194. https://doi.org/10.1080/00218464.2013.772052.

(13) Roman, M. Toxicity of Cellulose Nanocrystals: A Review. *Industrial Biotechnology* **2015**, *11* (1), 25–33. https://doi.org/10.1089/ind.2014.0024.

(14) de France, K. J.; Badv, M.; Dorogin, J.; Siebers, E.; Panchal, V.; Babi, M.; Moran-Mirabal, J.; Lawlor, M.; Cranston, E. D.; Hoare, T. Tissue Response and Biodistribution of Injectable Cellulose Nanocrystal Composite Hydrogels. *ACS Biomater Sci Eng* **2019**, *5* (5), 2235–2246. https://doi.org/10.1021/acsbiomaterials.9b00522.

(15) Jia, B.; Li, Y.; Yang, B.; Xiao, D.; Zhang, S.; Rajulu, A. V.; Kondo, T.; Zhang, L.; Zhou, J. Effect of Microcrystal Cellulose and Cellulose Whisker on Biocompatibility of Cellulose-Based Electrospun Scaffolds. *Cellulose* **2013**, *20* (4), 1911–1923. https://doi.org/10.1007/s10570-013-9952-0.

(16) Seabra, A. B.; Bernardes, J. S.; Fávaro, W. J.; Paula, A. J.; Durán, N. Cellulose Nanocrystals as Carriers in Medicine and Their Toxicities: A Review. *Carbohydr Polym* **2018**, *181*, 514–527. https://doi.org/10.1016/j.carbpol.2017.12.014.

(17) Carreño, N. L. V; Barbosa, A. M.; Noremberg, B. S.; Salas, M. M. S.; Fernandes, S. C. M.; Labidi, J. *Advances in Nanostructured Cellulose-Based Biomaterials*; Kacprzyk J, Ed.; SpringerBriefs in Applied Sciences and Technology; Cham, 2017. https://doi.org/10.1007/978-3-319-58158-3.

(18) Giese, M.; Blusch, L. K.; Khan, M. K.; MacLachlan, M. J. Functional Materials from Cellulose-Derived Liquid-Crystal Templates. *Angewandte Chemie International Edition* **2015**, *54* (10), 2888–2910. https://doi.org/10.1002/anie.201407141.

(19) Voisin, H.; Bergström, L.; Liu, P.; Mathew, A. Nanocellulose-Based Materials for Water Purification. *Nanomaterials* **2017**, *7* (3), 57. https://doi.org/10.3390/nano7030057.

(20) Lahiji, R. R.; Xu, X.; Reifenberger, R.; Raman, A.; Rudie, A.; Moon, R. J. Atomic Force Microscopy Characterization of Cellulose Nanocrystals. *Langmuir* **2010**, *26* (6), 4480–4488. https://doi.org/10.1021/la903111j.

(21) Lagerwall, J. P. F.; Schütz, C.; Salajkova, M.; Noh, J.; Hyun Park, J.; Scalia, G.; Bergström, L. Cellulose Nanocrystal-Based Materials: From Liquid Crystal Self-Assembly and Glass Formation to Multifunctional Thin Films. *NPG Asia Mater* **2014**, *6* (1), e80–e80. https://doi.org/10.1038/am.2013.69.

(22) Buffa, J. M.; Casado, U.; Mucci, V.; Aranguren, M. I. Cellulose Nanocrystals in Aqueous Suspensions: Rheology of Lyotropic Chiral Liquid Crystals. *Cellulose* **2019**, *26* (4), 2317–2332. https://doi.org/10.1007/s10570-019-02278-3.

(23) Sheltami RM, Kargarzadeh H, Abdullah I, A. I. Thermal Properties of Cellulose Nanocomposite. In *Handbook of nanocellulose and cellulose nanocomposites*; Wiley, 2017; pp 523–552.

(24) Lin, N.; Huang, J.; Dufresne, A. Preparation, Properties and Applications of Polysaccharide Nanocrystals in Advanced Functional Nanomaterials: A Review. *Nanoscale* **2012**, *4* (11), 3274. https://doi.org/10.1039/c2nr30260h.

(25) Qie, L.; Dubé, M. A. Manipulation of Chain Transfer Agent and Cross-Linker Concentration to Modify Latex Micro-Structure for Pressure-Sensitive Adhesives. *Eur Polym J* **2010**, *46* (6), 1225–1236. https://doi.org/10.1016/j.eurpolymj.2010.02.014.

(26) Qie, L.; Dubé, M. A. Manipulating Latex Polymer Microstructure Using Chain Transfer Agent and Cross-Linker to Modify PSA Performance and Viscoelasticit **y**. *Macromol React Eng* **2011**, *5* (2), 117–128. https://doi.org/10.1002/mren.201000046.

(27) Rose, S.; Prevoteau, A.; Elzière, P.; Hourdet, D.; Marcellan, A.; Leibler, L. Nanoparticle Solutions as Adhesives for Gels and Biological Tissues. *Nature* **2014**, *505* (7483), 382–385. https://doi.org/10.1038/nature12806.

(28) Ávila Ramírez, J. A.; Fortunati, E.; Kenny, J. M.; Torre, L.; Foresti, M. L. Simple Citric Acid-Catalyzed Surface Esterification of Cellulose Nanocrystals. *Carbohydr Polym* **2017**, *157*, 1358–1364. https://doi.org/10.1016/j.carbpol.2016.11.008.

(29) Kale, R. D.; Gorade, V. G.; Madye, N.; Chaudhary, B.; Bangde, P. S.; Dandekar, P. P. Preparation and Characterization of Biocomposite Packaging Film from Poly(Lactic Acid) and Acylated Microcrystalline Cellulose Using Rice Bran Oil. *Int J Biol Macromol* **2018**, *118*, 1090–1102. https://doi.org/10.1016/j.ijbiomac.2018.06.076.

(30) Shojaeiarani, J.; Bajwa, D. Functionalized Cellulose Nanocrystals for Improving the Mechanical Properties of Poly(Lactic Acid). In *12*; Am. Soc. Mech. Eng., 2018. https://doi.org/10.1115/IMECE2018-87691.

(31) Robles, E.; Urruzola, I.; Labidi, J.; Serrano, L. Surface-Modified Nano-Cellulose as Reinforcement in Poly(Lactic Acid) to Conform New Composites. *Ind Crops Prod* **2015**, *71*, 44–53. https://doi.org/10.1016/j.indcrop.2015.03.075.

(32) Zhou, L.; Ke, K.; Yang, M.-B.; Yang, W. Recent Progress on Chemical Modification of Cellulose for High Mechanical-Performance Poly(Lactic Acid)/Cellulose Composite: A Review. *Composites Communications* **2021**, *23*, 100548. https://doi.org/10.1016/j.coco.2020.100548.

(33) Biswas, A.; Shogren, R. L.; Willett, J. L. Solvent-Free Process to Esterify Polysaccharides. *Biomacromolecules* **2005**, *6* (4), 1843–1845. https://doi.org/10.1021/bm0501757.

(34) Abedi, F.; Dubé, M. A.; Emadzadeh, D.; Kruczek, B. Improving Nanofiltration Performance Using Modified Cellulose Nanocrystal-Based TFN Membranes. *J Memb Sci* **2023**, *670*, 121369. https://doi.org/10.1016/j.memsci.2023.121369.

(35) Abedi, F.; Emadzadeh, D.; Dubé, M. A.; Kruczek, B. Modifying Cellulose Nanocrystal Dispersibility to Address the Permeability/Selectivity Trade-off of Thin-Film Nanocomposite Reverse Osmosis Membranes. *Desalination* **2022**, *538*. https://doi.org/10.1016/j.desal.2022.115900.

(36) Abraham, E.; Kam, D.; Nevo, Y.; Slattegard, R.; Rivkin, A.; Lapidot, S.; Shoseyov, O. Highly Modified Cellulose Nanocrystals and Formation of Epoxy-Nanocrystalline Cellulose (CNC)

Nanocomposites. *ACS Appl Mater Interfaces* **2016**, *8* (41), 28086–28095. https://doi.org/10.1021/acsami.6b09852.

(37) Long, W.; Ouyang, H.; Hu, X.; Liu, M.; Zhang, X.; Feng, Y.; Wei, Y. State-of-Art Review on Preparation, Surface Functionalization and Biomedical Applications of Cellulose Nanocrystals-Based Materials. *Int. J. Biol. Macromol.* **2021**, *186*, 591–615. https://doi.org/10.1016/j.ijbiomac.2021.07.066.

(38) Lin, N.; Huang, J.; Chang, P. R.; Feng, J.; Yu, J. Surface Acetylation of Cellulose Nanocrystal and Its Reinforcing Function in Poly(Lactic Acid). *Carbohydr Polym* **2011**, *83* (4), 1834–1842. https://doi.org/10.1016/j.carbpol.2010.10.047.

(39) Trinh, B. M.; Mekonnen, T. Hydrophobic Esterification of Cellulose Nanocrystals for Epoxy Reinforcement. *Polymer (Guildf)* **2018**, *155*, 64–74. https://doi.org/10.1016/j.polymer.2018.08.076.

(40) Doan Van Hong, T.; Tran Thao, N.; Do Thi Kieu, T.; Nguyen, C.-N.; Pham Van, T.; Van-Pham, D.-T. Effects of Reaction Conditions on the Degree of Substitution in Acetylated Nanocellulose. *Vietnam Journal of Catalysis and Adsorption* **2020**, *9* (4), 22–28. https://doi.org/10.51316/jca.2020.065.

(41) Leszczyńska, A.; Radzik, P.; Szefer, E.; Mičušík, M.; Omastová, M.; Pielichowski, K. Surface Modification of Cellulose Nanocrystals with Succinic Anhydride. *Polymers (Basel)* **2019**, *11* (5), 866. https://doi.org/10.3390/polym11050866.

(42) Kajtna, J.; Krajnc, M.; Golob, J. The Role of Components in Waterbased Microsphere Acrylic PSA Adhesive Properties. *Macromol Symp* **2006**, *243*, 132–146. https://doi.org/10.1002/masy.200651114.

(43) Rana, P. K.; Swain, S. K.; Sahoo, P. K. Synthesis, Characterization, and Properties of Intercalated Poly(2-Ethyl Hexylacrylate)/Silicate Nanocomposites: XRD, TEM, IR, TGA, Superabsorbency, Pressure-Sensitive Adhesion, and Biodegradation. *J Appl Polym Sci* **2004**, *93* (3), 1007–1011. https://doi.org/10.1002/app.20568.

(44) Kedzior, S. A.; Gabriel, V. A.; Dubé, M. A.; Cranston, E. D. Nanocellulose in Emulsions and Heterogeneous Water-Based Polymer Systems: A Review. *Advanced Materials*. Wiley-VCH Verlag 2020. https://doi.org/10.1002/adma.202002404.

(45) Mabrouk, A. ben; Kaddami, H.; Magnin, A.; Belgacem, M. N.; Dufrensne, A.; Boufi, S. Preparation of Nanocomposite Dispersions Based on Cellulose Whiskers and Acrylic Copolymer by Miniemulsion Polymerization: Effect of the Silane Content Ayman. *Polym Eng Sci* **2011**. https://doi.org/10.1002/pen.21778.

(46) Elmabrouk, A. ben; Wim, T.; Dufrensne, A.; Boufi, S. Preparation of Poly(Styrene-Co-Hexylacrylate)/Cellulose Whiskers Nanocomposites via Miniemulsion Polymerization. *Polymers and Polymer Science* **2009**, No. 7, 449–456. https://doi.org/10.1002/app.30886.

(47) Bettaieb, F.; Khiari, R.; Dufresne, A.; Mhenni, M. F.; Belgacem, M. N. Mechanical and Thermal Properties of Posidonia Oceanica Cellulose Nanocrystal Reinforced Polymer. *Carbohydr Polym* **2015**, *123*, 99–104. https://doi.org/10.1016/j.carbpol.2015.01.026.

(48) Kedzior, S. A.; Kiriakou, M.; Niinivaara, E.; Dubé, M. A.; Fraschini, C.; Berry, R. M.; Cranston, E. D. Incorporating Cellulose Nanocrystals into the Core of Polymer Latex Particles via Polymer Grafting. *ACS Macro Lett* **2018**, *7* (8), 990–996. https://doi.org/10.1021/acsmacrolett.8b00334.

(49) Dastjerdi, Z.; Cranston, E. D.; Dubé, M. A. Pressure Sensitive Adhesive Property Modification Using Cellulose Nanocrystals. *Int J Adhes Adhes* **2018**, *81*, 36–42. https://doi.org/10.1016/j.ijadhadh.2017.11.009.

(50) Ouzas, A.; Niinivaara, E.; Cranston, E. D.; Dubé, M. A. In Situ Semibatch Emulsion Polymerization of 2-Ethyl Hexyl Acrylate/ n -Butyl Acrylate/Methyl Methacrylate/Cellulose Nanocrystal Nanocomposites for Adhesive Applications. *Macromol React Eng* **2018**, *12* (3), 1700068. https://doi.org/10.1002/mren.201700068.

(51) Benedek, I. *Pressure-Sensitive Adhesives and Applications*; CRC Press, 2004. https://doi.org/10.1201/9780203021163.

(52) Lin, S. B.; Durfee, L. D.; Ekeland, R. A.; McVie, J.; Schalau, G. K. Recent Advances in Silicone Pressure-Sensitive Adhesives. *J Adhes Sci Technol* **2007**, *21* (7), 605–623. https://doi.org/10.1163/156856107781192274.

(53) Benedek, I. *Pressure-Sensitive Adhesives and Applications*; 2004.

(54) Creton, C. Pressure-Sensitive Adhesives: An Introductory Course. *Materials Research Society* **2003**, 434–439.

(55) Dubé, M. A.; Gabriel, V. A.; Pakdel, A. S.; Zhang, Y. Sustainable Polymer Reaction Engineering: Are We There Yet? *Can J Chem Eng* **2021**, *99* (1), 31–60. https://doi.org/10.1002/cjce.23865.

(56) Jovanović, R.; Dubé, M. A. Emulsion-Based Pressure-Sensitive Adhesives: A Review. *Journal of Macromolecular Science, Part C: Polymer Reviews* **2004**, *44* (1), 1–51. https://doi.org/10.1081/MC-120027933.

(57) ASTM D3654-06 (Reapproved 2011) Standard Test Methods for Shear Adhesion of Pressure-Sensitive Tapes. *America Sociaty for Testing and Materials*. 2006. https://doi.org/10.1520/D3654.

(58) ASTM D3330-04 (Reapproved 2018) Standard Test Method for Peel Adhesion of Pressure-Sensitive Tape. 2004. https://doi.org/10.1520/D3330.

(59) ASTM D6463-06 (Reapproved 2012) Standard Test Method for Time to Failure of Pressure Sensitive Articles Under Sustained Shear Loading. 2012. https://doi.org/10.1520/D6463.

(60) *Pressure Sensitive Tape Council. Test Methods for Pressure Sensitive Adhesive Tapes.*

(61) Czech, Z. Synthesis and Cross-Linking of Acrylic PSA Systems. *J Adhes Sci Technol* **2007**, *21* (7), 625–635. https://doi.org/10.1163/156856107781192337.

(62) Roberge, S.; Dubé, M. A. The Effect of Particle Size and Composition on the Performance of Styrene/Butyl Acrylate Miniemulsion-Based PSAs. *Polymer (Guildf)* **2006**, *47* (3), 799–807. https://doi.org/10.1016/j.polymer.2005.12.024.

(63) Edward Petrie. *Acrylic Adhesives: Leader Among Waterborne PSAs*. https://foreverest.cn/news-list/acrylic-adhesives-leader-among-waterborne-psas.

(64) Maguire, R. A. V. and J. F. Polymer Nanocomposites with Prescribed Morphology: Going beyond Nanoparticle-Filled Polymers. *Chemistry of Materials* **2007**, *19* (11), 2736–2751. https://doi.org/doi.org/10.1021/cm062693%2B.

(65) Tobing, S. D.; Klein, A. Molecular Parameters and Their Relation to the Adhesive Performance of Acrylic Pressure-Sensitive Adhesives. *J Appl Polym Sci* **2001**, *79* (12), 2230–2244. https://doi.org/10.1002/1097-4628(20010321)79:12<2230::AID-APP1030>3.0.CO;2-2.

(66) Czech, Z. , and R. Milker. Development Trends in Pressure-Sensitive Adhesive Systems. *Materials Science* **2005**, 0137–1339.

(67) Lovell, P. A.; Schork, F. J. Fundamentals of Emulsion Polymerization. *Biomacromolecules* **2020**, *21* (11), 4396–4441. https://doi.org/10.1021/acs.biomac.0c00769.

(68) Qiu, J.; Charleux, B.; Matyjaszewski, K. Controlled/Living Radical Polymerization in Aqueous Media: Homogeneous and Heterogeneous Systems. *Progress in Polymer Science (Oxford)*. 2001. https://doi.org/10.1016/S0079-6700(01)00033-8.

(69) Chern, C. S. Emulsion Polymerization Mechanisms and Kinetics. *Prog Polym Sci* **2006**, *31* (5), 443–486. https://doi.org/10.1016/j.progpolymsci.2006.02.001.

(70) Ahmadi-Dehnoei, A.; Ghasemirad, S. Designing of Desired Nanocomposite Pressure-Sensitive Adhesives through Tailoring the Structural Characteristics of Polysilsesquioxane-Acrylic Core-Shell Nanoparticles. *Int J Adhes Adhes* **2021**, *111*, 102973. https://doi.org/10.1016/j.ijadhadh.2021.102973.

(71) Wang, T.; Lei, C.-H.; Dalton, A. B.; Creton, C.; Lin, Y.; Fernando, K. A. S.; Sun, Y.-P.; Manea, M.; Asua, J. M.; Keddie, J. L. Waterborne, Nanocomposite Pressure-Sensitive Adhesives with High Tack Energy, Optical Transparency, and Electrical Conductivity. *Advanced Materials* **2006**, *18* (20), 2730–2734. https://doi.org/10.1002/adma.200601335.

(72) Khan, U.; May, P.; Porwal, H.; Nawaz, K.; Coleman, J. N. Improved Adhesive Strength and Toughness of Polyvinyl Acetate Glue on Addition of Small Quantities of Graphene. *ACS Appl Mater Interfaces* **2013**, *5* (4), 1423–1428. https://doi.org/10.1021/am302864f.

(73) Oh, J.-K.; Park, C.-H.; Lee, S.-W.; Park, J.-W.; Kim, H.-J. Adhesion Performance of PSA–Clay Nano-Composites by the in-Situ Polymerization and Mechanical Blending. *Int J Adhes Adhes* **2013**, *47*, 13–20. https://doi.org/10.1016/j.ijadhadh.2013.09.002.

(74) Niinivaara, E.; Ouzas, A.; Fraschini, C.; Berry, R. M.; Dubé, M. A.; Cranston, E. D. How Latex Film Formation and Adhesion at the Nanoscale Correlate to Performance of Pressure Sensitive Adhesives with Cellulose Nanocrystals. *Philosophical Transactions of the Royal Society A: Mathematical, Physical and Engineering Sciences* **2021**, *379* (2206). https://doi.org/10.1098/rsta.2020.0330.

(75) Pakdel, A. S.; Cranston, E. D.; Dubé, M. A. Incorporating Hydrophobic Cellulose Nanocrystals inside Latex Particles via Mini-Emulsion Polymerization. *Macromol. React. Eng.* **2021**, *15* (5), 2100023. https://doi.org/10.1002/mren.202100023.

(76) Pakdel, A. S.; Niinivaara, E.; Cranston, E. D.; Berry, R. M.; Dubé, M. A. Cellulose Nanocrystal (CNC)–Latex Nanocomposites: Effect of CNC Hydrophilicity and Charge on Rheological, Mechanical, and Adhesive Properties. *Macromol. Rapid. Commun.* **2021**, *42* (3), 2000448. https://doi.org/10.1002/marc.202000448.

(77) Dastjerdi, Z.; Cranston, E. D.; Dubé, M. A. Synthesis of Poly(n -Butyl Acrylate/Methyl Methacrylate)/CNC Latex Nanocomposites via In Situ Emulsion Polymerization. *Macromol React Eng* **2017**, *11* (6), 1700013. https://doi.org/10.1002/mren.201700013.

(78) Ouzas, A.; Niinivaara, E.; Cranston, E. D.; Dubé, M. A. Synthesis of Poly(Isobutyl Acrylate/N-butyl Acrylate/Methyl Methacrylate)/CNC Nanocomposites for Adhesive Applications via in Situ Semi-batch Emulsion Polymerization. *Polym Compos* **2019**, *40* (4), 1365–1377. https://doi.org/10.1002/pc.24869.

(79) Abitbol, T.; Marway, H.; Cranston, E. D. Surface Modification of Cellulose Nanocrystals with Cetyltrimethylammonium Bromide. *Nord Pulp Paper Res J* **2014**, *29* (1), 46–57. https://doi.org/10.3183/npprj-2014-29-01-p046-057.

(80) Brinatti, C.; Huang, J.; Berry, R. M.; Tam, K. C.; Loh, W. Structural and Energetic Studies on the Interaction of Cationic Surfactants and Cellulose Nanocrystals. *Langmuir* **2016**, *32* (3), 689–698. https://doi.org/10.1021/acs.langmuir.5b03893.

(81) Kedzior, S. A.; Marway, H. S.; Cranston, E. D. Tailoring Cellulose Nanocrystal and Surfactant Behavior in Miniemulsion Polymerization. *Macromolecules* **2017**, *50* (7), 2645–2655. https://doi.org/10.1021/acs.macromol.7b00516.

(82) Gabriel, V. A.; Cranston, E. D.; Dubé, M. A. Pushing the Limits with Cellulose Nanocrystal Loadings in Latex-Based Pressure-Sensitive Adhesive Nanocomposites. *Macromol. React. Eng.* **2020**, *14* (6), 2000027. https://doi.org/10.1002/mren.202000027.

(83) Gabriel, V. A.; Champagne, P.; Cunningham, M. F.; Dubé, M. A. In-situ Addition of Carboxylated Cellulose Nanocrystals in Seeded Semi-batch Emulsion Polymerization. *Can. J. Chem. Eng.* **2022**, *100* (4), 767–779. https://doi.org/10.1002/cjce.24299.

(84) Gabriel, V. A.; Tousignant, M. N.; Wilson, S. M. W.; Faure, M. D. M.; Cranston, E. D.; Cunningham, M. F.; Lessard, B. H.; Dubé, M. A. Improving Latex-Based Pressure-Sensitive Adhesive Properties Using Carboxylated Cellulose Nanocrystals. *Macromol. React. Eng.* **2022**, *16* (3), 2100051. https://doi.org/10.1002/mren.202100051.

(85) Klemm, D.; Kramer, F.; Moritz, S.; Lindström, T.; Ankerfors, M.; Gray, D.; Dorris, A. Nanocelluloses: A New Family of Nature-Based Materials. *Angew. Chem., Int. Ed.* **2011**, *50* (24), 5438–5466. https://doi.org/10.1002/anie.201001273.

(86) Ferreira, E. S.; Lanzoni, E. M.; Costa, C. A. R.; Deneke, C.; Bernardes, J. S.; Galembeck, F. Adhesive and Reinforcing Properties of Soluble Cellulose: A Repulpable Adhesive for Wet and Dry Cellulosic Substrates. *ACS Appl. Mater. Interfaces.* **2015**, *7* (33), 18750–18758. https://doi.org/10.1021/acsami.5b05310.

(87) Mokhena, T. C.; Sefadi, J. S.; Sadiku, E. R.; John, M. J.; Mochane, M. J.; Mtibe, A. Thermoplastic Processing of PLA/Cellulose Nanomaterials Composites. *Polymers (Basel)* **2018**, *10* (12), 1363. https://doi.org/10.3390/polym10121363.

(88) Arrieta, M. P.; Peltzer, M. A.; López, J.; Peponi, L. PLA-Based Nanocomposites Reinforced with CNC for Food Packaging Applications: From Synthesis to Biodegradation. In *Industrial Applications of Renewable Biomass Products*; Springer International Publishing: Cham, 2017; pp 265–300. https://doi.org/10.1007/978-3-319-61288-1_11.

(89) Vatansever, E.; Arslan, D.; Nofar, M. Polylactide Cellulose-Based Nanocomposites. *Int. J. Biol. Macromol.* **2019**, *137*, 912–938. https://doi.org/10.1016/j.ijbiomac.2019.06.205.

(90) Nofar, M.; Sacligil, D.; Carreau, P. J.; Kamal, M. R.; Heuzey, M.-C. Poly (Lactic Acid) Blends: Processing, Properties and Applications. *Int J Biol Macromol* **2019**, *125*, 307–360. https://doi.org/10.1016/j.ijbiomac.2018.12.002.

(91) Sema Sarul, D.; Arslan, D.; Vatansever, E.; Kahraman, Y.; Durmus, A.; Salehiyan, R.; Nofar, M. Preparation and Characterization of PLA/PBAT/CNC Blend Nanocomposites. *Colloid Polym Sci* **2021**, *299* (6), 987–998. https://doi.org/10.1007/s00396-021-04822-9/Published.

(92) Muiruri, J. K.; Liu, S.; Teo, W. S.; Kong, J.; He, C. Highly Biodegradable and Tough Polylactic Acid-Cellulose Nanocrystal Composite. *ACS Sustain Chem Eng* **2017**, *5* (5), 3929–3937. https://doi.org/10.1021/acssuschemeng.6b03123.

(93) Mohammadi, M.; Bruel, C.; Heuzey, M. C.; Carreau, P. J. CNC Dispersion in PLA and PBAT Using Two Solvents: Morphological and Rheological Properties. *Cellulose* **2020**, *27* (17), 9877–9892. https://doi.org/10.1007/s10570-020-03460-8.

(94) Paul, D. R.; Robeson, L. M. Polymer Nanotechnology: Nanocomposites. *Polymer (Guildf)* **2008**, *49* (15), 3187–3204. https://doi.org/10.1016/j.polymer.2008.04.017.

(95) Kamal, M. R.; Khoshkava, V. Effect of Cellulose Nanocrystals (CNC) on Rheological and Mechanical Properties and Crystallization Behavior of PLA/CNC Nanocomposites. *Carbohydr Polym* **2015**, *123*, 105–114. https://doi.org/10.1016/j.carbpol.2015.01.012.

(96) Gois, G. da S.; Santos, A. S. F.; Hernandéz, E. P.; Medeiros, E. S.; Almeida, Y. M. B. Biodegradation of PLA/CNC Composite Modified with Non-Ionic Surfactants. *Polymer Bulletin* **2023**, *80* (10), 11363–11377. https://doi.org/10.1007/s00289-022-04618-z.

(97) Vatansever, E.; Arslan, D.; Sarul, D. S.; Nofar, M. The CNC Dispersion Quality in Various PLA Grades. In *AIP Conference Proceedings*; American Institute of Physics Inc., 2023; Vol. 2607. https://doi.org/10.1063/5.0135790.

(98) Spinella, S.; Lo Re, G.; Liu, B.; Dorgan, J.; Habibi, Y.; Leclère, P.; Raquez, J. M.; Dubois, P.; Gross, R. A. Polylactide/Cellulose Nanocrystal Nanocomposites: Efficient Routes for Nanofiber Modification and Effects of Nanofiber Chemistry on PLA Reinforcement. *Polymer (Guildf)* **2015**, *65*, 9–17. https://doi.org/10.1016/j.polymer.2015.02.048.

(99) Trifol, J.; Plackett, D.; Sillard, C.; Hassager, O.; Daugaard, A. E.; Bras, J.; Szabo, P. A Comparison of Partially Acetylated Nanocellulose, Nanocrystalline Cellulose, and Nanoclay as Fillers for High-Performance Polylactide Nanocomposites. *J Appl Polym Sci* **2016**, *133* (14). https://doi.org/10.1002/app.43257.

(100) Alanalp, M. B.; Ozdemir, B.; Nofar, M.; Durmus, A. Isothermal and Non-Isothermal Cold Crystallization Kinetics of Polylactide/Cellulose Nanocrystal (PLA/CNC) Nanocomposites. *J Therm Anal Calorim* **2022**, *147* (24), 14211–14227. https://doi.org/10.1007/s10973-022-11598-9.

(101) Bhiogade, A.; Kannan, M. Studies on Thermal and Degradation Kinetics of Cellulose Micro/Nanoparticle Filled Polylactic Acid (PLA) Based Nanocomposites. *Polymers and Polymer Composites* **2021**, *29* (9), S85–S98. https://doi.org/10.1177/0967391120987170.

(102) Lam, E.; Hemraz, U. D. Preparation and Surface Functionalization of Carboxylated Cellulose Nanocrystals. *Nanomaterials* **2021**, *11* (7), 1641. https://doi.org/10.3390/nano11071641.

(103) Dhar, P.; Tarafder, D.; Kumar, A.; Katiyar, V. Thermally Recyclable Polylactic Acid/Cellulose Nanocrystal Films through Reactive Extrusion Process. *Polymer (Guildf)* **2016**, *87*, 268–282. https://doi.org/10.1016/j.polymer.2016.02.004.

(104) Bagheriasl, D.; Carreau, P. J.; Riedl, B.; Dubois, C.; Hamad, W. Y. Shear Rheology of Polylactide (PLA)–Cellulose Nanocrystal (CNC) Nanocomposites. *Cellulose* **2016**, *23* (3), 1885–1897. https://doi.org/10.1007/s10570-016-0914-1.

(105) Khoshkava, V.; Kamal, M. R. Effect of Surface Energy on Dispersion and Mechanical Properties of Polymer/Nanocrystalline Cellulose Nanocomposites. *Biomacromolecules* **2013**, *14* (9), 3155–3163. https://doi.org/10.1021/bm400784j.

(106) Mukherjee, T.; Tobin, M. J.; Puskar, L.; Sani, M.-A.; Kao, N.; Gupta, R. K.; Pannirselvam, M.; Quazi, N.; Bhattacharya, S. Chemically Imaging the Interaction of Acetylated Nanocrystalline Cellulose (NCC) with a Polylactic Acid (PLA) Polymer Matrix. *Cellulose* **2017**, *24* (4), 1717–1729. https://doi.org/10.1007/s10570-017-1217-x.

(107) Habibi, Y.; Lucia, L. A.; Rojas, O. J. Cellulose Nanocrystals: Chemistry, Self-Assembly, and Applications. *Chem Rev* **2010**, *110* (6), 3479–3500. https://doi.org/10.1021/cr900339w.

(108) Minggang Fang; Luo, C.; Guo, X.; Sun, J.; Chen, M.; Chen, W. The Effect of Cellulose Nanocrystals and Acetylated Nanocellulose on the Crystallization Kinetics and Thermal Stability of Polylactic Acid. *Polymer Science - Series A* **2022**, *64* (6), 802–817. https://doi.org/10.1134/S0965545X22700523.

Chapter 3

The Effect of Cellulose Nanocrystal Reassembly on Latex-Based Pressure-Sensitive Adhesive Performance

Parisa Bayat[a], Kelly M. Meek[a], Maryam Movafagh[a], Emily D. Cranston[b], Michael F. Cunningham[c], Pascale Champagne[d], Timothy Morse[e], Michael V. Kiriakou[e], Sean R. George[f], and Marc A. Dubé[a]

[a]Department of Chemical and Biological Engineering, University of Ottawa, Ottawa, ON, Canada
[b]Department of Wood Science and Department of Chemical and Biological Engineering, University of British Columbia, Vancouver, BC, Canada
[c]Department of Chemical Engineering, Queen's University, Kingston, ON, Canada
[d]Energy Mining & Environment Research Centre, National Research Council, Montreal, QC, Canada
[e]Anomera Inc., Montreal, QC, Canada
[f]BASF Corp., Charlotte, NC, United States

This chapter is a manuscript published in Biomacromolecules (2024; 25,5: 3018-3032)

3.1 Abstract

Different cellulose nanocrystal (CNC) forms (dried vs. never-dried) can lead to different degrees of CNC reassembly, the formation of nanofibril-like structures, in nanocomposite latex-based pressure-sensitive adhesive (PSA) formulations. CNC reassembly is also affected by CNC sonication and loading, as well as the protocol used for CNC addition to the polymerization. In this study, carboxylated CNCs (cCNCs) were incorporated into a seeded, semi-batch, 2-ethyl hexyl acrylate/methyl methacrylate/styrene emulsion polymerization and cast as pressure-sensitive adhesive (PSA) films. The addition of CNCs led to a simultaneous increase in tack, peel strength, and shear adhesion, avoiding the typical trade-off between adhesive and cohesive strength. Increased CNC reassembly resulted from the use of dried, redispersed, and sonicated cCNCs, along with increased cCNC loading and the addition of the cCNCs at the seed stage of the polymerization. The increased degree of CNC reassembly was shown to significantly increase shear adhesion by enhancing the elastic modulus of the PSA films.

Keywords: Carboxylated cellulose nanocrystals, emulsion polymerization, zeta potential, sulfated cellulose nanocrystals, pressure-sensitive adhesives, self-assembly

3.2 Introduction

Pressure-sensitive adhesives (PSAs) offer the potential of permanent tackiness (or stickiness) by firmly bonding to a surface upon the application of light pressure (i.e., the pressure applied with one's finger).[1,2] What gives PSAs this property includes the use of polymers exhibiting natural tack at the application temperature and a certain degree of flowability, i.e., a low glass transition temperature (T_g) and a molecular weight that allow sufficient molecular movement for the polymers to migrate into the surface topography and maximize contact with the surface.[3] This is achieved by combining so-called "soft" monomers (i.e., monomers having a low homopolymer T_g, such as acrylic monomers) with "hard" monomers (i.e., monomers having a high homopolymer T_g, such as many methacrylic monomers). The "soft" monomers impart the tackiness required to adhere to the substrate but often lack sufficient cohesive (internal) strength, thus, the "hard" monomers are added to provide the necessary cohesive strength to the adhesive.[4] Acrylic PSAs are popular in many applications (e.g., self-adhesive tapes, labels, and protective films) because of their processability, cost, properties and compatibility with additives.[5] In recent decades, more sustainable industrial practices have led to the reduction of volatile organic compounds (VOCs), which has ultimately steered the adhesives industry toward the production of latex-based (emulsion-based, water-based) PSAs[6] rather than solvent-based and hot melt PSAs.[7]

PSAs are evaluated based on three key performance properties: tack, peel strength, and shear adhesion.[4] Because latex polymers are produced as individual particles, generally and unlike their solvent-based counterparts, the resulting films do not possess a continuous gel structure. As a result, latex-based PSAs tend to underperform, especially concerning shear adhesion.[4] Many strategies have been used to improve latex-based PSA performance, including the modification of the reaction conditions and the monomer formulation or the use of additives.[8–12] Alternative approaches using nanomaterials have shown positive results, but environmental concerns related to the toxicity of these nanomaterials have been raised.[13–16] Cellulose nanocrystals (CNCs), however, are non-toxic, renewable, and part of a sustainable approach to polymer nanocomposite production as they are often derived from forest products (e.g., wood pulp).[17] CNCs, are the crystalline parts of cellulose microfibrils and are typically isolated from the amorphous sections of the microfibrils using controlled acid-hydrolysis.[18]

The acid used during the extraction of the CNCs from wood pulp can yield CNCs with unique surface functional groups.[19,20] Sulfated CNCs, which are the most frequently used in recent research, are produced using sulfuric acid hydrolysis. As a result, some CNC surface hydroxy groups are substituted by anionic sulfate half-ester groups, ultimately leading to colloidally stable CNC dispersions in water.[21] Anomera Inc. recently developed a more sustainable method to extract CNCs from wood pulp using hydrogen peroxide oxidation. The result is that some hydroxy groups on the CNCs are substituted by carboxylate groups to produce carboxylated CNCs (cCNCs).[18] The cCNCs have a length of ~100 nm and an average diameter of ~5 nm, which is shorter in length than sulfated CNCs (~183 nm).[19,22] In addition, cCNCs possess a lower surface charge density (e.g., 0.16 e/nm^2) than sulfated CNCs (e.g., 0.29-0.49 e/nm^2).[19] The CNC surface groups affect various properties, specifically, their self-assembly behavior.[23] This behavior plays an important role in the creation of nanofibril-like structures.[24]

Several studies have demonstrated the effectiveness of sulfated CNCs in improving latex-based PSA performance.[9,25–27] Surprisingly, adding sulfated CNCs to latex-based PSAs led to the simultaneous improvement of all three performance properties (i.e., tack, peel strength, shear adhesion) without the use of hazardous CTAs and cross-linkers in the formulation. This is counter to typical PSA behavior because factors that positively influence adhesive properties (tack and peel strength) often have a negative influence on cohesion (shear adhesion) and vice-versa.[28,29] In addition, the sulfated CNCs acted as a rheology modifier, leading to latex viscosity increases and improved film formation properties.[8] It was also shown that CNC concentrations ranging from 0.25 to 1 phm (mass parts per hundred parts monomer) led to improved PSA performance via in situ polymerization.[8] Dastjerdi et al. showed that higher sulfated CNC loadings led to higher PSA gel contents and elasticity due to polymer chain mobility limitations, resulting in improved cohesive strength (shear adhesion) using blending and in-situ techniques. A subsequent study showed that the sulfated CNC/latex nanocomposite films outperformed the base case formulations (i.e., without sulfated CNCs) for all adhesive properties (i.e., tack, peel strength, and shear adhesion), and the viscosity increased with sulfated CNC loading, suggesting that sulfated CNCs were not located within the latex particles but rather somewhere near the particle-water interface.[30] It has been demonstrated, using atomic force microscopy (AFM) imaging of dried sulfated CNC-latex films, that during an in-situ latex polymerization, the sulfated CNCs (50-200 nm in length) reassembled to form nanofibril-like structures (typically several microns in length).[24,27] The degree of reassembly was shown to depend on a few factors,

including sulfated CNC loading and surface chemistry. Any adhesive and mechanical property enhancements were like that from the addition of nanofibrils to a polymer matrix but without the stability and mixing challenges presented by, for example, cellulose nanofibrils.[24,27]

It has been shown that the presence of carboxyl groups in latex monomers has the potential to improve latex film formation properties.[11] This raises the question of whether the presence of carboxyl groups in cCNCs would have a similar impact and, ultimately, an impact on PSA performance. In the first study of cCNCs in PSA formulations, Gabriel et al.[31] encountered latex stability problems with the use of cCNCs at 1 phm. To lower the number of interactions of the cCNCs with the other latex components, they successfully preserved a low ionic strength of the latex by using a non-conventional semi-batch emulsion polymerization method. Improved PSA performance was demonstrated; however, the base case formulation was sub-optimal in terms of its applicability as a PSA on its own. Thus, the current work aims to shed light on the potential further enhancements which cCNCs can bring to an industry-standard high-performance PSA formulation.

Furthermore, most studies have used sonication, as an important step in CNC preparation to break up CNC aggregates prior to their addition to the polymer formulation,[8,30,32–34] but recent work has questioned the need for this processing step.[23,24]

This study incorporated cCNCs into a commercially viable PSA formulation using a seeded, semi-batch emulsion polymerization. Aside from the impact of different cCNC forms (dried-redispersed vs. never-dried suspensions) and their quality of dispersion (sonication) on PSA performance, various strategies were applied to seek further improvement in the properties of a typical commercial PSA formulation. This included exploring the effect of cCNC addition protocols, i.e., in the seed versus feed stage, on PSA performance. Moreover, we studied the role of CNC surface chemistry (sulfated CNCs vs. cCNCs) on our commercial PSA performance. This work presents the first deep study on the effect of different cCNC forms, their preparation protocol, and their addition location (seed vs. feed stage) on PSA performance. The PSA formulation consisting of a “soft” monomer: 2-ethyl hexyl acrylate (2-EHA), and “hard” monomers: methyl methacrylate (MMA) and styrene (STY), was devised to mimic a high-performance commercial PSA formulation.

3.3 Experimental

3.3.1 Materials

All chemicals were purchased through Sigma-Aldrich, unless otherwise specified. 2-Ethyl hexyl acrylate (2-EHA), styrene (STY), and methyl methacrylate (MMA) were used as monomers and purified by passing them drop-wise through an inhibitor removal column. Alkyldiphenyloxide disulfonate (commercially named Dowfax 2A1, from Dow Chemical Co.) and poly(ethylene glycol tert-octylphenyl ether) (commercially named Triton X-405) served as the anionic and non-ionic surfactants, respectively. The radical initiator sodium persulfate (NaPS). Sodium bicarbonate was used as a buffer. De-ionized distilled water (DIW) with a resistivity of 18.0 ± 0.2 MΩ cm was used for synthesis and characterization purposes. Finally, cCNCs were supplied by Anomera Inc. in two forms: a "never-dried" form (a 6.6 wt.% suspension in water) and a "dried-redispersed" form (a spray-dried powder, readily dispersible in water). The carboxylate groups on the cCNC surface were in the sodium-salt form. The carboxylate content of the cCNCs was 0.22 and 0.23 mmol.g^{-1} cCNC for dried-redispersed and never-dried cCNCs, respectively. The “apparent” nanoparticle length via dynamic light scattering (DLS) for the “dried-redispersed” cCNCs was 81±0.4 nm. For further investigation, sulfated CNCs (CelluForce Inc., Windsor, QC) were obtained as a spray-dried powder (dimensions: 183±8 nm long and 6±2 nm in cross-section) and had a nominal sulfate half-ester content of 0.25 mmol.g^{-1} CNC.[22]

3.3.2 CNC preparation

Two different cCNC types were used: a "never-dried" form consisting of a 6.6 wt.% suspension in water and a "dried-redispersed" form. Prior to use, both cCNC types were diluted with water allocated to the seed or feed stage, depending on which location the cCNCs were added, and stirred on a magnetic stir plate for 1-3 hours until visibly dispersed. Then, the dispersions were sonicated using a Fisher Scientific 550 sonic dismembrator at 75% amplitude in three 5-minute intervals, with 5-minute rest periods in between. An ice bath was used to maintain a low sample temperature during sonication. Afterwards, the sonicated dispersion was filtered three times using 2.7 µm filter paper (Whatman, Grade 50, 110 mm diameter) to eliminate any metal that may have leached from the sonicator probe tip. In some cases, sonication was omitted to investigate its effect. The same CNC preparation procedure was used for the sulfated CNCs.

3.3.3 PSA synthesis

PSAs were generated using a conventional seeded, semi-batch emulsion polymerization, carried out under a nitrogen blanket in a 1.25 L stainless steel reactor (Mettler Toledo LabMax Automatic Lab Reactor), mixed at 250 rpm and heated to 80°C for the entire reaction. The composition of the ingredients in the PSA formulation is listed in Table 3.1. Surfactants were mixed with DIW at a concentration greater than the critical micelle concentration to form micelles in the aqueous phase. For most of the runs, the cCNC suspensions in water were added to the seed charge. Prior to its addition, the surfactant mixture was added to the cCNC suspension and mixed until visibly homogeneous with a magnetic stir bar (~15 min). The cCNC-surfactant mixture was then poured into the reactor. Reactor mixing (250 rpm) and heating to 80°C was begun. Once the set point temperature was reached, 10% of the total monomer mixture was added to the reactor and allowed to mix for 5 min. The seed polymerization was started by injecting the seed stage initiator solution (NaPS, buffer, and DIW) into the reactor and allowing it to react for 30 min. The total number of particles generated during the polymerization was produced by the end of the seed stage, and the seed monomer was completely consumed. The remaining 90% of the monomer was fed by pump to the reactor over 240 min in the form of a pre-emulsion that was pre-mixed with surfactants and DIW. A parallel feed pump provided an initiator solution containing NaPS and buffer in DIW for a total of 270 min (30 min longer than the pre-emulsion feed). Following the completion of the feed stage, the reaction mixture was stirred and heated for 30 min (as the final cook stage) to ensure that any residual monomer was reacted. Five runs were completed by adding the cCNC suspension at the feed stage rather than the seed stage. In those cases, the cCNC was added to the pre-emulsion mixture. First, the cCNC was dispersed in the DIW allocated to the feed stage. Next the remaining 90% of the monomers and surfactants were added and mixed until visibly homogeneous prior to beginning the feed pump.

Table 3.1. Seeded semi-batch emulsion-based PSA formulation

Component	Seed stage	Feed stage	Total
EHA/MMA/STY:90/8/2 (w/w/w)	20 g	180 g	200 g
CNCs	0-0.7 phm	0-1.5 phm	0-1.5 phm
Dowfax 2A1	0.13 phm	0.53 phm	0.66 phm
Triton X-405	0.07 phm	0.27 phm	0.34 phm
Sodium persulfate (NaPS)	0.08 phm	0.72 phm	0.8 phm
Buffer	0.056 phm	0.504 phm	0.56 phm
Water	195 g	105 g	300 g

*phm; mass parts per hundred parts monomer

3.3.4 Latex characterization

The latex was sampled at 30 min, 1 h, and every hour thereafter to measure the solids content, monomer conversion, pH and particle size. The final latex was analyzed for viscosity. The final latex was cast as a PSA film and tested for adhesive performance (tack, peel strength, and shear adhesion).

A standard gravimetric method was applied to measure the conversion and solids content of the latex; ~0.5 g of latex was weighed in an aluminum dish and dried at ambient temperature under the fume hood until a constant weight was achieved (24 h). The solids content was calculated using:

$$Solids\ content\ (\%) = \frac{W_{dried\ sample}}{W_{latex}} \times 100\% \quad (3.1)$$

Upon taking samples during the reaction, the instantaneous monomer conversion was calculated based on the amount of monomer and other ingredients charged to the reactor as:

$$X_{ins} = \frac{Solids\ content - w_i - w_{surf} - w_{CNC} - w_{buffer}}{w_m} \quad (3.2)$$

where w_i, w_{surf}, $w_{CNC,}$ w_{buffer} and w_m represent the weight fractions of initiator, surfactant, CNC, buffer, and monomer, respectively, which were introduced to the reaction mixture up to that time. The overall monomer conversion was calculated via Equation (3.2) using the total weight fractions of the ingredients added throughout the reaction.

The pH was measured using a Fisher Scientific/Accumet Research AR50 Dual Channel pH meter. A Malvern Zetasizer 2000 was used to measure the particle size and polydispersity index of diluted samples, to a concentration of 0.025 wt.%, with no added salt suspensions at room temperature (25 °C) by DLS. The zeta potential was then calculated assuming Smoluchowski behaviour using measuring the electrophoretic mobility of the latex particles in diluted suspension, to a concentration of 0.25 wt.% with 10 mM NaCl. Each measurement was conducted in triplicate for both techniques, and the presented values represent the averages.

The sessile water contact angle was measured using a VCA Optima surface analysis system (AST Products, Inc., Billerica, MA). The cCNC films were dried in dishes lined with silicone release paper at room temperature to a constant thickness of 1.8±0.2 mm and then removed from the release paper. At least 10 droplets of DIW (each droplet = 1 µL) at different locations on each sample were measured at ambient temperature.

AFM imaging of cCNC dispersions was done using drop casting on clean silicon wafers. The wafers were placed on a hot plate for drop casting, where a single drop (~1 mL) of the diluted CNC suspension (0.5 mg/L) was placed onto the wafer surface and dried for 10 minutes at 80 ^{o}C on the hot plate. Dried-redispersed and never-dried cCNCs, either sonicated or non-sonicated, were imaged. The AFM images were captured using a Park NX10 AFM. Tapping mode was employed at room temperature, utilizing a 40 N/m spring constant and a 300 kHz resonance frequency. Imaging was conducted at a scan rate of 0.01 Hz, with a resolution of 512 measurements per line (512 lines). The CNC dimensions, specifically the length measured from the particle height, were quantified from flattened height images using Gwyddion v.2.55 freeware.

The final latex viscosities were characterized using a Thermo Scientific HAAKE Viscotester (Model D) using spindle R2 or R3 at 100 rpm. The uncertainty in the measurements was ±5 mPa s. Gel content was measured for all final latexes. Around 0.03 g of polymer was placed in a poly(vinylidene fluoride) Durapore™ membrane pouch with a pore size of 0.45 µm and a diameter of 47 mm from Millipore and heat sealed. Each pouch was soaked in THF for 8

hours and gently shaken for 12 hours. Each pouch was dried to a constant weight, and the gel content was calculated.

Dynamic oscillatory frequency tests were performed using an RDA III dynamic mechanical analyzer (DMA, TA Instruments). The geometry used was a pair of 25 mm parallel plates, and the sample thickness was 1.80 ± 0.2 mm. The PSA samples were prepared as follows: first, a certain amount of latex was put in a silicon release paper dish (3.5 cm in diameter). The latex was dried for four weeks until reaching a constant weight and was cut to prepare disk-shaped specimens. Frequency sweep tests were performed at 23 °C (i.e., ~78 °C higher than the polymer T_g) over an oscillation frequency (ω) range of 0.01- 100 Hz; measured values had 10% uncertainty.

3.3.5 PSA characterization

Based on the PSTC-16 standard,[27] final PSA latex films were cast on 30 µm corona-treated Mylar sheets using a #30 Meyer rod and dried at controlled conditions (temperature: 23±1 °C, and relative humidity: 50±5 %) for 24 h before testing (2 films per sample). A dried latex film with a dry film weight of 20±2 g/m^2 was used for the PSA tests, i.e., tack, peel strength and shear adhesion. Bluehill 2 Materials Testing Software was used on an Instron 3000 Universal Tester, and Pressure Sensitive Tape Council (PSTC) methods were employed for loop tack, peel strength, and shear adhesion measurements.[35] Strips of 1″ × 6″ were cut for tack, and a drop loop was formed by taping 1″ of each end of the strip, which was then secured in the upper grip of the Instron tester. The upper grip was moved downward at a rate of 2 mm/s until an area of 1″ × 1″ of a stainless-steel substrate mounted on the lower grip was covered. The upper grip was then pulled up at a 5 mm/s rate, and the maximum force (N/m) required for removal was recorded as tack.

Peel strength was measured by separating an adhesive from a substrate at a 180° angle with respect to the substrate. Strips of 1″ × 5″ were cut and adhered to a stainless-steel substrate via application of a 2040 g roll coater (twice front-to-back movement along the length of the strip) at a rate of 10 mm/s. Subsequently, the substrate and the PSA strip were fixed in the lower and upper grips, respectively. The upper grip was then pulled upward at a rate of 5 mm/s, and the average force required for peeling (N/m) was reported as peel strength. All tack and peel strength measurements resulted in adhesive failure.

A custom-made shear tester was used to record the time a PSA strip could hold against a constant vertical force. Strips of 1" × 5" were cut, and one end of the strip was laminated to a stainless-steel substrate to cover a 1" × 0.5" area using the roll coater (2040 g) in a similar way to specimen preparation for peel strength (four passes at a rate of 10 mm/s). A C-clamp was used to hang a 500 g weight at the other end of the strip. The time (h) to cohesive failure (i.e., the hung weight dropped) was reported as shear adhesion. Each test was repeated six times for each latex film (three samples per film for each test), and the average results and standard deviations were reported. In the case of normally distributed data, a range of ±3 standard deviations corresponds to 95% of the expected variability, and the analysis ensures that most of the observed values lie within this range.

3.4 Results and discussion

A series of preliminary experiments using seeded semi-batch emulsion polymerization was conducted to formulate a base case high-performance adhesive (Table 3.1). A feed composition of 90/8/2 2-EHA/MMA/STY (w/w/w) was used in all runs to obtain a T_g of -55 ºC (using differential scanning calorimetry; described in the Appendix I, Figure AI.1). The formation of homogeneous latex films from the initial base case formulation was impeded by the low viscosity of the latex and various surface forces acting between the latex and the Mylar backing sheet. Various strategies were explored to improve the castability of the base case latex. These strategies included increasing the initiator and surfactant concentrations to 0.8 and 1 phm, respectively, reducing particle size and increasing the latex viscosity. Further improvements in film castability were achieved by using a combination of anionic and non-ionic surfactants in a 2:1 mass ratio.

The initial introduction of cCNCs into the base case latex formulation led to coagulation. To address this, further adjustments were made to the base case formulation. These adjustments included reducing the solids content from 50 to 40 wt.%, redistributing the water content in the seed and feed (65 and 35 wt.%, respectively), and allocating 20 wt.% of the total surfactant to the seed stage. Furthermore, given the low pH of the system (pH~2), the necessity of including a buffer to produce a stable latex with cCNCs was investigated. The pH stability range for cCNCs falls between 3 and 11.[19,36] The addition of cCNCs did not significantly alter the pH of the overall system compared to the base case formulations. These measures collectively

led to achieving a reproducible, stable base case latex formulation that was also stable in the presence of cCNCs (Table 3.1). Details of the preliminary runs are shown in the Appendix (Table AI.1).

For all colloidally stable runs (with and without cCNCs), overall monomer conversion and instantaneous conversion vs. time exhibited similar trends, culminating in final conversions exceeding 99 wt.% (Figure 3.1). A monomer starved-feed approach controlled the kinetics, and despite some changes in latex particle size from run to run (latex particle sizes ranged from 160 to 323 nm), the conversion trajectories were generally similar (see Appendix I, Figures AI.2-4). The polymerization began with a seed stage of 30 min, followed by a 270 min feed stage, and culminated in a 30 min cook stage; this protocol was chosen based on our previous studies and was modeled after a typical commercial approach.[8,37] The base case formulation was modelled after a high-performance commercial latex, and the PSA performance of the base case adhesive film compared well with that of a commercial PSA designed for use as a sealing tape (Table 3.2).

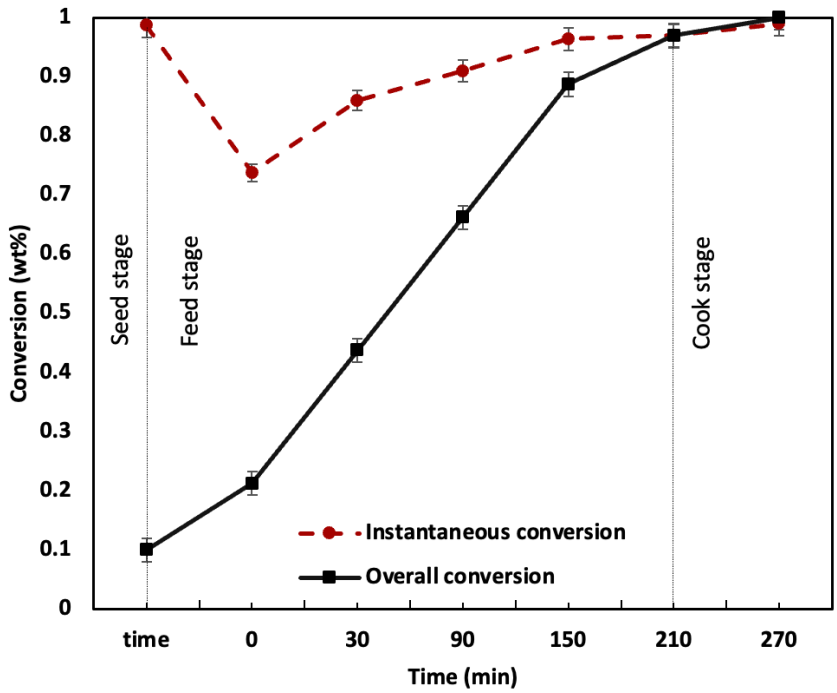

Figure 3.1. Typical instantaneous and overall monomer conversion (base case run is shown as an example).

Table 3.2. Base case latex and commercial adhesive properties

Run ID	Particle size (nm)	Viscosity (mPa s)	Tack (N/m)	Peel strength (N/m)	Shear adhesion (h)
Base case	173.0±0.7	60	316±25	386±40	4±1
Commercial latex (BASF)	307.0±0.5	27	485±41	245±16	13±2

3.4.1 Effect of cCNC sonication and cCNC form (dried-redispersed vs. never-dried)

A key factor impacting application performance is the quality of the suspension of CNCs in water before addition to the latex; ensuring CNCs are uniformly distributed is crucial for consistent nanocomposite properties. As noted, the cCNCs were supplied as a spray-dried powder and a never-dried 6.6 wt.% suspension in water. Inadequate dispersion of the CNCs in water before addition to the latex can lead to significant CNC-latex particle aggregation, resulting in heterogeneous nanocomposite films, compromised adhesive performance, and possibly latex coagulation.[22,38] The redispersion of the dried CNC powder in water has been shown to be necessary for dispersion in the latex – in other words, direct addition of the dried powder does not work.[31] A typical protocol in bench scale settings involves sonication of the CNC suspensions before addition to the latex formulation.[31,34,39] Given that redispersion and dilution of CNCs in DIW without sonication is normally employed at the industrial scale, we sought to clarify the impact of sonication on PSA performance while comparing the cCNC form used.

Before adding the cCNCs to the latex, one can envision four different cCNC treatments: never-dried cCNCs vs. dried-redispersed cCNCs, each either sonicated or not sonicated. These treatments were first compared using particle size analysis via DLS (Table 3.3). The particle size data showed apparent differences when sonication was applied. The sonication process is known to disintegrate CNC aggregates, resulting in reduced "apparent" particle sizes (recalling that CNCs are non-spherical). In fact, it is possible to over-sonicate and damage the CNCs. The population distributions of cCNC particles at the sonication levels in this study (~1776 J/mL) have been shown to migrate from an aggregated state to a discrete nanoparticle state.[40,41] Thus,

sonication reduces the particle size of the dried-redispersed and never-dried cCNCs to similar values. However, without sonication, the particle sizes of the dried-redispersed cCNCs were larger than those of the never-dried cCNCs. This suggests the presence of more aggregates for the dried-redispersed cCNCs. The polydispersity index data also support this observation. AFM imaging also led to the same conclusion (Figure 3.2). The higher surface charge density observed for never-dried cCNCs compared to the dried-redispersed cCNCs in recent work resulted in superior water stability and a lower degree of aggregation in the never-dried cCNCs.[19,34] This difference in surface charge density between the two different cCNC forms in our previous study was attributed to the use of different cCNC batches.[34] However, the dried-redispersed and never-dried cCNCs used in the current study were from the same batch and did not demonstrate any differences in surface charge density (0.22 and 0.23 $mmol.g^{-1}$ cCNC for dried-redispersed and never-dried cCNCs, respectively). The surface charge density values reveal the accumulated net charge on a nanoparticle's surface, offering insights into the fundamental source of charge on the shear plane and directly reflecting the nanoparticle's surface chemistry.[42] The presence of surface charge induces a stern potential across each nanoparticle in the dispersion medium, forming a zeta potential layer due to phase differences between the medium and the nanoparticle surface. Consequently, zeta potential becomes a crucial indicator for assessing the stability of colloidal dispersions. Nevertheless, in this study, the sonication process acted as a mechanical equalizer, mitigating the zeta potential differences between the two cCNC forms and yielding similar particle sizes and polydispersities.

Table 3.3. Particle size distribution and zeta potential of dried and never-dried cCNCs (0.5 phm in water) before and after sonication

cCNC form	cCNC dispersion method	Particle size (nm)	Polydispersity Index*	Zeta potential (mV)	Surface charge density (e/nm^2)
Dried-redispersed	Sonicated	67.5±1.3	0.27±0.01	-34.4±0.6	0.22
Dried-redispersed	Non-sonicated	133.0±2.4	0.40±0.01	-28.9±1.2	-
Never-dried	Sonicated	70.5±1.2	0.27±0.01	-49.8±2.2	0.23
Never-dried	Non-sonicated	108.0±1.5	0.24±0.01	-35.1±3.0	-

*A polydispersity index below 0.1 is considered monomodal, whereas a measurement of 0.1 or greater is considered a broad distribution.[43]

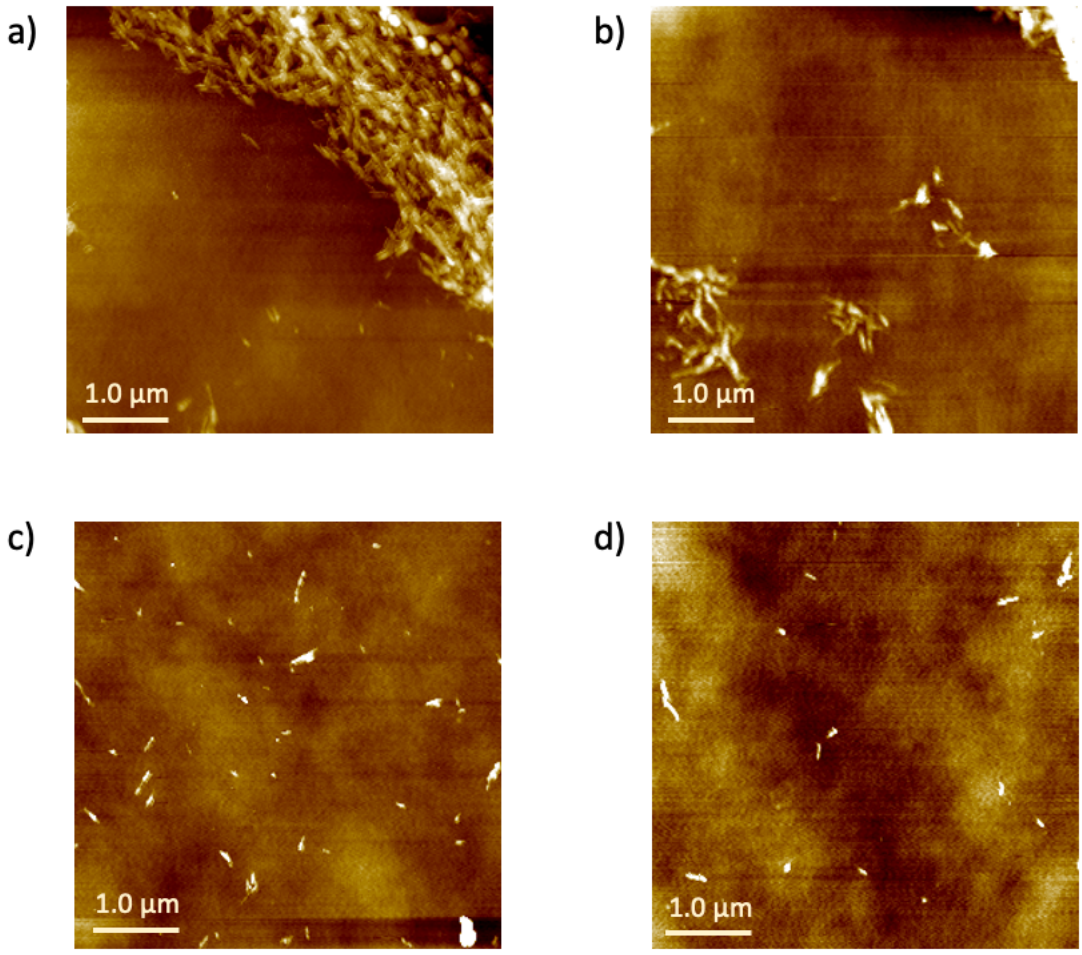

Figure 3.2. AFM height images of (a) non-sonicated dried-redispersed cCNCs, (b) non-sonicated never-dried cCNCs, (c) sonicated dried-redispersed cCNCs, (d) sonicated never-dried cCNCs.

Next, the addition of the cCNC suspensions to the latex formulation was investigated. After polymerization, analysis of the final latex revealed that adding cCNCs increased the latex particle size, polydispersity index, latex viscosity and gel content compared to the base case (Table 3.4). These increases suggest some interaction between the cCNCs and the polymer particles. Previous studies, which included AFM imaging, also support this claim.[24] In other words, the cCNCs do not necessarily reside in isolation in the water phase. They are more likely to reside near the polymer particle surfaces but not within the polymer particles. If the cCNCs resided within the polymer particles, geometric considerations would have led to the formation of even larger latex particles due to the relative size of the cCNCs compared to the latex particles

(compare results from Tables 3.3 and 3.4). As noted in the discussion related to the cCNC suspensions (Table 3.3), sonication resulted in the de-aggregation of the cCNCs.[44,45] As sonication increased the zeta potential values, lower cCNC reassembly was expected regardless of the form of cCNCs. On the other hand, it has been shown that shorter CNCs are more prone to form highly ordered structures through reassembly.[44,45] Thus, by extension, sonicated CNCs should reassemble to a greater extent than would non-sonicated CNCs. In fact, regardless of the cCNC form used, the runs with the sonicated cCNCs gave larger polydispersities and higher gel contents, supporting the idea that there was greater cCNC reassembly compared to the non-sonicated cCNCs.

Table 3.4. Latex properties for 0.5 phm cCNC addition at seed stage in 40 wt.% solids latexes

Run ID*	Particle size (nm)	Polydispersity index	Viscosity (mPa s)	Gel content (%)
Base case	173.0±0.7	0.010±0.004	60	43±7
S-D-0.5	200.0±0.4	0.270±0.030	186	60±9
NS-D-0.5	196.0±3.0	0.230±0.030	132	50±8
S-ND-0.5	202.0±2.2	0.310±0.013	270	63±10
NS-ND-0.5	182.0±2.8	0.250±0.020	180	53±9

* S: sonicated / NS: non-sonicated; D: dried-redispersed / ND: never-dried.

From the above discussion, a view of the four stages of cCNC incorporation before and after addition to the latex formulation emerges (Figure 3.3):

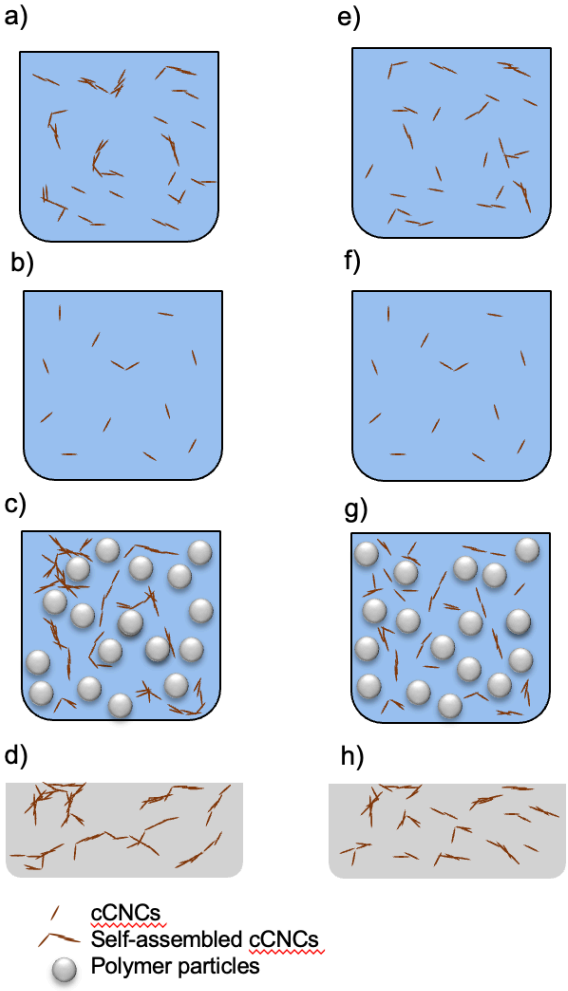

Figure 3.3. Dried-redispersed cCNCs in water, a) before and b) after sonication; and in the latex, c) after polymerization and d) in the dried film. Never-dried cCNCs in water, e) before and f) after sonication; and in the latex, g) after polymerization, and h) in the dried film. For images c), d), g) and h), cCNC addition is assumed to be at the seed stage.

(1) Dispersion of cCNCs in water before sonication: The dried-redispersed cCNCs had a zeta potential of -28.9 mV, which was lower in magnitude than their never-dried counterparts at -35.1 mV (Table 3.3). Upon dispersion in water, the lower repulsive forces in the dried-redispersed cCNCs lead to a greater level of reassembly and a higher "apparent" aspect ratio than the never-dried cCNCs. As a result, they display more side-by-side and end-to-end association, i.e., aggregation.[24,46] Figures 3.3a and 3.3e, depict the characteristics of dried

(lower zeta potential in terms of absolute value) and never-dried (higher zeta potential in terms of absolute value) cCNCs dispersed in water.

(2) cCNC dispersions after sonication: Sonication serves to disintegrate the cCNC aggregates, resulting in reduced "apparent" aspect ratios (Figures 3.3b and 3.3f). The sonication process equalized the dried-redispersed and never-dried cCNCs in terms of their “apparent” particle sizes (Table 3.3). To gain a better understanding of the characteristics of these two types of cCNCs, their surface features were examined using AFM imaging. The AFM images revealed that the suspension of dried-redispersed cCNCs (Figure 3.2a) exhibited greater aggregation prior to sonication compared to their never-dried counterparts (Figure 3.2b). Dried-redispersed cCNCs, possessing a lower absolute value zeta potential, demonstrated higher concentrations of self-assembly and end-to-end aggregation. The average particle diameters calculated from the AFM images for dried-redispersed and never-dried cCNCs were 137 and 124 nm, respectively, surpassing the average particle diameters obtained via DLS (Table 3.3). However, determining the lengths of cCNCs manually, proved challenging due to their nanofibril-like appearance in AFM images, arising from both end-to-end and side-by-side interactions. Sonication effectively separated individual cCNC particles that were either aligned end-to-end or stuck side-by-side before the process. In line with the DLS findings, sonication of cCNCs resulted in smaller particle diameters (74 nm and 78 nm for dried-redispersed and never-dried forms, respectively). It is important to note that the reported cCNC dimensions are meant for comparative purposes only among the different samples.

(3) Dispersion of sonicated cCNCs inside the latex formulation: It has been well-established that in a latex formulation, the hydrophilic CNCs tend to reside close to the polymer particles but still within the aqueous phase.[9,26,30,47] The negatively charged latex particles encourage cCNC reassembly via latex particle-cCNC repulsion. As described earlier, the cCNCs with a lower absolute value zeta potential (i.e., dried-redispersed) will tend to reassemble into nanofibrillar structures to a greater extent than their high zeta potential counterparts (i.e., never-dried) (Figures 3.3c and 3.3g).[48] It is noted that 2 hours after the feed stage began, a bimodal particle size distribution was observed via DLS; 1 to 8% of the particle population had an average particle size of 5000 nm. This points to the formation of latex particle-cCNC aggregates. The second peak area observed in DLS measurements for the never-dried cCNCs (~8%) compared to that of the dried-redispersed cCNCs (~5.6%) confirmed a higher degree of

aggregation of the latex particles in the presence of never-dried cCNCs. In this case, it is important to distinguish cCNC reassembly from latex particle-cCNC aggregation.

(4) cCNCs in dried PSA films: The dissimilarity in the self-assembly behaviour of dried-redispersed and never-dried cCNCs was expected to have been sustained throughout the film drying process. As shown in Figures 3.3d and 3.3h, the occurrence of cCNC end-to-end assemblies in the PSA films containing dried-redispersed cCNCs was expected to be greater than those containing never-dried cCNCs. This higher tendency towards reassembly of CNCs after incorporation into PSA formulation has been shown in prior work.[24] This depiction is further supported by water contact angle measurements on the dried cCNC films mm (without latex) (Figure 3.4). The measured water contact angles for the dried-redispersed cCNC films showed a rapid decrease from 35 ±5° to 12 ±4° within 100 seconds, indicative of rapid water absorption due to the porous nature of the cCNC film. This suggests a less densely packed film due to the nanofibrillar structures. In contrast, the water contact angles of the never-dried cCNC films decreased more gradually from 37 ±5° to 14 ±2° over 4 minutes. This illustrated slower water droplet penetration into the more densely packed film. These findings align with previous investigations on sulfated CNCs in spray-dried and never-dried forms, revealing evidence of insufficient pore space within the never-dried cCNC films.[49]

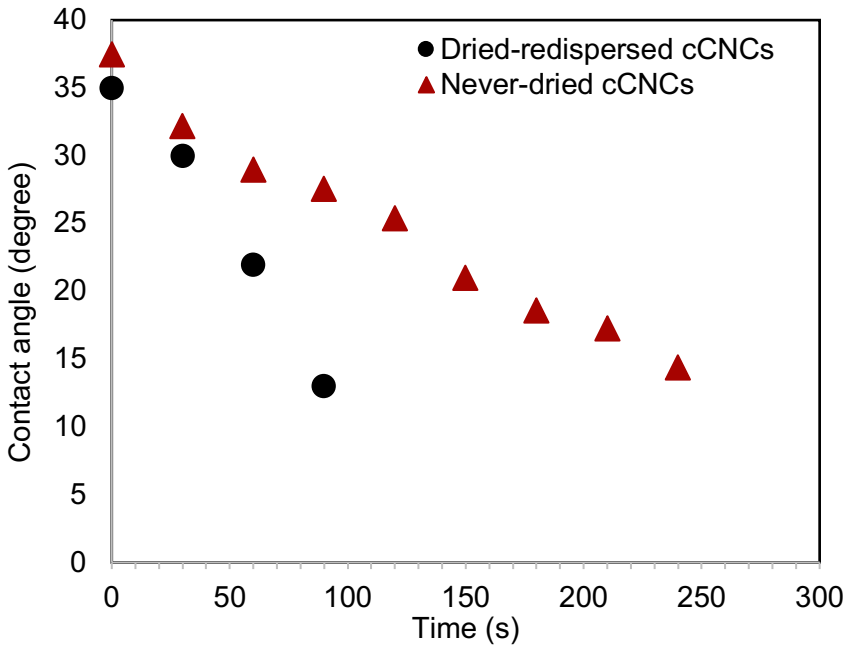

Figure 3.4. Changes in the contact angle of a water droplet (1 µL) on never-dried and spray-dried cCNC dried films.

The PSA performance showed a simultaneous increase in all three key PSA performance measures: tack, peel strength, and shear adhesion with the addition of cCNC at 0.5 phm loading (Figures 3.5 and 3.6). The impact on tack was significant (131% average increase), whereas for peel strength the increase was moderate (11% average increase). There were no significant differences between the four treatments for tack and peel strength. On the other hand, shear adhesion showed significant increases (increases ranging from 325 to 1350%) and they differed widely from one treatment to the next. It is worth noting that the simultaneous increase in all three PSA performance measurements is unlike other interventions in PSA formulations, which tend to result in a trade-off between tack and peel strength vs. shear adhesion.[4] This behaviour is consistent with previous CNC studies but is noteworthy because of the higher quality base case adhesive formulation used.[8,31,32]

The increased tack can be attributed to the improved wettability of PSA films due to the hydrophilicity of the cCNCs.[9] The polar hydroxy groups on the cCNCs positively interacted with those on the stainless-steel test panels.[30] In Figure 3.4, although not statistically significant, the trend towards lower water contact angles for the cCNC-containing PSA films points to a greater work of adhesion; previous work supports this idea.[30] The improvement in peel strength was due to increased wettability and higher elasticity of the latex when cCNCs were added to the formulation. Evidence for the higher elasticity was measured using DMA and will be discussed later. In other words, the addition of cCNCs improved the capability of the polymer chains to fibrillate and stretch through their entanglement with the polymers coupled with their increased end-to-end self-assembly.[50] Finally, the entanglement of the diffusing polymer chains with the cCNCs during film drying increased shear adhesion by creating a more networked microstructure than the base case formulation.[8,9]

As noted earlier, tack was affected equally by the various treatments, i.e., the use of sonication and the cCNC form (Figure 3.5). Given that tack is a surface-contact phenomenon, this would imply that the cCNCs were equally distributed at the PSA film surface. The lack of change in the water contact angles between the four treatments aligns with the idea that the PSA film surfaces did not differ (Figure 3.5). Peel strength was similarly affected between the four treatments (Figure 3.5). Peel strength measures the ability of an adhesive to intimately contact the adherend surface and dissipate energy during the debonding process. Thus, increasing PSA flowability and wettability toward a surface increases the adhesive forces. The lack of difference in peel strength from treatment to treatment aligns with the findings for tack,

which suggested a consistent cCNC concentration at the surface of all PSA films during the drying process.

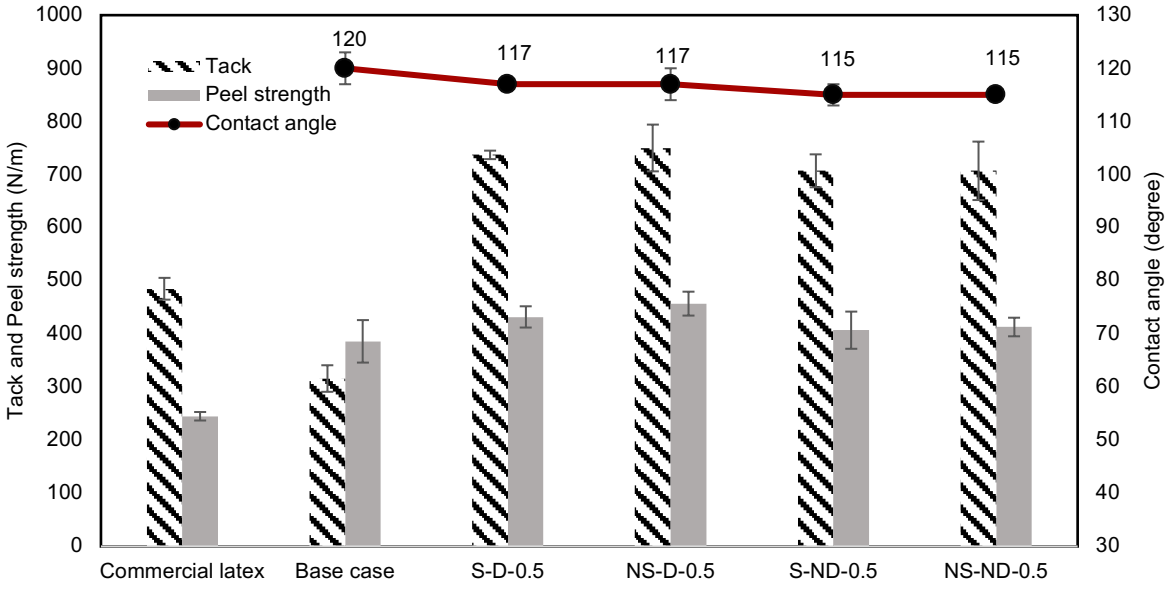

Figure 3.5. Tack, peel strength and water contact angle for commercial latex, cCNC-PSA dried films (0.5 phm cCNC) for sonicated (S), non-sonicated (NS), dried-redispersed (D) and never-dried (ND) treatments. Tack and peel strength values on left axis; contact angle values on right axis.

As mentioned above, significant differences between the treatments were observed in the shear adhesion results (Figure 3.6). The never-dried cCNC-PSA films showed lower shear adhesion than the dried-redispersed cCNC-PSA films. As depicted in Figures 3.3d and 3.3h, the dried-redispersed cCNCs would present a more branched, nanofibrillar structure leading to a more extensive cCNC self-assembly than the never-dried cCNCs. This, coupled with cCNC-polymer entanglements, led to higher elasticity and higher cohesive strength. The sonication of the cCNCs also impacted shear adhesion, particularly for the dried-redispersed cCNCs. The sonicated cCNCs were better distributed in the latex, forming more highly ordered nanostructures,[44,45] and a more continuous network in the PSA films than in the non-sonicated case. Thus, the greater cCNC-latex particle interactions led to higher shear adhesion.

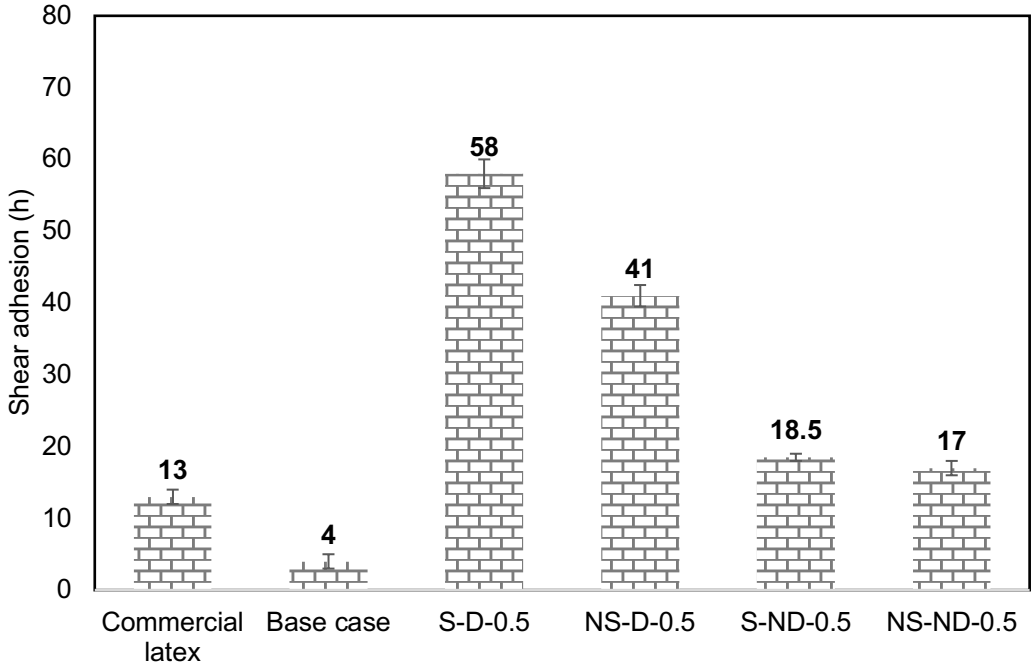

Figure 3.6. Shear adhesion of commercial latex, cCNC-PSA dried films (0.5 phm cCNC) for sonicated (S), non-sonicated (NS), dried-redispersed (D) and never-dried (ND) treatments.

In summary, the addition of cCNC allowed for simultaneous improvement in all three PSA performance indicators, in particular, shear adhesion. Apart from the influence of the cCNC forms (dried-redispersed vs. never-dried) and their dispersion quality (sonication) on PSA performance, the addition of cCNCs led to performance improvements compared to both the base case and commercial latex (Figures 3.4 and 3.5). Sonication, though not preferred in commercial settings, has a strong positive impact on cCNC dispersion in water and eventually in the latex and dried PSA films. The dried-redispersed cCNC form is preferred from both a PSA performance angle and practical transportation considerations.

3.4.2 Effect of cCNC loading

To uncover whether further improvements in adhesive performance and mechanical properties could be achieved, additional cCNC loadings of 0.3 and 0.7 phm were explored for two distinct preparation methods: non-sonicated, never-dried and sonicated, dried-redispersed cCNCs. Attempts to use cCNC concentrations greater than 0.7 phm by adding them at the seed stage led to colloidal instabilities and reaction failure (coagulation). [8,9,27,30,51] As cCNC content

was increased, regardless of the cCNC form, there was an increase in particle size, distribution broadness, and viscosity, which can be attributed to cCNC-latex particle interactions (Table 3.6). The particle size reported in Table 3.5 is that for the first peak in a bimodal distribution; that peak consisted of 93 to 99% of the particle population. As noted earlier, a second peak at a particle size of ~5000 nm was observed for all the runs when cCNC was charged via the seed stage. Higher cCNC loadings led to greater cCNC self-assembly and cCNC-latex aggregation, regardless of whether sonication was used. This is consistent with the increased particle size (for peak 1, Table 3.5), polydispersity index (Table 3.5), viscosity and percentage of the second peak (particle size of ~5000 nm) from 1 to 7% (Table 3.5).

Table 3.5. Latex properties of PSAs containing cCNCs at different loadings for sonicated, dried-redispersed vs. non-sonicated never-dried cCNCs.

Run ID*	cCNC loading (phm)	Particle size Peak 1 (nm)	Particle size Peak 2 area (%)	Polydispersity index	Viscosity (mPa s)	Gel content (wt.%)
Base case	0	173.0±0.7	-	0.010±0.004	60	43±7
S-D-0.3	0.3	172.0±2.7	1.1±0.00	0.130±0.019	87	64±9
S-D-0.5	0.5	200.0±0.4	5.60±0.01	0.270±0.030	186	60±9
S-D-0.7	0.7	274.0±3.2	7.00±0.80	0.450±0.018	347	57±6
NS-ND-0.3	0.3	170.0±1.8	5.00±0.02	0.170±0.005	84	66±11
NS-ND-0.5	0.5	182.0±2.8	6.50±0.50	0.250±0.020	180	53±8
NS-ND-0.7	0.7	356.0±18.2	7.40±1.01	0.660±0.123	300	61±11

* S: sonicated / NS: non-sonicated; D: dried-redispersed / ND: never-dried.

As shown earlier in Figures 3.5 and 3.6, all three PSA properties increased simultaneously relative to the base case when cCNCs were added. The tack and peel strength remained invariant to the increased cCNC content regardless of the cCNC form or use of sonication (Figure 3.7). Only run NS-ND-0.7 showed a slight decrease in tack from the other cCNC-containing runs. On the other hand, dramatic increases in shear adhesion for the sonicated, dried-redispersed cCNC runs were observed with increasing cCNC content (Figure 3.7). Run S-D-0.7 exhibited the largest increase in shear adhesion (>3,500 % compared to the base case). The gel content data showed no consistent trends except that adding cCNCs led to higher gel content measures, attributed to the entrapment of polymer particles via polymer-cCNC entanglements[32] (Table 3.5). Certainly, the gel content results were not consistent with the shear adhesion results (Figure 3.7). Normally, one interprets gel content as a measure of cross-linked polymer in the dried latex. However, it has been previously determined that the cCNCs were unlikely to engage in cross-linking reactions, thus, we can speculate that because of their hydrophilicity and entanglement with the polymer chains, the cCNCs formed a barrier to the escape of some of the long-chained polymers from the sample pouch.[32]

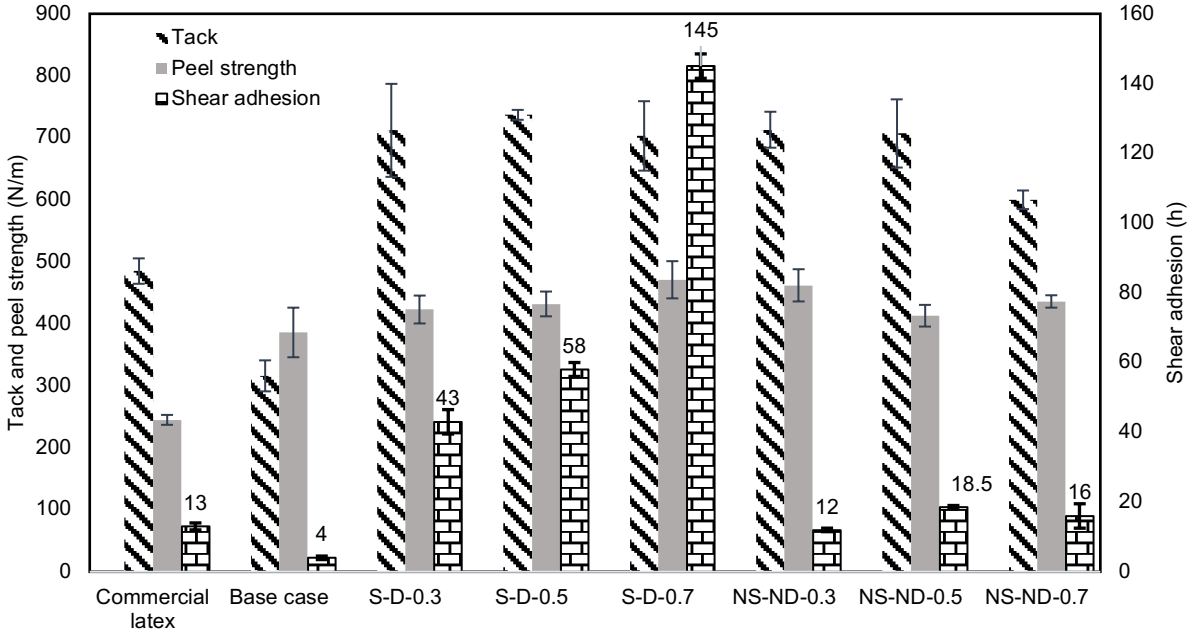

Figure 3.7. PSA properties of dried latex films at different cCNC loadings for sonicated (S), dried-redispersed (D) cCNCs vs. non-sonicated (NS), never-dried (ND) cCNCs. Numbers in run ID refer to cCNC loading in phm. Tack and peel strength values are on the left axis; shear adhesion values are on the right axis.

The shear adhesion results do, however, align with our previous depiction of the cCNC microstructure (Figure 3.3). According to our depiction, the sonicated, dried-redispersed (S-D runs) cCNCs formed a more nanofibrillar-like structure within the latex compared to the non-sonicated, never-dried (NS-ND runs) cCNCs. The greater reassembly of the S-D-cCNCs led to a higher "apparent" aspect ratio and coupled with the increasing polymer cCNC entanglements (due to increased cCNC loading), higher cohesive strengths were achieved; thus, higher shear adhesion measurements. The impact of increased cCNC loading was not as significant for the NS-ND-cCNCs because they failed to produce the same type of nanofibrillar network as in the S-D-cCNCs.

In summary, the impact of cCNC addition on tack and shear adhesion was significant. The impact on peel strength, though the base case statistically exceeded the commercial latex, was less powerful. In addition, the cCNC treatment via sonication and the cCNC form used had a major impact on shear adhesion. The different zeta potential of the different forms and their subsequent reassembly after sonication can lead to nanofibrillar structures in the dried PSA films. This nanofibrillar structure directly impacts increasing cohesive strength and, thus, shear adhesion.

3.4.3 cCNC feed strategies

The significant increase in shear adhesion for the sonicated, dried-redispersed cCNC (S-D) runs (Figure 3.7), in addition to the limitations to loading the cCNCs at the seed stage encountered above, led to further investigation into achieving even higher shear adhesion. While using the same S-D case, the addition of the cCNCs via the feed stage was investigated.

When the cCNCs were added at the feed stage, the conversion profile was not significantly different from the previous runs where the cCNCs were added at the seed stage. The final gel contents were similar to the runs where cCNCs were added at the seed stage (Table 3.6). However, monomodal particle size distributions were observed for the cCNCs added to the feed stage, whereas bimodal distributions were seen for all the seed stage runs (see Appendix I, Figure AI.6-7). As noted earlier, the bimodality in the seed stage runs began to appear after 2 h from the beginning of the feed stage. Recalling the depiction of the cCNCs added at the seed stage (Figures 3.8a and b), one can envision that when the cCNCs were added to the seed stage, they were in a dilute environment, encouraging their reassembly into large

nanofibrillar structures. These large nanofibrillar structures led to their eventual aggregation with the latex particles. This aggregation only occurred at higher polymer particle concentrations later in the reaction, and these were detectable as a second peak in the particle size analysis (earlier samples were monomodal). Recall that the aggregates made up no more than 8% of the particle size distribution. In addition to the monomodal particle size distribution in the feed stage runs the particle size was significantly smaller compared to that in the seed stage runs (Table 3.6). In the feed stage addition case, the cCNCs were added over a longer time, which allowed them to mix with the latex particles and interact with them rather than reassembling with other cCNCs. Thus, they were less likely to form the nanofibrillar structures formed when they were added at the seed stage.

Table 3.6. Latex properties of PSA formulations with sonicated, dried-redispersed cCNCs added at the feed stage (F) compared with seed stage addition and the base case.

Run ID*	cCNC loading (phm)	Particle size (nm)	Polydispersity index	Viscosity (mPa s)	Gel content (%)
Base case	0	173.0±0.7	0.010±0.004	60	43±7
S-D-0.5	0.50	200.0±0.4	0.270±0.030	186	60±9
S-D-0.7	0.70	274.0±3.2	0.450±0.018	347	57±6
S-D-0.5-F	0.50	160.0±1.7	0.090±0.009	93	60±12
S-D-0.75-F	0.75	223.0±4.2	0.180±0.024	105	53±6
S-D-1-F	1.00	209.0±1.8	0.200±0.008	190	53±8
S-D-1.25-F	1.25	228.0±1.2	0.220±0.007	175	57±6
S-D-1.5-F	1.50	220.0±2.0	0.280±0.035	460	63±9

* S: sonicated / NS: non-sonicated; D: dried-redispersed / ND: never-dried.

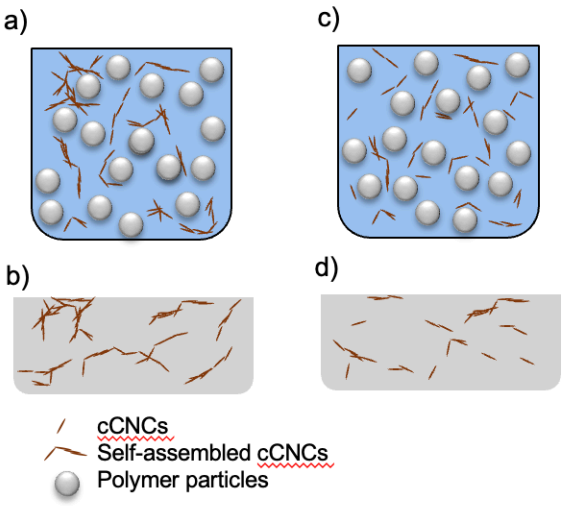

Figure 3.8. Dried-redispersed cCNCs added in the seed stage in the latex, a) after polymerization and b) in the dried film. Dried-redispersed cCNCs added in the feed stage in the latex, c) after polymerization, and d) in the dried film.

As noted in Table 3.6 and in other studies[26], the cCNCs acted as a rheology modifier, leading to latex viscosity increases and improved film formation properties.[8] The ultimate viscosity of the latex increased with cCNC loading, irrespective of the addition protocol (seed vs. feed). The similarity in the base case formulation for all the runs in this study (Tables 3.4 and 3.6) confirmed that the viscosity increases were due solely to the presence of cCNCs in the formulations. The limitations observed earlier when adding the cCNCs at the seed stage were attributed to increased latex viscosity resulting from cCNC-component interactions during the seed stage and cCNC reassembly throughout the polymerization. Adding cCNCs at the feed stage vs. the seed stage showed a drastic decrease in the latex viscosity (Table 3.6). Normally, a lower particle size and, therefore, a larger number of particles would be expected to generate a higher viscosity. The same behavior was noted in another study when the addition of sonicated, dried-redispersed, sulfated CNCs at the feed stage decreased latex viscosity.[32] Given the particle size analysis and the viscosity data, one can conclude that something else was at play in this situation. With the addition of the cCNCs at the seed stage, aggregation due to the greater cCNC-latex particle interactions occurred (observed second peak in DLS measurements) and led to a higher viscosity compared to the runs when the cCNCs were added at the feed stage. In other words, the addition of all the cCNCs at the seed stage allowed for a longer period

of cCNC-latex interaction at a higher cCNC concentration, whereas the feed stage addition of the cCNCs provided a relatively lower cCNC concentration throughout the latex synthesis. Therefore, by adding the cCNCs at the feed stage, stable latexes with cCNC loadings of up to 1.5 phm were achieved compared to the limit of 0.7 phm when the cCNCs were added at the seed stage.

As seen earlier with the seed stage addition of the cCNCs, the use of cCNCs in the latex adhesives simultaneously increased tack, peel strength, and shear adhesion compared to the base case (Figure 3.9).[24,30,32] The average tack and peel strength for the PSA films in which the cCNCs were added at the seed stage were 717 and 442 N/m, whereas those added at the feed stage were 719 and 460 N/m, respectively. It was only at higher loadings (1.25 and 1.5 phm) that tack (at 1.25 phm), and peel strength (at 1.5 phm) showed moderate increases beyond the average PSA performance of the other samples in this study (Figure 3.9).[32]

The shear adhesion was significantly higher for the seed stage addition compared to the feed stage addition cases (Figure 3.9). This aligns with our earlier discussion regarding the impact of cCNC-latex particle aggregation on shear adhesion. In other words, the addition of the cCNCs at the feed stage led to less cCNC reassembly and lower cCNC-latex particle aggregation compared to the seed stage addition cases.[27,52–55]

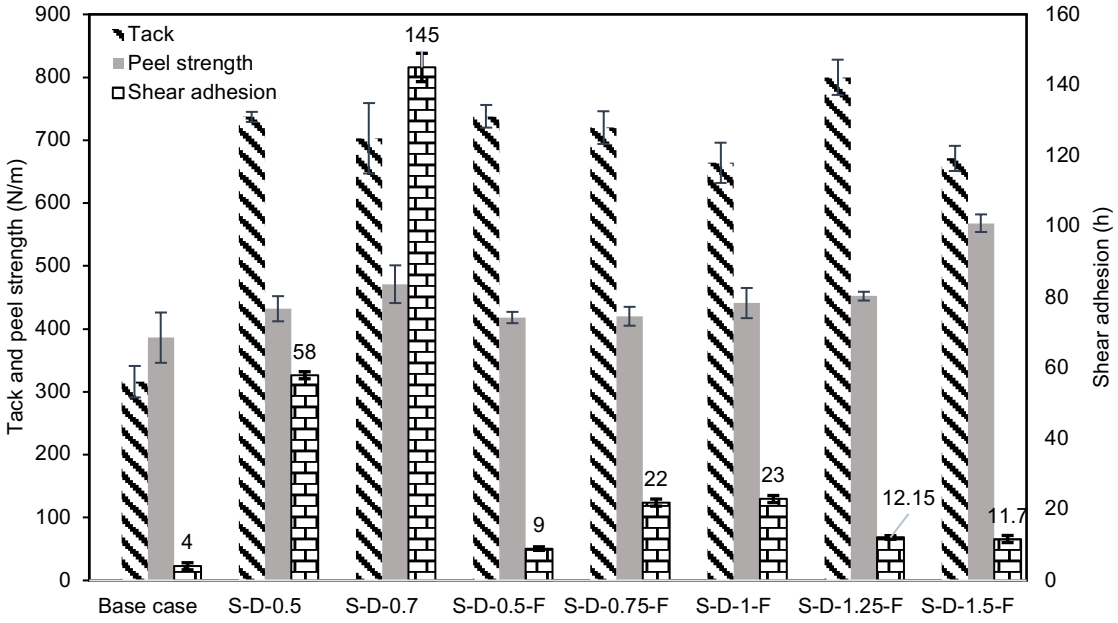

Figure 3.9. PSA properties of dried latex films for the base case formulation vs. latexes with the cCNCs added at the feed stage (F) vs. the seed stage (run ID ending without F) with increasing cCNC loading. All cCNCs were sonicated (S) and of the dried-redispersed (D) form. Numbers in run ID indicate cCNC loading in phm. Tack and peel strength values on left axis; shear adhesion values on right axis.

Previous studies using sulfated CNC dispersions[38] showed that higher surface-charged CNCs with similar aspect ratios and surface groups were found to become metastable above 2.5 gCNC.L^{-1} water.[38] The cCNC dispersion concentrations in this study's seed and feed stage cases were considerably higher (3.68 and 41.95 gCNC.L^{-1}, respectively), suggesting that surface chemistry was a critical factor in controlling latex stability. In addition, cCNC reassembly to form nanofibrillar microstructures and, ultimately, cCNC-latex particle aggregation significantly impacted PSA performance and, in particular, shear adhesion. Furthermore, the lower limits to cCNC loading to avoid colloidal instability were not necessarily limiting regarding their significant impact on PSA performance.[32]

3.4.4 Dynamic Mechanical Analysis

PSA adhesive and cohesive performance are closely linked to the viscoelastic properties of the polymer.[56] For instance, the process of adhesive removal from a substrate typically occurs at high frequencies (around 100 Hz), making G' and G" values at ≈100 Hz indicative of debonding strength. Conversely, the bonding process frequently unfolds at lower frequencies (0.01–1 Hz), making G' at low frequencies a measure of bonding efficiency.[57–59] Dynamic oscillatory frequency tests using a DMA were conducted at room temperature (approximately 75°C above the polymer's glass transition temperature) under a constant strain of 1% to investigate the impact of cCNC concentration and cCNC addition protocol on the viscoelastic properties of the PSA films (see Appendix I, Figures AI.8-10). Results at a frequency of 1 Hz are shown in Table 3.7.

Table 3.7. Dynamic mechanical analysis of PSAs with different loadings of cCNCs at different locations at a frequency of 1 Hz. All cCNC runs were for sonicated (S), dried-redispersed (D) cCNCs with addition at the feed stage (F) or seed stage. Numbers in run ID indicate cCNC loading in phm.

Run ID	G' (kPa)	G" (kPa)	Tan δ
Base case	9.6	3.3	0.40
S-D-0.3	54.7	20.1	0.37
S-D-0.5	59.7	21.2	0.37
S-D-0.7	62.8	23.0	0.35
S-D-0.5-F	44.0	16.1	0.37
S-D-0.75-F	46.1	17.2	0.35
S-D-1-F	48.2	19.4	0.34
S-D-1.25-F	32.9	13.0	0.36
S-D-1.5-F	30.8	10.9	0.37

The hydrophilic cCNCs, when dispersed in a nonpolar polymeric environment, tend to reassemble in the water phase near the latex particles due to robust interparticle interactions involving hydrogen bonds, van der Waals forces, and their substantial specific surface area.[60] Nevertheless, if hydrogen bonding transpires at the interface between the polymer and cCNCs, cCNC-polymer chain entanglements could serve as conduits for transferring mechanical forces generated during analysis, such as strain, from the nanocomposite to these structures[51], which has been observed by increasing the cCNC content in runs S-D-0.3 to S-D-0.7 and S-D-0.5-F to S-D-1-F (Table 3.7). An alternate study has shown that during strain-sweep tests at lower deformations, CNC aggregates behaved cohesively, enhancing the nanocomposite's elasticity with a Hookean response to applied stresses (comparing runs S-D-0.5 vs S-D-0.5-F in Table 3.7).[26]

As the cCNC loading increased up to 1 phm, regardless of cCNC addition protocol, the storage modulus (G') of the latex nanocomposite increased at a frequency of 1 Hz (Table 3.7). This was an indication of increased nanocomposite elasticity due to the restrictions on polymer chain mobility by the cCNCs with greater levels of reassembly.[37] Thus, higher cCNC loadings contributed to greater reassembly as did the addition of cCNCs via the seed stage. The loss

modulus (G"), characterizes the nanocomposite's ability to resist viscous flow and deformation, thus reflecting the cCNCs' ability to limit the motion of the polymer chains.[26] G" followed the same trends as G', and for all formulations, remained lower than G', signifying the dominance of polymer elasticity over viscous flow behavior. Typically, tan δ decreases with increasing filler content, reflecting the addition of a stiff particle to a softer polymer matrix.[59] Up to 1 phm cCNC loadings, the tan δ behaved as expected. At cCNC loadings greater than 1 phm, the deformations from the DMA test generate strong enough forces to break apart the interactions between the cCNCs and the polymers, leading to the disintegration of aggregates into individual components. This resulted in reduced G' and G" (Table 3.7).

3.4.5 Comparing cCNCs with sulfated CNCs

Because of our extensive experience with sulfated CNCs and because of their commercial availability, we compared their performance using the current formulation with the cCNCs. Attempts to increase the sulfated CNC loading via the seed stage beyond 0.3 phm led to latex coagulation. This limit was lower than that for the cCNC addition (0.7 phm cCNC loading) and points to the surface characteristics of cCNCs and sulfated CNCs.[17,19] The higher zeta potential of sulfated CNCs (41.8 mV compared to 34.3 mV for cCNCs)[23,61] led to an increase in the second peak area (4.8%) compared to the cCNCs (1.1%) at the same loading (0.3 phm), suggesting the presence of more aggregation of sulfated CNC-latex particles. This was supported by higher viscosity measurements (Table 3.8) and the lower CNC loading limit for the sulfated CNCs relative to the cCNCs. For this reason, the sulfated CNC runs at 0.5 phm were conducted via feed stage addition of the CNCs.

Table 3.8. Latex properties for cCNC and sulfated CNC nanocomposite latexes. CNCs were sonicated and redispersed from dried powder.

Run ID	CNC (phm)	Particle size (nm)	Polydispersity index	Viscosity (mPa s)	Gel content %
Base case	0	173.0±0.7	0.010±0.004	60	43±7
S-D-0.3	0.3-cCNC	172.0±2.7	0.130±0.019	87	64±9
S-D-0.3-sulfated	0.3-sulfated CNC	219.0±3.0	0.240±0.020	106	46±8
S-D-0.5-F	0.5-cCNC	160.0±1.7	0.090±0.009	105	60±12
S-D-0.5-sulfated-F	0.5-sulfated CNC	185.0±2.1	0.200±0.008	170	47±7

There were notable differences in the latex properties (Table 3.8) and PSA performance (Figure 3.10) when comparing the use of cCNCs and sulfated CNCs. Comparisons were made for two CNC loadings (0.3 and 0.5), one with addition at the seed stage (0.3 phm sulfated CNC) and the other added at the feed stage (0.5 phm sulfated CNC). In both cases, a larger average particle size and more dispersed particle size distribution were observed for the sulfated CNC cases. This may partly have been due to the "apparent" length of 183 ±8 nm for the sulfated CNCs compared to that of the cCNCs of 81 ±0.4 nm.[19,22] The higher viscosities observed for the sulfated CNC nanocomposite latexes with higher zeta potential were due to the higher repulsive interactions between the CNCs and latex particles. The addition of sulfated CNCs did not significantly impact gel content compared to the base case formulation. On the other hand, the lower zeta potential of the dried-redispersed cCNCs increased entanglements with polymer chains, particularly at the seed stage, leading to higher gel content measures.

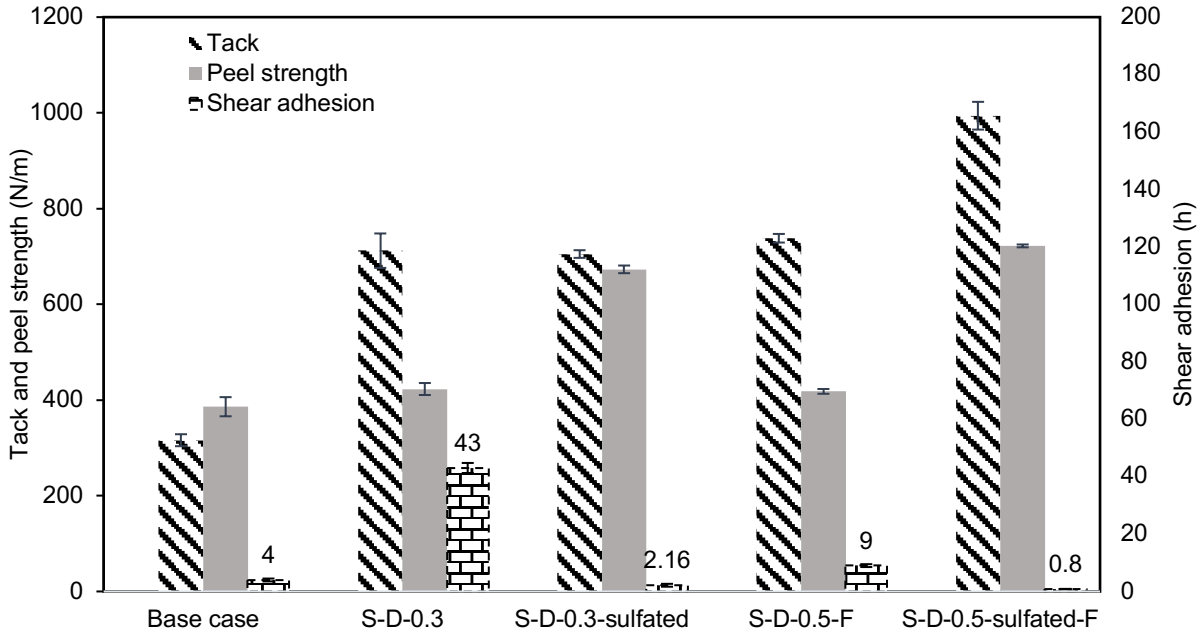

Figure 3.10. Sulfated CNC latex performance versus the cCNC incorporated latexes at two different conditions (location and loading). Run ID denotes CNC source (sulfated vs. carboxylated), CNCs added at the feed stage (F) vs. the seed stage (run ID ending without F) with numbers denoting CNC loading in phm. All cCNCs were sonicated (S) and of the dried-redispersed (D) form. Tack and peel strength values on left axis; shear adhesion values on right axis.

The influence of the sulfated CNCs' addition location (seed vs. feed stage) on shear adhesion mirrored that of the cCNCs, with lower shear adhesion observed when the sulfated CNCs were added at the feed stage (Figure 3.8d) compared to the seed stage (Figure 3.8b). However, for the sulfated CNCs, at the higher CNC loading with feed stage addition, tack increased significantly. The increased tack was attributed to improved wettability facilitated by comparable surface interactions with both sulfated CNCs and cCNCs. As explained earlier, the presence of CNCs on the film surface enhanced film wettability and the required debonding force (i.e., tack).[51,62] The higher zeta potential of the sulfated CNCs, combined with their addition at the feed stage, increased the amount of individualized CNCs contacting the stainless-steel test panels, thereby enhancing tack. The sulfated CNCs' lower affinity for forming nanofibrillar structures due to their high zeta potential, led to significant influences of their addition location on tack.

When comparing the dried latex films of the different CNC types used, moderate differences in peel strength were observed, especially when the CNCs were added at the feed stage (Figure 3.10). Adding sulfated CNCs at the seed stage instead of cCNCs increased the peel strength. The observed effect on peel strength is linked to the hydrophilicity differences between the sulfated CNCs and cCNCs. As discussed earlier, the lower hydrophilicity of the sulfated CNCs and lower number of nanofibril-like structures (due to its higher zeta potential) led to the migration of more sulfated CNC particles to the film surface during drying. This resulted in greater contact between the sulfated CNCs and the stainless-steel test panels, leading to higher peel strengths compared to the cCNCs.

Recall our earlier observations that the general trends in PSA performance often involve a compromise between tack and peel strength versus shear adhesion.[4] The lower zeta potential of the cCNCs resulted in stronger interactions among the cCNCs, leading to nanofibril-like networks (Figure 3.3d). The higher shear adhesion observed in latexes with cCNCs, regardless of addition protocol, can be attributed to the presence of those nanofibril-like structures for the cCNC latexes (Figure 3.3d) compared to latexes with sulfated CNCs (Figure 3.3h). In summary, the zeta potential differences in the two CNCs led to important performance differences from their latex properties all the way to their adhesive properties.

3.5 Conclusion

In this study, we explored the impact of reassembly of CNCs on high-performance latex-based PSAs. The zeta potential differences observed between two cCNC forms (dried-redispersed vs. never-dried suspensions) prompted a deeper exploration of how zeta potential influences their reassembly. [24]Through AFM imaging we showed that a lower zeta potential can facilitate CNC reassembly to form nanofibril-like structures. This higher tendency towards reassembly for the dried-redispersed (lower zeta potential) cCNCs was correlated to a rapid decrease in the water contact angle measurements for their dried films (without latex) relative to the never-dried ones. In other words, the dried-redispersed cCNC films were less densely packed due to the presence of nanofibrillar structures. In the latex formulation, the ability of the cCNCs, because of their lower zeta potential, to interact favorably with the polymer matrix led to their organized reassembly, especially after sonication, and ultimately led to significant improvements in shear adhesion. While tack and peel strength were moderately impacted, their improvements were comparatively less pronounced than for shear adhesion. Regardless, all three PSA performance measures increased significantly compared to that of the base case latex films.

The observations regarding the zeta potential above were further supported using sulfated CNCs, which had a comparatively higher zeta potential than dried-redispersed cCNCs. The lower zeta potential of cCNCs emerged as a distinct advantage over the sulfated CNCs, at least in promoting enhanced shear adhesion.

Further exploration into achieving higher shear adhesion led to a shift in focus on the other factors affecting cCNC reassembly, including the cCNC addition protocol. A comparison of seed and feed stage addition suggested that the latter exhibited less cCNC reassembly, lower cCNC-latex particle aggregation, and lower viscosity, allowing for higher cCNC loadings. PSA performance, including tack, peel strength, and shear adhesion, saw improvements with cCNC addition at both stages. However, consistent with the impact of zeta potential and cCNC reassembly throughout this study, the cCNCs added at the seed stage led to greater cohesive performance compared to when the cCNCs were added at the feed stage.

This study highlights the role of the CNC zeta potential in CNC reassembly into nanofibril-like structures to simultaneously enhance tack, peel strength, and shear adhesion in latex-based PSAs. Other factors contributing to reassembly include the CNC processing conditions (e.g.,

extraction methods, product forms), loading, sonication, and addition protocol. These should all be considered depending on the ultimate nanocomposite application. These considerations can also be extended to other applications such as packaging, sustainable barrier films, and coatings. This work underscores the transformative potential of CNCs, particularly cCNCs, in the development of new nanocomposite applications.

3.6 Acknowledgements

The authors gratefully acknowledge the financial contribution of the Natural Science and Engineering Council of Canada (NSERC) Alliance Grant #ALLRP 560215-20, and Anomera, Inc. Mr. Joseph Costello is acknowledged for his technical assistance with some of the analyses. Assistance with AFM imaging was provided by Rahil Ghalamboland.

3.7 Supporting information

Supporting Information is reproduced in Appendix I, including additional data on preliminary experiments, characterization, and performance property measurements.

3.8 References

(1) Lin, S. B.; Durfee, L. D.; Ekeland, R. A.; McVie, J.; Schalau, G. K. Recent Advances in Silicone Pressure-Sensitive Adhesives. *J Adhes Sci Technol* **2007**, *21* (7), 605–623. https://doi.org/10.1163/156856107781192274.

(2) Wang, Q.; Griffith, W. B.; Einsla, M.; Zhang, S.; Pacholski, M. L.; Shull, K. R. Bulk and Interfacial Contributions to the Adhesion of Acrylic Emulsion-Based Pressure-Sensitive Adhesives. *Macromolecules* **2020**, *53* (16), 6975–6983. https://doi.org/10.1021/acs.macromol.0c01354.

(3) Khan, I.; Poh, B. T. Natural Rubber-Based Pressure-Sensitive Adhesives: A Review. *J Polym Environ* **2011**, *19* (3), 793–811. https://doi.org/10.1007/s10924-011-0299-z.

(4) Jovanović, R.; Dubé, M. A. Emulsion-Based Pressure-Sensitive Adhesives: A Review. *Journal of Macromolecular Science, Part C: Polymer Reviews* **2004**, *44* (1), 1–51. https://doi.org/10.1081/MC-120027933.

(5) Wahdat, H.; Hirth, C.; Johannsmann, D.; Gerst, M.; Rückel, M.; Adams, J. Film Formation of Pressure-Sensitive Adhesives (PSAs) Studied with Förster Resonance Energy Transfer (FRET) and Scattering Intensity. *Macromolecules* **2018**, *51* (12), 4718–4726. https://doi.org/10.1021/acs.macromol.8b00423.

(6) Aguirre, M.; Ballard, N.; Gonzalez, E.; Hamzehlou, S.; Sardon, H.; Calderon, M.; Paulis, M.; Tomovska, R.; Dupin, D.; Bean, R. H.; Long, T. E.; Leiza, J. R.; Asua, J. M. Polymer Colloids: Current Challenges, Emerging Applications, and New Developments. *Macromolecules* **2023**, *56* (7), 2579–2607. https://doi.org/10.1021/acs.macromol.3c00108.

(7) Creton, C.; Ciccotti, M. Fracture and Adhesion of Soft Materials: A Review. *Reports on Progress in Physics* **2016**, *79* (4), 046601. https://doi.org/10.1088/0034-4885/79/4/046601.

(8) Dastjerdi, Z.; Cranston, E. D.; Dubé, M. A. Pressure Sensitive Adhesive Property Modification Using Cellulose Nanocrystals. *Int J Adhes Adhes* **2018**, *81*, 36–42. https://doi.org/10.1016/j.ijadhadh.2017.11.009.

(9) Ouzas, A.; Niinivaara, E.; Cranston, E. D.; Dubé, M. A. In Situ Semibatch Emulsion Polymerization of 2-Ethyl Hexyl Acrylate/n-Butyl Acrylate/Methyl Methacrylate/Cellulose Nanocrystal Nanocomposites for Adhesive Applications. *Macromol React Eng* **2018**, *12* (3), 1–10. https://doi.org/10.1002/mren.201700068.

(10) Ahmadi-Dehnoei, A.; Ghasemirad, S. Designing of Desired Nanocomposite Pressure-Sensitive Adhesives through Tailoring the Structural Characteristics of Polysilsesquioxane-Acrylic Core-Shell Nanoparticles. *Int J Adhes Adhes* **2021**, *111*, 102973. https://doi.org/10.1016/j.ijadhadh.2021.102973.

(11) Khanjani, J.; Zohuri, G. H.; Gholami, M.; Shojaei, B.; Dalir, R. Emulsion Semi-Batch Terpolymerization Process Using Hybrid Emulsifiers for Synthesizing New Emulsion Pressure Sensitive Adhesives (EPSAs). *J Adhes* **2014**, *90* (2), 174–194. https://doi.org/10.1080/00218464.2013.772052.

(12) Udagama, R.; Degrandi-Contraires, E.; Creton, C.; Graillat, C.; McKenna, T. F. L.; Bourgeat-Lami, E. Synthesis of Acrylic−Polyurethane Hybrid Latexes by Miniemulsion Polymerization and Their Pressure-Sensitive Adhesive Applications. *Macromolecules* **2011**, *44* (8), 2632–2642. https://doi.org/10.1021/ma200073d.

(13) Rana, P. K.; Swain, S. K.; Sahoo, P. K. Synthesis, Characterization, and Properties of Intercalated Poly(2-Ethyl Hexylacrylate)/Silicate Nanocomposites: XRD, TEM, IR, TGA,

Superabsorbency, Pressure-Sensitive Adhesion, and Biodegradation. *J Appl Polym Sci* **2004**, *93* (3), 1007–1011. https://doi.org/10.1002/app.20568.

(14) Wang, T.; Lei, C.-H.; Dalton, A. B.; Creton, C.; Lin, Y.; Fernando, K. A. S.; Sun, Y.-P.; Manea, M.; Asua, J. M.; Keddie, J. L. Waterborne, Nanocomposite Pressure-Sensitive Adhesives with High Tack Energy, Optical Transparency, and Electrical Conductivity. *Advanced Materials* **2006**, *18* (20), 2730–2734. https://doi.org/10.1002/adma.200601335.

(15) Czech, Z.; Kowalczyk, A.; Ortyl, J.; Świderska, J. Acrylic Pressure-Sensitive Adhesives Containing SiO_2 Nanoparticles. *pjct* **2013**, *15* (1), 12–14. https://doi.org/10.2478/pjct-2013-0003.

(16) Desroches, G.; Wang, Y.; Kubiak, J.; Macfarlane, R. Crosslinking of Pressure-Sensitive Adhesives with Polymer-Grafted Nanoparticles. *ACS Appl Mater Interfaces* **2022**, *14* (7), 9579–9586. https://doi.org/10.1021/acsami.1c22997.

(17) Moon, R. J.; Martini, A.; Nairn, J.; Simonsen, J.; Youngblood, J. Cellulose Nanomaterials Review: Structure, Properties and Nanocomposites. *Chem Soc Rev* **2011**, *40* (7), 3941. https://doi.org/10.1039/c0cs00108b.

(18) Habibi, Y.; Lucia, L. A.; Rojas, O. J. Cellulose Nanocrystals: Chemistry, Self-Assembly, and Applications. *Chem Rev* **2010**, *110* (6), 3479–3500. https://doi.org/10.1021/cr900339w.

(19) Delepierre, G.; Vanderfleet, O. M.; Niinivaara, E.; Zakani, B.; Cranston, E. D. Benchmarking Cellulose Nanocrystals Part II: New Industrially Produced Materials. *Langmuir* **2021**, *37* (28), 8393–8409. https://doi.org/10.1021/acs.langmuir.1c00550.

(20) Masese, F. K.; Njenga, P. K.; Ndaya, D. M.; Kasi, R. M. Recent Advances and Opportunities for Cellulose Nanocrystal-Based Liquid Crystalline Polymer Hybrids and Composite Materials. *Macromolecules* **2023**, *56* (17), 6567–6588. https://doi.org/10.1021/acs.macromol.3c00369.

(21) Kedzior, S. A.; Marway, H. S.; Cranston, E. D. Tailoring Cellulose Nanocrystal and Surfactant Behavior in Miniemulsion Polymerization. *Macromolecules* **2017**, *50* (7), 2645–2655. https://doi.org/10.1021/acs.macromol.7b00516.

(22) Reid, M. S.; Villalobos, M.; Cranston, E. D. Cellulose Nanocrystal Interactions Probed by Thin Film Swelling to Predict Dispersibility. *Nanoscale* **2016**, *8* (24), 12247–12257. https://doi.org/10.1039/C6NR01737A.

(23) Antoniw, J. M.; Hallman, M. T.; Kiriakou, M. V.; Morse, T.; Cranston, E. D. Colloidal Stability Window for Carboxylated Cellulose Nanocrystals: Considerations for Handling,

Characterization, and Formulation. *Langmuir* **2023**, *39* (30), 10321–10334. https://doi.org/10.1021/acs.langmuir.3c00319.

(24) Gabriel, V. A.; Tousignant, M. N.; Wilson, S. M. W.; Faure, M. D. M.; Cranston, E. D.; Cunningham, M. F.; Lessard, B. H.; Dubé, M. A. Improving Latex-Based Pressure-Sensitive Adhesive Properties Using Carboxylated Cellulose Nanocrystals. *Macromol. React. Eng.* **2022**, *16* (3), 2100051. https://doi.org/10.1002/mren.202100051.

(25) Pakdel, A. S.; Cranston, E. D.; Dubé, M. A. Incorporating Hydrophobic Cellulose Nanocrystals inside Latex Particles via Mini-Emulsion Polymerization. *Macromol React Eng* **2021**, *15* (5), 1–10. https://doi.org/10.1002/mren.202100023.

(26) Pakdel, A. S.; Niinivaara, E.; Cranston, E. D.; Berry, R. M.; Dubé, M. A. Cellulose Nanocrystal (CNC)–Latex Nanocomposites: Effect of CNC Hydrophilicity and Charge on Rheological, Mechanical, and Adhesive Properties. *Macromol Rapid Commun* **2021**, *42* (3), 1–12. https://doi.org/10.1002/marc.202000448.

(27) Niinivaara, E.; Ouzas, A.; Fraschini, C.; Berry, R. M.; Dubé, M. A.; Cranston, E. D. How Latex Film Formation and Adhesion at the Nanoscale Correlate to Performance of Pressure Sensitive Adhesives with Cellulose Nanocrystals. *Philosophical Transactions of the Royal Society A: Mathematical, Physical and Engineering Sciences* **2021**, *379* (2206). https://doi.org/10.1098/rsta.2020.0330.

(28) Czech, Z.; Maciejewski, Z.; Kondratowicz-Maciejewska, K. Water-Borne Pressure-Sensitive Adhesives Acrylics Modified Using Amorphous Silica Nanoparticles. *Polish Journal of Chemical Technology* **2016**, *18* (4), 124–128. https://doi.org/10.1515/pjct-2016-0081.

(29) Lakrout, H.; Creton, C.; Ahn, D.; Shull, K. R. Influence of Molecular Features on the Tackiness of Acrylic Polymer Melts. *Macromolecules* **2001**, *34* (21), 7448–7458. https://doi.org/10.1021/ma0020279.

(30) Ouzas, A.; Niinivaara, E.; Cranston, E. D.; Dubé, M. A. Synthesis of Poly(Isobutyl Acrylate/N-butyl Acrylate/Methyl Methacrylate)/CNC Nanocomposites for Adhesive Applications via in Situ Semi-batch Emulsion Polymerization. *Polym Compos* **2019**, *40* (4), 1365–1377. https://doi.org/10.1002/pc.24869.

(31) Gabriel, V. A.; Champagne, P.; Cunningham, M. F.; Dubé, M. A. In-situ Addition of Carboxylated Cellulose Nanocrystals in Seeded Semi-batch Emulsion Polymerization. *Can. J. Chem. Eng.* **2022**, *100* (4), 767–779. https://doi.org/10.1002/cjce.24299.

(32) Gabriel, V. A.; Cranston, E. D.; Dubé, M. A. Pushing the Limits with Cellulose Nanocrystal Loadings in Latex-Based Pressure-Sensitive Adhesive Nanocomposites. *Macromol. React. Eng.* **2020**, *14* (6), 2000027. https://doi.org/10.1002/mren.202000027.

(33) Gabriel, V. A.; Dubé, M. A. Toward a Fully Biobased Pressure-Sensitive Adhesive. *Ind. Eng. Chem. Res.* **2023**, *62* (1), 478–488. https://doi.org/10.1021/acs.iecr.2c03756.

(34) Antoniw, J. M.; Gabriel, V. A.; Kiriakou, M. V.; Dubé, M. A.; Cunningham, M. F.; Cranston, E. D. Influence of Cellulose Nanocrystal Surface Chemistry and Dispersion Quality on Latex Nanocomposite Stability, Film Formation and Adhesive Properties. *RSC Applied Polymers* **2024**, *2* (2), 262–274. https://doi.org/10.1039/D3LP00244F.

(35) *Pressure Sensitive Tape Council. Test Methods for Pressure Sensitive Adhesive Tapes.*

(36) Dastjerdi, Z.; Cranston, E. D.; Dubé, M. A. Synthesis of Poly(n -Butyl Acrylate/Methyl Methacrylate)/CNC Latex Nanocomposites via In Situ Emulsion Polymerization. *Macromol React Eng* **2017**, *11* (6), 1700013. https://doi.org/10.1002/mren.201700013.

(37) Pakdel, A. S.; Niinivaara, E.; Cranston, E. D.; Berry, R. M.; Dubé, M. A. Cellulose Nanocrystal (CNC)–Latex Nanocomposites: Effect of CNC Hydrophilicity and Charge on Rheological, Mechanical, and Adhesive Properties. *Macromol Rapid Commun* **2021**, *42* (3), 2000448. https://doi.org/10.1002/marc.202000448.

(38) Cherhal, F.; Cousin, F.; Capron, I. Influence of Charge Density and Ionic Strength on the Aggregation Process of Cellulose Nanocrystals in Aqueous Suspension, as Revealed by Small-Angle Neutron Scattering. *Langmuir* **2015**, *31* (20), 5596–5602. https://doi.org/10.1021/acs.langmuir.5b00851.

(39) Gabriel, V. A.; Champagne, P.; Cunningham, M. F.; Dubé, M. A. In-situ Addition of Carboxylated Cellulose Nanocrystals in Seeded Semi-batch Emulsion Polymerization. *Can J Chem Eng* **2021**. https://doi.org/10.1002/cjce.24299.

(40) Parton, T. G.; Parker, R. M.; van de Kerkhof, G. T.; Narkevicius, A.; Haataja, J. S.; Frka-Petesic, B.; Vignolini, S. Chiral Self-Assembly of Cellulose Nanocrystals Is Driven by Crystallite Bundles. *Nat Commun* **2022**, *13* (1). https://doi.org/10.1038/s41467-022-30226-6.

(41) Johns, M. A.; Lam, C.; Zakani, B.; Melo, L.; Grant, E. R.; Cranston, E. D. Comparison of Cellulose Nanocrystal Dispersion in Aqueous Suspension via New and Established Analytical Techniques. *Cellulose* **2023**, *30* (13), 8259–8274. https://doi.org/10.1007/s10570-023-05348-9.

(42) Lowry, G. V.; Hill, R. J.; Harper, S.; Rawle, A. F.; Hendren, C. O.; Klaessig, F.; Nobbmann, U.; Sayre, P.; Rumble, J. Guidance to Improve the Scientific Value of Zeta-Potential Measurements in NanoEHS. *Environ Sci Nano* **2016**, *3* (5), 953–965. https://doi.org/10.1039/C6EN00136J.

(43) Raval, N.; Maheshwari, R.; Kalyane, D.; Youngren-Ortiz, S. R.; Chougule, M. B.; Tekade, R. K. Importance of Physicochemical Characterization of Nanoparticles in Pharmaceutical Product Development. In *Basic Fundamentals of Drug Delivery*; Elsevier, 2019; pp 369–400. https://doi.org/10.1016/B978-0-12-817909-3.00010-8.

(44) Browne, C.; Raghuwanshi, V. S.; Lin, M.; Garnier, G.; Batchelor, W. Characterisation of Cellulose Nanocrystals by Rheology and Small Angle X-Ray Scattering (SAXS). *Colloids Surf A Physicochem Eng Asp* **2022**, *651*, 129532. https://doi.org/10.1016/j.colsurfa.2022.129532.

(45) Raghuwanshi, V. S.; Browne, C.; Batchelor, W.; Garnier, G. Self-Assembly of Cellulose Nanocrystals of Different Lengths. *J Colloid Interface Sci* **2023**, *630*, 249–259. https://doi.org/10.1016/j.jcis.2022.10.100.

(46) Abitbol, T.; Kam, D.; Levi-Kalisman, Y.; Gray, D. G.; Shoseyov, O. Surface Charge Influence on the Phase Separation and Viscosity of Cellulose Nanocrystals. *Langmuir* **2018**, *34* (13), 3925–3933. https://doi.org/10.1021/acs.langmuir.7b04127.

(47) Kedzior, S. A.; Kiriakou, M.; Niinivaara, E.; Dubé, M. A.; Fraschini, C.; Berry, R. M.; Cranston, E. D. Incorporating Cellulose Nanocrystals into the Core of Polymer Latex Particles via Polymer Grafting. *ACS Macro Lett* **2018**, *7* (8), 990–996. https://doi.org/10.1021/acsmacrolett.8b00334.

(48) Liu, Y.; Stoeckel, D.; Gordeyeva, K.; Agthe, M.; Schütz, C.; Fall, A. B.; Bergström, L. Nanoscale Assembly of Cellulose Nanocrystals during Drying and Redispersion. *ACS Macro Lett* **2018**, *7* (2), 172–177. https://doi.org/10.1021/acsmacrolett.7b00964.

(49) Han, J.; Zhou, C.; Wu, Y.; Liu, F.; Wu, Q. Self-Assembling Behavior of Cellulose Nanoparticles during Freeze-Drying: Effect of Suspension Concentration, Particle Size, Crystal Structure, and Surface Charge. *Biomacromolecules* **2013**, *14* (5), 1529–1540. https://doi.org/10.1021/bm4001734.

(50) Qie, L.; Dubé, M. A. Manipulating Latex Polymer Microstructure Using Chain Transfer Agent and Cross-Linker to Modify PSA Performance and Viscoelasticit **y**. *Macromol. React. Eng.* **2011**, *5* (2), 117–128. https://doi.org/10.1002/mren.201000046.

(51) Pakdel, A. S.; Gabriel, V.; Berry, R. M.; Fraschini, C.; Cranston, E. D.; Dubé, M. A. A Sequential Design Approach for in Situ Incorporation of Cellulose Nanocrystals in Emulsion-Based Pressure Sensitive Adhesives. *Cellulose* **2020**, *27* (18), 10837–10853. https://doi.org/10.1007/s10570-020-03060-6.

(52) Wang, Y.; Yao, B.; Chen, H.; Wang, H.; Li, C.; Yang, Z. Preparation of Anisotropic Conductive Graphene Aerogel/Polydimethylsiloxane Composites as LEGO® Modulars. *Eur Polym J* **2019**, *112*, 487–492. https://doi.org/10.1016/j.eurpolymj.2019.01.036.

(53) Zhang, Y.; Cunningham, M. F.; Dubé, M. A. Modification of Adhesive and Latex Properties for Starch Nanoparticle-Based Pressure Sensitive Adhesives. *Macromol. React. Eng.* **2020**, *14* (1), 1900023. https://doi.org/10.1002/mren.201900023.

(54) Fonseca, G. E.; McKenna, T. F.; Dubé, M. A. Miniemulsion vs. Conventional Emulsion Polymerization for Pressure-Sensitive Adhesives Production. *Chem Eng Sci* **2010**, *65* (9), 2797–2810. https://doi.org/10.1016/j.ces.2010.01.017.

(55) Fonseca, G. E.; McKenna, T. F. L.; Dubé, M. A. Preparation of Stable Miniemulsions of Poly(2-Ethyl Hexyl Acrylate-Co-Vinyl Acetate). *Macromol Symp* **2010**, *289* (1), 72–85. https://doi.org/10.1002/masy.200900009.

(56) Guo, H.; Saed, M. O.; Terentjev, E. M. Mechanism of Pressure-Sensitive Adhesion in Nematic Elastomers. *Macromolecules* **2023**, *56* (16), 6247–6255. https://doi.org/10.1021/acs.macromol.3c01038.

(57) Chen, D.; Lawton, D.; Thompson, M. R.; Liu, Q. Biocomposites Reinforced with Cellulose Nanocrystals Derived from Potato Peel Waste. *Carbohydr Polym* **2012**, *90* (1), 709–716. https://doi.org/10.1016/j.carbpol.2012.06.002.

(58) Flauzino Neto, W. P.; Mariano, M.; da Silva, I. S. V.; Silvério, H. A.; Putaux, J.-L.; Otaguro, H.; Pasquini, D.; Dufresne, A. Mechanical Properties of Natural Rubber Nanocomposites Reinforced with High Aspect Ratio Cellulose Nanocrystals Isolated from Soy Hulls. *Carbohydr Polym* **2016**, *153*, 143–152. https://doi.org/10.1016/j.carbpol.2016.07.073.

(59) C. A. Dahlquist. Treatise on Adhesion and Adhesives. In *Oxford University Press*; R. L. Patrick, Ed.; New York, 1969; Vol. 42, pp 219–260.

(60) Khoshkava, V.; Kamal, M. R. Effect of Surface Energy on Dispersion and Mechanical Properties of Polymer/Nanocrystalline Cellulose Nanocomposites. *Biomacromolecules* **2013**, *14* (9), 3155–3163. https://doi.org/10.1021/bm400784j.

(61) Ataeian, P.; Shi, Q.; Ioannidis, M.; Tam, K. C. Effect of Hydrophobic Modification of Cellulose Nanocrystal (CNC) and Salt Addition on Pickering Emulsions Undergoing Phase-Transition. *Carbohydrate Polymer Technologies and Applications* **2022**, *3*, 100201. https://doi.org/10.1016/j.carpta.2022.100201.

(62) Ben Mabrouk, A.; Kaddami, H.; Magnin, A.; Belgacem, M. N.; Dufresne, A.; Boufi, S. Preparation of Nanocomposite Dispersions Based on Cellulose Whiskers and Acrylic Copolymer by Miniemulsion Polymerization: Effect of the Silane Content. *Polym Eng Sci* **2011**, *51* (1), 62–70. https://doi.org/10.1002/pen.21778.

Chapter 4

Enhancing Pressure Sensitive Adhesive Performance Using Acetylated Carboxylated Cellulose Nanocrystals

Parisa Bayat[1], Kelly M. Meek[1,2], Emily D. Cranston[3], Michael Cunningham[4], Pascale Champagne[5], Timothy Morse[6], Arthur Werner[6], Sean George[7], Cecilia Cancellara[3], and Marc A. Dubé[*,1]

[1]Department of Chemical and Biological Engineering, University of Ottawa, Ottawa, ON, Canada, K1N 6N5
[2]Chemical and Material Engineering, Concordia University, Montreal, QC, Canada, H3G 1M8
[3]Department of Wood Science and Department of Chemical and Biological Engineering, University of British Columbia, Vancouver, BC, Canada, V6T 1Z4
[4]Department of Chemical Engineering, Queen's University, Kingston, ON, Canada, K7L 3N6
[5]Energy Mining & Environment Research Centre, National Research Council, Montreal, QC, Canada, K1A 0R6
[6]Anomera Inc., Montreal, QC, Canada, H3B 1A7
[7]BASF Corp., Charlotte, NC, United States, 28273

This chapter is a manuscript published in Industrial & Engineering Chemistry Research (2025, 64, 9, 4932–4941)

4.1 Abstract

Carboxylated cellulose nanocrystals (cCNCs) were acetylated to varying degrees of substitution to enhance their compatibility with the hydrophobic acrylic polymer matrix in pressure-sensitive adhesives (PSAs). The contact angle measurements showed the transition of the cCNCs from hydrophilic to hydrophobic properties. The least hydrophilic acetylated cCNCs, with a degree of substitution of 0.42, significantly enhanced PSA performance, improving tack, peel strength, and shear adhesion, compared to the base formulation and that with unmodified cCNCs. The findings emphasize the crucial role of nanoparticle dispersion, where lower interfacial tension leads to improved dispersion and enhanced latex particle coalescence during film drying, consequently yielding, superior mechanical, thermal, and barrier properties of the nanocomposite PSAs. Overall, the ability to fine-tune the degree of substitution of the acetylated cCNCs points to their broader potential applications in coatings, hydrogels, and other advanced materials, allowing for adjustments in hydrophilicity to match specific application needs.

KEYWORDS: Pressure sensitive adhesive, Modification, Cellulose Nanocrystal, Cellulose, Emulsion, Acetylation

4.2 Introduction

Acrylic pressure-sensitive adhesives (PSAs) are highly adaptable adhesives made from viscoelastic polymers possessing a low glass transition temperature (T_g) (typically < 0 °C), enabling them to bond to solid surfaces with minimal pressure.[1] Adhesive performance is mainly assessed according to three characteristics: tack, peel strength, and shear adhesion.[2] So-called "soft" monomers (low T_g) contribute the natural tack required for substrate adhesion but may lack adequate cohesive (internal) strength. Consequently, "hard" monomers (high T_g) are incorporated to enhance the adhesive's cohesive strength.[2] Environmental concerns have led to the use of water-based synthesis approaches (i.e., emulsion polymerization) rather than the environmentally hazardous solvent-based approaches, albeit frequently with a performance trade-off.[3–5]

The combination of emulsion polymerization and a bio-based nanomaterial, such as starch nanoparticles,[6] lignin nanoparticles,[7] and cellulose nanocrystals (CNCs),[8,9] has led to more sustainable PSA production with improved mechanical, rheological, thermal, and barrier properties.[3,10] CNCs have emerged as superior substitutes for other nanoparticles, offering reduced health risks, cost-effectiveness, biocompatibility, high aspect ratios, and impressive mechanical properties.[11,12] CNCs, typically derived from wood pulp, are isolated from cellulose microfibrils using controlled acid-hydrolysis, with their surface functional groups determined by the acid utilized during extraction.[11] Recently, a sustainable technique involving hydrogen peroxide oxidation to replace hydroxy groups with carboxylate groups to create carboxylated CNCs (cCNCs) has been developed.[13,14] It should be noted that heretofore when we use the term CNCs we are referring to all CNC types, whereas when cCNC is used, we are specifically referring to the carboxylated form.

Our recent work has demonstrated how cCNC/latex nanocomposite films outperform PSA base case formulations for all adhesive properties (i.e., tack, peel strength, and shear adhesion).[8,15] In addition, the latex viscosity increased with cCNC loading, suggesting that the cCNCs were not located within the latex particles,[16] which was also confirmed with AFM studies.[17] Interestingly, the literature points to an increased likelihood for reassembly of cCNCs into nanofibril-like structures

when they are incorporated into PSA formulations.[17,18] The effect of cCNC reassembly on high-performance latex-based PSAs was examined in our previous study.[8] It was shown that cCNC reassembly was correlated with a reduced zeta potential, which eventually contributed to a considerable improvement in PSA performance, particularly shear adhesion.[8]

While the simultaneous improvement of three PSA properties and utilizing the hydrophilic nature of cCNCs for emulsion polymerization offer promising advantages,[16,19] their hydrophilicity presents challenges in dispersing them into nonpolar hydrophobic polymeric matrices.[20–22] Previous research demonstrated how the incorporation of partially hydrophilic CNCs in conventional emulsion polymerization improved PSA performance compared to unmodified, hydrophilic CNCs.[23] However, the use of highly hydrophobic CNCs inside polymer particles in a mini-emulsion polymerization led to the deterioration of all three key PSA performance properties.[19] In those studies, the exact nature of the hydrophobic modifications to the CNCs was unknown due to proprietary reasons.[19,23]

Numerous chemical modification strategies including grafting,[24] esterification,[25] alkylation,[26] and cationic modification[27], have been used to improve the mechanical and adhesive properties of polymers and to regulate CNC dispersion in hydrophobic latexes.[25,28–30 2427]One CNC esterification technique of interest in this study, acetylation, introduces acetyl functional groups ($COCH_3$) to the CNC surfaces through the condensation of a carboxylic acid group and a hydroxy group.[29,30 31,32]A decrease in the negative surface charge on the acetylated CNCs due to the substitution of the hydroxy (OH) groups was confirmed via zeta potential measurements.[31–33] Based on our recent work,[8] we hypothesize that the less hydrophilic cCNCs have a lower zeta potential, which should lead to more nanofibril-like structures and enhance PSA performance.

Finally, a straightforward and environmentally benign acetylation process[32] enables us to decrease the hydrophilicity of cCNC surfaces and quantify that hydrophilicity via zeta potential measurements. As a result, a range of cCNCs with varying propensity towards reassembly in the latex will be produced in a controlled manner. These cCNCs are then incorporated into a 2-ethyl hexyl acrylate (2-EHA), methyl methacrylate (MMA) and styrene (STY) PSA formulation to observe their impact on latex properties and nanocomposite adhesive performance.

4.3 Experimental

4.3.1 Materials

The monomers 2-ethyl hexyl acrylate (2-EHA), styrene (STY), and methyl methacrylate (MMA) were purchased through Sigma-Aldrich (Oakville ON, Canada) and purified by passing them drop-wise through an inhibitor removal column. The anionic and non-ionic surfactants were, respectively, Dowfax 2A1 (alkyldiphenyloxide disulfonate, from Dow Chemical Co., Midland MI, US) and Triton X-405 (poly(ethylene glycol tert-octylphenyl ether), from Sigma-Aldrich). The radical initiator used was sodium persulfate (NaPS) and the buffer was sodium bicarbonate. De-ionized distilled water (DIW) with a resistivity of 18.0 ± 0.2 MΩ cm was utilized for synthesis and characterization. A spray-dried powder of cCNCs in the sodium-salt form (Dextracel^{TM} COOH content of 0.22 mmol.g^{-1}) was donated by Anomera Inc. (Montreal QC, Canada). Ethanol (purity > 99%), acetone (purity >99%), acetic anhydride (ACS REAGENT, >98.0%) and iodine (ACS REAGENT, >99.8%) used for the modification of the cCNCs, were provided from Sigma-Aldrich. Other solvents used for characterization (e.g., tetrahydrofuran (THF, HPLC)) were purchased from Sigma-Aldrich. All materials were used as received without further purification/modification unless otherwise specified.

4.3.2 cCNC acetylation

Following the protocol of Abedi et al.[32], cCNCs were acetylated in a controlled process. A mixture containing 0.57 g of cCNCs, 9 mL of acetic anhydride, and varying amounts of iodine as catalyst (0.02, 0.04, 0.06, and 0.08 g) was agitated at 100 °C for 10 minutes in a glass vial equipped with a magnetic stirrer. After the reaction mixture had cooled to room temperature, it was agitated for 15 minutes using 0.9 mL of acetone. A 75% volume ethanol/DIW solution (60 mL) was then added, and the mixture was agitated for ten minutes. A neutral pH suspension of acetylated cCNCs (AcCNCs) was obtained by three cycles of centrifugation and washing using DIW (80 mL each cycle). Finally, the AcCNCs were dispersed in DIW (10 mL) and freeze-dried for 48 hours at -70 °C. The degree of substitution of acetylation was evaluated via FTIR spectroscopy.[31]

4.3.3 cCNC dispersion

The cCNCs or AcCNCs were dispersed in the DIW allocated to the seed stage (Table 4.1) and mixed on a magnetic stir plate overnight. Subsequently, the dispersions underwent three cycles of 5-minute on/off sonication at 75% amplitude using a Fisher Scientific 550 sonic dismembrator. During sonication, the sample temperature was maintained near 0 ^{o}C using an ice bath. Subsequently, the sonicated dispersion was filtered three times with Whatman filter paper (Grade 50, 110 mm diameter, 2.7 µm) to remove any metals that may have leached from the sonicator probe tip.

Table 4.1. Seeded semi-batch emulsion-based PSA formulation

Component	Seed stage	Feed stage	Total
EHA/MMA/STY:90/8/2 (w/w/w)	20 g	180 g	200 g
cCNCs/AcCNCs	0-0.5 phm	-	0-0.5 phm
Dowfax 2A1	0.13 phm	0.53 phm	0.66 phm
Triton X-405	0.07 phm	0.27 phm	0.34 phm
Sodium persulfate (NaPS)	0.08 phm	0.72 phm	0.8 phm
Buffer	0.028 phm	0.252 phm	0.56 phm
Water	195 g	105 g	300 g

*phm: mass parts per hundred parts monomer

4.3.4 PSA synthesis

The production of PSAs via seeded semi-batch emulsion polymerization was outlined in our earlier work.[8] The reaction formulation is shown in Table 4.1. Briefly, the process involved adding the surfactants into the cCNC/AcCNC DIW dispersion, stirring by magnetic stirrer for ~5 min and charging the dispersion to a 1.25 L stainless steel reactor (Mettler Toledo LabMax Automatic Lab Reactor), under a nitrogen blanket. Upon reaching the set point temperature (80°C) and the desired reactor mixing speed (250 rpm), 10% of the total monomer mixture and initiator solution were added to the reactor to initiate the seed polymerization for 30 min. The remaining 90% of the

monomer was fed in the form of a pre-emulsion (i.e., monomer, surfactant and DIW), pre-mixed with surfactants and DIW into the reactor via a pump over 240 min. A parallel feed pump supplied 90% of the initiator solution (i.e., NaPS and buffer in DIW) for a total of 270 min (30 min longer than the pre-emulsion feed). After the feed stage, a redox initiation system was added as a shot to the reaction mixture and the reaction conditions were maintained for an additional 30 min (final cook stage) to ensure the complete reaction of any residual monomer. Samples were taken periodically throughout the reaction and tested for monomer conversion, pH, and particle size and distribution. The final latex was characterized for conversion, pH, particle size and distribution, viscosity, gel content, and PSA testing (i.e., loop tack, peel strength, shear adhesion). Selected dry final latex films were imaged using AFM.

4.3.4 cCNC characterization

An Agilent Cary 630 FTIR spectrometer (Agilent Technologies, Santa Clara CA, US) with a diamond attenuated total reflectance technique (ATR-FTIR) was used to determine the degree of acetylation at a resolution of 16 cm^{-1} over a range of wave numbers between 650 and 4000 cm^{-1} using the MicroLab Expert software. For quantitative analysis, the spectra were normalized to the C-O stretching vibration at 1060 cm^{-1}. [31] The percent ratio of grafted acetyl groups relative to the total number of OH groups in the cCNCs (Ac/OH%) was determined via the calculation of the $I_{C=O}/I_{C-O}$ peak height ratio, which represents the ratio of the intensity of the C=O stretching of the grafted acetyl group (at 1740 cm^{-1}) to that of the C–O stretching of cellulose (at 1060 cm^{-1}). The peak heights at 1740 cm^{-1} ($I_{C=O}$) and 1060 cm^{-1} (I_{C-O}) were calculated using a baseline constructed between 1790 and 1690 cm^{-1}, and between 1500 and 860 cm^{-1}, respectively. The wt.% acetylation was calculated using

$$wt.\%\ acetyl = \frac{I_{C=O}/I_{C-O}}{0.0282} \qquad (4.1)$$

The constant 0.0282 in Equation 4.1 was derived from calibration curves by Tinguat et al.[34] for commercial cellulose acetate samples. This equation has been widely used for the determination of the percentage of acetyl groups in cellulosic materials.[31] The wt.% acetyl is a measure of the percentage of acetyl groups per anhydroglucose unit in the cCNCs. The percent ratio of the number of acetyl groups to the total number of OH groups in the cCNCs, Ac/OH%, can then be calculated from [31,34]

$$Ac/OH\ \% = \frac{(wt.\%\ acetyl \times 162)}{(3\times 43)} \quad (4.2)$$

where the molecular weight of the anhydroglucose unit (162 g mol^{-1}), the molecular weight of the acetyl group (43 g mol^{-1}) and the number of available OH groups per anhydroglucose unit (3) are used. To calculate the degree of substitution (DS) of acetyl groups, the following equation was used[35]:

$$DS = \frac{162 * \mathrm{Ac/OH\%}}{4300 - 42 * \mathrm{Ac/OH\%}} \quad (4.3)$$

where 4300 (g mol^{-1}) is the molecular weight of the acetyl group multiplied by 100, and 42 g mol^{-1} is the molecular weight of the acetyl group minus 1.[35] Because only the hydroxy groups located at the cCNC surfaces are accessible for acetylation, the DS provided by Equation 3 should only be considered as an "apparent DS". For the purposes of the current work, it was deemed sufficient to demonstrate that the cCNCs were acetylated to different degrees. To quantify the exact DS on the cCNC surfaces, one could use a titration method, but this would require more time and could lead to greater analytical error.[36] Alternatively, the number of accessible hydroxy groups compared to the number of inaccessible ones could be estimated using AFM techniques, which would require significant additional effort.[37]

Solid-state ^{13}C-NMR spectra of cCNCs and AcCNCs were used to qualitatively confirm the different DS. The spectra were obtained at a frequency of 200 MHz with an MAS rate of 4.5 kHz at room temperature using a Bruker AVANCE III 400 NMR spectrometer with a single crystal solid-state probe. All spectra were recorded with a contact time of 2000 µs and a repetition time of 2 s. The acquired data were processed using Bruker TopSpin software. The sessile water contact angles of the cCNC and AcCNC dried powders were measured using a VCA Optima surface analysis system (AST Products, Inc., Billerica, MA). The pressed disc samples were prepared using a hydraulic press at 10 MPa pressure for 1 minute to ensure a smooth and flat surface. The discs were then stored in a desiccator before measurement to prevent moisture absorption. At least 20 droplets (1 µL) of DIW in at least seven different locations on each sample were tested at ambient temperature. Each droplet was allowed to settle for 5 seconds before measurement to ensure consistent spreading behavior. The reported values represent the average of all measurements.

Dynamic light scattering (DLS) was used to measure the apparent hydrodynamic particle sizes (Z-average particle size) and distribution of cCNC and AcCNC dispersions in DIW after probe sonication at three 5-minute intervals at 75% amplitude. Using a Malvern Zetasizer 2000, the polydispersity index and particle size of diluted samples were measured at room temperature (25 ^{o}C) up to a concentration of 0.025 wt.% without the addition of salt. Every measurement was done three times, and the numbers shown are the averages. A zeta analyzer (Zetasizer PSS0012-22, Malvern Instruments), assuming Smoluchowski behavior, was used to identify the cCNC and AcCNC surfaces' zeta potential and surface charge. The cCNCs and AcCNCs were probe-sonicated and dispersed in DIW at a concentration of 0.25 weight percent with 10 mM NaCl prior to surface potential analysis. Every measurement was done three times, and the numbers shown are the averages.

4.3.5 Latex characterization

The latex was sampled at 30 min and 1 h and collected every hour thereafter to measure the solids content and instantaneous and overall monomer conversion (via gravimetry), pH (using a Fisher Scientific/Accumet Research AR50 Dual Channel pH meter), and particle size and distribution (using a Malvern Zetasizer 2000). The final latex was analyzed for viscosity (using a Thermo Scientific HAAKE Viscotester (Model D) using spindle R2 or R3 at 100 rpm). Gel content was measured in all final latexes using Millipore's Durapore™ membrane pouch to heat seal approximately 0.03 g of polymer. Each pouch was soaked in THF for 8 hours before gently shaking for 12 hours. The gel content was estimated after drying of pouches to a consistent weight. Details on the above methods are reported elsewhere.[8] Atomic force microscopy (AFM) height imaging of latexes was done using spin-coated 100x diluted samples (0.4 wt.%) solids on Piranha-cleaned wafers. In-phase AFM imaging was performed on spin-coated undiluted latex samples (40 wt.% solids). AFM images were captured using AC160 probes (nominal spring constant 26 N/m, measured spring constant 29.57-49.88 N/m). The resolution of the measurements was 512 points per line for height imaging.

4.3.6 Adhesive characterization

Dried films from the final latexes with a dry film weight of 20±2 g/m^2 were used for the PSA tests, i.e., tack, peel strength and shear adhesion, according to the PSTC-16, PSTC-101, and PSTC-107 standards, respectively.[38] Films were cast on 30 µm corona-treated Mylar sheets using a #30 Meyer rod and conditioned at 50% relative humidity and room temperature. In the tack test, 1" x 6" strips with taped ends were looped over the upper grip of an Instron tester. A stainless-steel substrate on the lower grip, measuring 1" x 1", was used. The upper grip was lowered at a rate of 2 mm/s until an area of 1” × 1” of a stainless-steel substrate mounted on the lower grip was covered and then raised at specific speed of at a rate of 5 mm/s, recording the maximum force (N/m) required for detachment as tack. Peel strength was measured by recording the average force required for separating 1" x 5" strips of adhesive from a stainless-steel substrate at a 180° angle. A custom shear tester assessed the duration a PSA strip could withstand a constant vertical force. 1" x 5" strips were affixed to a stainless-steel substrate using a roll coater (2040 g) as in peel strength testing. A 500 g weight was hung from the strip using a C-clamp. The time (h) until cohesive failure (i.e., the weight dropped) was recorded as shear adhesion. Each of the three tests were conducted six times for each latex film, and average results with standard deviations were reported. All tack and peel strength measurements resulted in adhesive failure.

4.4 Results and discussion

4.4.1 cCNC acetylation

The cCNCs were acetylated using the technique described earlier, and their degree of acetylation (or degree of substitution, DS) was controlled by varying the iodine content in the process (Table 4.2). The DS was determined using ATR-FTIR and calculated according to Equations 4.1-4.3. Recall that the DS is an “apparent DS” corrected for the surface hydroxy groups available for acetylation. The DS indicates the average number of acetyl groups replacing hydroxy groups on the cCNC surface, with a maximum DS of 3.[39] From Table 4.2, DS is shown to increase with iodine concentration. The acetylation reaction is depicted in Figure 4.1. The ATR-FTIR spectra (Figure 4.2) show increases in absorption at the carbonyl (C=O) (1750 cm^{-1}), methyl (C–H) (1370 cm^{-1}), and acetyl

(C–O) (1240 cm^{-1}) group stretching vibrations due to the acetylation reaction (Figure 4.1), and a decrease in the anhydroglucose hydroxy group (O–H) (3300 and 1643 cm^{-1}) absorbance, giving a clear indication of successful acetylation. The acetylation process did not alter the basic cellulose structure of the cCNCs, with the −CH bending (1352 cm^{-1}) and C–O stretching (1220 and 1026 cm^{-1}) peaks remaining unchanged with increased iodine content (Figure 4.2). These results were confirmed qualitatively using ^{13}C-NMR spectroscopy (Figure 4.3). The chemical shifts for cCNC, C1 (105 ppm), C4 (89 ppm), C2, C3, C5 (72 and 75 ppm), and C6 (65 ppm) were unchanged with DS.[40] The peaks at 172 and 21 ppm, which correspond to the methyl (C–H) and (C–O) groups of the acetyl ester, respectively, confirm the increase in DS with iodine content.

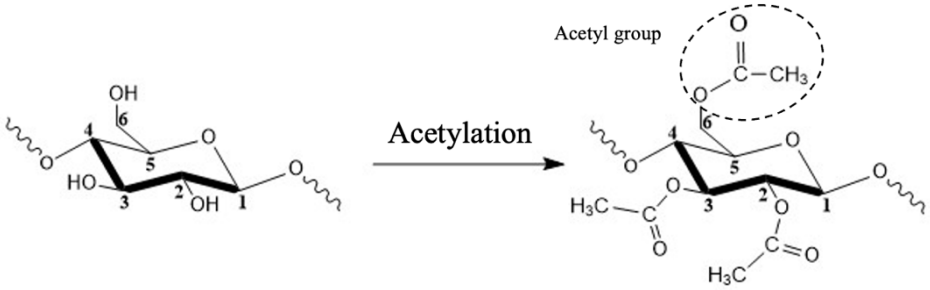

Figure 4.1. Acetylation of cCNC.

Table 4.2. Characterization of cCNC and AcCNCs with varying degree of acetylation (DS).

cCNC type	Iodine content (g)	DS	Contact angle (°)	Zeta potential (mV)	Particle size (nm)
cCNC	0	0	30±2	-34.4	67.5±0.2
0.06-AcCNC	0.02	0.06	60±4	-30.0	71.7±0.5
0.10-AcCNC	0.04	0.10	80±3	-26.2	80.7±1.5
0.25-AcCNCs	0.06	0.25	90±2	-23.3	151.0±0.3
0.42-AcCNCs	0.08	0.42	101±4	-20.0	173.0±1.0

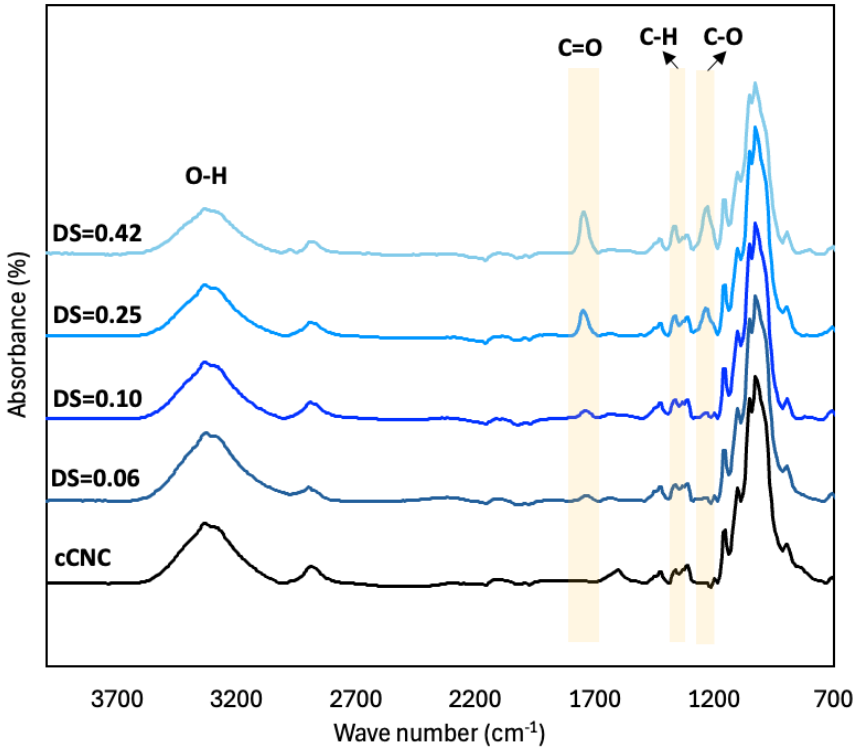

Figure 4.2. ATR-FTIR spectra of cCNC and AcCNC with varying DS.

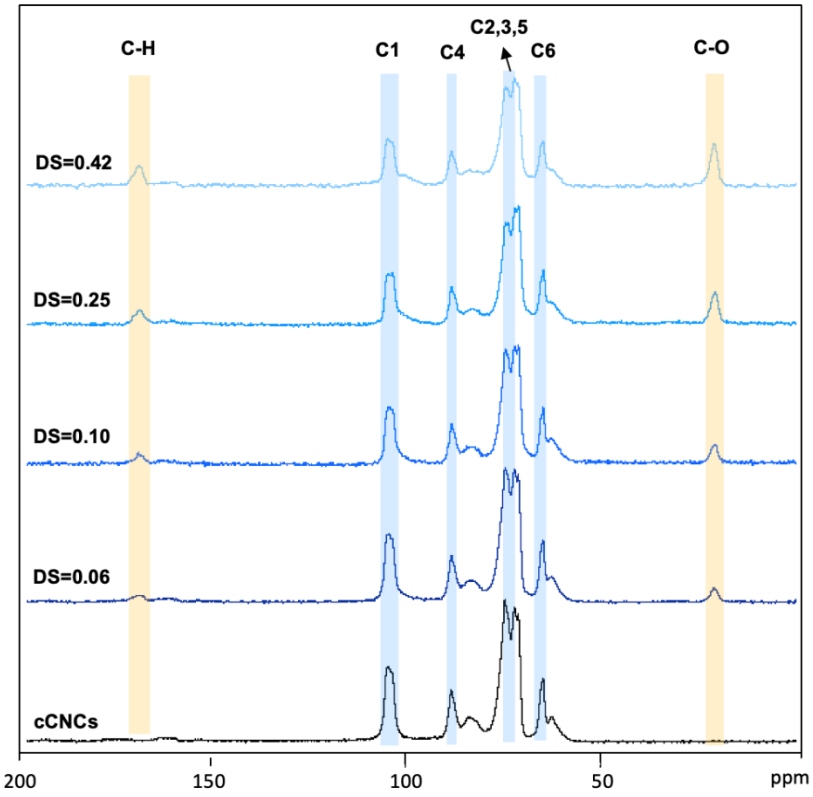

Figure 4.3. ^{13}C-NMR spectra of cCNC and AcCNC with varying DS.

The water contact angle of cCNC and AcCNC films ranged from 30° for cCNC to 101° for 0.42-AcCNC, indicating decreased hydrophilicity with increasing DS, ultimately transitioning to the hydrophobic range (contact angle > 90°).[41] The effect of iodine content on the surface charge density of the AcCNCs was quantified using zeta potential measurements. The zeta potential of the cCNCs decreased in magnitude from -34.4 mV to -20.0 mV after acetylation, attributed to a decreased negative surface charge density due to the substitution of neutral methyl groups.[40,42] The decrease in surface charge led to increased aggregations between AcCNC particles compared to the cCNC particles. This was confirmed by the increase in apparent particle size from 67.5 nm (cCNC) to 173.0 nm (0.42-AcCNC) (Table 4.2). This was another indication of decreased hydrophilicity. Abedi et al. previously dispersed AcCNCs of increasing DS in n-hexane and showed how the average particle size decreased with decreasing hydrophilicity.[32] This suggests that in a mixed-phase environment such as emulsion polymerization, the AcCNCs should disperse better with increasing hydrophobicity due to the presence of the organic polymer particle phase.

Both cCNCs and AcCNCs with varying degrees of substitution (DS) were dispersed in deionized water (DIW) at 0.5 phm to observe partitioning in the water or monomer phase. While both cCNCs and AcCNCs could be dispersed in DIW (Figure 4.4a), the observed clearer dispersion of cCNCs suggests a stronger affinity to DIW (hydrophilicity) compared to the AcCNCs with increasing DS. The difference between the acetylated cCNC samples before sonication was not initially apparent. After sonication (Figure 4.4b), the higher DS samples appeared more opaque, consistent with their larger particle sizes and degrees of aggregation (Table 4.2). Next, monomer, at the same concentrations as in the formulation (Table 4.1), was added to each vial. The vials were shaken and vortexed. The higher DS correlates with a greater likelihood of partitioning at the interface, as shown by the diminishing transparency in the monomer phase and a larger water/monomer interface (Figure 4.4c).

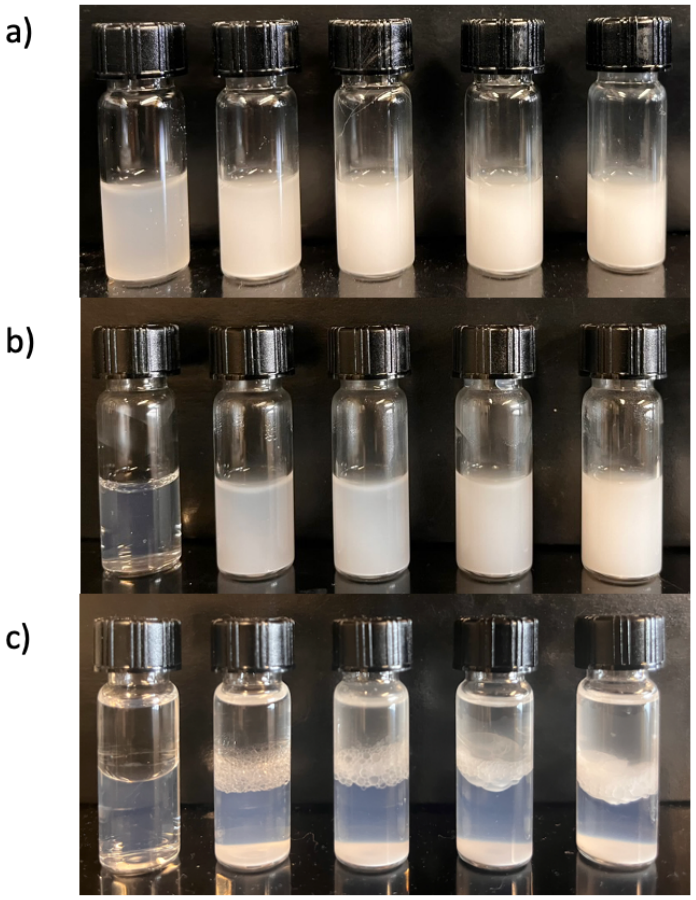

Figure 4.4. Visual observation of dispersion of cCNCs/AcCNCs with increasing DS (from left to right: 0, 0.06, 0.10, 0.25, and 0.42, respectively) in DIW (a) before sonication, (b) after sonication, and (c) after monomer addition and vortexing.

4.4.2 Latex characterization

Table 4.3 details the final latex characterization results for the in-situ incorporation of cCNCs or AcCNCs into the PSA formulation at a concentration of 0.5 phm. The overall and instantaneous monomer conversions for all runs, both with cCNCs and AcCNCs, followed similar trajectories, ultimately achieving final conversions greater than 99 wt.%; the solids content was ~40 wt.%. Conversion and pH plots are shown in the Appendix II.

Table 4.3. Final latex characterization results

Latex ID	Particle size (nm)	PDI	Viscosity (mPa s)	Zeta potential (mV)	Gel content (%)
Base case	173 ±0.7	0.010	60 ±3	-62.1	43 ±7
cCNC-PSA	200 ±0.4	0.270	270 ±5	-84.2	60 ±9
0.06-AcCNC-PSA	171 ±3.0	0.030	40 ±2	-79.0	60 ±12
0.10-AcCNC-PSA	180 ±0.7	0.020	39 ±2	-77.4	55 ±10
0.25-AcCNC-PSA	180 ±0.7	0.014	38 ±3	-73.0	53 ±3
0.42-AcCNC-PSA	185 ±2.0	0.003	34 ±2	-64.3	50 ±7

In comparison to the base case formulation, the addition of cCNCs increased the latex particle size, polydispersity index (PDI), viscosity, and gel content (Table 4.3). The increased particle size was due to some minor aggregation of the polymer particles resulting from the repulsive forces between the cCNCs and the polymer particles, as discussed in an earlier study.[8] Further evidence of this phenomenon was the increased PDI and the presence of a bimodal particle size distribution, compared to the monomodal distribution for the base case. As a result, the latex viscosity increased significantly. In contrast, the AcCNC-based formulations exhibited particle sizes like those of the base case formulation and similarly exhibited monomodal distributions (low PDI). As a result, the AcCNC-based formulations exhibited comparatively low latex viscosities. This suggests a far lower degree of repulsive forces between the AcCNCs and the polymer particles and, thus, lower particle-particle aggregation, which aligns with the zeta potential measurements of the final latexes (Table 4.3). The particle size trajectories for all runs showed non-significant differences in particle size after the seed stage, with the differences only manifesting towards the end of the polymerization (see Appendix II). The observed rise in gel content is likely due to the formation of 3D cCNC structures, which physically entrap polymer chains or swell during testing.[43] A statistically significant trend in gel content measurements with respect to DS was not observed.

4.4.3 PSA characterization

Incorporating cCNCs or AcCNCs into a high-performance latex-based PSA formulation resulted in the *simultaneous* improvement of all three key adhesive performance measures: tack, peel strength, and shear adhesion (Figure 4.5 and 4.6). One should recall that PSA properties often trend in opposing directions; for example, increases in tack and peel strength are often compensated by decreases in shear adhesion.[24] While the commercial formulation showed marginally higher tack and shear adhesion compared to the base case with slightly lower peel strength, these differences were not statistically significant (Figure 4.5 and 4.6).[8,15]

In the cCNC-latex nanocomposite films, the tack and peel strength increases (tack = 133% increase, peel strength = 12% increase) were attributed to improved wettability and higher latex elasticity imparted by the hydrophilic cCNCs (Figure 4.5).[8] The reassembly of cCNCs in the dried latex films led to a higher "apparent" aspect ratio of the cCNC dimensions; that is, the cCNCs tend toward reassembling as nanofibril-like structures.[8] Coupled with increased polymer-cCNC entanglements, this resulted in higher cohesive strengths and, thus, remarkably higher shear adhesion (1350% increase) (Figure 4.6).[8] The incorporation of the most hydrophilic of the AcCNCs (DS = 0.06) led to a decrease in tack, peel strength and shear adhesion compared to the cCNCs. Nonetheless, all three performance measures for the lowest DS AcCNC still exceeded that of the base formulation. With increasing DS, all three measures increased and eventually surpassed the performance of the cCNC-latex nanocomposite films once the AcCNCs crossed the threshold of being considered hydrophobic (contact angle >90^{o}, DS = 0.42).[41] Thus, in comparison to the base formulation, the best AcCNC (DS = 0.42) adhesive performance gave a 251% increase in tack, a 66% increase in peel strength, and a 1650% increase in shear strength. Even in comparison to the commercial latex, the 0.42-AcCNC-PSA adhesive performance increased by 129% (tack), 162% (peel strength), and 438% (shear adhesion). This highlights the importance of the compatibility of the nanoparticle with the polymer matrix as an additional factor to significantly enhance PSA performance.[8,15]

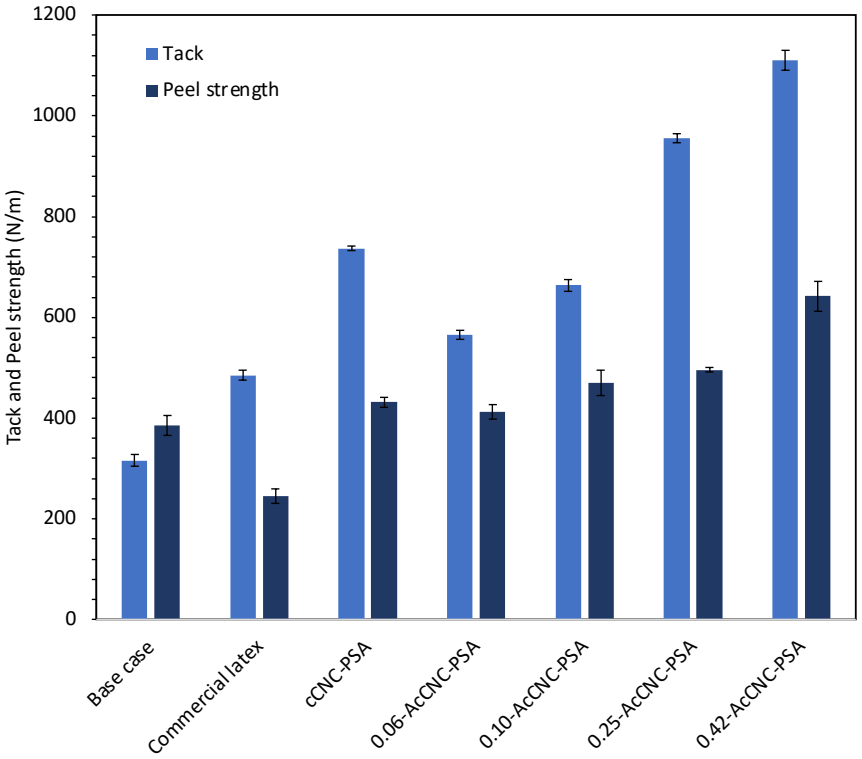

Figure 4.5. Effect of acetylation on tack and peel strength

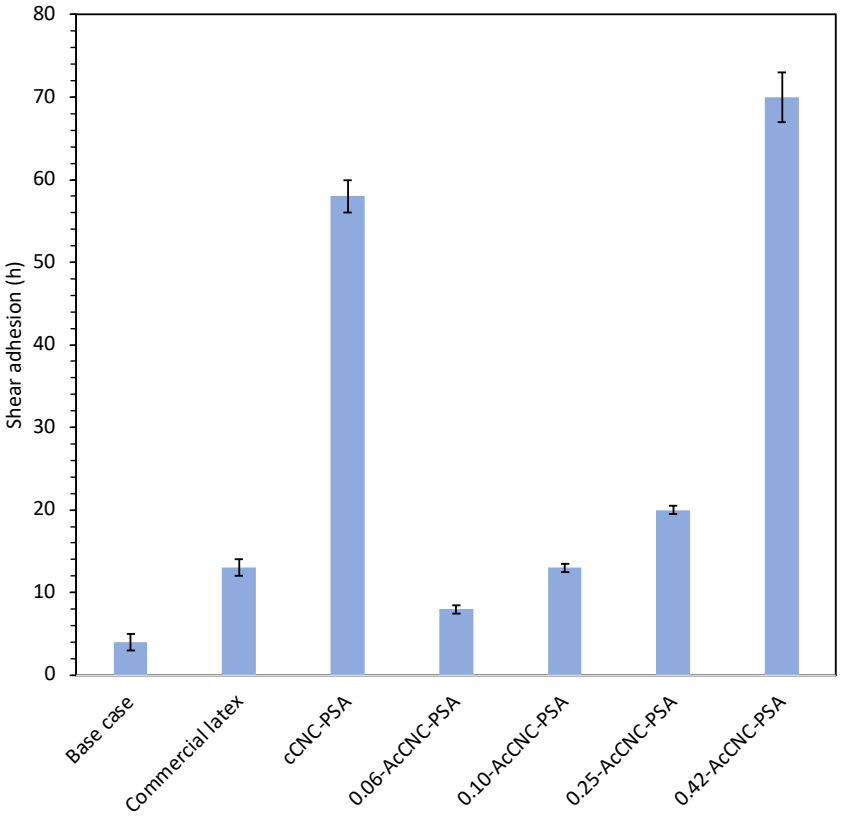

Figure 4.6. Effect of acetylation on shear adhesion.

To further explain the changes in adhesive performance after the addition of cCNCs or AcCNCs, it is useful to schematically illustrate the relationship between the cCNCs and latex particles from synthesis to film formation (Figure 4.7). A similar schematic was described for cCNCs previously.[8] Because they are hydrophilic, the cCNCs were principally located in the water phase, albeit near the polymer particle surfaces, rather than within the particles (Figure 4.7a).[18] The cCNCs were repelled from the latex particles due to their more hydrophilic nature and surface charge (Table 4.2). The hydrophilic cCNCs tended to aggregate in the water phase, and evidence of this is seen in this system's high latex viscosity (Table 4.3). As mentioned, the cCNC nanocomposite latex exhibited a bimodal particle size distribution and this provided the greatest contribution to the viscosity increase. On the other hand, the AcCNCs were increasingly less hydrophilic with increasing DS, up to the point of being considered hydrophobic for DS = 0.42 (Table 4.2). Thus, with decreasing hydrophilicity and lower surface charge (Table 4.2), the AcCNCs tended to reside increasingly closer to the particle surfaces up to the hydrophobic AcCNCs, which interacted more directly with the polymer particles (Figure 4.7b-e). This, in turn, resulted in less AcCNC aggregation and improved dispersibility in the latex. In addition, the AcCNC nanocomposite latexes had a monomodal particle size distribution and exhibited significantly lower latex viscosities (Table 4.3).

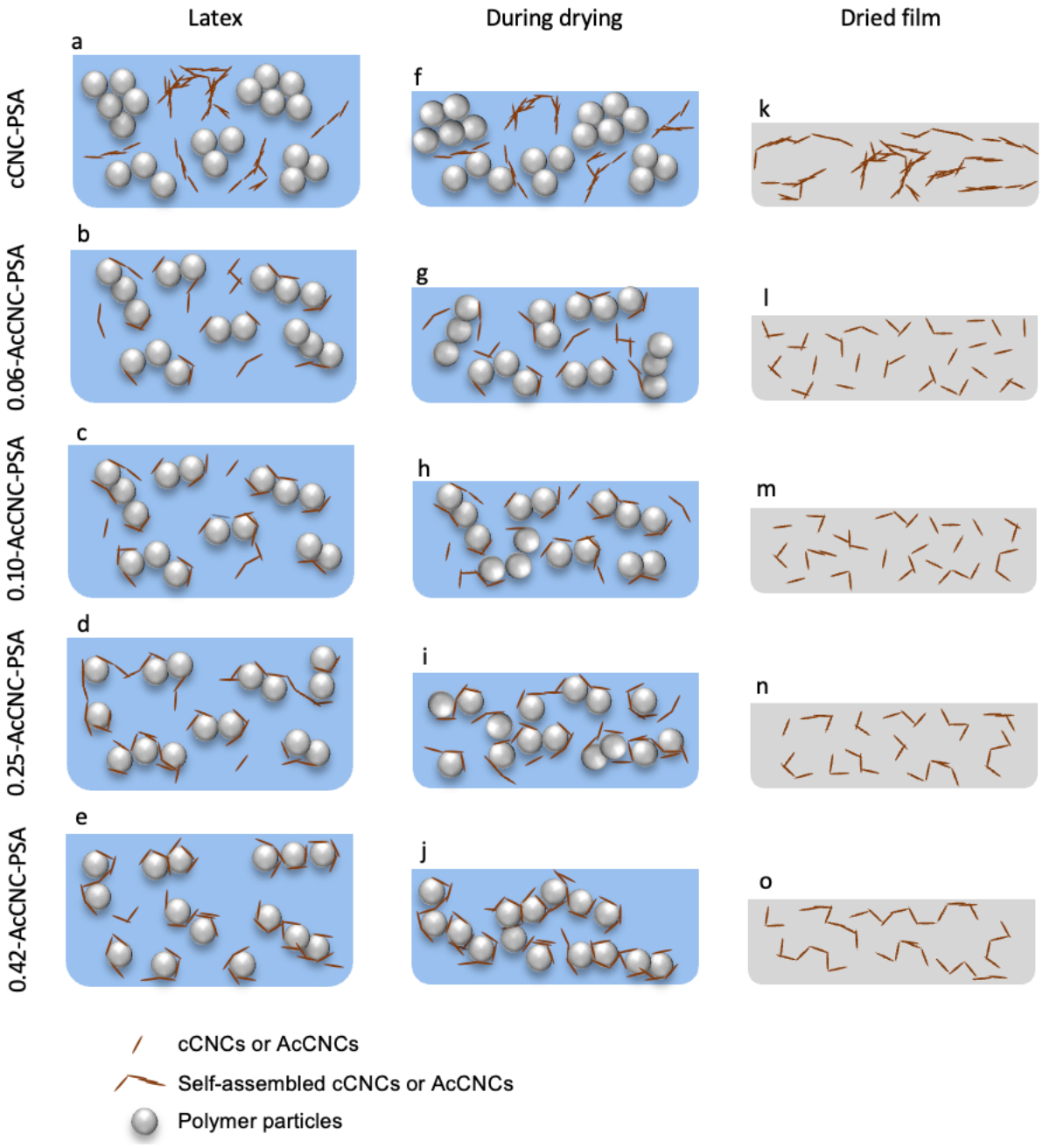

Figure 4.7. Schematic of cCNC (a-c) and AcCNC (d-o) location relative to latex particles and cCNC/AcCNC reassembly during film formation. (Note: CNCs are shown larger than actual size for clarity).

During the film casting and drying process, water evaporated from the cast films and the polymer particles began to pack together (Figure 4.7f-j). For the cCNC nanocomposite latexes, the cCNC aggregates persisted and maintained a fibril-like structure (Figure 4.7f). In other words, the apparent aspect ratio of the cCNCs was quite high. For the AcCNC nanocomposites, the particle packing entrained the AcCNCs and induced their reassembly during the drying process, while maintaining an even AcCNC distribution throughout the drying latex (Figure 4.7g-j).

In the dried films, the cCNCs and AcCNCs adopted the structure imposed by the packed particles and their original degree of interaction with the particles (Figure 4.7k-o). Thus, in the case of the cCNCs, the cCNC aggregates were retained in the dried films. These long cCNC self-assemblies allowed the cCNCs to act as nanofibrils and impart significant influence on the PSA properties, in particular shear adhesion (Figure 4.5, 4.6 and 4.7k).[8,44] The AcCNCs exhibited increasing self-assembly behaviour with increasing DS (Figure 4.7l-o). The better dispersion of the AcCNCs led to their uniform distribution in the dried latex films. However, with decreasing hydrophilicity (increasing DS), the AcCNCs were more prone to create end-to-end assemblies because the lower repulsive forces between the AcCNCs and the polymer particles allowed the AcCNCs to interact with and cover the polymer particles (Figure 4.7l-o). Then, a more uniformly distributed nanoparticle arrangement and greater amount of end-to-end reassembly led to smoother dried film surfaces and more nanofibril-like structures, which significantly improved the PSA properties. Of particular note was the significant increase in shear adhesion from 0.25-AcCNC-PSA to 0.42-AcCNC-PSA. This denotes the point where the AcCNCs crossed the threshold of hydrophobicity. Thus, significantly more re-assembly occurred, resulting in a significant increase in shear adhesion.

In a prior study, we demonstrated that incorporating partially hydrophilic sulfated CNCs increased tack, peel strength and shear adhesion compared to a CNC-free formulation.[19,23] As noted earlier, the exact nature of the modifications to the CNCs was not known. In that case, the tack and peel strength improved with decreasing hydrophilicity, while the shear adhesion did not.[19,23] In another study, with so-called hydrophobic sulfated CNCs a mini-emulsion process was used to synthesize the nanocomposites.[19,23] This forced the CNCs to the interior of the polymer particles, and while tack and peel strength increased, the shear adhesion fell below that of the base case formulation. This points to the importance of how the CNCs (or in this case, cCNCs and AcCNCs) are

added to the latex formulation. One would prefer to follow the procedure used in the current work to maximize cCNC or AcCNC reassembly to achieve the greatest impact on shear adhesion.

4.4.4 Morphology and dispersibility

AFM height imaging was used to support our understanding of the morphological changes in and the distribution of the cCNCs and AcCNCs within the latex (Figure 4.8). Additionally, in-phase AFM imaging of the cCNC-PSA films was done (Appendix II). Of particular interest were the latex particle-particle interactions that occurred during the deformation and interdiffusion of polymer chains associated with film drying.[2] Differentiating the cCNCs and AcCNCs from the polymer matrix was difficult due to small height differences (~50 nm), but the effects of the nanoparticles on particle coalescence during film drying were observable (Figure 4.8). The relatively low T_g of the polymer led to particle deformation during drying, making size measurements useful for comparison rather than precise differentiation.[18] The base case latex had a monomodal particle size distribution induced by the anionic surfactants through lateral repulsive capillary forces (Table 4.3). Only a minor flocculation was observed during film drying due to convective particle movement (Figure 4.8a). Consistent with our prior work, incorporating cCNCs reduced the spacing between the anionic latex particles due to increased repulsive forces between the latex particles and the cCNCs, leading to a bimodal latex particle size distribution and high initial latex viscosity (Table 4.3).[8,38] During film formation, aggregates formed on the substrate because the cCNCs were more repelled by the latex particles, leading to a higher likelihood of latex particle-particle interactions with the cCNCs distributed around these flocs (Figure 4.8b). This mechanism is called “depletion flocculation” of the polymer particles.[23,45,46]

When the AcCNCs were added, the AFM imaging pointed to a “bridging flocculation” mechanism (Figure 4.8, Table 4.3). This mechanism suggests that more than one latex particle interacts with the same AcCNC, forming bridges that enhance particle coalescence.[23,45,46] The lower surface charge and repulsive electrostatic forces of the AcCNCs compared to the cCNCs (Table 3.2) are consistent with these different flocculation mechanisms. The AFM images of the 0.06-AcCNC (Figure 4.8c) were like that of the base case latex (Figure 4.8a), implying little change to latex particle-particle spacing during film drying. As the DS of the AcCNCs increased (Figure 4.8c, d), the AcCNCs

with increasingly reduced surface charge and hydrophilicity (Table 3.2) resulted in greater latex particle-AcCNC-particle bridging.[23,46] This increasing bridging flocculation with DS was reflected in the increasing shear adhesion measurements (Figure 4.6). In summary, the increased DS correlates with enhanced particle coalescence during film drying and supports the increased degree of AcCNC reassembly.

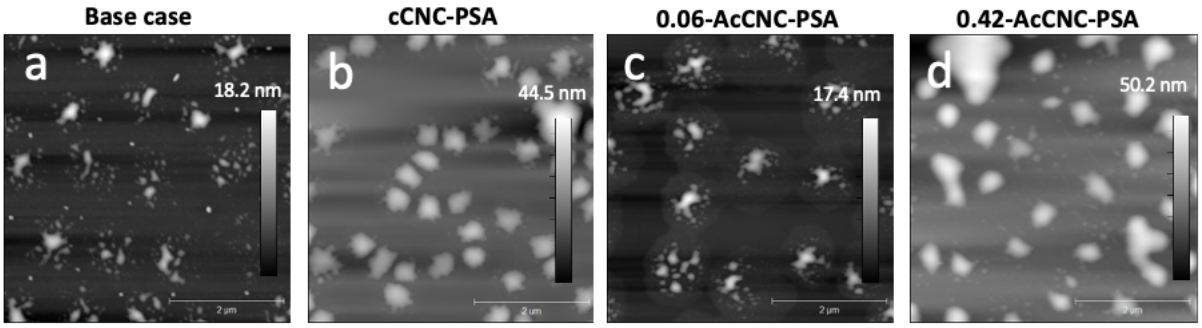

Figure 4.8. Height AFM images of diluted latexes (0.4 wt.%) a) Base case, b) cCNC-PSA, c) 0.06-AcCNC-PSA, d) 0.42-AcCNC-PSA.

4.5 Conclusion

Incorporating cCNCs into high-performance acrylic PSAs offers significant improvements in key adhesive properties such as tack, peel strength, and shear adhesion. However, the inherent hydrophilicity of cCNCs poses challenges in their dispersion within nonpolar hydrophobic polymer matrices, which were addressed through acetylation. In this study, acetylation was controlled by varying the iodine content. The DS was measured using ATR-FTIR spectroscopy and confirmed by ^{13}C-NMR spectroscopy. Water contact angle measurements indicated a transition from hydrophilic to hydrophobic properties with increasing DS.

A key finding in this work demonstrated that the use of hydrophobic cCNCs (i.e., AcCNCs with a DS = 0.42) provides the best increases in PSA performance. The cCNCs be added *in situ* during the latex synthesis at the seed stage (and not simply blended into an existing latex). This will ensure a better cCNC distribution in the PSA films and, with the higher DS AcCNCs, will lead to greater cCNC reassembly into nanofibril-like structures. In turn, the nanofibril-like structures impart the greatest impact on shear adhesion while the presence of the cCNCs simultaneously improves tack and peel strength.

These findings revealed the distinct localization and self-assembly behavior of cCNCs and AcCNCs (with varying DS) within the polymer matrix. The distribution of nanoparticles within a polymer matrix is significantly affected by interfacial tension, which was consistent with AFM imaging. When the interfacial tension is lower, it facilitates better dispersion because it decreases the energy needed to evenly spread the nanoparticles throughout the polymer matrix. This enhanced dispersion usually leads to superior mechanical, thermal, and barrier properties in the nanocomposite.[47] Because of the similarity of the water contact angles for the 0.42-AcCNCs (101±4°), with that of the base case polymer (120°), the dispersion of the AcCNCs was effective. The ability to control the DS, in other words, the hydrophilicity of the AcCNCs, points to the opportunity for their broader use in coatings,[48] hydrogels, and other advanced materials where one could fine-tune the DS to match the hydrophilicity to the application.

4.6 Supporting information

Additional data on conversion, pH, average particle size; description of gel content method and in-phase AFM image of dried cCNC-PSA film (PDF).

4.7 Author information

Corresponding Author: * Marc A. Dubé - Department of Chemical and Biological Engineering, University of Ottawa, Ottawa, ON, Canada; orcid.org/0000-0003-2718-9221; E-mail: marc.dube@uottawa.ca

4.8 Acknowledgement

The authors gratefully acknowledge the financial contribution of the Natural Science and Engineering Council of Canada (NSERC) Alliance Grant #ALLRP 560215-20 and Anomera, Inc.

4.9 References

(1) Dastjerdi, Z.; Cranston, E. D.; Berry, R.; Fraschini, C.; Dubé, M. A. Polymer Nanocomposites for Emulsion-Based Coatings and Adhesives. *Macromol. React. Eng.* **2019**, *13* (2), 1800050. https://doi.org/10.1002/mren.201800050.

(2) Jovanović, R.; Dubé, M. A. Emulsion-Based Pressure-Sensitive Adhesives: A Review. *Journal of Macromolecular Science, Part C: Polymer Reviews* **2004**, *44* (1), 1–51. https://doi.org/10.1081/MC-120027933.

(3) Dubé, M. A.; Gabriel, V. A.; Pakdel, A. S.; Zhang, Y. Sustainable Polymer Reaction Engineering: Are We There Yet? *Can J Chem Eng* **2021**, *99* (1), 31–60. https://doi.org/10.1002/cjce.23865.

(4) Stouten, J.; Cao, H.; Pich, A.; Bernaerts, K. V. Renewable and Functional Latexes Synthesized by Polymerization-Induced Self-Assembly for UV-Curable Films. *ACS Appl. Mater. Interfaces* **2023**, *15* (45), 52939–52952. https://doi.org/10.1021/acsami.3c11657.

(5) Fang, C.; Zhu, X.; Cao, Y.; Xu, X.; Wang, S.; Dong, X. Toward Replacement of Methyl Methacrylate by Sustainable Bio-Based Isobornyl Methacrylate in Latex Pressure Sensitive Adhesive. *Int. J. Adhes. Adhes.* **2020**, *100*, 102623. https://doi.org/10.1016/j.ijadhadh.2020.102623.

(6) Zhang, Y.; Cunningham, M. F.; Dubé, M. A. Modification of Adhesive and Latex Properties for Starch Nanoparticle-Based Pressure Sensitive Adhesives. *Macromol. React. Eng.* **2020**, *14* (1), 1900023. https://doi.org/10.1002/mren.201900023.

(7) Nasiri, A.; Wearing, J.; Dubé, M. A. The Use of Lignin in Emulsion-Based Pressure-Sensitive Adhesives. *Int. J. Adhes. Adhes.* **2020**, *100*, 102598. https://doi.org/10.1016/j.ijadhadh.2020.102598.

(8) Bayat, P.; Meek, K. M.; Movafagh, M.; Cranston, E. D.; Cunningham, M. F.; Champagne, P.; Morse, T.; Kiriakou, M. V.; George, S. R.; Dubé, M. A. The Effect of Cellulose Nanocrystal Reassembly on Latex-Based Pressure-Sensitive Adhesive Performance. *Biomacromolecules* **2024**, *25* (5), 3018–3032. https://doi.org/10.1021/acs.biomac.4c00138.

(9) Gabriel, V. A.; Dubé, M. A. Toward a Fully Biobased Pressure-Sensitive Adhesive. *Ind. Eng. Chem. Res.* **2023**, *62* (1), 478–488. https://doi.org/10.1021/acs.iecr.2c03756.

(10) Gandini, A.; Lacerda, T. M. From Monomers to Polymers from Renewable Resources: Recent Advances. *Prog. Polym. Sci.* **2015**, *48*, 1–39. https://doi.org/10.1016/j.progpolymsci.2014.11.002.

(11) Delepierre, G.; Vanderfleet, O. M.; Niinivaara, E.; Zakani, B.; Cranston, E. D. Benchmarking Cellulose Nanocrystals Part II: New Industrially Produced Materials. *Langmuir* **2021**, *37* (28), 8393–8409. https://doi.org/10.1021/acs.langmuir.1c00550.

(12) Fu, D.; Yang, R.; Wang, Y.; Guo, X.; Cheng, C.; Hua, F. Nanocellulose-Enhanced, Easily Processable Cellulose-Based Flexible Pressure Sensor for Wearable Epidermal Sensing. *ACS Appl. Mater. Interfaces* **2024**, *16* (16), 21242–21254. https://doi.org/10.1021/acsami.4c03541.

(13) Lam, E.; Hemraz, U. D. Preparation and Surface Functionalization of Carboxylated Cellulose Nanocrystals. *Nanomaterials* **2021**, *11* (7), 1641. https://doi.org/10.3390/nano11071641.

(14) Ávila Ramírez, J. A.; Fortunati, E.; Kenny, J. M.; Torre, L.; Foresti, M. L. Simple Citric Acid-Catalyzed Surface Esterification of Cellulose Nanocrystals. *Carbohydr. Polym.* **2017**, *157*, 1358–1364. https://doi.org/10.1016/j.carbpol.2016.11.008.

(15) Movafagh, M.; Meek, K. M.; Bayat, P.; Cranston, E. D.; Cunningham, M.; Champagne, P.; Morse, T.; Kiriakou, M.; George, S.; Dubé, M. A. Improved Pressure-sensitive Adhesive Performance Using Carboxylated Cellulose Nanocrystals via Blending. *Polym. Eng. Sci.* **2024**, *64* (2), 798–816. https://doi.org/10.1002/pen.26585.

(16) Gabriel, V. A.; Champagne, P.; Cunningham, M. F.; Dubé, M. A. In-situ Addition of Carboxylated Cellulose Nanocrystals in Seeded Semi-batch Emulsion Polymerization. *Can. J. Chem. Eng.* **2022**, *100* (4), 767–779. https://doi.org/10.1002/cjce.24299.

(17) Antoniw, J. M.; Gabriel, V. A.; Kiriakou, M. V.; Dubé, M. A.; Cunningham, M. F.; Cranston, E. D. Influence of Cellulose Nanocrystal Surface Chemistry and Dispersion Quality on Latex Nanocomposite Stability, Film Formation and Adhesive Properties. *RSC Applied Polymers* **2024**, *2* (2), 262–274. https://doi.org/10.1039/D3LP00244F.

(18) Gabriel, V. A.; Tousignant, M. N.; Wilson, S. M. W.; Faure, M. D. M.; Cranston, E. D.; Cunningham, M. F.; Lessard, B. H.; Dubé, M. A. Improving Latex-Based Pressure-Sensitive

Adhesive Properties Using Carboxylated Cellulose Nanocrystals. *Macromol. React. Eng.* **2022**, *16* (3), 2100051. https://doi.org/10.1002/mren.202100051.

(19) Pakdel, A. S.; Cranston, E. D.; Dubé, M. A. Incorporating Hydrophobic Cellulose Nanocrystals inside Latex Particles via Mini-Emulsion Polymerization. *Macromol. React. Eng.* **2021**, *15* (5), 2100023. https://doi.org/10.1002/mren.202100023.

(20) Klemm, D.; Kramer, F.; Moritz, S.; Lindström, T.; Ankerfors, M.; Gray, D.; Dorris, A. Nanocelluloses: A New Family of Nature-Based Materials. *Angew. Chem., Int. Ed.* **2011**, *50* (24), 5438–5466. https://doi.org/10.1002/anie.201001273.

(21) Miao, C.; Hamad, W. Y. Critical Insights into the Reinforcement Potential of Cellulose Nanocrystals in Polymer Nanocomposites. *Curr. Opin. Solid State Mater. Sci.* **2019**, *23* (4), 100761. https://doi.org/10.1016/j.cossms.2019.06.005.

(22) Ferreira, E. S.; Lanzoni, E. M.; Costa, C. A. R.; Deneke, C.; Bernardes, J. S.; Galembeck, F. Adhesive and Reinforcing Properties of Soluble Cellulose: A Repulpable Adhesive for Wet and Dry Cellulosic Substrates. *ACS Appl. Mater. Interfaces.* **2015**, *7* (33), 18750–18758. https://doi.org/10.1021/acsami.5b05310.

(23) Pakdel, A. S.; Niinivaara, E.; Cranston, E. D.; Berry, R. M.; Dubé, M. A. Cellulose Nanocrystal (CNC)–Latex Nanocomposites: Effect of CNC Hydrophilicity and Charge on Rheological, Mechanical, and Adhesive Properties. *Macromol. Rapid. Commun.* **2021**, *42* (3), 2000448. https://doi.org/10.1002/marc.202000448.

(24) Kedzior, S. A.; Gabriel, V. A.; Dubé, M. A.; Cranston, E. D. Nanocellulose in Emulsions and Heterogeneous Water-Based Polymer Systems: A Review. *Adv. Mater.* **2021**, *33* (28), 2002404. https://doi.org/10.1002/adma.202002404.

(25) Espino-Pérez, E.; Domenek, S.; Belgacem, N.; Sillard, C.; Bras, J. Green Process for Chemical Functionalization of Nanocellulose with Carboxylic Acids. *Biomacromolecules* **2014**, *15* (12), 4551–4560. https://doi.org/10.1021/bm5013458.

(26) Lee, J. H.; Park, S. H.; Kim, S. H. Surface Alkylation of Cellulose Nanocrystals to Enhance Their Compatibility with Polylactide. *Polymers (Basel)* **2020**, *12* (1), 1–16. https://doi.org/10.3390/polym12010178.

(27) Kaboorani, A.; Riedl, B. Surface Modification of Cellulose Nanocrystals (CNC) by a Cationic Surfactant. *Ind. Crops. Prod.* **2015**, *65*, 45–55. https://doi.org/10.1016/j.indcrop.2014.11.027.

(28) Long, W.; Ouyang, H.; Hu, X.; Liu, M.; Zhang, X.; Feng, Y.; Wei, Y. State-of-Art Review on Preparation, Surface Functionalization and Biomedical Applications of Cellulose Nanocrystals-Based Materials. *Int. J. Biol. Macromol.* **2021**, *186*, 591–615. https://doi.org/10.1016/j.ijbiomac.2021.07.066.

(29) Abraham, E.; Kam, D.; Nevo, Y.; Slattegard, R.; Rivkin, A.; Lapidot, S.; Shoseyov, O. Highly Modified Cellulose Nanocrystals and Formation of Epoxy-Nanocrystalline Cellulose (CNC) Nanocomposites. *ACS Appl. Mater. Interfaces* **2016**, *8* (41), 28086–28095. https://doi.org/10.1021/acsami.6b09852.

(30) Ullah, M. W.; Manan, S.; Kiprono, S. J.; Ul-Islam, M.; Yang, G. Synthesis, Structure, and Properties of Bacterial Cellulose. In *Nanocellulose*; Wiley, 2019; pp 81–113. https://doi.org/10.1002/9783527807437.ch4.

(31) Werner, A.; Schmitt, V.; Sèbe, G.; Héroguez, V. Synthesis of Surfactant-Free Micro- and Nanolatexes from Pickering Emulsions Stabilized by Acetylated Cellulose Nanocrystals. *Polym. Chem.* **2017**, *8* (39), 6064–6072. https://doi.org/10.1039/C7PY01203A.

(32) Abedi, F.; Emadzadeh, D.; Dubé, M. A.; Kruczek, B. Modifying Cellulose Nanocrystal Dispersibility to Address the Permeability/Selectivity Trade-off of Thin-Film Nanocomposite Reverse Osmosis Membranes. *Desalination* **2022**, *538*, 115900. https://doi.org/10.1016/j.desal.2022.115900.

(33) Montanheiro, T. L. A.; Montagna, L. S.; de Farias, M. A.; Magalhães, J. A.; Tada, D. B.; Passador, F. R.; Machado, J. P. B.; Lemes, A. P. Cytotoxicity and Physico-Chemical Evaluation of Acetylated and Pegylated Cellulose Nanocrystals. *J. Nanopart. Res.* **2018**, *20* (8), 206. https://doi.org/10.1007/s11051-018-4306-3.

(34) Tingaut, P.; Zimmermann, T.; Lopez-Suevos, F. Synthesis and Characterization of Bionanocomposites with Tunable Properties from Poly(Lactic Acid) and Acetylated Microfibrillated Cellulose. *Biomacromolecules* **2010**, *11* (2), 454–464. https://doi.org/10.1021/bm901186u.

(35) Xu, J.; Wu, Z.; Wu, Q.; Kuang, Y. Acetylated Cellulose Nanocrystals with High-Crystallinity Obtained by One-Step Reaction from the Traditional Acetylation of Cellulose. *Carbohydr. Polym.* **2020**, *229*, 115553. https://doi.org/10.1016/j.carbpol.2019.115553.

(36) Fei, P.; Liao, L.; Cheng, B.; Song, J. Quantitative Analysis of Cellulose Acetate with a High Degree of Substitution by FTIR and Its Application. *Anal. Methods* **2017**, *9* (43), 6194–6201. https://doi.org/10.1039/c7ay02165h.

(37) Habibi, Y.; Chanzy, H.; Vignon, M. R. TEMPO-Mediated Surface Oxidation of Cellulose Whiskers. *Cellulose* **2006**, *13* (6), 679–687. https://doi.org/10.1007/s10570-006-9075-y.

(38) Niinivaara, E.; Ouzas, A.; Fraschini, C.; Berry, R. M.; Dubé, M. A.; Cranston, E. D. How Latex Film Formation and Adhesion at the Nanoscale Correlate to Performance of Pressure Sensitive Adhesives with Cellulose Nanocrystals. *Philos. Trans. R. Soc., A* **2021**, *379* (2206), 20200330. https://doi.org/10.1098/rsta.2020.0330.

(39) Moon, J. D.; Freeman, B. D.; Hawker, C. J.; Segalman, R. A. Can Self-Assembly Address the Permeability/Selectivity Trade-Offs in Polymer Membranes? *Macromol.* **2020**, *53* (14), 5649–5654. https://doi.org/10.1021/acs.macromol.0c01111.

(40) Wu, Z.; Xu, J.; Gong, J.; Li, J.; Mo, L. Preparation, Characterization and Acetylation of Cellulose Nanocrystal Allomorphs. *Cellulose* **2018**, *25* (9), 4905–4918. https://doi.org/10.1007/s10570-018-1937-6.

(41) Renate Förch; Holger Schönherr; A. Tobias A. Jenkins. Contact Angle Goniometry. In *Surface design: applications in bioscience and nanotechnology.*; Förch, R., Schönherr, H., Jenkins, A. T. A., Eds.; Wiley, 2009; p 471. https://doi.org/10.1002/9783527628599.

(42) Hu, W.; Chen, S.; Xu, Q.; Wang, H. Solvent-Free Acetylation of Bacterial Cellulose under Moderate Conditions. *Carbohydr. Polym.* **2011**, *83* (4), 1575–1581. https://doi.org/10.1016/j.carbpol.2010.10.016.

(43) Gabriel, V. A.; Cranston, E. D.; Dubé, M. A. Pushing the Limits with Cellulose Nanocrystal Loadings in Latex-Based Pressure-Sensitive Adhesive Nanocomposites. *Macromol. React. Eng.* **2020**, *14* (6), 2000027. https://doi.org/10.1002/mren.202000027.

(44) Qie, L.; Dubé, M. A. Manipulating Latex Polymer Microstructure Using Chain Transfer Agent and Cross-Linker to Modify PSA Performance and Viscoelasticit **y**. *Macromol. React. Eng.* **2011**, *5* (2), 117–128. https://doi.org/10.1002/mren.201000046.

(45) Dickinson, E. A Model of a Concentrated Dispersion Exhibiting Bridging Flocculation and Depletion Flocculation. *J. Colloid Interface Sci.* **1989**, *132* (1), 274–278. https://doi.org/10.1016/0021-9797(89)90237-3.

(46) Sun, X.; Danumah, C.; Liu, Y.; Boluk, Y. Flocculation of Bacteria by Depletion Interactions Due to Rod-Shaped Cellulose Nanocrystals. *Chem. Eng. J.* **2012**, *198–199*, 476–481. https://doi.org/10.1016/j.cej.2012.05.114.

(47) Khoshkava, V.; Kamal, M. R. Effect of Surface Energy on Dispersion and Mechanical Properties of Polymer/Nanocrystalline Cellulose Nanocomposites. *Biomacromolecules* **2013**, *14* (9), 3155–3163. https://doi.org/10.1021/bm400784j.

(48) Liu, X.; Teng, R.; Fu, C.; Wang, R.; Chen, Z.; Li, W.; Liu, S. Design and Synthesis of a Robust and Multifunctional Superhydrophobic Coating with a Three-Dimensional Network Structure on a Paper-Based Material. *ACS Appl. Mater. Interfaces* **2024**, *16* (28), 37111–37121. https://doi.org/10.1021/acsami.4c08089.

Chapter 5
Effect of Carboxylated Cellulose Nanocrystal Acetylation on PLA Nanocomposite Properties

Parisa Bayat[1], Andrew Anstey[1], Marc A. Dubé[1], Timothy Morse[2], Michael F. Cunningham[3], Kelly M. Meek[*4]

[1]Department of Chemical and Biological Engineering, University of Ottawa, Ottawa, ON, Canada, K1N 6N5
[2]Anomera Inc., Montreal, QC, Canada, H3B 1A7
[3]Department of Chemical Engineering, Queen's University, Kingston, ON, Canada, K7L 3N6
[4]Chemical and Material Engineering, Concordia University, Montreal, QC, Canada, H3G 1M8

This chapter is a manuscript to be submitted to a refereed journal.

5.1 Abstract

Polylactic acid (PLA) has garnered increasing attention as a biodegradable polymer derived from renewable resources; however, its relatively slow crystallization rate restricts its broader use in wider applications. We address this challenge by producing PLA nanocomposites with carboxylated cellulose nanocrystals (cCNCs) and acetylated cCNCs (AcCNCs) in ethyl lactate (EtLa), a bio-based, non-toxic solvent. The crystallization behaviour and thermomechanical properties of the nanocomposites were measured using X-ray diffraction (XRD), differential scanning calorimetry (DSC), thermogravimetric analysis (TGA), dynamic mechanical analysis (DMA), and polarized optical microscopy (POM). For the PLA-cCNC nanocomposites, Avrami analysis confirmed a transition from two- to three-dimensional spherulitic growth. The inclusion of 1.5 wt.% cCNCs provided the greatest increase in PLA crystallization rate at 100°C, as did the AcCNCs with a degree of substitution of 0.06 at higher temperatures (i.e., 110, 120°C). This demonstrated that the cCNCs enhanced heterogeneous nucleation and the use of EtLa chain mobility. XRD measurements revealed an increase in average crystallite size from 0.78 nm in pure PLA to 21.17 nm in the PLA nanocomposite with 2.5 wt.% cCNCs, signifying improved crystal development. Although both cCNCs and AcCNCs promoted PLA crystallization, the nucleating efficacy of AcCNCs was hampered by reduced compatibility with the EtLa solvent, leading to AcCNC aggregation. The results show how leveraging a greener solvent (EtLa) and utilizing cCNCs can effectively address PLA's crystallization rate limitation, thereby expanding opportunities for

the development of high-performance, sustainable materials in packaging, additive manufacturing, and biomedical engineering.

Keywords: polylactic acid, cellulose nanocrystals, crystallization, nanocomposite, acetylation, Avrami, crystallite

5.2 Introduction

Polylactic acid (PLA) is regarded as one of the most promising bio-sourced polymers, with applications in packaging, textiles, drug delivery, and biomedical equipment, because of its biodegradability, biocompatibility, and UV stability.[1,2] PLA is noted for its ability to be produced in either amorphous or semi-crystalline forms, depending on the concentration of L- and D-type stereoisomers and other process conditions.[3] PLA's inherently slow crystallization kinetics lead to longer processing times, and poor thermal stability, hindering its scalability for broader application.[4–6] These restrictions could be overcome by copolymerization,[7] blending with other polymers,[8] and the use of nanofillers.[9] Nanofillers such as carbon nanotubes, layered silicates, hydroxyapatite, layered titanate, and aluminum hydroxide improve polymer characteristics such as crystallization rate, even at low concentrations due to their high aspect ratio and specific surface area.[10] However, the main concern is that most of them are suspected to be toxic.[3]

Cellulose nanocrystals (CNCs), derived from abundant natural resources, have gained increasing attention as a sustainable nanomaterial.[11,12] CNCs, with a modulus ranging from 140 to 220 GPa and a tensile strength of 7.5 to 77 GPa, demonstrate exceptional mechanical performance, improving the performance of polymer composites even at low concentrations.[13] Their low thermal expansion, high aspect ratio, and unique rheological properties make these rod-like nanoparticles ideal for improving the crystallization rate of PLAs as a "green" alternative nucleating agent.[14]

The surface chemistry of CNCs depends on the acid used for their extraction from wood pulp. Sulfuric acid hydrolysis introduces anionic sulfate half-ester groups, replacing some hydroxyl groups and yielding colloidally stable CNC dispersions in water.[15] The addition of sulfated CNCs to PLA has been shown to enhance the cold crystallization of PLA by promoting

faster and more uniform crystal formation due to the CNCs ability to act as a nucleating agent.[11,15–19] The decrease in the cold crystallization temperature was attributed to the reduction of strong intermolecular interactions between the PLA chains in the rubbery state by the CNCs.[14] Recently, carboxylated CNCs (cCNCs) have been derived using a more sustainable approach, hydrogen peroxide oxidation.[20] The lower surface charge density of cCNCs (0.16 e/nm²) compared to sulfated CNCs (0.29–0.49 e/nm²) is a crucial factor in their self-assembly in nanocomposites.[21] The incorporation of sulfated CNCs into PLA resulted in lower thermal stability of the nanocomposite, as shown by the lower degradation onset temperatures with higher sulfated CNC content.[22] cCNCs have substantially higher thermal stability compared to sulfated CNCs [20] and could have a less deleterious effect on nanocomposite thermal stability.

Achieving a homogeneous dispersion in the matrix material is a significant challenge for any nanocomposite material.[16] Numerous efforts to produce PLA nanocomposites with good CNC dispersion have been explored.[3,23] The dispersion of CNCs in PLA through solution casting has been shown to be more effective compared to direct melt mixing, as it promotes the wetting of the hydrophilic CNCs and prevents irreversible agglomeration after drying.[17,24–26] Alanalp et al. investigated the effect of solvents on crystallization behavior and kinetics, discovering that dimethyl sulfoxide (DMSO) had a lower onset temperature for cold crystallization and a broader exothermic peak than dimethylformamide (DMF)-based samples.[14] However, polar solvents used in similar research, such as DMF,[14,25] chloroform,[3] and dichloromethane,[27] are more hazardous. To our knowledge, no studies have been conducted on PLA processed with ethyl lactate (EtLa), an eco-friendly solvent. Ethyl lactate, a bio-based, benign, and economically viable solvent,[28] is proposed in this study for this purpose. Therefore, the dispersion of CNCs in ethyl lactate can be achieved through a solvent exchange process, maintaining high environmental and safety standards.

The effectiveness of solution casting to achieve a uniform dispersion of CNCs in PLA is challenged by the hydrophilicity of the CNCs, which makes them prone to rapid aggregation in semi-polar matrices like PLA.[29,30] The CNC hydrophilicity primarily stems from the presence of interacting hydroxyl groups on the CNC surfaces, making dispersion within the hydrophobic PLA difficult. Thus, this limits the ability of the CNCs to effectively reinforce the polymer matrix and

diminishes their potential as reinforcing agents.[31] Various surface modification techniques have been explored to reduce the hydrophilicity of CNCs and expand their use as nanofillers in PLA.[32,33] Acetylated sulfated CNCs have yielded positive results leading to increased crystallization rates and capacity without affecting thermal stability.[33] Another concern is that the CNC modification methods used often involve toxic solvents and are time- and energy-intensive, while achieving only minimal improvements in CNC dispersion within the PLA.[3,34] Recently, we demonstrated a simple, safe, and effective acetylation method to improve CNC dispersion in hydrophobic materials in membranes and adhesives.[21,35,36] The reassembly of the AcCNCs was shown to increase adhesive properties.[21,35,36] Acetylating cCNCs can further increase their thermal stability by substituting the hydroxyl groups with acetyl groups, which is critical for blending CNCs with PLA in high-temperature processes like extrusion.[32]

In this study, PLA-based nanocomposites were produced using a range of concentrations of cCNCs and a series of acetylated cCNCs with different degrees of substitution (DS) suspended in EtLa. The effects of these nanomaterials on various PLA nanocomposite properties were assessed using x-ray diffraction (XRD), differential scanning calorimetry (DSC), thermal gravimetric analysis (TGA), dynamic mechanical analysis (DMA), and polarized optical microscopy (POM). Of particular interest was the use of the Avrami method to investigate the impact of these nanomaterials on PLA crystallization kinetics.

5.3 Experimental

5.3.1 Materials

Polylactide (PLA, trade name 3001D) with a D-lactic acid content of 1.5%, a commercial product from NatureWorks Co., Ltd., USA, was used in this study. The PLA had a specific gravity of 1.24 g cm^{-3} and a melt flow index of 22 g 10 min^{-1} (210°C, 2.16 kg) with a molecular weight ranging from 100,000 to 200,000 g/mol. Ethyl lactate (EtLa, ≥98%, Sigma-Aldrich) was employed as-received to disperse carboxylated cellulose nanocrystals (cCNCs) within the PLA matrix. Never-dried cCNC dispersed in EtLa and spray-dried cCNC powder in the sodium-salt form (Dextracel™ COOH content of 0.22 mmol/g) was supplied by Anomera Inc. (Montreal QC, Canada). De-ionized distilled water (DIW) with a resistivity of 18.0 ± 0.2 MΩ cm was utilized for modification of cCNCs.

Ethanol (purity > 99%), acetone (purity >99%), acetic anhydride (ACS REAGENT, >98.0%) and iodine (ACS REAGENT, >99.8%) were used for the modification of the cCNCs and were purchased from Sigma-Aldrich.

5.3.2. cCNC acetylation and dispersion in EtLa

The cCNCs were acetylated using a solvent-free technique developed in our previous work.[37,38] In a glass vial with a magnetic stirrer, 0.57 g of cCNCs, 9 mL of acetic anhydride, and varying amounts of iodine catalyst (0.02, 0.04, 0.06, 0.08 g) were stirred at 100°C for 10 minutes. After cooling, 0.9 mL of acetone was added to quench the acetylation reaction and the contents were stirred for 15 minutes, followed by the addition of 60 mL of 75% ethanol/DIW. The mixture was stirred for 10 minutes, and the acetylated cCNCs (AcCNCs) were washed and centrifuged three times to neutralize the pH. The AcCNCs were then dispersed in ethyl lactate, using a solvent-exchange process in a rotary evaporator, to achieve a final concentration of 3 wt% in EtLa.[21,35] As a result of the change in iodine catalyst concentration, four different degrees of substitution (DS) were achieved (i.e., 0.06, 0.10, 0.25, 0.42), which were estimated via FTIR spectroscopy[39]. A detailed description of the acetylation process and a complete characterization of the AcCNCs is available in previous work.[38]

5.3.3. PLA/cCNC nanocomposites

In a 500 mL stainless steel beaker equipped with a heating mantle, temperature control probe, and mechanical stirrer under a fume hood, 150 g of PLA granules were added and heated to 200°C until fully melted. The temperature was then reduced to 150°C, and 100 g of EtLa was added to the melted PLA. The mixture was stirred to achieve homogeneity. Once uniform, maintaining a 1:1 proportion of PLA to EtLa, the remaining EtLa, along with the cCNCs dispersed in EtLa at the specified concentration, was added. The mixture was stirred for 30 minutes at 160°C. Afterward, it was poured into a silicone mold and placed in a vacuum chamber for 48 hours to allow complete evaporation of the EtLa. The solidified material was then chopped into small pieces using a grinder, washed with DIW three times, and dried in a vacuum oven for 24 hours. The resulting PLA/cCNC composites (Table 5.1) were then prepared for characterization.

Table 5.1. Experimental design of PLA-cCNC/AcCNC samples

Sample ID[a]	cCNC type	cCNC/AcCNC concentration (wt.%)	Degree of substitution (DS)[b]
PLA	-	-	-
PLA+EtLa	-	-	-
PLA+0.5% cCNC	cCNC	0.5	0
PLA+1.5% cCNC	cCNC	1.5	0
PLA+2.5% cCNC	cCNC	2.5	0
PLA+1.5% AcCNC-0.06	AcCNC	1.5	0.06
PLA+1.5% AcCNC-0.10	AcCNC	1.5	0.10
PLA+1.5% AcCNC-0.25	AcCNC	1.5	0.25
PLA+1.5% AcCNC-0.42	AcCNC	1.5	0.42

[a] Sample IDs are as follows: PLA represents pure PLA polymer; PLA+EtLa represents PLA processed with EtLa, after EtLa evaporation; for PLA+xx% cCNC, xx represents concentration of cCNCs; and for PLA+1.5% AcCNC-y.yy, y.yy represents the degree of substitution.
[b] See reference 35 for the detailed characterization of the AcCNCs.

5.4 Characterization

Contact angle: The sessile water/EtLa contact angle of the cCNC and AcCNC dried powders, pressed into discs, was measured using a VCA Optima surface analysis system (AST Products, Inc., Billerica, MA). At least 20 droplets (3 µL) of water/EtLa in at least seven different locations on each sample were tested at ambient temperature.

TGA: Thermogravimetric analysis (TGA) was carried out using an SDT Q600 thermogravimetric analyzer (TA Instruments Inc, Delaware, USA) under nitrogen from 27 to 800°C at a heating rate of 10°C/min with 5-10 mg of sample used to measure the thermal stability of the nanocomposites.

DMA: The viscoelastic properties of the blends were evaluated using Dynamic Mechanical Analysis (DMA) to measure the loss modulus, storage modulus, and tan delta. DMA tests were conducted on rectangular compression-molded samples with dimensions of 3.7 mm in thickness, 12.5 mm in width, and 35 mm in length, using a DMAQ800 (TA Instruments). The specimens were

analyzed in the dual cantilever bending mode with a 30-micron amplitude, 1 Hz frequency, and a heating rate of 3°C/min, over a temperature range from 25 to 145°C, under ambient conditions. Each nanocomposite formulation was tested in triplicate, with data variability within a range of 0.7%.

DSC: The kinetics of crystallization were examined using differential scanning calorimetry (DSC). Conventional 3-stage heat-cool-heat tests were performed on each sample from 0 to 200°C at a rate of 10°C/min to determine the effect of cCNC concentration and degree of acetylation. The enthalpy of cold crystallization and melting, the crystallization onset point, peak temperature, and melting temperature were measured during the second heating stage.

Isothermal crystallization and melting behaviour were studied using DSC. Flat solid specimens weighing 8-12 mg were prepared for each sample. To remove any seed crystals, the samples were first heated to 200°C at a rate of 10°C/min and held isothermally for 3 minutes. The samples were then cooled at a maximum cooling rate of 40°C/min to the designated isothermal crystallization temperatures (90, 100, 110, and/or 120°C) and held until complete crystallization was observed.

The influence of cCNCs on crystallization kinetics was investigated at cCNC concentrations of 0, 0.5, 1.5, and 2.5 wt.% (Table 5.1). Additionally, to assess the effect of acetylation on crystallization, unmodified cCNCs and AcCNCs with varying DS were examined at a constant concentration of 1.5 wt.%. The isothermal crystallization data were analyzed using the Avrami method to determine the Avrami exponent (n) and rate constant (k), which were used to calculate the crystallization half-time ($t_{1/2}$) for each nanocomposite at each specific temperature.

XRD: X-ray diffraction (XRD) was employed to measure the crystallinity of the cCNCs/AcCNCs and nanocomposites. At ambient temperature, the XRD test was performed using Cu Kα radiation (λ = 1.5418 Å) using a Bragg-Brentano geometry. With a scan speed of 3°/min (for cCNCs/AcCNCs) and 0.02°/sec (for PLA) and a step width of 0.02°, the 2θ range spanning from 4° to 80° was covered. The Segal empirical equation was used to calculate crystallinity (*X*) of cCNCs/AcCNCs.

$$\mathrm{X}(\%) = \frac{I_{16^\circ} - I_{22^\circ}}{I_{22^\circ}} 100\% \qquad (5.1)$$

where I_{22° (arbitrary units) represents the peak diffraction intensity corresponding to the crystalline cellulose, and I_{16° is the peak diffraction intensity corresponding to the amorphous sections.[40]

The crystallite sizes for cCNCs/AcCNCs blended PLA nanocomposites were calculated by using the Scherrer equation:

$$D = \frac{k \times \lambda}{\beta \, Cos\,(\theta)} \qquad (5.2)$$

where D represents the average size of the ordered (crystalline) regions in nm within a material, λ is the radiation wavelength (1.54Å), 2θ is the diffraction angle, β is the peak width at half maximum intensity in radian, and k=0.9 is a dimensionless shape factor.[22] Prior to the XRD measurements, the nanocomposite samples were heated to 200°C at a rate of 10°C/min and held isothermally for 3 minutes, then rapidly cooled at 40°C/min to 130°C, and the samples were kept at this temperature for 60 minutes to crystallize.

POM: The nucleating ability of the PLA nanocomposites was investigated using a polarized optical microscope (POM; BX53 Microscope (Olympus, Tokyo, Japan)) equipped with a heating stage (CSS450 (Linkam Scientific Instruments Ltd., Salfords, United Kingdom)). To visualize the crystallization behaviour of PLA in the presence of cCNCs/AcCNCs, a thin film of approximately 15–40 µm thick was placed on the heating stage. Films were prepared via compression moulding at 200°C temperature for 3 minutes between Teflon sheets with a 5000 psi pressure increase every 3 seconds until 15000 psi and were held at that pressure for 1 minute. The pressure was released for 30 s, and rapidly raised to 15000 psi for another 30 seconds, before the film was removed from the hot press. The sample placed between two thin glass coverslips, was heated from room temperature to 200°C at a rate of 10°C/min and held isothermally for 3 minutes to erase any thermal history in the PLA matrix. After this initial heating, the samples were rapidly cooled at 40°C/min to the isothermal crystallization temperature of 130°C, and the samples were crystallized at this temperature for 25 minutes. Images were captured to observe the crystallization process of PLA and cCNC/AcCNC-PLA nanocomposites at this temperature, with snapshots taken at intervals of 5, 15, and 25 min. The goal was to see the difference in

crystallization rate between samples by increasing the cCNC content and DS through acetylation of the cCNCs.

5.5 Results and discussion

5.5.1 cCNC and AcCNC characterization results

XRD spectra (Figure 5.1) were used to calculate the degree of crystallinity of the cCNCs and AcCNCs. The spectra show three distinct diffraction peaks at 16°, 22°, and 34.9°, which are characteristic of cellulose. The peaks at 16° and 22° were used to calculate the degree of crystallinity. The degree of crystallinity of the cCNCs was 65±0.9% compared to that of the AcCNCs, which were 60±0.2% for DS = 0.06, 55±0.5% for DS = 0.10, 53±0.3% for DS = 0.25, and 51±0.2% for DS = 0.42. With an increasing degree of acetylation, the crystal structure of the cCNCs decreased, due to the substitution of hydroxy groups with the larger acetyl groups, thereby breaking some inter- and intramolecular hydrogen bonds in the cellulose structure.[41,42]

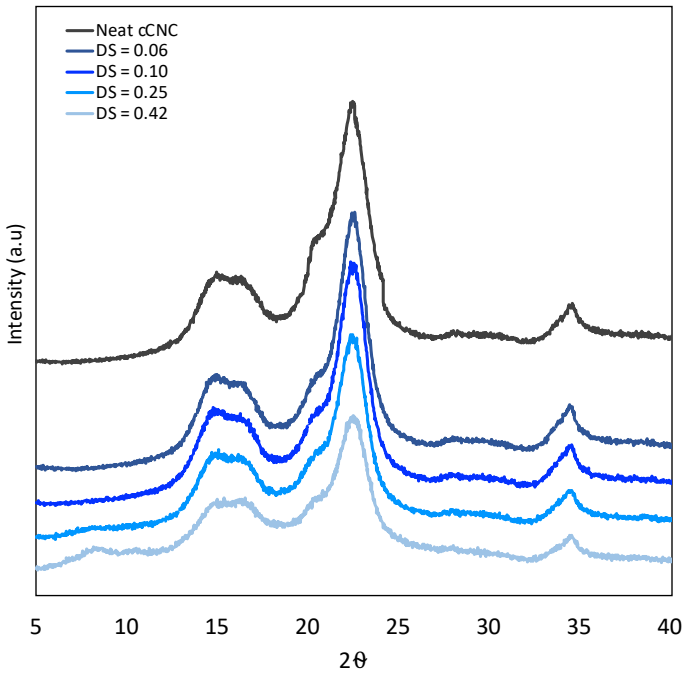

Figure 5.1. The XRD spectra of cCNCs and AcCNCs with different DS.

Table 5.2. cCNC and AcCNC properties.

cCNC ID	Crystallinity (%)	Water contact angle (°)[38]	EtLa contact angle (°)	$T_{d5\%}$ (°C)
cCNC	65%	30±2	5±1	216.6
AcCNC-0.06	60%	60±4	15±2	270.0
AcCNC-0.10	55%	80±3	39±3	265.0
AcCNC-0.25	53%	90±2	49±3	256.8
AcCNC-0.42	51%	101±4	52±3	257.0

As seen in Table 5.2, the hydrophobicity of the cCNCs was increased with acetylation. This is evident from the increasing water contact angle with DS. While EtLa is less polar than water, it still exhibits hydrophilic characteristics, and a similar increase in EtLa contact angle with DS was observed.[28,32] The thermal stability of the cCNCs/AcCNCs, analyzed by TGA, was compared using the degradation temperature at 5% weight loss ($T_{d5\%}$). The acetylation of the cCNCs greatly increased thermal stability, consistent with previous work.[18,32] The moderate thermal stability of the unmodified cCNCs (216.6°C) was improved by substituting stable acetyl groups for less stable hydroxy groups, which can be beneficial for PLA nanocomposites during processing at higher temperatures.[43,44]

5.5.2 PLA nanocomposite characterization

The XRD patterns of cCNC/AcCNC-based PLA nanocomposites are shown in Figure 5.2, where two main diffraction peaks are visible at 2θ = 16.7 and 19.1°, which represent the (110/200) and (203) crystalline planes of PLA, respectively.[45] The peak at 16.7° was further intensified by the addition of cCNCs, suggesting that a greater crystal fraction was present within the nanocomposite. In the PLA+2.5% cCNC sample, a small increase in the intensity of the peak at 19.1° was apparent, indicating the creation of a higher fraction of ordered structures in PLA. The Scherrer equation was utilized to obtain the crystallite size (D) for the crystalline planes of (110/200) in order to evaluate the effect of cCNCs and AcCNCs on crystallite size.[22] As shown in Table 5.3, the crystallite size of PLA, which was measured at 0.78 nm, grew dramatically to 21.17 nm at 2.5 wt.% cCNCs, confirming its influence on more ordered growth. The crystallite size of PLA-AcCNC nanocomposites, on the other hand, showed an opposite trend, with an increase in the DS. For instance, the crystallite size was 13.87 nm at DS = 0.06 and dropped to 1.09 nm at DS

= 0.42. In contrast to previous studies,[44,46] our results indicate that the XRD patterns of PLA significantly changed after the incorporation of AcCNCs, demonstrating that the acetylation of cCNCs impact their ability to nucleate PLA crystals.

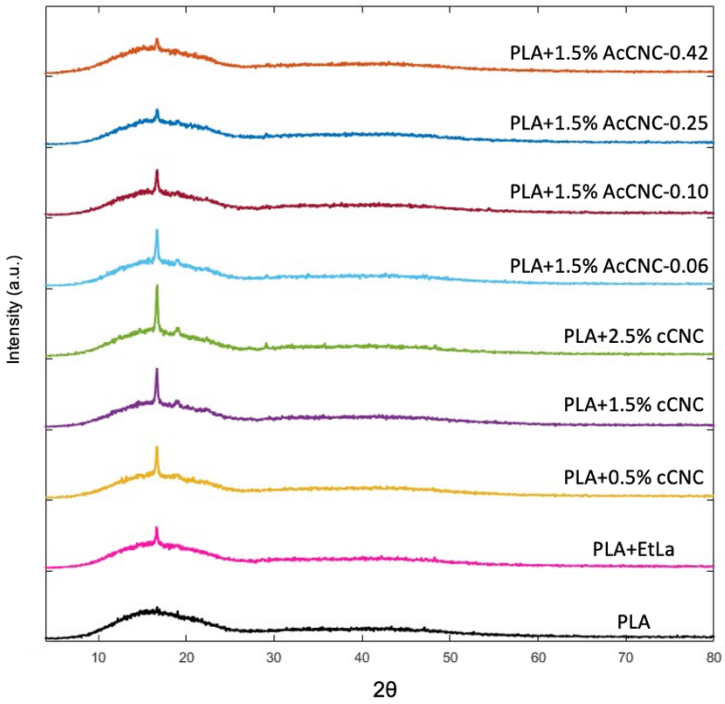

Figure 5.2. The X-ray diffraction pattern of PLA and cCNC/AcCNC based PLA nanocomposites.

Table 5.3. The crystallite size of nanocomposites at maximum observed peak using Scherrer equation.

Sample	Crystallite size (nm) at plane (110/200)
PLA	0.78
PLA+EtLa	2.15
PLA+0.5% CNC	14.89
PLA+1.5% CNC	14.90
PLA+2.5% CNC	21.17
PLA+1.5% AcCNC-0.06	13.87
PLA+1.5% AcCNC-0.10	7.31
PLA+1.5% AcCNC-0.25	1.22
PLA+1.5% AcCNC-0.42	1.09

5.5.3. Differential scanning calorimetry

The DSC thermograms to assess the thermal characteristics of PLA and PLA-based nanocomposites with cCNCs and AcCNCs are shown in Figure 5.3. The key transitions, including the glass transition temperature (T_g), cold crystallization temperature (T_{cc}), melting temperatures (T_{m1} and T_{m2}), and the associated enthalpy changes, are detailed in Table 5.4.

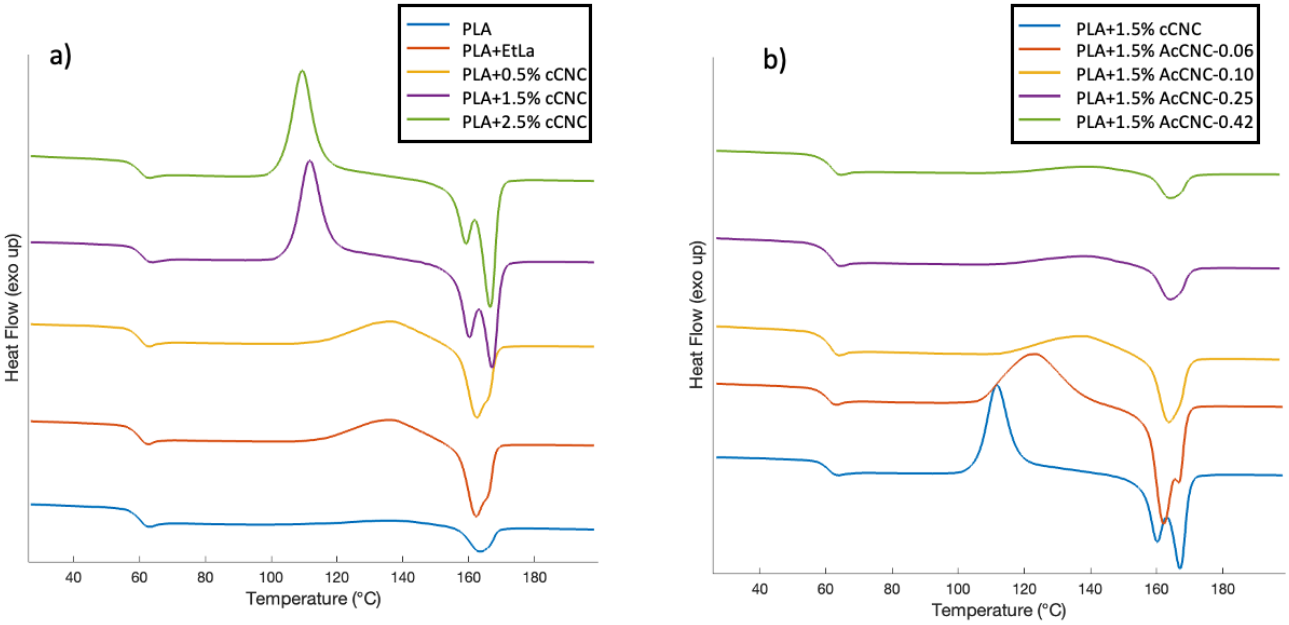

Figure 5.3. DSC thermograms of PLA and cCNC/AcCNC-PLA nanocomposites vs a) cCNC content and b) at 1.5 wt.% cCNC/AcCNC vs DS.

Table 5.4. Differential scanning calorimetry data of PLA and PLA-cCNC/AcCNC nanocomposites.

Sample	T_g/°C	T_{cc}/°C	ΔH_{cc} (J/g)	T_{m1}/°C	T_{m2}/°C	ΔH_m (J/g)	$T_{d5\%}$
PLA	58.9	136.6	4.7	163.4	-	6.6	320.4
PLA+EtLa	58.7	136.2	19.0	161.7	166.2	18.7	318.1
PLA+0.5% cCNC	59.2	135.8	14.2	162.4	166.3	21.5	309.3
PLA+1.5% cCNC	60.3	111.7	30.7	160.0	167.0	33.1	296.9
PLA+2.5% cCNC	59.3	109.4	33.9	159.0	166.4	34.4	286.2
PLA+1.5% AcCNC-0.06	59.2	123.5	38.5	161.9	166.9	37.4	315.7
PLA+1.5% AcCNC-0.10	60.2	137.8	13.2	163.7	167.0	11.0	314.4
PLA+1.5% AcCNC-0.25	60.6	139.6	6.4	164.0	-	7.4	315.4
PLA+1.5% AcCNC-0.42	60.9	139.7	4.0	164.0	-	5.5	315.6

There were no significant differences between the T_gs of the various PLA nanocomposites (Figure 5.3). PLA exhibited a T_g of 58.9°C, while its nanocomposites displayed slightly higher T_g values, up to a maximum of 60.9°C for PLA+1.5%AcCNC-0.42 (Table 5.4). This minor increase in T_g can be attributed to the slightly restricted mobility of the PLA chains due to the lower free volume resulting from the addition of the nanomaterials.[47] All nanocomposites exhibited no crystallization during the cooling run; the cold crystallization peak emerged during the second heating step for all PLA and nanocomposite samples. PLA exhibited a slight exothermic peak, indicating minor cold crystallization. Adding EtLa to PLA significantly increased the crystallization enthalpy from 4.7 to 19.0 J/g. Most of the EtLa was extracted prior to testing, but some residual EtLa (<1% according to TGA results, see Appendix III) provided a plasticizing effect by minimizing intermolecular interactions and facilitating the reorganization of the polymer chains into crystalline domains. This structure promoted improved cold crystallization by enabling the chains to realign more effectively after reheating.[16]

Because cCNCs function as heterogeneous nucleation sites during cooling, their improved nucleation effectiveness was reflected in an exothermic peak, which gradually increased with cCNC content (Figure 5.3a). Furthermore, the decrease in cold crystallization temperature (T_{cc}) with increased cCNC loading suggests that crystallization took place at lower temperatures because of the availability of more nucleation sites. Interestingly, the acetylation of the cCNCs to increase PLA compatibility led to greater T_{cc}, but a higher enthalpy of cold crystallization (Figure 5.3b). Nevertheless, the cold crystallization enthalpy ($\triangle H_{cc}$) dramatically dropped with the DS. The lowest enthalpy value (4.073 J/g) was measured for PLA+1.5wt.% AcCNC-0.42, suggesting low-efficiency crystallization during cooling (Table 5.4). This pattern was observed by Fang et al. for increased modified CNC content in PLA due to the hindrance effect of modified CNCs on PLA chain mobility.[33] The $\triangle H_{cc}$ results correlate with the increase in AcCNC hydrophobicity after acetylation (Table 5.2), suggesting increased AcCNC aggregation in the PLA during processing, which impacts crystal nucleation due to the reduction of available AcCNC surface area.

The second heating curves of the PLA and PLA-based nanocomposites revealed significant differences in melting behavior. PLA exhibited a single, monomodal melting peak at 163.4°C, corresponding to the melting of α' crystals with an imperfect structure. In contrast, PLA+EtLa and

cCNC-PLA nanocomposites demonstrated a bimodal melting behavior, with one peak at a lower temperature and another at a higher temperature (Figure 5.3). The lower-temperature peak (T_{m1}) is attributed to the melting of imperfect and defective α' crystals, grown during cold crystallization at lower temperatures, while the higher-temperature peak (T_{m2}) corresponds to the melting of more perfect and stable α crystals.[47] With increasing amount of cCNCs, the T_{m2} peak became increasingly prominent due to the accelerated cold crystallization of crystals nucleated by the cCNCs during cooling. This bimodal melting behavior highlights the role of the cCNCs in promoting the formation of a broader range of crystal structures. The cCNC concentration of 2.5 wt.% successfully balanced nucleation and crystal development to yield more perfect α crystals in PLA, indicating that higher cCNC content facilitated heterogeneous crystallization. The creation of well-ordered α crystals was made challenging by the introduction of AcCNC-0.06, which can be attributed to the aggregation of AcCNC, which reduces the availability of nucleating surfaces and limits PLA chain mobility and hinder crystal perfection.

PLA demonstrated a $T_{d5\%}$ of 320.4°C, suggesting moderate thermal stability (Table 5.4). The inclusion of EtLa resulted in a drop in $T_{d5\%}$, which decreased the thermal stability likely due to the volatility of the residual EtLa. As cCNCs were added, thermal stability deteriorated further; PLA+0.5wt.% cCNC, for instance, demonstrated a $T_{d5\%}$ of 309.3°C, and PLA+2.5wt.% cCNC displayed a noticeably lower $T_{d5\%}$ of 286.2°C. In contrast to earlier research,[33] the use of AcCNCs (e.g., AcCNC-0.06, AcCNC-0.10) greatly showed higher thermal stability compared to the unmodified cCNCs, highlighting the significance of functionalization optimization for PLA nanocomposites.

PLA and cCNC/AcCNC-PLA nanocomposites were isothermally crystallized at 100, 110, and 120°C to examine the impact of cCNCs (or AcCNCs) on the crystallization behavior of PLA. The relative crystallinity is plotted as a function of time at various isothermal crystallization temperatures in Figure 5.4. The duration of isothermal crystallization of the cCNC-PLA nanocomposites at 1.5 and 2.5 wt.% was significantly shorter than that of PLA and PLA+EtLa at a constant crystallization temperature, demonstrating that cCNCs more efficiently accelerate PLA's isothermal crystallization. The maximum crystallization rate was for the cCNC concentration of 2.5 wt.% (Figures 5.4c and 5.4e), reflecting an optimum balance between nucleation sites and

chain mobility. Isothermal crystallization at 100 and 110°C yielded faster crystallization rates due to higher supercooling that enhanced both nucleation and crystal growth for all samples. However, at higher temperatures, such as at 120°C, of the opposite is observed for crystallization rate because the driving force for nucleation decreases.[47]

The crystallization at 110 and 120°C for samples with AcCNCs with lower DS (e.g., AcCNC-0.06 and AcCNC-0.10) outperformed the unmodified cCNCs, even with high concentrations (e.g., 1.5 wt.% or 2.5 wt.% cCNCs). The thermodynamic driving force for nucleation and crystal development was significantly reduced at 120°C, which decreased crystallization rates for all samples. The decreased nucleation potential at 120°C outweighed the benefit of higher temperatures, which typically increases chain mobility. For unmodified cCNCs, the presence of strong hydrogen bonding between the cCNCs, combined with increased PLA chain mobility, caused more frequent cCNC-cCNC contact, leading to greater cCNC aggregation. This increased aggregation reduced the number of nucleation sites, ultimately decreasing the crystallization rate. In contrast, the lower hydrophilicity of the AcCNCs and their weaker hydrogen bonding interactions led to fewer AcCNC aggregates compared to the cCNCs, which led to a higher number of nucleation sites compared to the cCNCs. As a result, at the higher temperatures, the AcCNCs were less prone to forming aggregates compared to the cCNCs, despite their poor dispersion. This underscores the significance of nanoparticle surface chemistry and temperature-dependent dynamics in affecting crystallization behaviour.

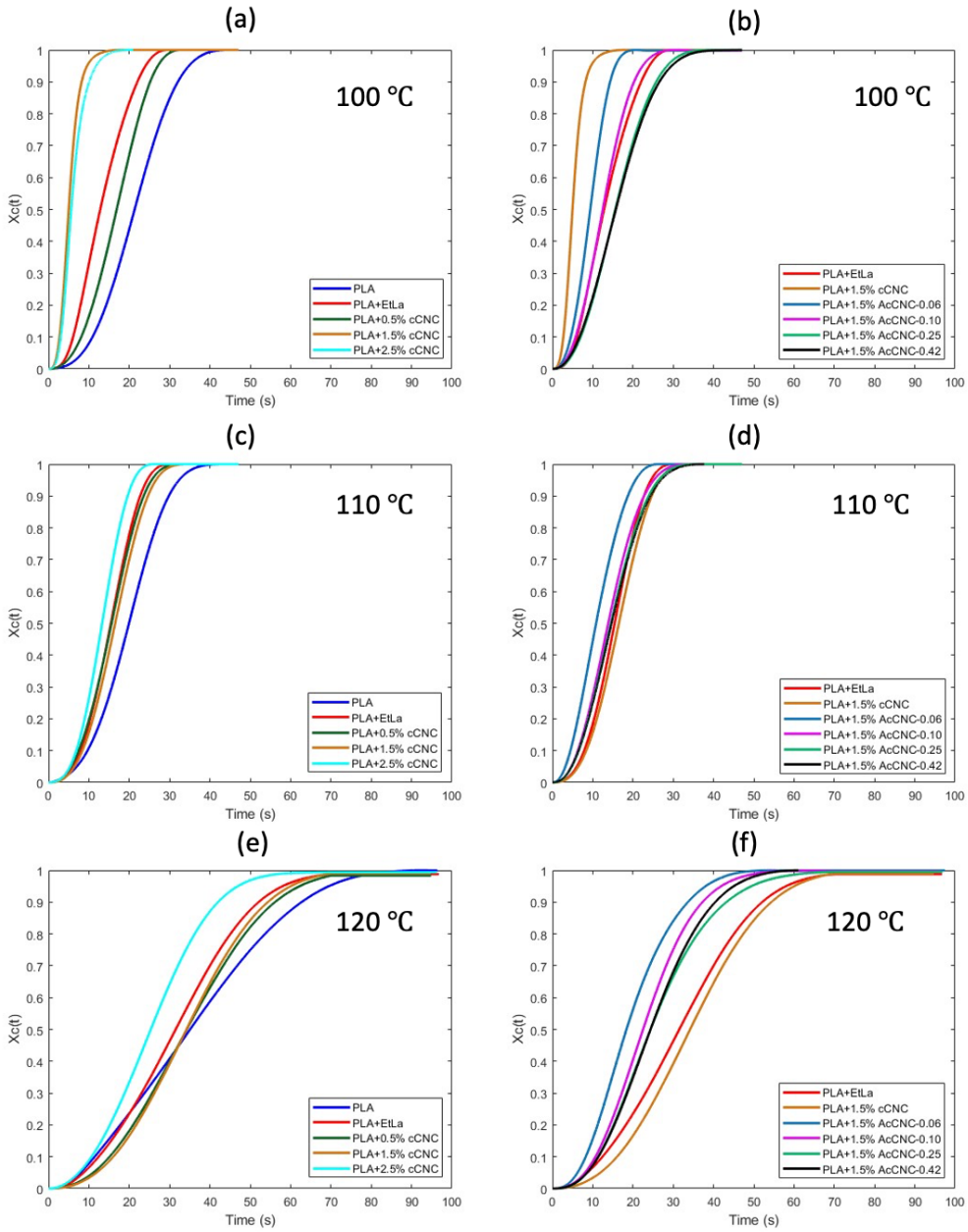

Figure 5.4. Relative crystallinity as a function of time (s) for nanocomposites, which isothermally melt crystallized at various temperatures of (a) and (b) 100°C, (c) and (d) 110°C, (e) and (f) 120°C characterized by DSC.

The Avrami equation was used to assess the relative crystallinity changes across the isothermal crystallization period to examine the isothermal crystallization kinetics of PLA and cCNC (or AcCNCs)-PLA nanocomposites. The following formula was used to determine the relative crystallinity (X_c) as a function of time:

$$1 - \mathrm{X}_c = \exp\left(-kt^n\right) \qquad (5.3)$$

The linear form of equation 3 is:

$$\ln[-\ln(1 - \mathrm{X}_c)] = \ln k + n \ln t \qquad (5.4)$$

where k is the total rate constant related to both nucleation and growth contributions and n is the Avrami exponent, depending on nucleation and growth geometry of crystals.[48,49] Figure 5.5 shows the comprehensive findings of the Avrami study for PLA, cCNC/PLA, and AcCNC/PLA nanocomposite materials, which are summarized in Table 5.5. It is evident from the results that the primary nucleation mechanism involves two- to three-dimensional growth modes, depending on the specific sample composition and temperature. For samples containing 1.5 wt.% and 2.5 wt.% cCNC, the value of n increased to roughly 3 at 100°C, indicating a shift to three-dimensional spherulitic crystal formation. cCNCs function as efficient nucleating agents, which raise the nucleation density and promote more consistent crystal formation in all dimensions.

The crystallization rate constant (k) provides crucial information about how quickly the crystallization process proceeds. Since they represent both the nucleation efficiency and the subsequent crystal growth rate, higher values correlate to faster overall crystallization rates. Because there are fewer nucleation sites in pure PLA, the values are lower than in PLA nanocomposites, suggesting slower crystallization. At a concentration of 1.5 wt.%, the balance between nucleation and chain mobility speeds up crystallization noticeably. The rapid crystal growth at 100°C for this composition demonstrates the efficacy of cCNCs as a nucleating agent. As the temperature rose up to 110°C, AcCNCs could surpass the crystallization rate of nanocomposites with non-acetylated cCNCs. Nonetheless, PLA blended with AcCNCs with higher DS showed lower crystallization rates, which can be explained by the acetylated cCNCs' restricted compatibility with EtLa and aggregations in the PLA matrix.

The overall rate of crystallization was further examined through the calculation of the half crystallization time ($t_{1/2}$) was introduced (Table 5.5), which quantifies the amount of time required for 50% completion of primary crystallization (Equation 5.5).[50]

$$t_{1/2} = (\frac{0.693}{k})^{1/n} \quad (5.5)$$

$t_{½}$ is comparatively high for PLA, indicating slower crystallization because there are fewer nucleation sites available. Consistent with earlier results, the half crystallization time for samples containing AcCNCs is significantly influenced by the DS. Because AcCNC is more evenly distributed throughout the PLA matrix at lower DS (i. e., AcCNC-0.06), $t_{½}$ are somewhat lower than those of plain PLA, suggesting the efficiency of modification. To evaluate the effect of lower temperature (i. e, 90°C) on the crystallization rate, isothermal DSC was performed on selected samples, including PLA, PLA+EtLA, and PLA+1.5 wt.% cCNC. The PLA with 1.5 wt.% of cCNC at 100°C showed the highest rate of crystallization. Interestingly, while the k values increased significantly, the half-crystallization times ($t_{½}$) showed only a slight decrease. This indicates a competing effect between the low mobility of the PLA chains and the nucleation efficiency, which influences the overall crystallization process.

Prior research revealed a lack of compatibility between PLA and sulfated CNC, which resulted in decreased crystallization ability, limited PLA chain mobility, and CNC agglomeration.[34] Our findings, however, indicate that cCNC demonstrated more PLA compatibility, which resulted in higher crystallinity. This emphasizes how crucial it is to improve the interaction between CNCs and PLA matrix by optimizing the CNC production process and functional groupings.

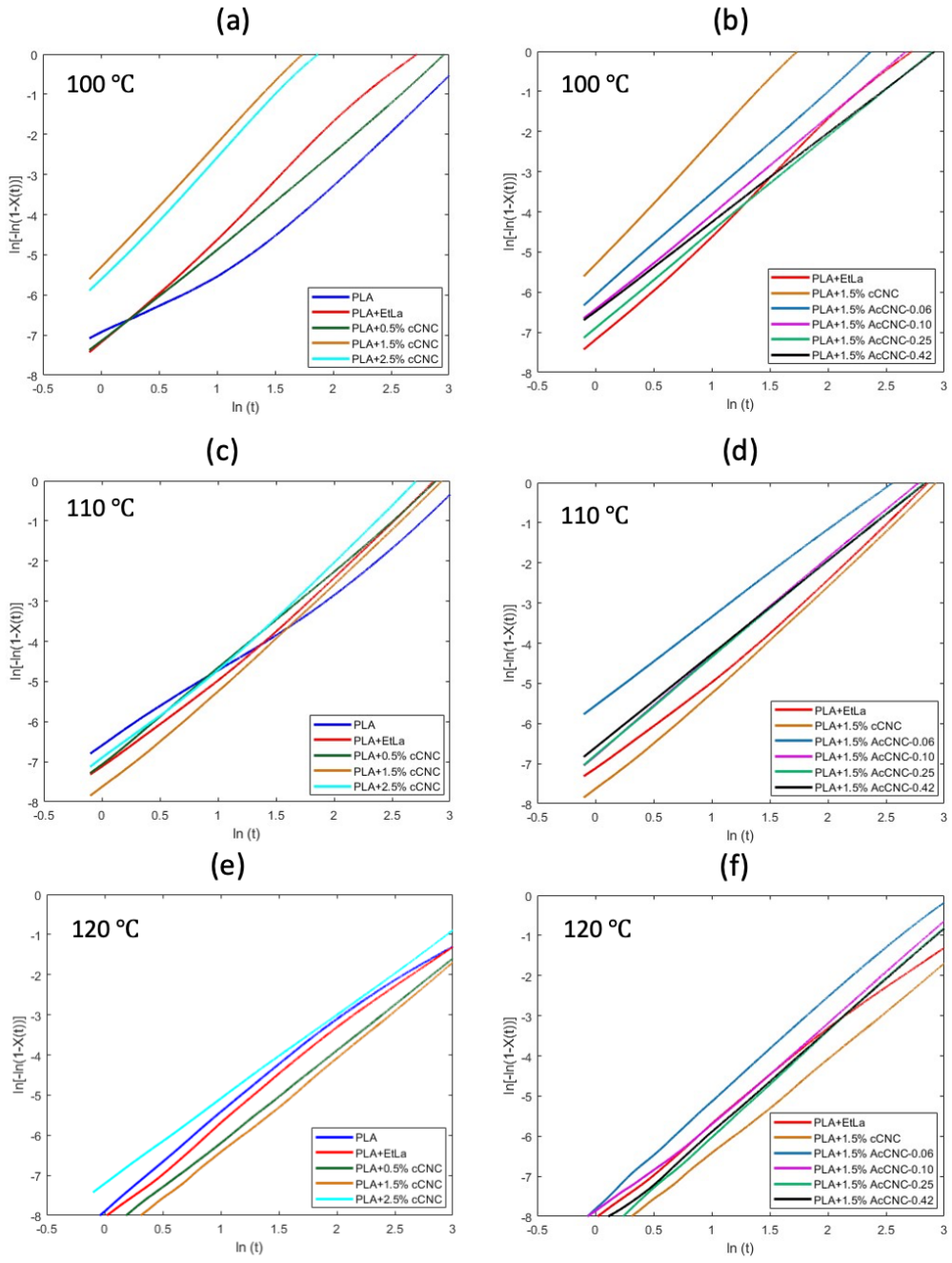

Figure 5.5. The Avrami plots of nanocomposites at various temperatures of (a) and (b) 100°C, (c) and (d) 110°C, (e) and (f) 120°C characterized by DSC.

Table 5.5. Isothermal crystallization kinetic parameters of PLA, and PLA nanocomposites with cCNCs/AcCNCs

Sample	T/°C	n	$k*10^{-4}$ min^{-1}	$t_{½}$ (min)
PLA	90	2.2871	11.0	17.73
	100	2.6286	2.1	21.31
	110	2.2947	6.5	19.90
	120	1.845	10.0	35.03
PLA+EtLa	90	2.0284	9.7	25.57
	100	2.6923	7.6	12.80
	110	2.7047	4.1	15.43
	120	2.0984	5.1	31.46
PLA+0.5% cCNC	100	2.4901	6.0	16.86
	110	2.4716	7.6	15.59
	120	2.2991	2.0	34.22
PLA+1.5% cCNC	90	2.7511	108.0	4.52
	100	3.0467	52.0	4.97
	110	2.7268	3.3	16.48
	120	2.4217	1.3	34.14
PLA+2.5% cCNC	100	3.0022	39.0	5.61
	110	2.7818	5.1	13.27
	120	2.1191	7.2	25.50
PLA+1.5% AcCNC-0.06	100	2.5729	22.0	9.37
	110	2.1397	43.0	10.81
	120	2.4555	5.6	18.36
PLA+1.5% AcCNC-0.10	100	2.4284	15.0	12.47
	110	2.4177	12.0	13.83
	120	2.5398	2.6	22.46
PLA+1.5% AcCNC-0.25	100	2.3455	11.0	15.60
	110	2.3617	13.0	14.50
	120	2.564	2.0	24.32
PLA+1.5% AcCNC-0.42	100	2.2132	16.0	15.71
	110	2.3108	14.0	14.68
	120	2.5221	2.2	24.31

5.5.4. Dynamic mechanical analysis

To quantify the stiffness and mechanical energy retention of the polymer in its unloaded condition, the storage modulus (E') of the nanocomposites was examined. The variation in E' and tan δ (damping factor) for all samples with temperature is shown in Figure 5.6. The storage modulus curves are similar in the initial glassy region, displayed as a plateau. However, all the samples exhibited a marked decrease in E' within the temperature range 60–80°C, which corresponds to the T_g of PLA (Figures 5.6a and 5.6b). The E' values rose once more above 100°C, demonstrating PLA's cold crystallization and confirming its semi-crystalline structure.

Table 6 presents an overview of how the addition of cCNC increases the storage modulus of PLA in the glassy region (35°C). The increase, however, is more significant in the rubbery region (75°C). Different concentrations of cCNC did not affect the PLA crystallization pattern except for 2.5 wt.%, where the nanocomposite showed a higher modulus in the rubbery plateau from 45±4 to 115±11 MPa. The increased compatibility between PLA and AcCNC could make a well-dispersed nanocomposites of PLA and AcCNCs, contributing to a higher modulus, whereas the incompatibility between AcCNC and EtLA reduced the homogeneity of the AcCNC dispersion in PLA. Due to this restriction and possible aggregations, the rubbery plateau modulus could not be surpassed by PLA with unmodified cCNC.

To further elucidate the role of surface chemistry in the interaction between PLA and cCNC/AcCNC, the tan δ (damping factor) peak was investigated (Figures 5.6c and d). Improved CNC-PLA interaction has been shown to be correlated to the broadening of the half-peak width, shift of the tan δ peak to higher temperatures, and decrease in intensity of tan δ.[18] The small decrease in tan δ at 0.5 wt.% cCNC suggests poor interfacial interactions, and the 20% decrease in tan δ at 2.5 wt.% cCNC suggests increased interaction between cCNC and PLA. AcCNC-0.42 showed the minimum intensity of the tan δ peak. Its 25% decrease in damping factor indicates the aggregations attributed to the incompatibility of the AcCNC-0.42 with EtLa, may have acted as stress concentration points.[51]

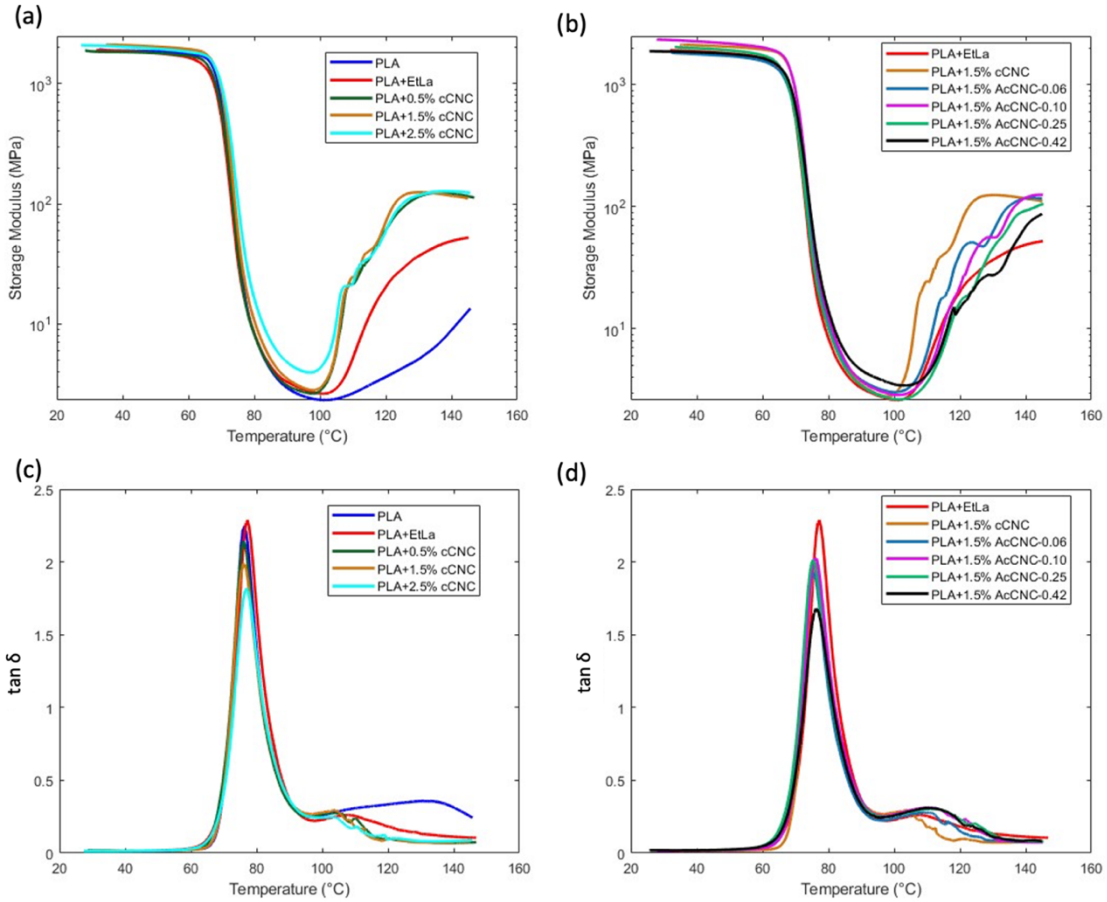

Table 5.6. Comparison of the storage modulus E’ of nanocomposites at glassy and rubbery region

Figure 5.6. (a) E’ and (c) tan δ curves of the neat PLA, PLA+EtLa, and PLA with cCNC nanocomposites, (b) E’ and (d) tan δ curves of PLA+EtLa, PLA+1.5% cCNC and PLA with AcCNC varying DS.

Sample	Storage Modulus E' (MPa, 35°C)	Storage Modulus E' (MPa, 75°C)
PLA	1908±12	45±4
PLA+EtLa	1898±10	36±5
PLA+0.5% CNC	1848±13	40±4
PLA+1.5% CNC	2130±22	63±3
PLA+2.5% CNC	2067±18	115±11
PLA+1.5% AcCNC-0.06	1805±14	44±5
PLA+1.5% AcCNC-0.10	2301±32	67±4
PLA+1.5% AcCNC-0.25	2016±14	43±5
PLA+1.5% AcCNC-0.42	1864±12	76±8

5.5.5 Polarized optical microscopy

Polarized optical microscopy was carried out for a few selected PLA blends at comparatively high isothermal temperatures (130°C) in order to evaluate the spherulitic growth rate over time and quantify the nuclei density (Figure 7). Even after 25 minutes, neat PLA (Figure 5.7a) showed very little spherulite production and delayed crystallization due to its fewer nucleation sites. The crystallization behavior was very slightly altered by the addition of EtLa (Figure 5.7b). Crystallization was accelerated by the pre-structured molecular arrangements that remained after the EtLa was removed. In contrast, the nucleation density and crystallization rate increased with the cCNC concentration, eventually producing more distinct and densely packed spherulites (Figures 5.7c–e). The nucleation density was much higher at 25 minutes at 2.5 wt.% cCNC (Figure 5.7e) than at lower concentrations, demonstrating that the cCNCs efficiently accelerated crystallization by offering heterogeneous nucleation sites. Also, higher cCNC contents led to a decrease in spherulite size observed at a specific time (Figure 5.7c-e), attributed to their role as nucleating agents, increasing nucleation density and causing earlier spherulite impingement. XRD analysis revealed an increase in crystallite size, suggesting that cCNCs promote better local molecular ordering and enhance individual crystal growth. This indicates that while cCNCs reduced the overall size of the PLA spherulites, they facilitated the formation of larger, more ordered crystallites within the polymer matrix.

The POM results of the cCNC- and AcCNC-PLA nanocomposites are compared in Figures 5.7d and f, and a clear crystallization pattern is seen. Sample AcCNC-0.06 has a substantially greater nuclei density at 5 minutes than the other samples, suggesting that AcCNC successfully started nucleation early in the crystallization process, likely due to the aggregations caused by the AcCNC and EtLa incompatibility. Nonetheless, as time went on, PLA chain mobility was restricted by the growing density of the nucleation sites and aggregations, which lengthened the crystallization process.

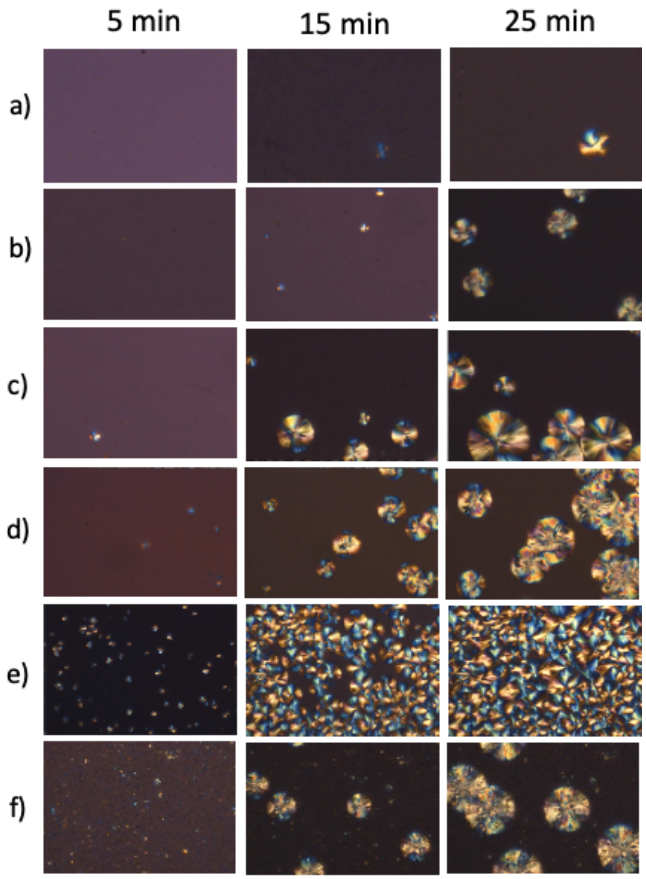

Figure 5.7. Polarized optical microscope of (a) PLA, (b) PLA+EtLa, PLA with cCNC at (c) 0.5, (d) 1.5, (e) 2.5 wt.%, and PLA with 1.5 wt.% (f) AcCNC-0.06 isothermally melt crystallized at 130°C for 5, 15, and 25 min.

5.6 Conclusion

This study highlights the potential of sustainable nanomaterials and safer solvents in enhancing the crystallization behavior of PLA-based nanocomposites. The use of EtLa as a sustainable solvent for PLA-based nanocomposites presents a promising eco-friendly alternative to conventional, hazardous solvents such as chloroform and DMF. Derived from renewable resources, EtLa is biodegradable and non-toxic with low volatility, making it an ideal choice for green polymer processing. In this study, EtLa not only served as a safe dispersion medium for cCNCs and AcCNCs but also promoted PLA chain mobility and facilitated organization processes.

This effect influenced crystallization kinetics, demonstrating the importance of solvent-polymer interactions in tailoring material properties while ensuring an environmentally responsible approach.

Our findings showed that cCNCs effectively promoted PLA crystallization by serving as heterogeneous nucleation sites, with crystallization kinetics analysis confirming an optimum balance between nucleation density and polymer chain mobility at a concentration of 1.5 wt.% cCNCs. The effect of EtLa on the mobility of PLA chains, along with cCNCs enhancing nucleation, led to faster crystallization rates, which were validated through a combination of DSC, XRD and POM. Avrami analysis also confirmed that cCNCs facilitated a transition to three-dimensional spherulitic growth, with an optimal balance between nucleation density and chain mobility observed at 1.5 wt.% cCNCs.

For AcCNCs, the degree of substitution (DS) significantly influenced the impact on PLA crystallization. Lower DS values (AcCNC-0.06 and AcCNC-0.10) correlated with better compatibility in EtLa, improved PLA dispersion, enhanced nucleation efficiency, and reduced crystallization half-time, compared to unmodified cCNCs, at higher temperatures of 110 and 120°C. Although AcCNCs with a DS of 0.42 led to higher storage modulus nanocomposites, they displayed lower nucleation efficiency, likely due to poor dispersion in EtLa and aggregate formation. POM showed that while aggregates led to early-stage high nucleation density, they limited chain mobility during spherulite growth, slowing the crystallization rate compared to unmodified cCNCs. Unlike previous studies that used acetylated CNCs with conventional solvents,[44,46] our findings shows that fine-tuning acetylation levels and using a safer solvent (EtLa) can significantly boost PLA crystallization performance.

This work demonstrates an improvement in PLA crystallization behaviour by incorporating cCNCs and AcCNCs. The results show how a greener solvent (EtLa) and nanomaterials (cCNCs) can be effectively utilized to address the property limitations of PLA. Future research should focus on refining AcCNC dispersion and tailoring solvent-polymer compatibility to further enhance PLA crystallization efficiency and broaden its applications in sustainable materials, such as 3D printing, food packaging, and biomedical applications.

5.7 Supporting information

Additional data on TGA, non-isothermal/isothermal DSC, and FTIR.

5.8 Acknowledgement

The authors gratefully acknowledge the financial contribution of the Natural Science and Engineering Council of Canada (NSERC) and Mitacs Grant #ALLRP 599870 – 24 and BASF and Anomera, Inc.

5.9 References

(1) Mokhena, T. C.; Sefadi, J. S.; Sadiku, E. R.; John, M. J.; Mochane, M. J.; Mtibe, A. Thermoplastic Processing of PLA/Cellulose Nanomaterials Composites. *Polymers (Basel)* **2018**, *10* (12), 1363. https://doi.org/10.3390/polym10121363.

(2) Arrieta, M. P.; Peltzer, M. A.; López, J.; Peponi, L. PLA-Based Nanocomposites Reinforced with CNC for Food Packaging Applications: From Synthesis to Biodegradation. In *Industrial Applications of Renewable Biomass Products*; Springer International Publishing: Cham, 2017; pp 265–300. https://doi.org/10.1007/978-3-319-61288-1_11.

(3) Vatansever, E.; Arslan, D.; Nofar, M. Polylactide Cellulose-Based Nanocomposites. *Int. J. Biol. Macromol.* **2019**, *137*, 912–938. https://doi.org/10.1016/j.ijbiomac.2019.06.205.

(4) Nofar, M.; Sacligil, D.; Carreau, P. J.; Kamal, M. R.; Heuzey, M.-C. Poly (Lactic Acid) Blends: Processing, Properties and Applications. *Int J Biol Macromol* **2019**, *125*, 307–360. https://doi.org/10.1016/j.ijbiomac.2018.12.002.

(5) Sema Sarul, D.; Arslan, D.; Vatansever, E.; Kahraman, Y.; Durmus, A.; Salehiyan, R.; Nofar, M. Preparation and Characterization of PLA/PBAT/CNC Blend Nanocomposites. *Colloid Polym Sci* **2021**, *299* (6), 987–998. https://doi.org/10.1007/s00396-021-04822-9/Published.

(6) Johansson, M.; Skrifvars, M.; Kadi, N.; Dhakal, H. N. Lignin-Polylactic Acid Biopolymer Blends for Advanced Applications – Effect of Impact Modifier. *Composites Part C: Open Access* **2024**, *14*, 100502. https://doi.org/10.1016/j.jcomc.2024.100502.

(7) Muiruri, J. K.; Liu, S.; Teo, W. S.; Kong, J.; He, C. Highly Biodegradable and Tough Polylactic Acid-Cellulose Nanocrystal Composite. *ACS Sustain Chem Eng* **2017**, *5* (5), 3929–3937. https://doi.org/10.1021/acssuschemeng.6b03123.

(8) Malayarom, P.; Pongpakdee, C.; Pattamaprom, C. Fine-Tuning Heat Resistance and Impact Toughness of Natural Rubber-Toughened PLA at Various Degrees of PLA/PDLA Stereocomplexation. *Composites Part C: Open Access* **2023**, *12*, 100391. https://doi.org/10.1016/j.jcomc.2023.100391.

(9) Keshtkar, M.; Nofar, M.; Park, C. B.; Carreau, P. J. Extruded PLA/Clay Nanocomposite Foams Blown with Supercritical CO2. *Polymer (Guildf)* **2014**, *55* (16), 4077–4090. https://doi.org/10.1016/j.polymer.2014.06.059.

(10) Paul, D. R.; Robeson, L. M. Polymer Nanotechnology: Nanocomposites. *Polymer (Guildf)* **2008**, *49* (15), 3187–3204. https://doi.org/10.1016/j.polymer.2008.04.017.

(11) Kamal, M. R.; Khoshkava, V. Effect of Cellulose Nanocrystals (CNC) on Rheological and Mechanical Properties and Crystallization Behavior of PLA/CNC Nanocomposites. *Carbohydr Polym* **2015**, *123*, 105–114. https://doi.org/10.1016/j.carbpol.2015.01.012.

(12) Gois, G. da S.; Santos, A. S. F.; Hernandéz, E. P.; Medeiros, E. S.; Almeida, Y. M. B. Biodegradation of PLA/CNC Composite Modified with Non-Ionic Surfactants. *Polymer Bulletin* **2023**, *80* (10), 11363–11377. https://doi.org/10.1007/s00289-022-04618-z.

(13) Dufresne, A. *Nanocellulose*; Huang, J., Dufresne, A., Lin, N., Eds.; Wiley, 2019. https://doi.org/10.1002/9783527807437.

(14) Alanalp, M. B.; Ozdemir, B.; Nofar, M.; Durmus, A. Isothermal and Non-Isothermal Cold Crystallization Kinetics of Polylactide/Cellulose Nanocrystal (PLA/CNC) Nanocomposites. *J Therm Anal Calorim* **2022**, *147* (24), 14211–14227. https://doi.org/10.1007/s10973-022-11598-9.

(15) Delepierre, G.; Vanderfleet, O. M.; Niinivaara, E.; Zakani, B.; Cranston, E. D. Benchmarking Cellulose Nanocrystals Part II: New Industrially Produced Materials. *Langmuir* **2021**, *37* (28), 8393–8409. https://doi.org/10.1021/acs.langmuir.1c00550.

(16) Vatansever, E.; Arslan, D.; Sarul, D. S.; Nofar, M. The CNC Dispersion Quality in Various PLA Grades. In *AIP Conference Proceedings*; American Institute of Physics Inc., 2023; Vol. 2607. https://doi.org/10.1063/5.0135790.

(17) Mohammadi, M.; Bruel, C.; Heuzey, M. C.; Carreau, P. J. CNC Dispersion in PLA and PBAT Using Two Solvents: Morphological and Rheological Properties. *Cellulose* **2020**, *27* (17), 9877–9892. https://doi.org/10.1007/s10570-020-03460-8.

(18) Spinella, S.; Lo Re, G.; Liu, B.; Dorgan, J.; Habibi, Y.; Leclère, P.; Raquez, J. M.; Dubois, P.; Gross, R. A. Polylactide/Cellulose Nanocrystal Nanocomposites: Efficient Routes for Nanofiber Modification and Effects of Nanofiber Chemistry on PLA Reinforcement. *Polymer (Guildf)* **2015**, *65*, 9–17. https://doi.org/10.1016/j.polymer.2015.02.048.

(19) Trifol, J.; Plackett, D.; Sillard, C.; Hassager, O.; Daugaard, A. E.; Bras, J.; Szabo, P. A Comparison of Partially Acetylated Nanocellulose, Nanocrystalline Cellulose, and Nanoclay as Fillers for High-Performance Polylactide Nanocomposites. *J Appl Polym Sci* **2016**, *133* (14). https://doi.org/10.1002/app.43257.

(20) Lam, E.; Hemraz, U. D. Preparation and Surface Functionalization of Carboxylated Cellulose Nanocrystals. *Nanomaterials* **2021**, *11* (7), 1641. https://doi.org/10.3390/nano11071641.

(21) Bayat, P.; Meek, K. M.; Movafagh, M.; Cranston, E. D.; Cunningham, M. F.; Champagne, P.; Morse, T.; Kiriakou, M. V.; George, S. R.; Dubé, M. A. The Effect of Cellulose Nanocrystal Reassembly on Latex-Based Pressure-Sensitive Adhesive Performance. *Biomacromolecules* **2024**, *25* (5), 3018–3032. https://doi.org/10.1021/acs.biomac.4c00138.

(22) Bhiogade, A.; Kannan, M. Studies on Thermal and Degradation Kinetics of Cellulose Micro/Nanoparticle Filled Polylactic Acid (PLA) Based Nanocomposites. *Polymers and Polymer Composites* **2021**, *29* (9), S85–S98. https://doi.org/10.1177/0967391120987170.

(23) dos Santos, F. A.; Iulianelli, G. C. V.; Tavares, M. I. B. Effect of Microcrystalline and Nanocrystals Cellulose Fillers in Materials Based on PLA Matrix. *Polym Test* **2017**, *61*, 280–288. https://doi.org/10.1016/j.polymertesting.2017.05.028.

(24) Dhar, P.; Tarafder, D.; Kumar, A.; Katiyar, V. Thermally Recyclable Polylactic Acid/Cellulose Nanocrystal Films through Reactive Extrusion Process. *Polymer (Guildf)* **2016**, *87*, 268–282. https://doi.org/10.1016/j.polymer.2016.02.004.

(25) Bagheriasl, D.; Carreau, P. J.; Riedl, B.; Dubois, C.; Hamad, W. Y. Shear Rheology of Polylactide (PLA)–Cellulose Nanocrystal (CNC) Nanocomposites. *Cellulose* **2016**, *23* (3), 1885–1897. https://doi.org/10.1007/s10570-016-0914-1.

(26) Khoshkava, V.; Kamal, M. R. Effect of Surface Energy on Dispersion and Mechanical Properties of Polymer/Nanocrystalline Cellulose Nanocomposites. *Biomacromolecules* **2013**, *14* (9), 3155–3163. https://doi.org/10.1021/bm400784j.

(27) Mukherjee, T.; Tobin, M. J.; Puskar, L.; Sani, M.-A.; Kao, N.; Gupta, R. K.; Pannirselvam, M.; Quazi, N.; Bhattacharya, S. Chemically Imaging the Interaction of Acetylated Nanocrystalline Cellulose (NCC) with a Polylactic Acid (PLA) Polymer Matrix. *Cellulose* **2017**, *24* (4), 1717–1729. https://doi.org/10.1007/s10570-017-1217-x.

(28) Kua, Y. L.; Gan, S.; Morris, A.; Ng, H. K. Ethyl Lactate as a Potential Green Solvent to Extract Hydrophilic (Polar) and Lipophilic (Non-Polar) Phytonutrients Simultaneously from Fruit and Vegetable by-Products. *Sustain Chem Pharm* **2016**, *4*, 21–31. https://doi.org/10.1016/j.scp.2016.07.003.

(29) Hossain, K. M. Z.; Ahmed, I.; Parsons, A. J.; Scotchford, C. A.; Walker, G. S.; Thielemans, W.; Rudd, C. D. Physico-Chemical and Mechanical Properties of Nanocomposites Prepared Using Cellulose Nanowhiskers and Poly(Lactic Acid). *J Mater Sci* **2012**, *47* (6), 2675–2686. https://doi.org/10.1007/s10853-011-6093-4.

(30) Pal, N.; Dubey, P.; Gopinath, P.; Pal, K. Combined Effect of Cellulose Nanocrystal and Reduced Graphene Oxide into Poly-Lactic Acid Matrix Nanocomposite as a Scaffold and Its Anti-Bacterial Activity. *Int J Biol Macromol* **2017**, *95*, 94–105. https://doi.org/10.1016/j.ijbiomac.2016.11.041.

(31) Habibi, Y.; Lucia, L. A.; Rojas, O. J. Cellulose Nanocrystals: Chemistry, Self-Assembly, and Applications. *Chem Rev* **2010**, *110* (6), 3479–3500. https://doi.org/10.1021/cr900339w.

(32) Lin, N.; Huang, J.; Chang, P. R.; Feng, J.; Yu, J. Surface Acetylation of Cellulose Nanocrystal and Its Reinforcing Function in Poly(Lactic Acid). *Carbohydr Polym* **2011**, *83* (4), 1834–1842. https://doi.org/10.1016/j.carbpol.2010.10.047.

(33) Minggang Fang; Luo, C.; Guo, X.; Sun, J.; Chen, M.; Chen, W. The Effect of Cellulose Nanocrystals and Acetylated Nanocellulose on the Crystallization Kinetics and Thermal Stability of Polylactic Acid. *Polymer Science - Series A* **2022**, *64* (6), 802–817. https://doi.org/10.1134/S0965545X22700523.

(34) Espino-Pérez, E.; Bras, J.; Almeida, G.; Plessis, C.; Belgacem, N.; Perré, P.; Domenek, S. Designed Cellulose Nanocrystal Surface Properties for Improving Barrier Properties in Polylactide Nanocomposites. *Carbohydr Polym* **2018**, *183*, 267–277. https://doi.org/10.1016/j.carbpol.2017.12.005.

(35) Abedi, F.; Emadzadeh, D.; Dubé, M. A.; Kruczek, B. Modifying Cellulose Nanocrystal Dispersibility to Address the Permeability/Selectivity Trade-off of Thin-Film Nanocomposite Reverse Osmosis Membranes. *Desalination* **2022**, *538*, 115900. https://doi.org/10.1016/j.desal.2022.115900.

(36) Movafagh, M.; Meek, K. M.; Bayat, P.; Cranston, E. D.; Cunningham, M.; Champagne, P.; Morse, T.; Kiriakou, M.; George, S.; Dubé, M. A. Improved Pressure-sensitive Adhesive Performance Using Carboxylated Cellulose Nanocrystals via Blending. *Polym. Eng. Sci.* **2024**, *64* (2), 798–816. https://doi.org/10.1002/pen.26585.

(37) Abedi, F.; Dubé, M. A.; Emadzadeh, D.; Kruczek, B. Improving Nanofiltration Performance Using Modified Cellulose Nanocrystal-Based TFN Membranes. *J Memb Sci* **2023**, *670*, 121369. https://doi.org/10.1016/j.memsci.2023.121369.

(38) Bayat, P.; Meek, K. M.; Cranston, E. D.; Cunningham, M.; Champagne, P.; Morse, T.; Werner, A.; George, S.; Cancellara, C.; Dubé, M. A. Enhancing Pressure Sensitive Adhesive Performance Using Acetylated Carboxylated Cellulose Nanocrystals. *Ind Eng Chem Res* **2025**, *64* (9), 4932–4941. https://doi.org/10.1021/acs.iecr.4c04649.

(39) Werner, A.; Schmitt, V.; Sèbe, G.; Héroguez, V. Synthesis of Surfactant-Free Micro- and Nanolatexes from Pickering Emulsions Stabilized by Acetylated Cellulose Nanocrystals. *Polym. Chem.* **2017**, *8* (39), 6064–6072. https://doi.org/10.1039/C7PY01203A.

(40) Xu, J.; Wu, Z.; Wu, Q.; Kuang, Y. Acetylated Cellulose Nanocrystals with High-Crystallinity Obtained by One-Step Reaction from the Traditional Acetylation of Cellulose. *Carbohydr. Polym.* **2020**, *229*, 115553. https://doi.org/10.1016/j.carbpol.2019.115553.

(41) Wohlert, J.; Chen, P.; Berglund, L. A.; Lo Re, G. Acetylation of Nanocellulose: Miscibility and Reinforcement Mechanisms in Polymer Nanocomposites. *ACS Nano* **2024**, *18* (3), 1882–1891. https://doi.org/10.1021/acsnano.3c04872.

(42) Wu, Z.; Xu, J.; Gong, J.; Li, J.; Mo, L. Preparation, Characterization and Acetylation of Cellulose Nanocrystal Allomorphs. *Cellulose* **2018**, *25* (9), 4905–4918. https://doi.org/10.1007/s10570-018-1937-6.

(43) Agustin, M. B.; Nakatsubo, F.; Yano, H. The Thermal Stability of Nanocellulose and Its Acetates with Different Degree of Polymerization. *Cellulose* **2016**, *23* (1), 451–464. https://doi.org/10.1007/s10570-015-0813-x.

(44) Mukherjee, T.; Sani, M.; Kao, N.; Gupta, R. K.; Quazi, N.; Bhattacharya, S. Improved Dispersion of Cellulose Microcrystals in Polylactic Acid (PLA) Based Composites Applying Surface Acetylation. *Chem Eng Sci* **2013**, *101*, 655–662. https://doi.org/10.1016/j.ces.2013.07.032.

(45) Tuccitto, A. V.; Anstey, A.; Sansone, N. D.; Park, C. B.; Lee, P. C. Controlling Stereocomplex Crystal Morphology in Poly(Lactide) through Chain Alignment. *Int J Biol Macromol* **2022**, *218*, 22–32. https://doi.org/10.1016/j.ijbiomac.2022.07.081.

(46) Dong, F.; Yan, M.; Jin, C.; Li, S. Characterization of Type-II Acetylated Cellulose Nanocrystals with Various Degree of Substitution and Its Compatibility in PLA Films. *Polymers (Basel)* **2017**, *9* (8). https://doi.org/10.3390/polym9080346.

(47) Kang, H.; Kim, D. S. A Study on the Crystallization and Melting of PLA Nanocomposites with Cellulose Nanocrystals by DSC. *Polym Compos* **2023**, *44* (11), 7727–7736. https://doi.org/10.1002/pc.27658.

(48) Li, Y.; Han, C. Isothermal and Nonisothermal Cold Crystallization Behaviors of Asymmetric Poly(L-Lactide)/Poly(D-Lactide) Blends. *I&ECR* **2012**, *51* (49), 15927–15935. https://doi.org/10.1021/ie302447e.

(49) Avrami, M. Kinetics of Phase Change. I General Theory. *J Chem Phys* **1939**, *7* (12), 1103–1112. https://doi.org/10.1063/1.1750380.

(50) Zhang, J.; Tsuji, H.; Noda, I.; Ozaki, Y. Structural Changes and Crystallization Dynamics of Poly(L-Lactide) during the Cold-Crystallization Process Investigated by Infrared and Two-Dimensional Infrared Correlation Spectroscopy. *Macromolecules* **2004**, *37* (17), 6433–6439. https://doi.org/10.1021/ma049288t.

(51) Arslan, D.; Vatansever, E.; Sarul, D. S.; Kahraman, Y.; Gunes, G.; Durmus, A.; Nofar, M. Effect of Preparation Method on the Properties of Polylactide/Cellulose Nanocrystal

Nanocomposites. *Polym Compos* **2020**, *41* (10), 4170–4180. https://doi.org/10.1002/pc.25701.

Chapter 6

General Discussion and Conclusion

6.1 General discussion

The objective of this study was to enhance polymer nanocomposite systems through the introduction of sustainable nanoparticles, i.e., carboxylated cellulose nanocrystals (cCNCs). By modifying the cCNCs to render them hydrophobic—and hence compatible with hydrophobic polymeric matrices—while also optimizing reaction conditions (i.e., using bio-based solvents), the performance and sustainability of the polymer nanocomposites were significantly improved. Ultimately, a promising route to reduce environmental impacts while maintaining—or even surpassing—conventional performance standards was presented.

6.2 Sustainability and performance in polymer nanocomposites

Polymers play a vital role across numerous industries, including automotive, aerospace, biomedical, electronics, and packaging.[1] The sustainability of petroleum-derived polymers has raised concerns, so researchers are focusing more on bio-based alternatives (e.g., bio-based polymers) and novel synthesis techniques (e.g., emulsion polymerization).[2] However, performance discrepancies between petroleum-based polymers and more environmentally sustainable materials continue to be a major focus of scientific inquiry.[3–6] In response, several bio-based composites, especially those that contain wood-derived nanoparticles, have been developed.[7]

Among these nanomaterials, CNCs have shown great promise because of their remarkable mechanical qualities, high aspect ratio, and biocompatibility for altering polymer characteristics and enhancing the sustainability of polymer nanocomposites.[8] The acid used during extraction affects the surface functional groups of CNCs.[9] cCNCs, which are made using a sustainable hydrogen peroxide oxidation process (Figure 6.1), have advantages over conventional sulfated CNCs (e.g., higher thermal and colloidal stability).[10–12] The dispersion and

reassembly of nanoparticles inside the polymer matrix are essential for attaining maximum performance in nanocomposites since they directly affect mechanical strength, barrier qualities, and overall stability.[13–16] Many hydrophobic polymers fail to fully exploit the potential of cCNCs; the challenge lies in achieving uniform dispersion and strong interfacial adhesion between the polymer and nanocellulose phases. CNCs' high hydroxy (OH) group density makes them more receptive to functionalization, creating new possibilities for enhancing reassembly and dispersion.[17,18] Research efforts have increasingly focused on better distribution of cCNCs within the hydrophobic polymeric matrix to boost their compatibility and enhanced material characteristics.

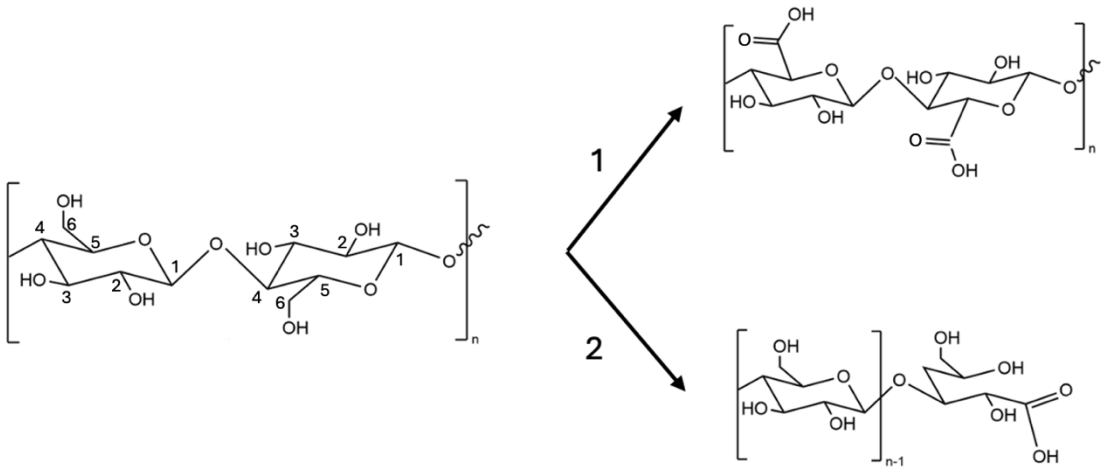

Figure 6.1. Chemical structure of carboxylated CNC. [taken from Chapter 2]

6.3 cCNC-based PSA nanocomposites

PSAs are adhesives that allow for instant adherence to a surface when mild pressure is applied, like a fingertip touch.[19] PSAs are typically assessed using three primary characteristics: (1) tack, which is the force needed to immediately separate the adhesive after it has soaked a surface; (2) peel strength, which is the force required to remove the adhesive from a surface after bonding; and (3) shear strength, which is the adhesive's ability to withstand creep or flow when stress is applied.[2,20,21] To promote sustainable polymers and reduce VOC emissions, emulsion (latex-based) polymerization replaces hazardous solvents with water as the reaction medium.[22] Water enhances reactant transport, heat dissipation, and viscosity control, making the process

environmentally benign. Conducted in batch, semi-batch, or continuous modes; the semi-batch process offers precise control over reaction rate and particle formation.[23,24]

In Chapter 3, I employed semi-batch emulsion polymerization to create a commercial PSA formulation. Although this technique provided a greener option to solution polymerization, the segmented structure of emulsion-based PSAs resulted in reduced shear adhesion. To overcome this challenge, I explored the incorporation of cCNCs to enhance PSA performance. In this chapter, I examined how cCNC end-to end reassembly plays a crucial part in improving the shear adhesion of PSAs made of latex. Although the cCNCs create side-by-side reassemblies, compelling indirect evidence in changes in shear adhesion has shown their higher tendency to create end-to-end reassemblies rather than side-by-side reassemblies. One important difference was made between dried-redispersed cCNCs, which had a greater tendency to reassemble into nanofibril-like structures because of their lower zeta potential, and never-dried cCNCs, which show superior dispersion but poorer reassembly. Reassembly by itself did not result in better PSA performance; rather, a well-dispersed reassembly was necessary to maximize shear adhesion. To better understand this equilibrium, cCNCs were sonicated before polymerization to enhance dispersion and encourage a more even and dispersed reassembly during PSA film creation (Figure 6.2). This ultimately resulted in a 1350% increase in shear adhesion when compared to the base case. Furthermore, an analysis of the timing of cCNC integration in emulsion polymerization showed that feed-stage addition improved dispersion, decreased viscosity, and permitted higher cCNC loadings, whereas seed-stage addition promoted increased nanofibril production and cohesive strength (Chapter 3). Comparisons with sulfated CNCs, which showed lower reassembly tendencies at greater zeta potentials, further demonstrated how crucial cCNC network formation is for increasing PSA cohesiveness. Ultimately, this study demonstrated that optimizing the interplay between dispersion and reassembly is crucial for enhancing PSA properties, particularly for achieving superior shear adhesion.[25]

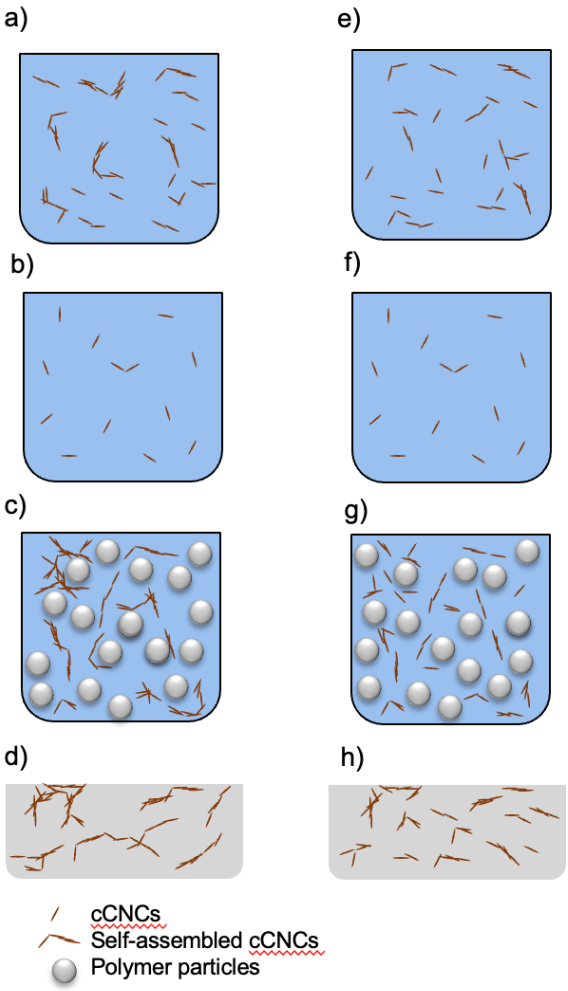

Figure 6.2. Dried-redispersed cCNCs in water, a) before and b) after sonication; and in the latex, c) after polymerization and d) in the dried film. Never-dried cCNCs in water, e) before and f) after sonication; and in the latex, g) after polymerization, and h) in the dried film. For images c), d), g) and h), cCNC addition is assumed to be at the seed stage [taken from Chapter 3].

The number of available hydroxy (OH) groups on cCNCs gives room to boost its compatibility (dispersion) in hydrophobic matrices. According to earlier research, using slightly hydrophilic CNCs in traditional emulsion polymerization produced better PSA characteristics than using totally hydrophilic, unmodified CNCs.[26] However, the precise hydrophobic alterations made

to CNCs in earlier studies were unknown due to proprietary restrictions.[26,27] In Chapter 4, I used a straightforward and eco-friendly acetylation procedure to modify cCNCs with different degrees of substitution (DS).[28] ATR-FTIR spectroscopy was used to assess the DS, and measurements of water contact angles showed that as DS increased, the hydrophilic (30±2°) behaviour changed to hydrophobic (101±4°) behaviour. This work revealed that acetylation decreased the zeta potential and, consequently, the interfacial tension.[29]

This investigation showed that acetylation improved dispersion in the polymer matrix by lowering the zeta potential. Since there were fewer repulsive forces between AcCNCs and polymer particles, AcCNCs showed a stronger tendency for end-to-end reassembly close to the surface of polymer particles (with higher DS). As seen in Figure 6.3, the most hydrophobic AcCNCs (DS = 0.42) showed remarkable shear adhesion increases of 1650%, peel strength increases of 66%, and tack increases of 251%.[29] These findings highlight how nanoparticle surface modification plays a crucial role in unlocking their full potential for enhancing PSA performance. By systematically adjusting the DS, the broader potential of cCNCs is underscored for tailoring nanoparticle behaviour for advanced applications beyond PSAs, such as coatings, hydrogels, and functional materials.

6.4 cCNC-based PLA nanocomposites

Polylactic acid (PLA) is considered one of the most promising bio-sourced polymers in medication delivery, packaging, textiles, and biomedical equipment due to its UV stability, biodegradability, and biocompatibility.[30,31] However, its slow crystallization and limited mechanical properties hinder its scalability for broader application.[32,33]

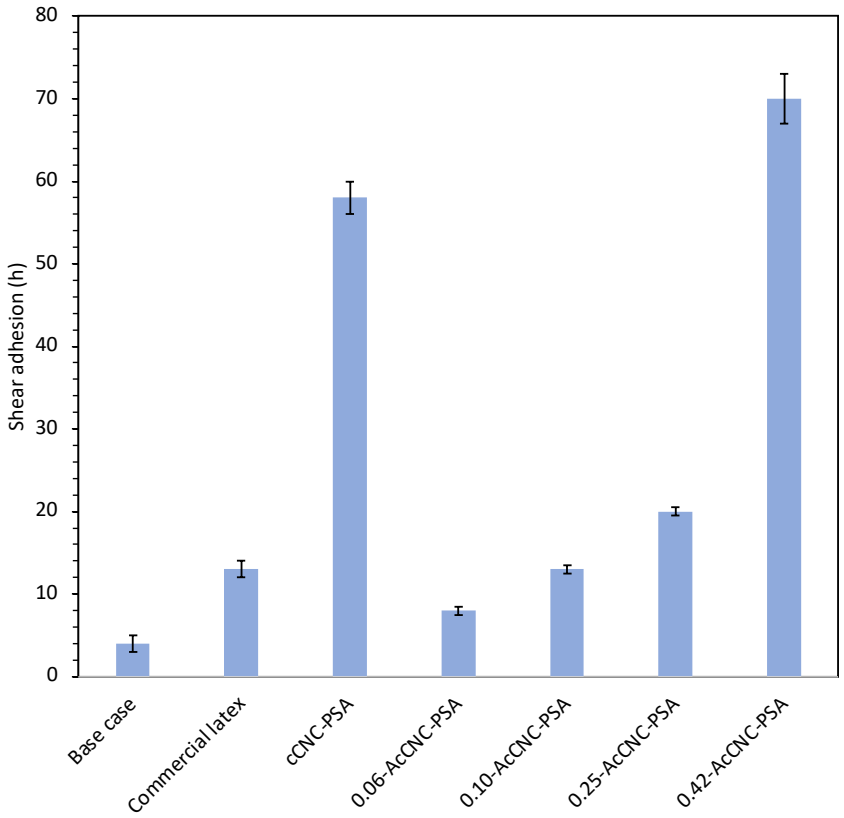

Figure 6.3. Effect of acetylation on shear adhesion.[taken from Chapter 4]

In Chapter 5, I studied how cCNCs and AcCNCs affect PLA-based nanocomposites' mechanical characteristics and crystallization behaviour. In contrast to earlier research that relied on toxic solvents such as dimethyl formamide, chloroform, and dichloromethane for CNC dispersion, this study showed that ethyl lactate (EtLa) is a practical, environmentally acceptable substitute that improves cCNC dispersion while maintaining environmental safety regulations.[34] EtLa served a dual function—acting as a plasticizer to increase chain mobility and reduce the cold crystallization temperature (T_{cc}) while simultaneously improving CNC dispersion in the PLA matrix.

Isothermal and non-isothermal DSC analyses confirmed that increasing cCNC content accelerated PLA crystallization, with Avrami analysis revealing a transition to three-dimensional spherulitic growth at an optimal 1.5 wt.% cCNC. The nucleation behaviour of AcCNCs was significantly influenced by the DS. At lower DS levels (AcCNC-0.06 and AcCNC-0.10), improved compatibility with EtLa led to a shorter crystallization half-time ($t_{1/2}$) and greater nucleation efficiency. However, excessive hydrophobicity at higher DS levels (AcCNC-0.25 and AcCNC-0.42)

caused poor dispersion in EtLa, which increased PLA aggregation and decreased nucleation effectiveness.

Our study demonstrated that EtLa serves as an effective bio-based solvent, offering a safer and more sustainable alternative for CNC dispersion, facilitating environmentally friendly nanocomposite processing. Additionally, cCNCs enhanced PLA crystallization kinetics and mechanical properties. Though cCNCs slightly reduced thermal stability, modifying cCNC surface chemistry (i.e., AcCNC) helped maintain PLA's original thermal stability. The interplay between AcCNC dispersion, cCNC nucleation, and EtLa plasticization highlights the importance of tailored formulation strategies in designing high-performance, biodegradable nanocomposites with enhanced properties.

This research expanded cCNC applications beyond PSA and PLA, providing Anomera Inc. with key insights into DextraCel™ behaviour in polymer systems. By modification of cCNCs, we facilitated broader applications in paints, coatings, and polymers. These findings, showcased in peer-reviewed publications, have led to a spin-off collaboration between Anomera, BASF, NSERC, and leading universities.

6.5 Future work

Building on the advances achieved in this research, several opportunities remain for further innovation and exploration:

1. **Explore the maximum DS to find the threshold of the highest PSA, PLA performance.**
   A deeper investigation into the maximum degree of substitution (DS) is essential to determine the optimal balance between functionality and material performance. Higher DS values can significantly impact the dispersion, compatibility, and crystallization behaviour of PLA. Understanding the upper DS limit will help identify at what point further substitution ceases to provide additional benefits or begins to hinder mechanical, thermal, or biodegradability properties.
2. **Fine-Tuning the Acetylation Protocol**
   A systematic study linking time, catalyst concentration, and temperature to the resulting DS would help pinpoint the most effective parameters for specific performance

objectives. Employing Design of Experiments (DoE) methods (e.g., Minitab) can efficiently map these process variables, ensuring precise control over the degree of substitution.

3. **Scaling Up Acetylation**

   Laboratory-scale acetylation was both challenging and time-consuming, particularly when dealing with small batches. Investigating protocols for larger-scale or continuous processes would streamline the production of AcCNCs, facilitating their broader commercial adoption.

4. **Substituting Biodegradable Monomers in PSA Formulations**

   Future work on pressure-sensitive adhesives can further reduce environmental impact by incorporating biodegradable monomers into the formulation.

5. **Exploring Alternative Bio-Solvents**

   While ethyl lactate (EtLa) proved effective, identifying other green solvents that are compatible with high-DS AcCNCs (e.g., limonene) could further optimize their dispersion and maximize PLA crystallinity.

6. **Investigating Other PLA Grades**

   Beyond crystallization and mechanical performance, evaluating permeability in different PLA grades (including copolymers) could reveal new applications for AcCNC/PLA nanocomposites in barrier packaging or controlled-release systems.

By pursuing these research directions, cCNC-based nanocomposite systems can be further refined, broadening the range of sustainable, high-performance materials suitable for applications from packaging and adhesives to biomedical and beyond.

6.6 References

(1) Thomas, S.; Joseph, K.; Malhotra, S. K.; Goda, K. *Polymers for Packaging Applications*; Alavi, S., Thomas, S., Sandeep, K. P., Kalarikkal, N., Varghese, J., Yaragalla, S., Eds.; Apple Academic Press, 2014. https://doi.org/10.1201/b17388.

(2) Dubé, M. A.; Gabriel, V. A.; Pakdel, A. S.; Zhang, Y. Sustainable Polymer Reaction Engineering: Are We There Yet? *Can J Chem Eng* **2021**, *99* (1), 31–60. https://doi.org/10.1002/cjce.23865.

(3) Dastjerdi, Z.; Cranston, E. D.; Dubé, M. A. Pressure Sensitive Adhesive Property Modification Using Cellulose Nanocrystals. *Int J Adhes Adhes* **2018**, *81*, 36–42. https://doi.org/10.1016/j.ijadhadh.2017.11.009.

(4) Ouzas, A.; Niinivaara, E.; Cranston, E. D.; Dubé, M. A. In Situ Semibatch Emulsion Polymerization of 2-Ethyl Hexyl Acrylate/n-Butyl Acrylate/Methyl Methacrylate/Cellulose Nanocrystal Nanocomposites for Adhesive Applications. *Macromol React Eng* **2018**, *12* (3), 1–10. https://doi.org/10.1002/mren.201700068.

(5) Ahmadi-Dehnoei, A.; Ghasemirad, S. Designing of Desired Nanocomposite Pressure-Sensitive Adhesives through Tailoring the Structural Characteristics of Polysilsesquioxane-Acrylic Core-Shell Nanoparticles. *Int J Adhes Adhes* **2021**, *111*, 102973. https://doi.org/10.1016/j.ijadhadh.2021.102973.

(6) Khanjani, J.; Zohuri, G. H.; Gholami, M.; Shojaei, B.; Dalir, R. Emulsion Semi-Batch Terpolymerization Process Using Hybrid Emulsifiers for Synthesizing New Emulsion Pressure Sensitive Adhesives (EPSAs). *J Adhes* **2014**, *90* (2), 174–194. https://doi.org/10.1080/00218464.2013.772052.

(7) Lin, N.; Huang, J.; Dufresne, A. Preparation, Properties and Applications of Polysaccharide Nanocrystals in Advanced Functional Nanomaterials: A Review. *Nanoscale* **2012**, *4* (11), 3274. https://doi.org/10.1039/c2nr30260h.

(8) Dufresne, A. *Nanocellulose*; Huang, J., Dufresne, A., Lin, N., Eds.; Wiley, 2019. https://doi.org/10.1002/9783527807437.

(9) Delepierre, G.; Vanderfleet, O. M.; Niinivaara, E.; Zakani, B.; Cranston, E. D. Benchmarking Cellulose Nanocrystals Part II: New Industrially Produced Materials. *Langmuir* **2021**, *37* (28), 8393–8409. https://doi.org/10.1021/acs.langmuir.1c00550.

(10) Delepierre, G.; Vanderfleet, O. M.; Niinivaara, E.; Zakani, B.; Cranston, E. D. Benchmarking Cellulose Nanocrystals Part II: New Industrially Produced Materials. *Langmuir* **2021**, *37* (28), 8393–8409. https://doi.org/10.1021/acs.langmuir.1c00550.

(11) Lam, E.; Hemraz, U. D. Preparation and Surface Functionalization of Carboxylated Cellulose Nanocrystals. *Nanomaterials* **2021**, *11* (7), 1641. https://doi.org/10.3390/nano11071641.

(12) Espino-Pérez, E.; Domenek, S.; Belgacem, N.; Sillard, C.; Bras, J. Green Process for Chemical Functionalization of Nanocellulose with Carboxylic Acids. *Biomacromolecules* **2014**, *15* (12), 4551–4560. https://doi.org/10.1021/bm5013458.

(13) Vatansever, E.; Arslan, D.; Sarul, D. S.; Nofar, M. The CNC Dispersion Quality in Various PLA Grades. In *AIP Conference Proceedings*; American Institute of Physics Inc., 2023; Vol. 2607. https://doi.org/10.1063/5.0135790.

(14) Sahlin, K.; Forsgren, L.; Moberg, T.; Bernin, D.; Rigdahl, M.; Westman, G. Surface Treatment of Cellulose Nanocrystals (CNC): Effects on Dispersion Rheology. *Cellulose* **2018**, *25* (1), 331–345. https://doi.org/10.1007/s10570-017-1582-5.

(15) Moon, R. J.; Martini, A.; Nairn, J.; Simonsen, J.; Youngblood, J. Cellulose Nanomaterials Review: Structure, Properties and Nanocomposites. *Chem Soc Rev* **2011**, *40* (7), 3941. https://doi.org/10.1039/c0cs00108b.

(16) Oksman, K.; Aitomäki, Y.; Mathew, A. P.; Siqueira, G.; Zhou, Q.; Butylina, S.; Tanpichai, S.; Zhou, X.; Hooshmand, S. Review of the Recent Developments in Cellulose Nanocomposite Processing. *Compos Part A Appl Sci Manuf* **2016**, *83*, 2–18. https://doi.org/10.1016/j.compositesa.2015.10.041.

(17) Ferreira, F. V.; Pinheiro, I. F.; Gouveia, R. F.; Thim, G. P.; Lona, L. M. F. Functionalized Cellulose Nanocrystals as Reinforcement in Biodegradable Polymer Nanocomposites. *Polym. Compos.* **2018**, *39* (S1), E9–E29. https://doi.org/10.1002/pc.24583.

(18) Hokkanen, S.; Bhatnagar, A.; Sillanpää, M. A Review on Modification Methods to Cellulose-Based Adsorbents to Improve Adsorption Capacity. *Water Res* **2016**, *91*, 156–173. https://doi.org/10.1016/j.watres.2016.01.008.

(19) Lin, S. B.; Durfee, L. D.; Ekeland, R. A.; McVie, J.; Schalau, G. K. Recent Advances in Silicone Pressure-Sensitive Adhesives. *J Adhes Sci Technol* **2007**, *21* (7), 605–623. https://doi.org/10.1163/156856107781192274.

(20) Jovanović, R.; Dubé, M. A. Emulsion-Based Pressure-Sensitive Adhesives: A Review. *Journal of Macromolecular Science, Part C: Polymer Reviews* **2004**, *44* (1), 1–51. https://doi.org/10.1081/MC-120027933.

(21) *Pressure Sensitive Tape Council. Test Methods for Pressure Sensitive Adhesive Tapes*.

(22) Lovell, P. A.; Schork, F. J. Fundamentals of Emulsion Polymerization. *Biomacromolecules* **2020**, *21* (11), 4396–4441. https://doi.org/10.1021/acs.biomac.0c00769.

(23) Asua, J. M. Emulsion Polymerization: From Fundamental Mechanisms to Process Developments. *Journal of Polymer Science, Part A: Polymer Chemistry*. 2004. https://doi.org/10.1002/pola.11096.

(24) Peter A. Lovell, M. S. E.-A. *Emulsion Polymerization and Emulsion Polymers*; 1997.

(25) Bayat, P.; Meek, K. M.; Movafagh, M.; Cranston, E. D.; Cunningham, M. F.; Champagne, P.; Morse, T.; Kiriakou, M. V.; George, S. R.; Dubé, M. A. The Effect of Cellulose Nanocrystal Reassembly on Latex-Based Pressure-Sensitive Adhesive Performance. *Biomacromolecules* **2024**, *25* (5), 3018–3032. https://doi.org/10.1021/acs.biomac.4c00138.

(26) Pakdel, A. S.; Niinivaara, E.; Cranston, E. D.; Berry, R. M.; Dubé, M. A. Cellulose Nanocrystal (CNC)–Latex Nanocomposites: Effect of CNC Hydrophilicity and Charge on Rheological, Mechanical, and Adhesive Properties. *Macromol. Rapid. Commun.* **2021**, *42* (3), 2000448. https://doi.org/10.1002/marc.202000448.

(27) Pakdel, A. S.; Cranston, E. D.; Dubé, M. A. Incorporating Hydrophobic Cellulose Nanocrystals inside Latex Particles via Mini-Emulsion Polymerization. *Macromol. React. Eng.* **2021**, *15* (5), 2100023. https://doi.org/10.1002/mren.202100023.

(28) Abedi, F.; Emadzadeh, D.; Dubé, M. A.; Kruczek, B. Modifying Cellulose Nanocrystal Dispersibility to Address the Permeability/Selectivity Trade-off of Thin-Film Nanocomposite Reverse Osmosis Membranes. *Desalination* **2022**, *538*, 115900. https://doi.org/10.1016/j.desal.2022.115900.

(29) Bayat, P.; Meek, K. M.; Cranston, E. D.; Cunningham, M.; Champagne, P.; Morse, T.; Werner, A.; George, S.; Cancellara, C.; Dubé, M. A. Enhancing Pressure Sensitive Adhesive Performance Using Acetylated Carboxylated Cellulose Nanocrystals. *Ind Eng Chem Res* **2025**, *64* (9), 4932–4941. https://doi.org/10.1021/acs.iecr.4c04649.

(30) Mokhena, T. C.; Sefadi, J. S.; Sadiku, E. R.; John, M. J.; Mochane, M. J.; Mtibe, A. Thermoplastic Processing of PLA/Cellulose Nanomaterials Composites. *Polymers (Basel)* **2018**, *10* (12), 1363. https://doi.org/10.3390/polym10121363.

(31) Arrieta, M. P.; Peltzer, M. A.; López, J.; Peponi, L. PLA-Based Nanocomposites Reinforced with CNC for Food Packaging Applications: From Synthesis to Biodegradation. In *Industrial Applications of Renewable Biomass Products*; Springer International Publishing: Cham, 2017; pp 265–300. https://doi.org/10.1007/978-3-319-61288-1_11.

(32) Nofar, M.; Sacligil, D.; Carreau, P. J.; Kamal, M. R.; Heuzey, M.-C. Poly (Lactic Acid) Blends: Processing, Properties and Applications. *Int J Biol Macromol* **2019**, *125*, 307–360. https://doi.org/10.1016/j.ijbiomac.2018.12.002.

(33) Sema Sarul, D.; Arslan, D.; Vatansever, E.; Kahraman, Y.; Durmus, A.; Salehiyan, R.; Nofar, M. Preparation and Characterization of PLA/PBAT/CNC Blend Nanocomposites. *Colloid Polym Sci* **2021**, *299* (6), 987–998. https://doi.org/10.1007/s00396-021-04822-9/Published.

(34) Kua, Y. L.; Gan, S.; Morris, A.; Ng, H. K. Ethyl Lactate as a Potential Green Solvent to Extract Hydrophilic (Polar) and Lipophilic (Non-Polar) Phytonutrients Simultaneously from Fruit and Vegetable by-Products. *Sustain Chem Pharm* **2016**, *4*, 21–31. https://doi.org/10.1016/j.scp.2016.07.003.

Appendix I

Supporting Information for Chapter 3: "The Effect of Cellulose Nanocrystal Surface Charge Density on PSA Performance"

Parisa Bayat[a], Kelly M. Meek[a], Maryam Movafagh[a], Emily D. Cranston[b], Michael F. Cunningham[c], Pascale Champagne[d], Timothy Morse[e], Michael V. Kiriakou[e], Sean R. George[f], and Marc A. Dubé[a]

[a]Department of Chemical and Biological Engineering, University of Ottawa, Ottawa, ON, Canada
[b]Department of Wood Science and Department of Chemical and Biological Engineering, University of British Columbia, Vancouver, BC, Canada
[c]Department of Chemical Engineering, Queen's University, Kingston, ON, Canada
[d]Energy Mining & Environment Research Centre, National Research Council, Montreal, QC, Canada
[e]Anomera Inc., Montreal, QC, Canada
[f]BASF Corp., Charlotte, NC, United States

This chapter is the Supporting Information for the manuscript published in Biomacromolecules (2024; 25,5: 3018-3032)

The differential scanning calorimetry (DSC) results are presented in Figure AI.1 for the base case formulation via seeded semi-batch emulsion polymerization. The DSC analysis gave a glass transition temperature (T_g) of -55 ºC, for a feed composition of 90/8/2 2-EHA/MMA/STY (w/w/w).

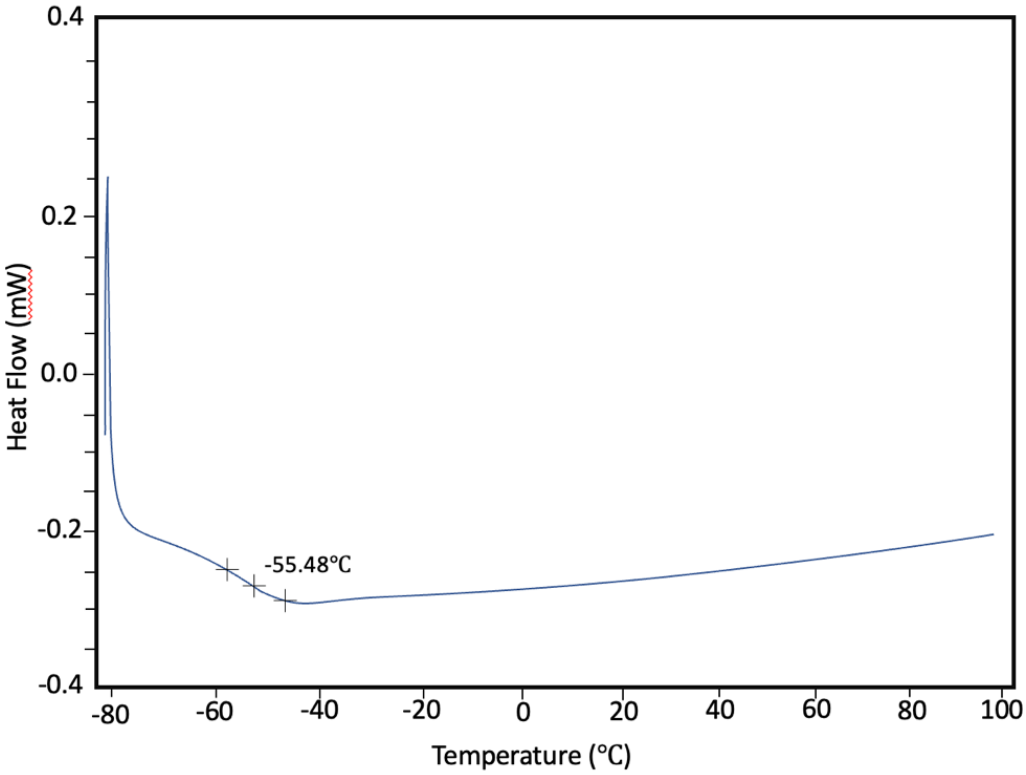

Figure AI.1. DSC result for base case formulation.

Appendix I

Preliminary experiments (Table AI.1) were conducted using a seeded semi-batch emulsion polymerization to formulate a base case high-performance adhesive. Challenges in achieving a stable latex and homogeneous dried latex films in Run #1 due to low latex viscosity were addressed by increasing the initiator and surfactant concentrations in Run #2, resulting in a reduced particle size and increased latex viscosity. Further enhancements in film castability were realized in Run #3 by employing a combination of anionic and non-ionic surfactants. The introduction of cCNCs initially led to coagulation in Run #4, prompting adjustments such as reducing the solids content, redistributing the water content between the seed and feed stages, and adding a buffer to achieve stability. These measures collectively resulted in a reproducible, stable base case latex formulation, even in the presence of cCNCs.

Table AI.1. Preliminary experiments

Run ID	Target solids (wt.%)	Water content		CNC type and loading (phm)			Sonicated (Y/N?)	Initiator Concn. (phm)	Buffer: Initiator (g:g)	Surfactant type and concentration (phm)		Final pH	Final particle size (nm)	Final PDI	Status
		Seed (wt.%)	Feed (wt%)	Sulfated CNC	Dried-redispersed cCNC	Never-dried cCNC				[Triton x-405]	[Dowfax 2A1]				
1	50	10	90		-			0.6	-		Seed (0.2) and Feed (1.8)	1	292	0.15	Stable / Not castable
2	50	30	70		-			0.8	0.75:1		Seed (0.4) and Feed (3.6)	7	108	0.30	Stable / Not castable
3	50	45	55		-			0.8	0.75:1	Seed (0.03) and Feed (0.3)	Seed (0.067) and Feed (0.6)	7	344	0.29	Stable/ Castable
4	50	45	55		0.3 Seed		Y	0.8	0.75:1	Seed (0.03) and Feed (0.3)	Seed (0.067) and Feed (0.6)				Coagulated
5	50	45	55		-			0.8	0.75:1	Seed (0.067) and Feed (0.6)	Seed (0.14) and Feed (1.2)				Coagulated
6	40	65	35		-			0.8	-	Seed (0.07) and Feed (0.27)	Seed (0.13) and Feed (0.53)	8	173	0.01	Stable / Castable
7	40	65	35		0.3 Seed		Y	0.8	-	Seed (0.07) and Feed (0.27)	Seed (0.13) and Feed (0.53)				Coagulated
Base case	40	65	35		-			0.8	0.35 :1	Seed (0.07) and Feed (0.27)	Seed (0.13) and Feed (0.53)	8	173	0.01	Stable / Castable

Figures AI.2 and AI.3 show the average particle size and polydispersity index trajectories (via DLS), respectively, for all the runs reported in the main manuscript.

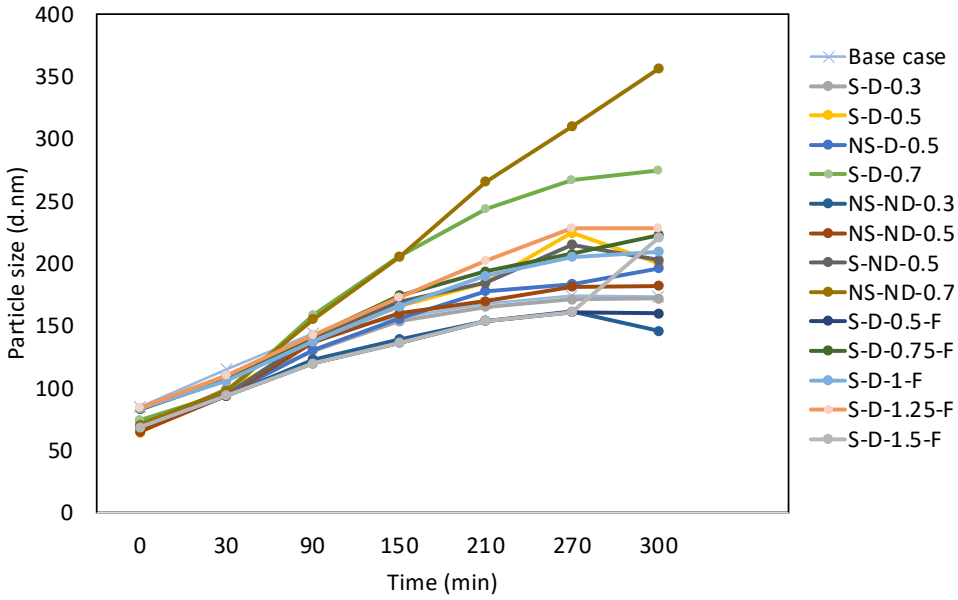

Figure AI.2. Average particle size trajectory for all runs.

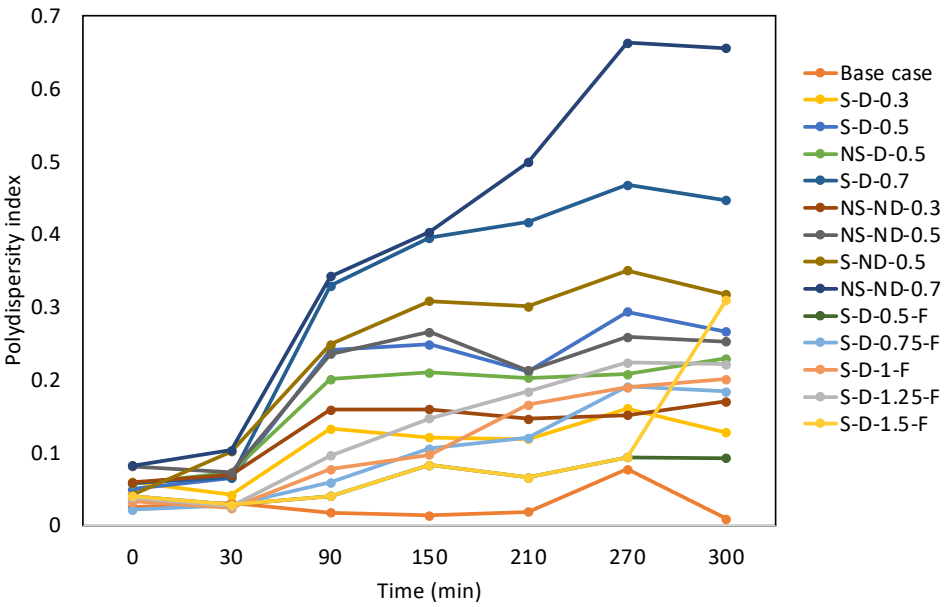

Figure AI.3. Polydispersity index trajectory for all runs.

Figures AI.4 and AI.5 show the instantaneous and overall conversion trajectories, respectively, for all the runs presented in the main manuscript. We note that the consistency in overall conversion rates for all of the runs, despite changes in latex particle size, underscores the robustness of the polymerization process and the reliability of the colloidally stable formulations.

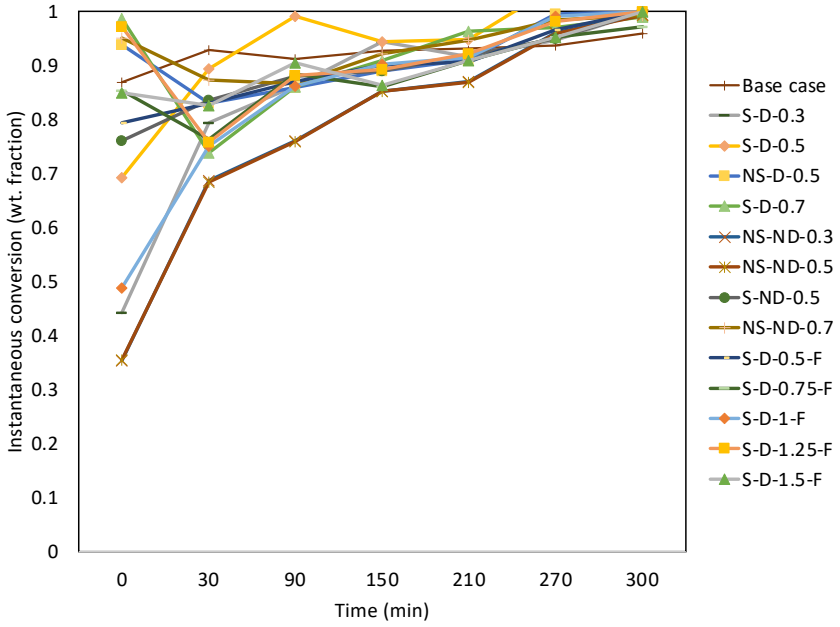

Figure AI.4. Instantaneous conversion trajectories for all runs.

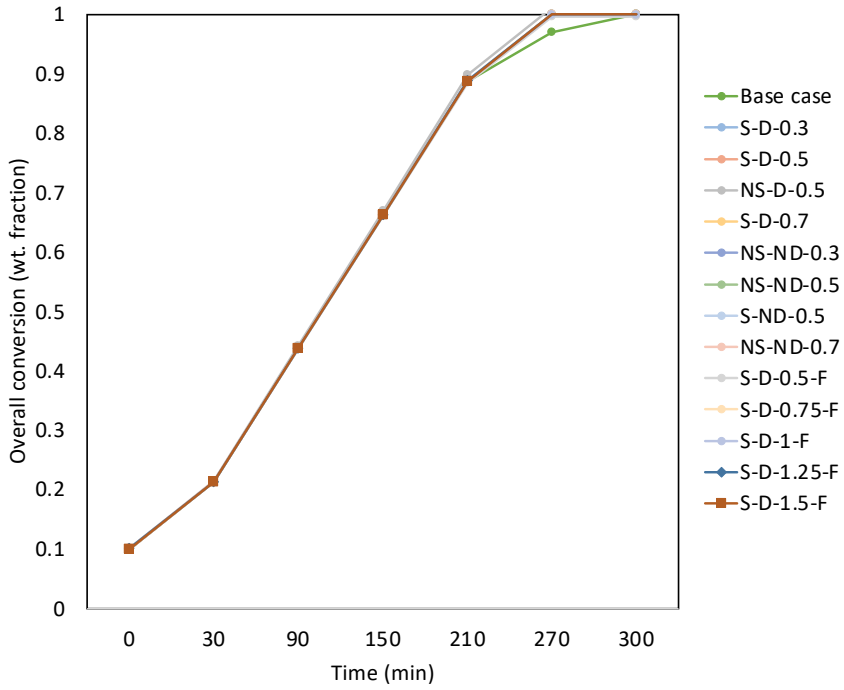

Figure AI.5. Overall conversion trajectories for all runs.

Figure AI.6 shows the difference in particle size distribution for runs in which cCNCs were introduced at the seed stage (Run S-D-0.5) versus the feed stage (Run S-D-0.5-F). The figure shows the second population of particles when cCNCs were added at the seed stage. All seed stage runs gave similar profiles, whereas all the feed stage runs showed a single particle size peak.

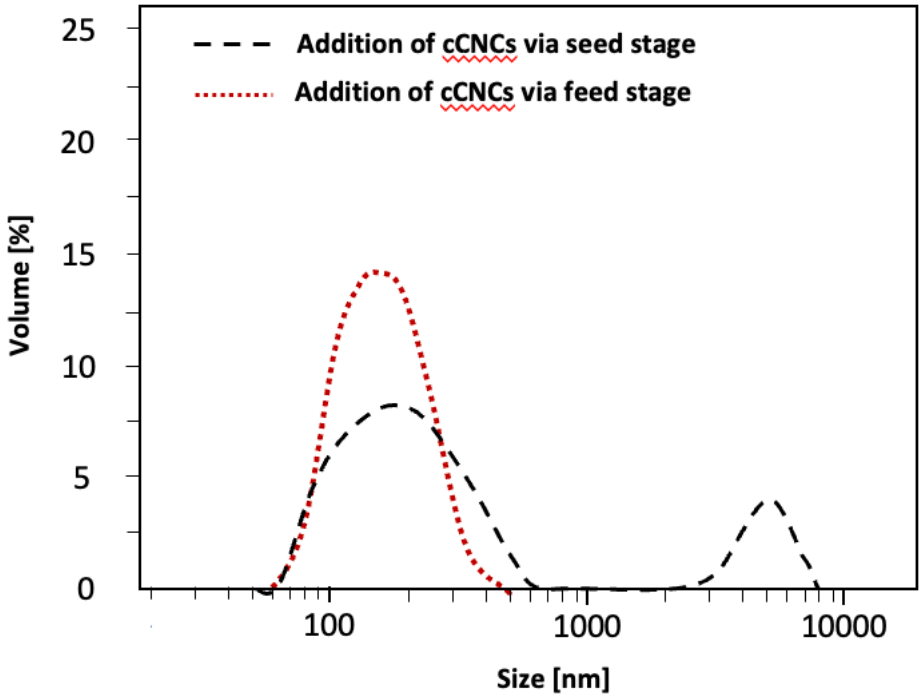

Figure AI.6. Particle size distribution of runs when cCNCs were added at the seed stage (S-D-0.5) versus the feed stage (S-D-0.5-F).

Figure AI.7 shows the particle size distribution for all runs.

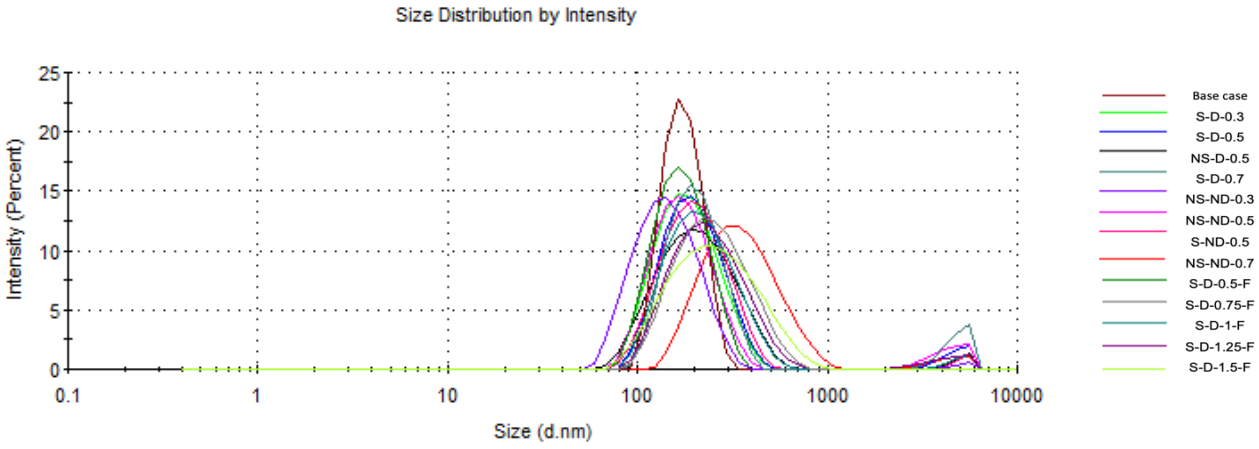

Figure AI.7. Particle size distribution of runs when cCNCs were added at the seed stage or the feed stage.

The pressure-sensitive adhesive performance, in terms of both adhesion and cohesion, is intricately tied to the viscoelastic characteristics of the polymer, measured using dynamic mechanical analysis (DMA). Figures AI.8-10 show the results for selected runs for G', G" and tan δ, respectively. The DMA tests were conducted at room temperature, approximately 75°C above the polymer's glass transition temperature, while maintaining a constant 1% strain.

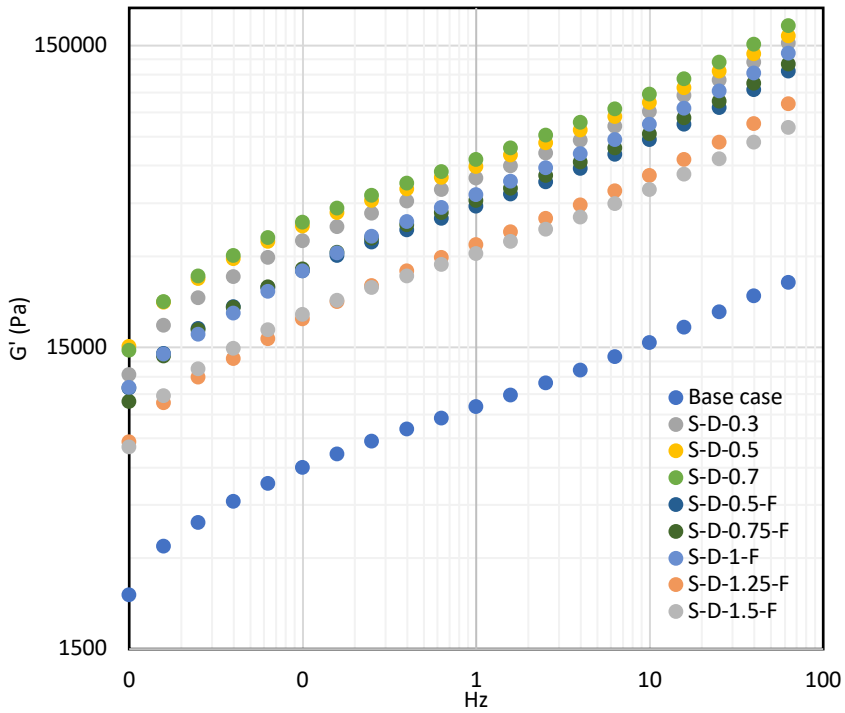

Figure AI.8. Elastic modulus, G', of runs at different cCNC loadings and different addition protocols (seed vs. feed (F)) versus frequency. All cCNCs were sonicated (S) and of the dried-redispersed (D) form. The numbers in the run IDs depict the cCNC loadings in phm.

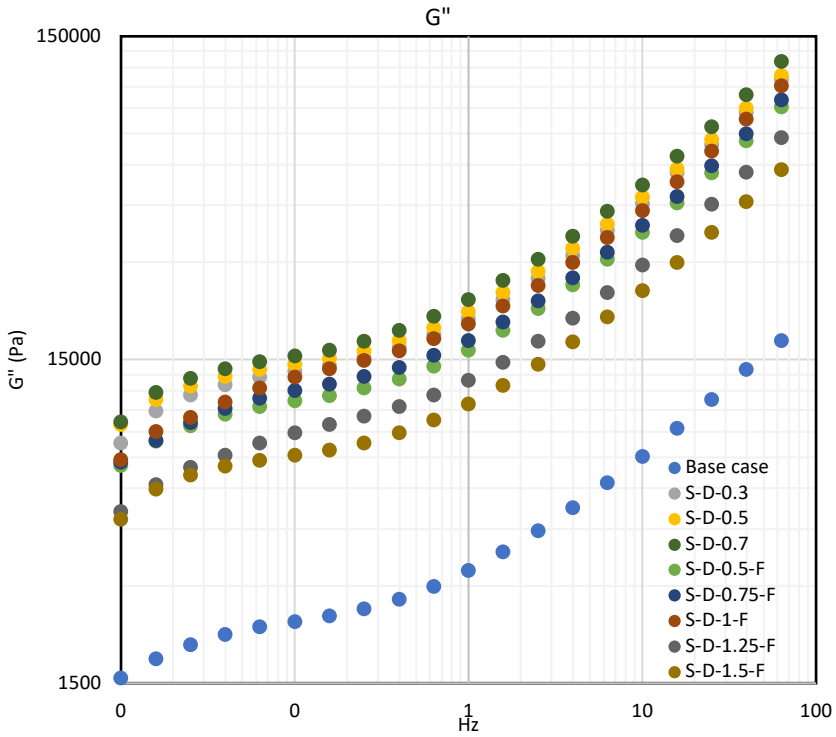

Figure AI.9. Viscous modulus, G" of runs at different cCNC loadings and different addition protocols (seed vs. feed (F)) versus the frequency. All cCNCs were sonicated (S) and of the dried-redispersed (D) form. The numbers in the run IDs depict the cCNC loadings in phm.

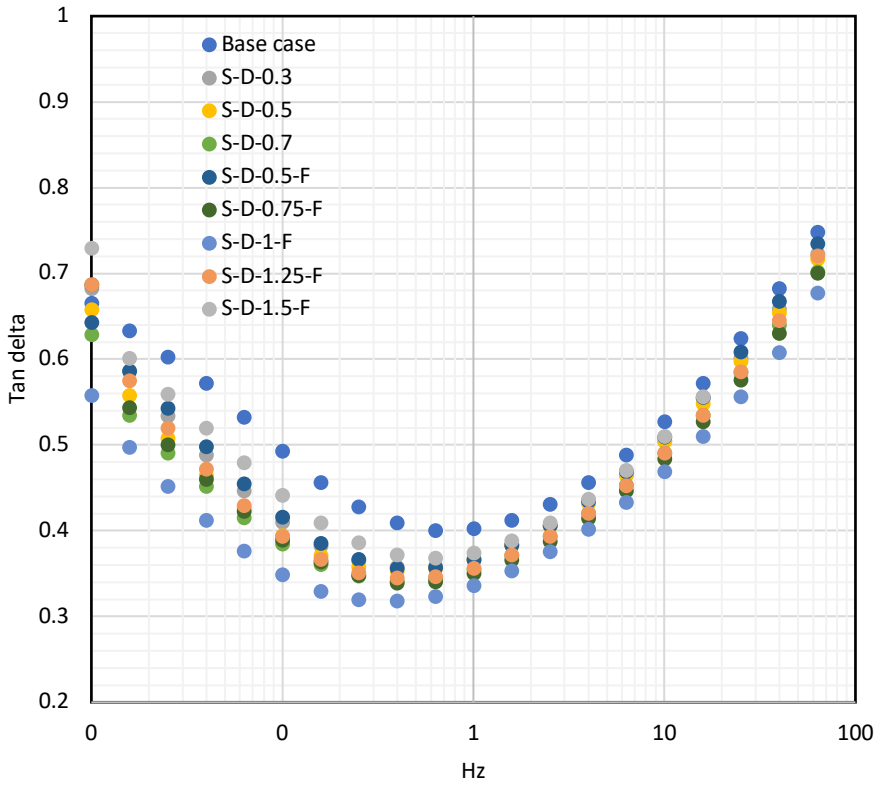

Figure AI.10. Tan δ for runs at different cCNC loadings and different addition protocols (seed vs. feed (F)) versus the frequency. All cCNCs were sonicated (S) and of the dried-redispersed (D) form. The numbers in the run IDs depict the cCNC loadings in phm.

Appendix II

Supporting Information for Chapter 4: "Enhancing Pressure Sensitive Adhesive Performance Using Acetylated Carboxylated Cellulose Nanocrystals"

Parisa Bayat[1], Kelly M. Meek[1,2], Emily D. Cranston[3], Michael Cunningham[4], Pascale Champagne[5], Timothy Morse[6], Arthur Werner[6], Sean George[7], Cecilia Cancellara[3], and Marc A. Dubé[*,1]

[1]Department of Chemical and Biological Engineering, University of Ottawa, Ottawa, ON, Canada, K1N 6N5
[2]Chemical and Material Engineering, Concordia University, Montreal, QC, Canada, H3G 1M8
[3]Department of Wood Science and Department of Chemical and Biological Engineering, University of British Columbia, Vancouver, BC, Canada, V6T 1Z4
[4]Department of Chemical Engineering, Queen's University, Kingston, ON, Canada, K7L 3N6
[5]Energy Mining & Environment Research Centre, National Research Council, Montreal, QC, Canada, K1A 0R6
[6]Anomera Inc., Montreal, QC, Canada, H3B 1A7
[7]BASF Corp., Charlotte, NC, United States, 28273

This chapter is Supporting Information for the manuscript published in Industrial & Engineering Chemistry Research (2025, 64, 9, 4932–4941)

The contact angle measurements of acetylated cCNCs with varying DS are shown in Figure AII.1. It should be noted that water contact angle measurements for the dried nanocomposite films were not performed as the impact of such low cCNC concentrations on this measurement was not significant according to our previous work (Ref. 8 in main manuscript).

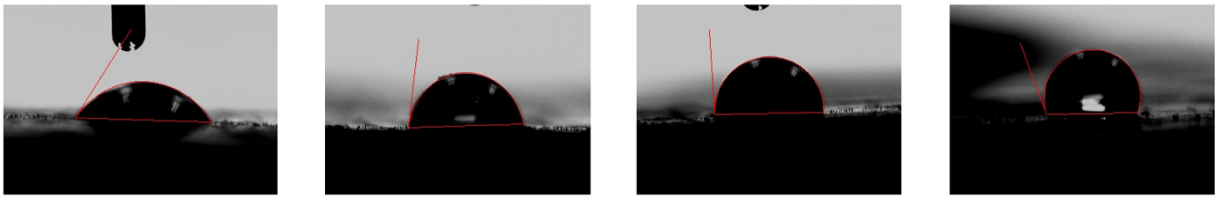

0.06 AcCNCs 0.10 AcCNCs 0.25 AcCNCs 0.42 AcCNCs

Figure AII.1. Change in the contact angle measurements of AcCNCs with increasing degree of substitution (DS).

In this study, the conversion was calculated using a standard gravimetric method; ~0.5 g of latex was weighed in an aluminum dish and dried at ambient temperature under the fume hood until a constant weight was achieved (~24 h). The solids content was calculated using:

$$Solids\ content\ (\%) = \frac{W_{dried\ sample}}{W_{latex}} \times 100\% \qquad \text{(AII.1)}$$

The instantaneous monomer conversion was calculated based on the amount of monomer and other ingredients charged to the reactor as:

$$X_{ins} = \frac{Solids\ content - w_i - w_{surf} - w_{CNC} - w_{buffer}}{w_m} \qquad \text{(AII.2)}$$

where w_i, ws_{surf}, w_{CNC}, w_{buffer} and w_m represent the weight fractions of initiator, surfactant, CNC, buffer, and monomer, respectively, which were introduced to the reaction mixture up to that time. The overall monomer conversion was calculated via Equation (AII.2) using the total weight fractions of the ingredients added throughout the reaction. As shown in Figures AII.2 and AII.3, the instantaneous and overall conversion of latexes with cCNCs/AcCNCs showed similar trends to those of the base case formulation.

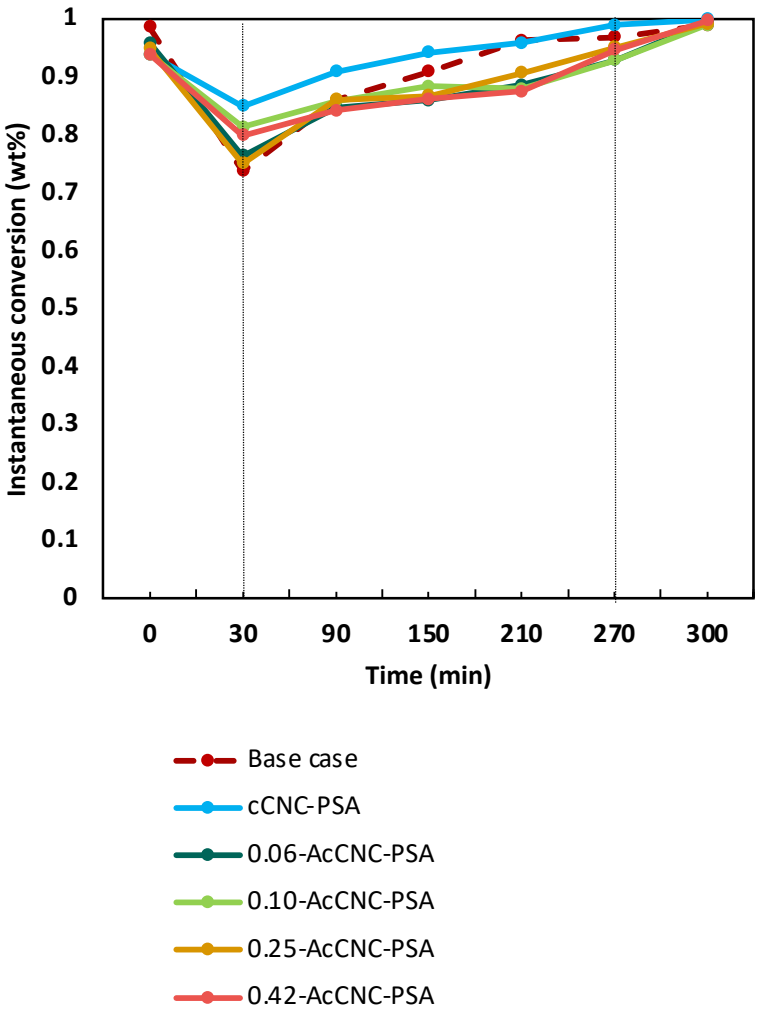

Figure AII.2. Instantaneous conversion of base case and latexes with cCNCs/AcCNCs.

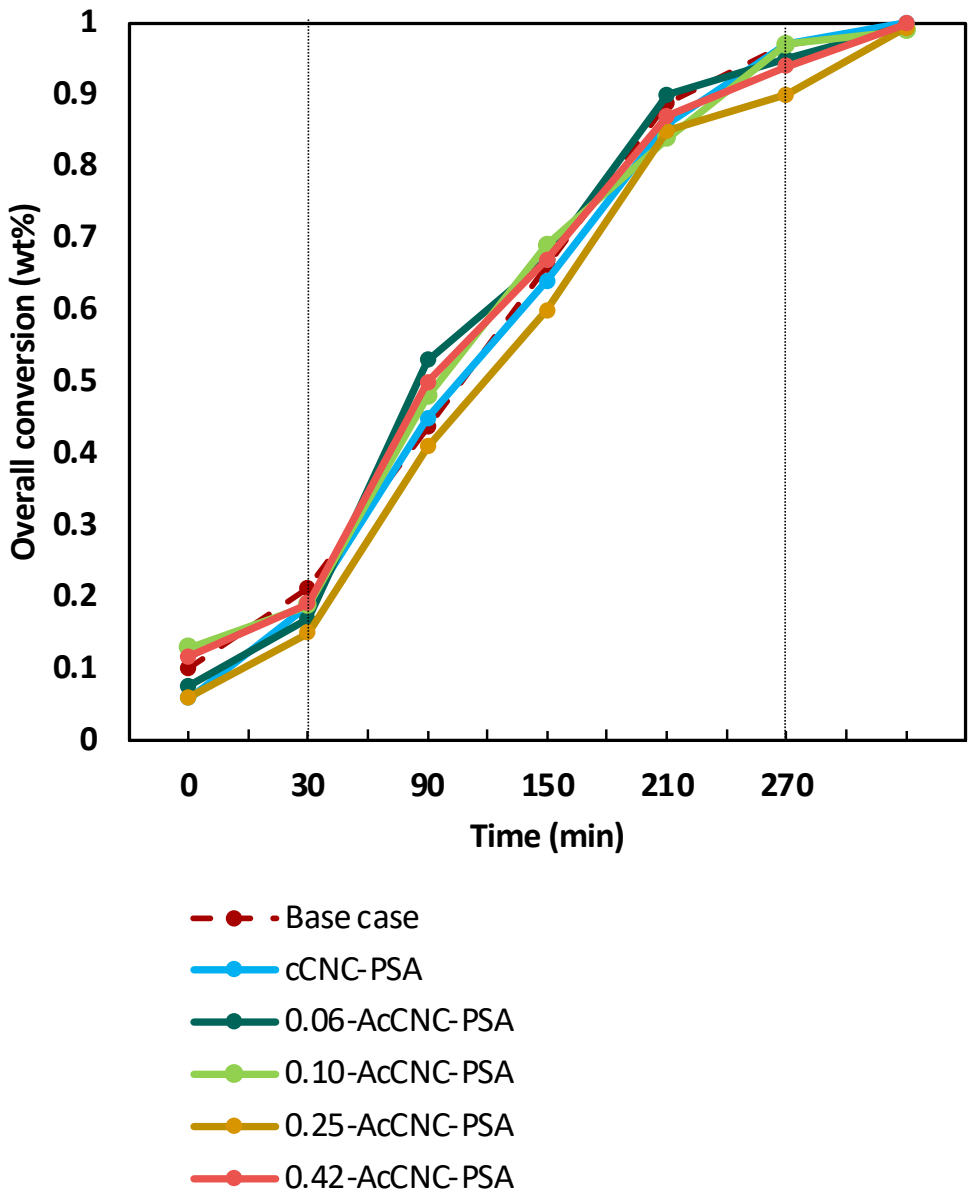

Figure AII.3. Overall conversion of base case and latexes with cCNCs/AcCNCs

The pH trajectories for each run followed similar trends, dropping from ~8 to ~7 during the reaction (Figure AII.4).

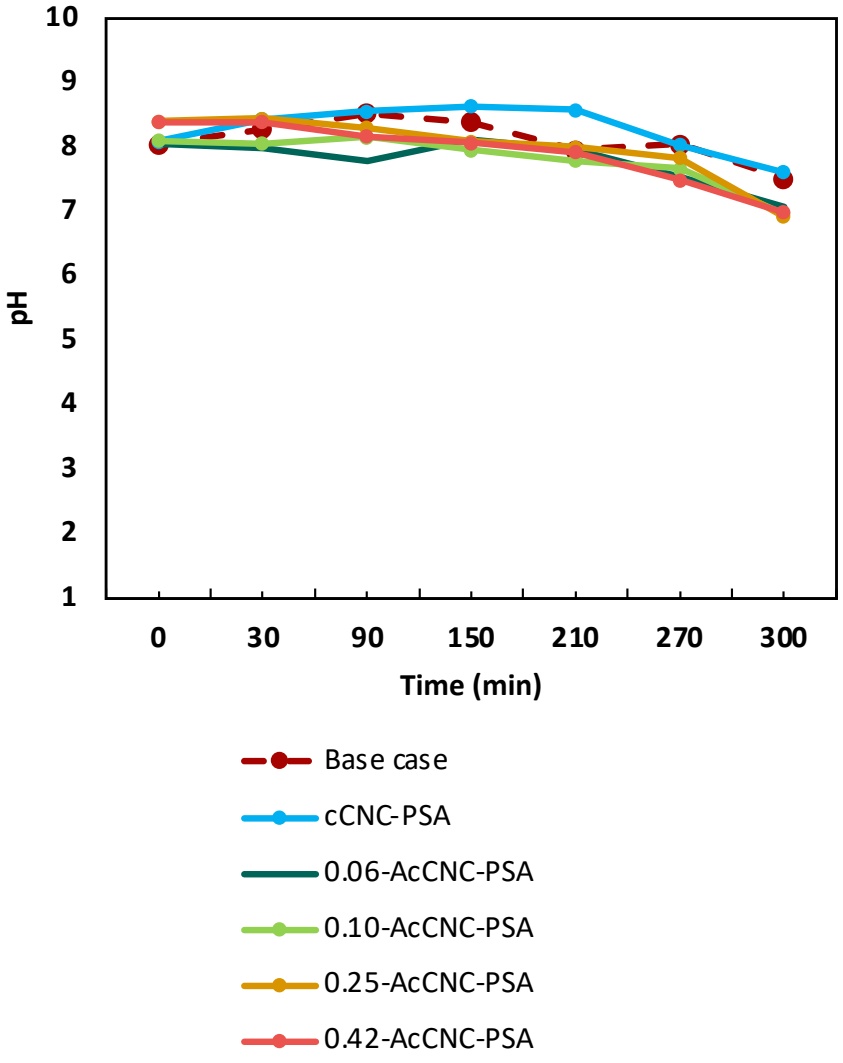

Figure AII.4. pH trajectory of base case and latexes with cCNCs/AcCNCs.

As seen in Figure AII.5, the presence of cCNCs or AcCNCs showed non-significant differences in particle size trajectories for all runs after the seed stage, with differences emerging only towards the end of the polymerization process.

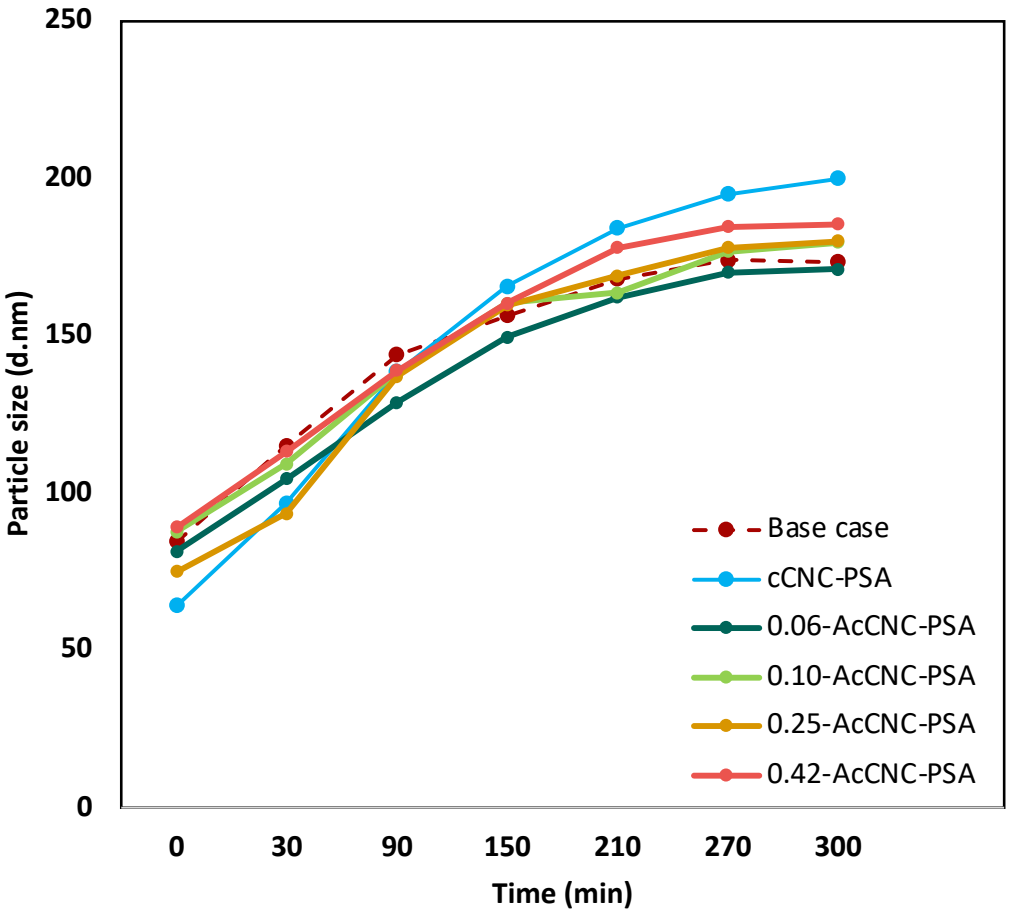

Figure AII.5. Particle size trajectory of base case and latexes with cCNCs/AcCNCs.

For every finished latex, the gel content was measured. A poly(vinylidene fluoride) Durapore™ membrane pouch measuring 47 mm in diameter and 0.45 µm in pore size held about 0.03 g of polymer, which was then heat sealed. Each pouch was immersed in tetrahydrofuran (THF) and gently shaken for a duration of 12 hours. After drying each pouch to a consistent weight, the amount of gel was determined using:

$$Gel\ content\ (\%) = \frac{weight\ of\ retained\ gel\ (g)}{weight\ of\ polymer\ sample\ (g)} \times 100 \qquad \text{Equation (AII.3)}$$

The in-phase AFM images of dried films from non-diluted latex nanocomposite samples (40 wt% solids) are shown in Figure AII.6. The unmodified cCNCs are clearly visible in the images (Figure AII.6).

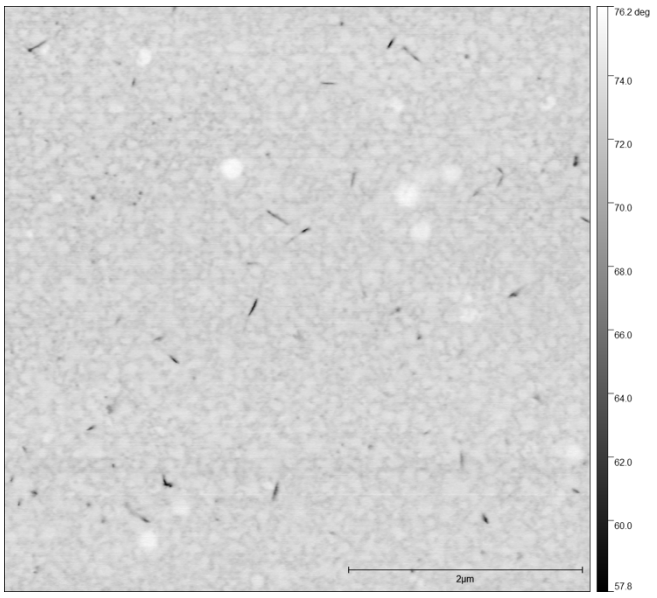

Figure AII.6. In-phase AFM images of stock latex (40 wt.%) cCNC-PSA.

Appendix III

Supporting Information for Chapter 5: "Effect of Carboxylated Cellulose Nanocrystal Acetylation on PLA Nanocomposite Properties"

Parisa Bayat[1], Andrew Anstey[1], Marc A. Dubé[1], Timothy Morse[2], Michael F. Cunningham[3], Kelly M. Meek[*4]

[1]Department of Chemical and Biological Engineering, University of Ottawa, Ottawa, ON, Canada, K1N 6N5
[2]Anomera Inc., Montreal, QC, Canada, H3B 1A7
[3]Department of Chemical Engineering, Queen's University, Kingston, ON, Canada, K7L 3N6
[4]Chemical and Material Engineering, Concordia University, Montreal, QC, Canada, H3G 1M8

Figure III.1 presents the thermal decomposition profiles (via DTG in the left column and TGA in the right column) of unmodified and acetylated cellulose nanocrystals (cCNC and AcCNC) as well as various PLA-based nanocomposites. The acetylation led to improve the thermal stability of unmodified cCNC. As shown in Figures III.1(c–f), a minor peak at about 150°C was detected in all PLA-based nanocomposites, indicating a small amount (<1%) of EtLa residue, even after an extended evaporation period (48 hours in a vacuum oven followed by 1 week under a fume hood).

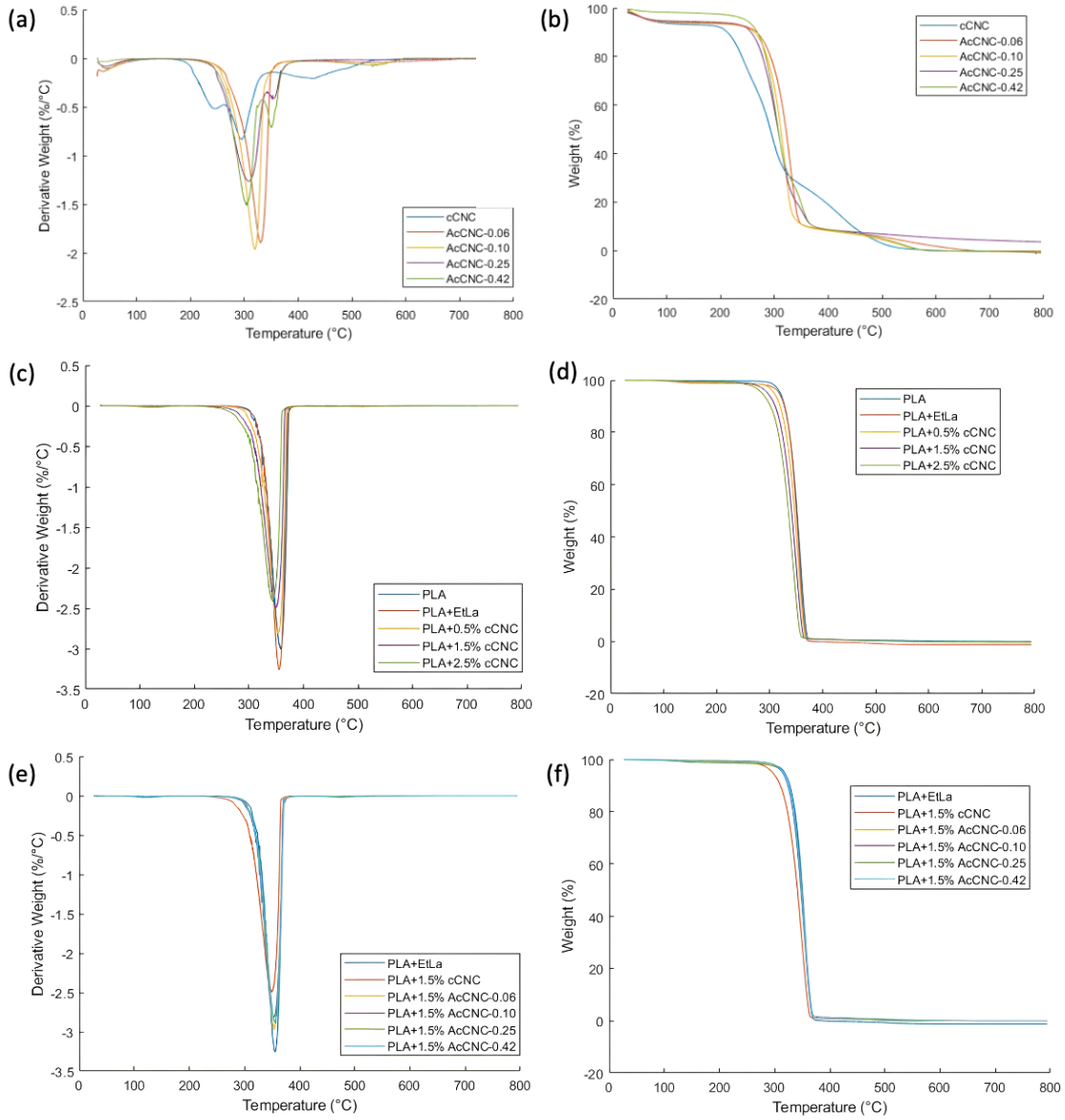

Figure III.1. DTG and TGA curves, respectively, for (a) and (b) cCNC and AcCNCs, (c) and (d) PLA-based nanocomposites with different cCNC levels, and (e) and (f) PLA-based nanocomposites with non-acetylated and acetylated cCNCs with different DS.

No crystallization peak emerged during the cooling run for all nanocomposites as shown in Figure III.2.

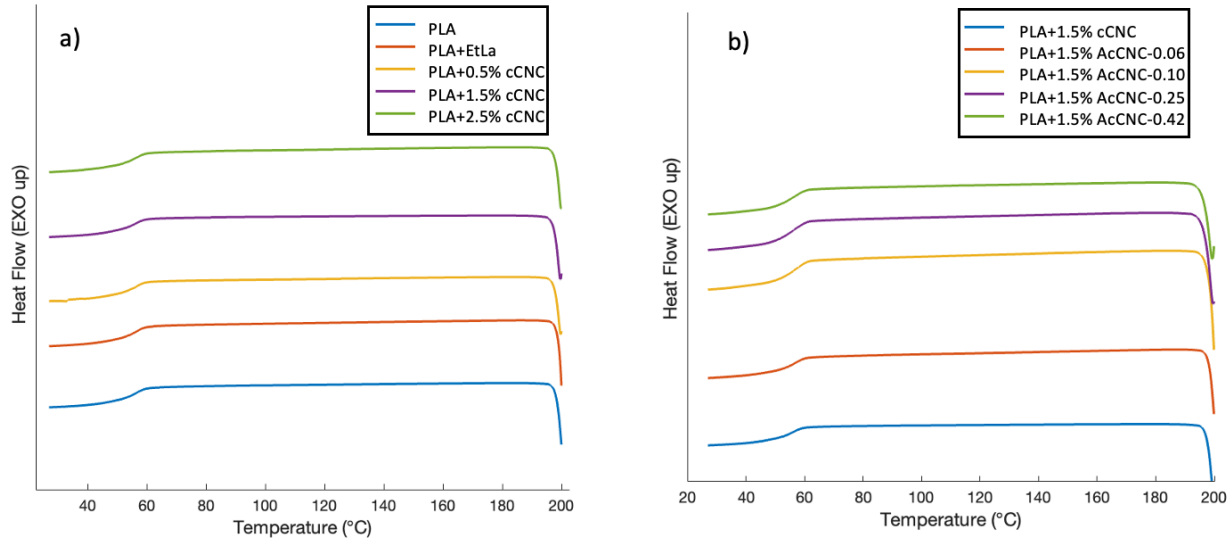

Figure III.2. DSC thermograms of cooling runs for PLA and PLA-based nanocomposites with a) cCNCs and b) AcCNCs. No crystallization was observed.

The measured heat flow using DSC under isotherm conditions at three different temperatures of 100, 110, and 120°C for pure PLA and PLA-based nanocomposites with cCNC/AcCNCs with various level has been shown in Figures III.3 and III.4.

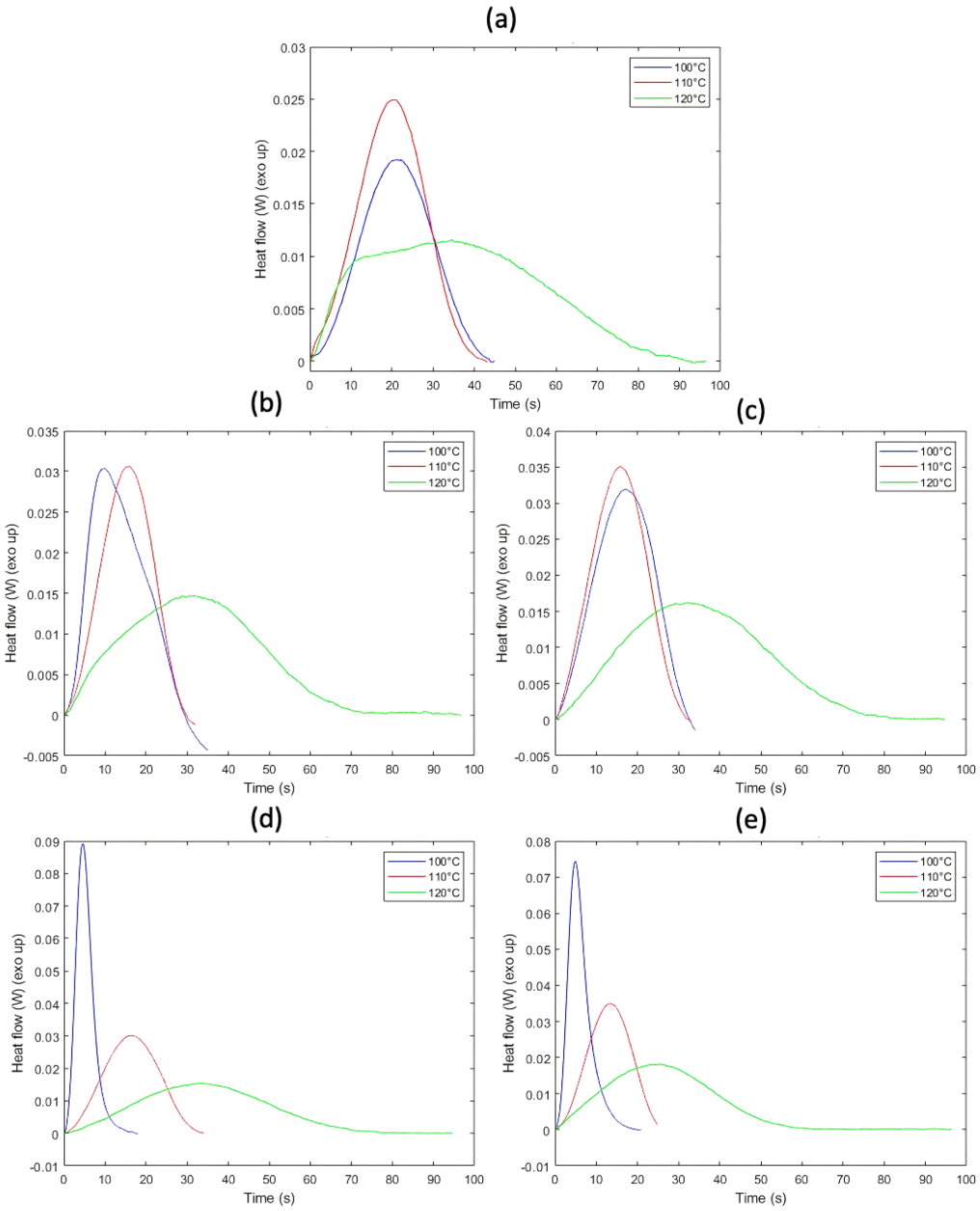

Figure III.3. Isothermal exotherms for a) PLA, b) PLA+EtLa and c-e) PLA-based nanocomposites with cCNC concentrations of c) 0.5 wt.%, d) 1.5 wt.%, and e) 2.5 wt.%.

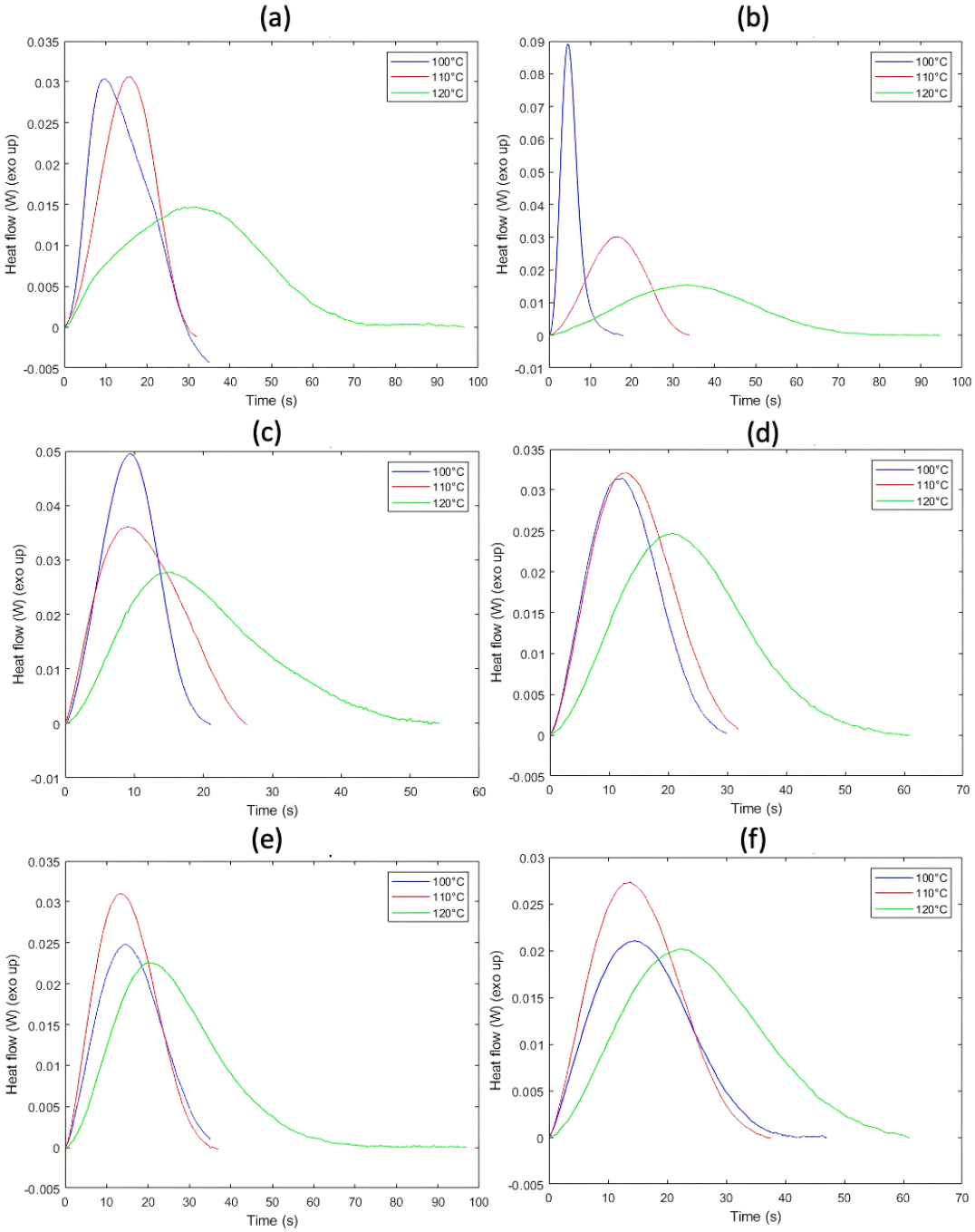

Figure III.4. Isothermal exotherms for a) PLA+EtLa, and b-f) PLA-based nanocomposites with AcCNC concentration of 1.5 wt.% at DS of b) 0 (i.e., cCNC), c) 0.06, d) 0.10, e) 0.25, and f) 0.42.

Based on the FTIR spectra for pure PLA, PLA+EtLA, and PLA with 0.5% and 1.5% cCNC (Figure III.5)—and consistent with TGA findings—it appears some EtLA may remain within the PLA matrix, even after prolonged evaporation.

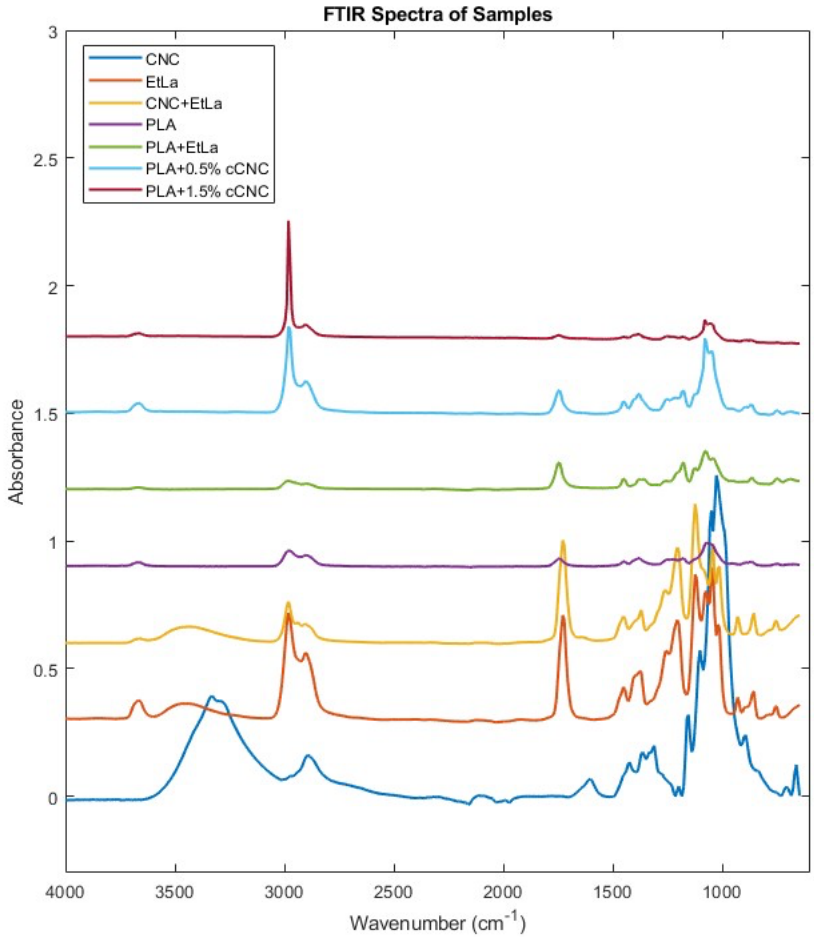

Figure III.5 ATR-FTIR spectra of cCNC, EtLa, cCNC+EtLa (in EtLa solution), PLA, PLA+EtLa (after EtLa evaporation), PLA+0.5% cCNC, and PLA+1.5% cCNC. Because of the similarity of PLA and EtLa FTIR spectra, detection of EtLa in the nanocomposites is inconclusive.

Appendix IV

Laboratory Safety Considerations

The hazards and personal protective equipment (PPE) requirements for all chemicals used throughout this project were derived from the manufacturer's safety data sheets and are mentioned below. PPE, such as a breathing mask, safety goggles, gloves, and lab coat, are used during reaction preparation and polymerization to avoid contact with monomer vapours (during reactor charging and sampling). The reactor temperature is automatically controlled (max 80-85 °C) in a jacketed stainless-steel reactor, coupled to a condenser to liquefy the monomer vapours. PLA is blended at a maximum temperature of ~190-200°C under a fume hood.

Table IV.1 Hazards and personal protective equipment required in this project.

Chemicals	Manufacturing company	Hazards	Personal protective equipment (PPE)
Acetic anhydride	Sigma Aldrich	Flammable liquid and vapour. Harmful if swallowed. Causes severe skin burns and eye damage. Fatal if inhaled.	Use equipment for eye. Tightly fitting safety goggles.
Acetone	Fischer Scientific	Highly flammable liquid and vapour Causes serious eye irritation May cause drowsiness	Protective clothing and gloves, eye protection
Alkyldiphenyloxide disulfonate (commercially named Dowfax 2A1)	Dow chemicals	Causes serious eye damage.	Wear eye protection and/or face protection.
Carboxylated Cellulose Nanocrystals (CNCs)	Anomera Co.	May cause respiratory irritation.	Protective clothing, a full-face respirator and gloves, eye protection

Ethyl alcohol	Sigma-Aldrich	Highly flammable liquid and vapor. Causes serious eye irritation	Protective clothing and gloves, eye protection and face protection
Ethyl Lactate	Sigma-Aldrich	Flammable liquid and vapour. May be corrosive to metals. Causes severe skin burns and eye damage. May cause respiratory irritation.	Protective clothing and gloves, eye protection and face protection. Respiratory protection required when vapours are generated
Hydroquinone	Sigma-Aldrich	May cause moderate skin and eye irritant	Protective clothing and gloves, eye protection
iodine	Sigma Aldrich	Harmful if swallowed, in contact with skin or if inhaled. Causes skin irritation. Causes serious eye irritation. May cause respiratory irritation. Causes damage to organs (Thyroid) through prolonged or repeated exposure if swallowed. H400 Very toxic to aquatic life.	Protective clothing and gloves, eye protection and face protection.
KCl	Sigma-Aldrich	Not hazardous	Protective clothing and gloves, eye protection. Respirator required when dusts are generated.
MMA	Sigma-Aldrich	Highly flammable liquid and vapor. Causes skin irritation. May cause an allergic skin reaction.	Tightly fitting safety goggles. Gloves, Complete suit, a full-face respirator

		May cause respiratory irritation.	
NaCl	Sigma-Aldrich	Not hazardous	Use gloves, eye protection
Nitrogen gas	Linde	High pressure May cause suffocation by displacing the oxygen in air	Storage upright and secure cylinders all time while in use and use appropriate hand truck designed for cylinder
Poly(lactate) acid	NatureWorks	May form combustible dust concentrations in air if small particles are generated during further processing. Not hazardous.	Protective clothing and gloves, eye Protection. Respirator required when dusts are generated.
Sodium bicarbonate	Sigma Aldrich	No Hazard. May cause eye and skin irritation	Use protective clothing and gloves, eye protection
Sodium hydroxide (NaOH)	Sigma-Aldrich	Causes severe skin burns and eye damage	Protective clothing and gloves, eye protection and face protection
Sodium persulfate (NaPS)	Sigma-Aldrich	May intensify fire; Harmful if swallowed. Causes skin irritation. May cause an allergic skin reaction. May cause allergy or asthma symptoms or breathing difficulties if inhaled. May cause respiratory irritation	Advice for non-emergency personnel: Avoid inhalation of dusts. Avoid substance contact. Ensure adequate ventilation.
Sulfated Cellulose Nanocrystals (sCNCs)	Celluforce	May cause respiratory irritation.	Protective clothing, a full-face respirator and gloves, eye protection

Styrene (STY)	Sigma-Aldrich	Flammable liquid and vapours. Causes skin and serious eye irritation, harmful if inhaled.	Tightly fitting safety goggles. Gloves, Complete suit, a full-face respirator
Triton X405	Dow chemicals	Not a hazardous substance or mixture	Slipping hazard Protective clothing and gloves, eye protection
2-EHA	Sigma-Aldrich	Causes skin irritation. May cause an allergic skin reaction. May cause respiratory irritation.	Tightly fitting safety goggles. Gloves, Complete suit, a full-face respirator

In compliance with safety protocols, a Hazard Identification and Risk Assessment (HIRA) on the emulsion polymerization process was completed and submitted to the Department of Chemical and Biological Engineering at the University of Ottawa. The assessment process led to the identification of potential hazards, the assessment of associated risks, the categorization of safety risk levels, and an outline of mitigation strategies to address the potential risks. This systematic approach ensured proactive management of safety concerns and promoted a secure research environment. The HIRA is available on the Office of Risk Management website at https://www.uottawa.ca/about-us/administration-services/office-chief-risk-officer/health-safety-environmental-management/occupational-health-safety/management-system/safety-procedures.

Appendix V

List of Publications and Conferences

AV.1 List of Publications

1. **Bayat, P.**; Meek, K. M.; Cranston, E. D.; Cunningham, M.; Champagne, P.; Morse, T.; Werner, A.; George, S.; Cancellara, C.; Dubé, M. A. Enhancing Pressure Sensitive Adhesive Performance Using Acetylated Carboxylated Cellulose Nanocrystals. *Ind Eng Chem Res* **2025**. https://doi.org/10.1021/acs.iecr.4c04649.
2. **Bayat, P.**; Meek, K. M.; Movafagh, M.; Cranston, E. D.; Cunningham, M. F.; Champagne, P.; Morse, T.; Kiriakou, M. V.; George, S. R.; Dubé, M. A. The Effect of Cellulose Nanocrystal Reassembly on Latex-Based Pressure-Sensitive Adhesive Performance. *Biomacromolecules* **2024**, *25* (5), 3018–3032. https://doi.org/10.1021/acs.biomac.4c00138.
3. Movafagh, M.; Meek, K. M.; **Bayat, P.**; Cranston, E. D.; Cunningham, M.; Champagne, P.; Morse, T.; Kiriakou, M.; George, S.; Dubé, M. A. Improved Pressure-sensitive Adhesive Performance Using Carboxylated Cellulose Nanocrystals via Blending. *Polym. Eng. Sci.* **2024**, *64* (2), 798–816. https://doi.org/10.1002/pen.26585.
4. **Bayat, P.**; Khorasani, M. Progress in Organic Coatings Synthesis and Characterization of Transparent 1-Package PUD Based on Castor Oil and Polyethylene Glycol. *Prog Org Coat* **2021**, *153* (1), 106148. https://doi.org/10.1016/j.porgcoat.2021.106148.

AV.2 List of Conference Presentations

1. **Bayat, P.**; Meek, K. M.; Movafagh, M.; Cranston, E. D.; Cunningham, M. F.; Champagne, P.; Morse, T.; Kiriakou, M. V.; George, S. R.; Dubé, M. A., "*Carboxylated Cellulose Nanocrystal Acetylation Improves Pressure Sensitive Adhesive Properties,"* Oral presentation, Canadian Chemical Engineering Conference, CCEC 2024, National, Toronto, ON, October 2024
2. **Bayat, P.**; Meek, K. M.; Movafagh, M.; Cranston, E. D.; Cunningham, M. F.; Champagne, P.; Morse, T.; Kiriakou, M. V.; George, S. R.; Dubé, M. A., "*The Effect of Cellulose Nanocrystal Reassembly on Latex-Based Pressure-Sensitive Adhesive Performance,"* Poster, Canadian Chemical Engineering Conference, CCEC 2024, National, Toronto, ON, October 2024
3. **Bayat, P.**; Meek, K. M.; Movafagh, M.; Cranston, E. D.; Cunningham, M. F.; Champagne, P.; Morse, T.; Kiriakou, M. V.; George, S. R.; Dubé, M. A., "*Improving Adhesive Properties of 2-Ethyl Hexyl Acrylate/Methyl Methacrylate/Styrene Emulsion Polymers Using Carboxylated Cellulose Nanocrystals,"* Poster, International Polymer Colloid Group, IPCG 2023, Kingstone, ON, June 2023
4. **Bayat, P.**; Meek, K. M.; Movafagh, M.; Cranston, E. D.; Cunningham, M. F.; Champagne, P.; Morse, T.; Kiriakou, M. V.; George, S. R.; Dubé, M. A., "*Improving Adhesive Properties of 2-Ethyl Hexyl Acrylate/Methyl Methacrylate/Styrene Emulsion Polymers Using Carboxylated Cellulose Nanocrystals,"* Poster, International Conference on Nanotechnology for Renewable Materials, TAPPI Nano 2023, Vancouver, BC, June 2023
5. **Bayat, P.**; Khorasani, M., "*Mechanical Improvement of Polyurethane Dispersion by Castor oil,"* Poster, The 6th international Congress on transportation, traffic, and safety coatings, Tehran, June 2019
6. **Bayat, P.**; Khorasani, M., "*The influence of molecular weight of polyol on properties of polyurethane dispersion,"* Oral presentation, The 6th international congress on transportation, traffic and safety coatings, Tehran, June 2019